Partial Discharge Pattern Analysis

By

Charles Chung Chang

M.Eng.Sc., Monash University

Submitted for the Degree of Doctor of Philosophy

This work was conducted within

The Department of Electrical and Computer Systems Engineering

Monash University

Clayton, Victoria 3168

Australia

December 2001

Contents

Summary

The main problem regarding discharge pattern analysis is that many discharge distributions have not been discovered, studied and utilized. To date, all data mining for PD analysis reported have been based only on a handful of distributions. This means that even sophisticated data mining techniques may not guarantee solid and reliable discharge pattern recognition, since the amount of information contained in those few distributions is limited to start with. It is therefore important to explore more discharge distributions, enabling the extraction of discriminating features. In this thesis, are presented some new method to analyze partial discharge patterns and identify different types of discharge sources. In order to break through the barrier and solve the problem in a broader base, great effort has been made in this research project on the establishment of various discharge distributions since every distribution contains unique information about discharge activities.

Many discharge distributions are innovated, classified and systematically established. New discharge distributions are derived from windowing statistics, which is based on measurable variables such as discharge amplitude, voltage when discharge occurs, voltage cycle index and the differences between consecutive discharge or discharge related properties. Parameters describing discharge distributions are extracted in order to have distribution pattern quantified and recognized. The new discharge distributions and the associated parameters in conjunction with a discharge measuring and evaluating system have been implemented and incorporated in a commercial partial discharge measuring and evaluating system as standard features.

With the support of established discharge distributions, reliable discharge pattern recognition is performed using three different types of neural network topologies in order to prove the effectiveness of the newly established discharge distributions and the extracted parameters. Successful discharge source recognition is achieved because extracted parameters for training the networks cover a wide range of discharge distributions that represents the nature of discharge activities. They have stronger

discriminating power than any other fingerprints used for this purpose. In order to reduce the dimension of discharge fingerprints, parameters are successfully compressed using a hybrid neural network constructed by a PCA cascading with a MLP network.

The significant parameter is a parameter that has strong discriminating power to separate different types of discharge sources. A small variation from a significant input channel causes a significant response of overall network output. Based on the sensitivity theory, this thesis innovates a general method to find the most significant parameters. Obviously, applying sensitivity theory in discharge pattern analysis makes it possible to link discharge physical mechanisms with discharge distributions.

All the new techniques presented in this thesis have great potential of future industrial application after further development.

Declaration

This thesis contains no material which has been accepted for the award of any other degree or diploma in any university or other institution and to the best of my knowledge and belief, it contains no material previously published or written by another person, except where due reference is made in the text of the thesis.
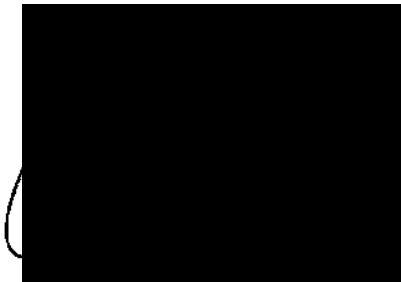
Charles Chung Chang

December 16, 2001

CHAPTER 1

INTRODUCTION

Partial discharge (PD) is the name given to electrical discharge involving a portion of a dielectric between two electrodes, which does not bridge the gap. PD may happen in a cavity in a solid insulating material, on a surface or around a sharp edge subjected to a high voltage (HV). PD occurs around conductors in air or other gases, which is referred to as corona. Electrical stress exceeding local field strength of insulation may cause the formation of PD. PD is both symptom and cause of deterioration in insulation. PD results in high frequency current pulses and radio frequency (RF) emission [1-6]. A lot of research activities have been devoted to investigate PD growth as a function of wide variety of parameters such as type and level of voltage, frequency, temperature, mechanical stressing, material properties and electrode geometry etc [7,8]. The reason to study PD phenomena is that PD has significant impact on the life of insulation of HV equipment. Every discharge event deteriorates the insulation material by the energy impact of high-energy electrons or accelerated ions, causing many types of chemical transformations [9]. PD occurs in solids, liquids, and gases in ways that will not affect the breakdown voltage during a non-destructive test. PD will eventually cause failure in most systems years after being placed in service.

For many years, an equivalent circuit has been used when discussing PDs as illustrated in figure 1. With respect to this equivalent circuit, C_a denotes the capacitance of the system. C_b is considered to be the capacitance of the dielectric in series with the void. C_c indicates that the gas-filled void breaks down when there is a sufficiently high field strength in the void. This well-known equivalent circuit is a useful tool in understanding how a PD produces a measurable signal. However, this model is valid only for a Laplacian field where the magnitude of charge carried by each conductor is directly proportional to the potential difference between the two conductors. Unfortunately, this proportionality does not exist in a Poissonian field where space charge exists in the volume between the electrodes. Therefore, the validity of this equivalent circuit is

limited to cases where the boundaries of a defect void are equipotential before and after PD taking place. Despite of the limitation or even error of this equivalent circuit, it is still a useful tool in understanding how a PD can be measured [10, 11].
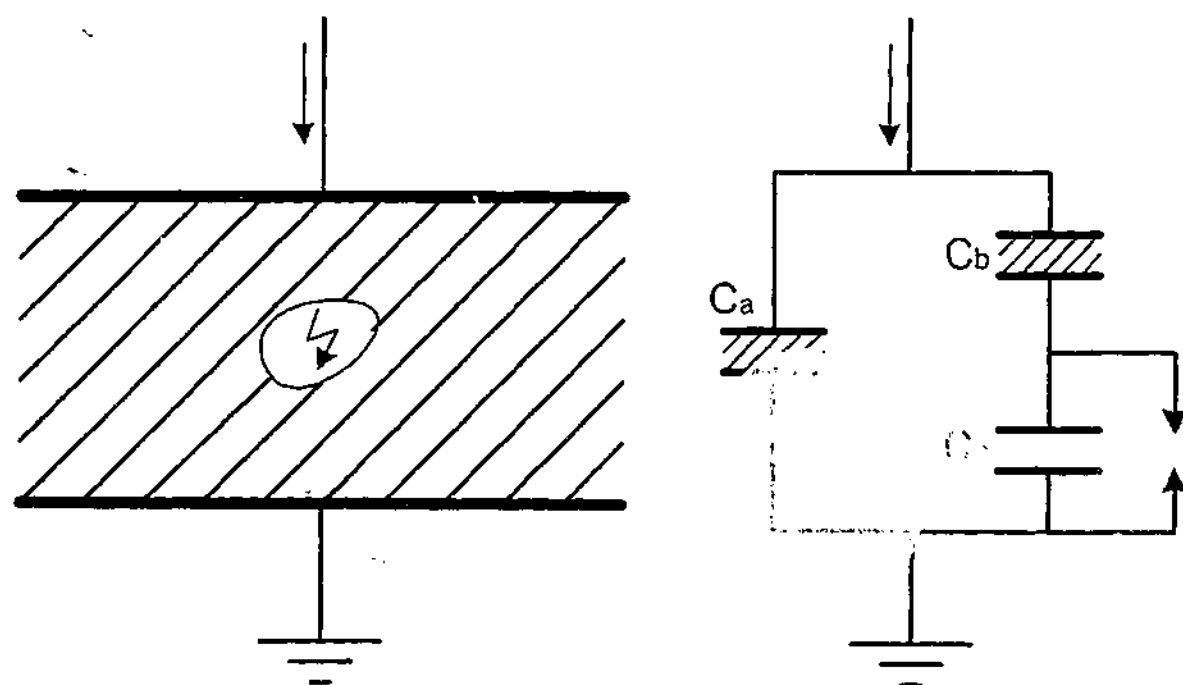
Fig 1.1 PD equivalent circuit

1.1 PARTIAL DISCHARGE MEASURING SYSTEM

The measurements of PD phenomena have been of interest since early 1940's. They were established as important tests for assessing the insulation condition of HV equipment in 1950s. A number of PD detectors were produced based on experimental development and research. The various developments, including application of the balanced circuit concept, were described by Kreuger [12]. The apparatus and techniques used in the early days were so basic that much went unrecorded. The early days of PD research included studies of PD in gas-filled cavities, in oil-impregnated paper, and in other dielectric materials. Studies were conducted in many HV apparatus, such as turbine generator and power transformers etc. [13-15].

The widespread acceptance of PD testing has made PD measuring system a diagnostic tool. The purpose of the diagnosis is not to check manufacturing quality, but rather to

determine if, or the degree to which, the insulation system is deteriorating during equipment operation. During operation, the thermal, electrical, and mechanical stresses, together with environmental factors, can combine to degrade the electrical insulation. For example, cracks and delaminating may occur within the insulation, insulation surfaces can become polluted and the oil or SF6 can degrade. Many of these processes lead to and, vice versa, are caused by PDs. Hence the detection of PD can facilitate preventive maintenance by monitoring the condition of insulation system. Several viable on-line PD tests have been developed to monitor the condition of the solid dielectric insulation in high voltage equipment with noise reduction techniques based on time and frequency domain filters [43, 44].

PD detection is based on the observable energy exchange as (1) electrical current due to some forms of electrical activity with the system, (2) dielectric loss, (3) electromagnetic radiation, (4) acoustic signals, and (5) chemical reaction. A number of PD detection techniques have been used for many years. The symptomatic nature and the available detection techniques have combined to make PD measurements the dominant basis for electrical quality control. PD tests detect many manufacturing and assembly problems, such as cavities in solid insulation, insulating surface contamination, metallic contaminants etc. However, in order to obtain reliable results in PD tests, it is essential to control all relevant factors in terms of the condition of test object and the choice of test procedure. PD measuring systems can be mainly divided into coupling device and measuring instrument that consists of a PD detector and a computer. Effective diagnosis of the insulation condition depends on the choice of measuring parameters, coupled with an extensive knowledge relating to particular physical conditions. The basic arrangement for a PD detection system can be represented by the simple block diagram in figure 1.2.
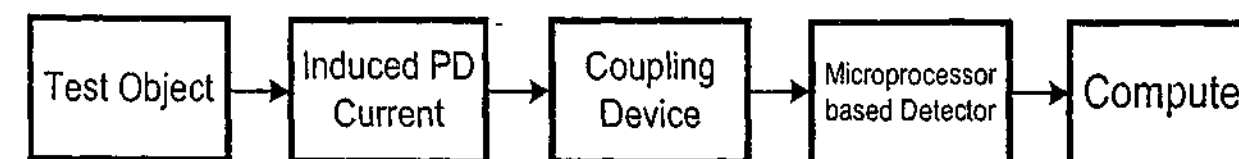
Fig. 1.2 General block diagram of a computer-based PD measuring system

1.1.1   Measuring Circuitry and Coupling Device

The coupling device is essentially an RLC network. It is an integral part of the measuring system and test circuit, with components specifically designed to achieve the optimum sensitivity with a specific test circuit. The choice of the impedance of the coupling device is governed by two main considerations. First, the power-frequency component of the applied voltage must be eliminated, second, the pulse component should be of sufficiently short duration to ensure resolution of rapidly successive pulses. The coupling device converts the input currents to output voltage signals that are transmitted to the measuring instrument through a connecting cable. The frequency response of the coupling device may be selected to reduce the noise. Coupling device can be connected in series with the coupling capacitor or the test object as shown in figure 1.3.
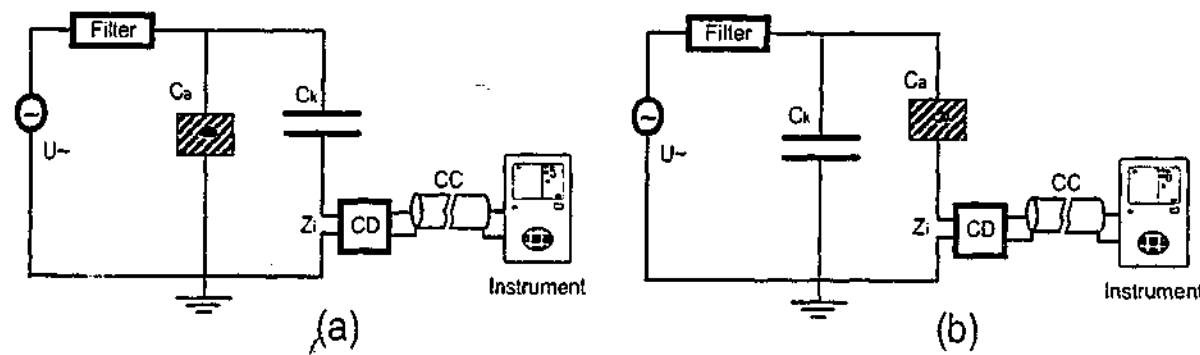
Fig. 1.3 PD detection circuit and measuring system
(a) CD in series with the coupling capacitor   (b) CD in series with the test object
U~: High voltage supply
C_a: Test Object
C_k: Coupling capacitor
Z_i: Input impedance of the measuring system
CD: Coupling device
CC: Connecting cable

In early days, the instruments that were ultimately used to detect discharges could be divided into two classes – namely, those responding to single discharge pulse and those responding to numerous pulses.

1.1.2   Microprocessor Based Detector

With the help of computer-based technologies, detailed analysis of PD behavior in HV insulation becomes possible. The electric signal produced by a PD is first transferred from its internal source to the terminals of the test object. Then it reaches the digital detector through a coupling device and a connecting cable. A large amount of quantitative information about the acquired PDs is transferred to a PC for a final evaluation.

The development of microprocessor technology has enabled the design of some digital instruments capable of measuring a wide range of PD parameters. Hence, many aspects of discharge activities relating to insulation deterioration can be taken into account. A large memory buffer is required in order to allow a sufficient number of PD data to be collected in a given time interval. The multi-channel detection techniques have made accurate and reliable measurement of basic PD quantities possible. Multi-channel pulse analyzers have been used for PD analysis since 1970's, mainly for the measurement and sorting of discrete pulse heights and corresponding discharge rates. This method of recording discharge patterns gave rise to statistical pulse distribution characteristics over a given period of time and for particularly applied voltage levels. Although this method of recording discharge activity can result in an in-depth analysis of insulation quality, there is still significant information that is lost. This type of digital recording is being substituted by PC oriented software. Many hardware and software systems are described in the literature [16-20].

Digital signal processing techniques involving the use of high-speed analog-to-digital (A/D) converters have been in use for more than three decades and appropriate calibration techniques developed [21, 22]. An important feature of the PD pulse is its rise time. The response of the PD detectors is contingent upon the rise time of the discharge pulse, which is a function of the voltage across the discharge site. When A/D converters are employed for discharge measurement, the response of the pulse detector will be influenced by the rise time of the discharge pulse [15]. In order to prevent inaccurate representation of rapid rise time PD pulses, the sampling rates had to be sufficiently high to accommodate all the high frequency components of the incident

pulses. The analog data was passed through an analog filter to attenuate the high frequencies due to the limits in the sampling rates available. The use of microcomputers has greatly facilitated the implementation of enormous amounts of PD information to be obtained with ease. The use of digital techniques has been largely contributed to research work in the area of PD where PD distribution measurements are of principal interest. Results from PD distribution may provide some insight into the insulation degradation process due to the presence of discharges and the nature of the discharges themselves [23].

A digital PD detection is in general based on analog measurement of apparent charge standardized in the IEC Publication 270 [24]. In other words, a digital PD detector is an extension of the analog systems used to record the PD quantities during the tests. Consequently, the digital part is used to process analog signals for further evaluation. The digitizing of discharge pulses is concerned with the peak values of the discharge pulses rather than on the shape of the PD pulse. This is because the pulse shape of a discharge is strongly influenced by the resonant frequency of the measuring circuit. To obtain the peak value of discharge pulses, two methods may be used. First, the discharge pulses are digitized at sufficiently high sampling rate and stored as numerical values. These stored numerical values must be interpolated using mathematical routines to produce a curve similar to the curve recorded by an analog detector. Second, an analog circuit can be used to capture the peak value of the discharge pulse using a peak hold circuit. In this approach, the resolution time of the digital detector need only be fast enough to match the resolution of the analog detector.

1.1.3. Host Computer

After digital processing of a PD sequence, the acquired PD data requires to be transferred to a host PC for further processing and displaying of the magnitude of app ˈ.e.nt charge. Numeric procedures are used to continuously process and display the acquired PD patterns and rel -vant feature quantities. Applicable statistical results can be calculated and selectively displayed on the PC screen.

To be at all effective, PD data must be manipulated to give outputs that summarize the results and present data in a form that does not require further scrutiny. The most common methods of presenting the results include graphic means, two or three dimension graphs, histograms, and other methods such as tabulations and arrays.

The procedure to calibrate a digital PD detector is the same as for an analog system. Before calibration, according to IEC Publication 270, the test object must be placed in the test circuit in which the digital detector is connected. It is important to observe PD parameters automatically over the whole period of measurement. PD parameters of interest include apparent charge, repetition rate, PD energy, and the phase position with respect to the ac voltage.

An interactive graphical user interface is one of the most important features of a host software package. It assists the operating engineer in performing real-time or non-real-time analysis. With such an interactive and intuitive environment, interface for the analysis of PDs in various distribution patterns is provided. With a sophisticated backend database and in-place graphic editing support, PD data types can be conveniently transformed from one format to another facilitating the investigation of the trend of PD activities over a selected period of time [44].

1.1.4 Application

Many applications have been published using computer-based measuring system to monitor condition of insulation system. Certain types of power apparatus have traditionally been tested for PD using a particular type of measuring circuit and instrumentation that has previously been considered as the most suitable ones for that application. For a particular apparatus, it is more relevant to use certain parameters than others in assessing the insulation quality. Indeed the availability of instrumentation for the measurement and the economics involved in the testing may be the deciding factors for the type and method of PD measurement being applied.

One of these applications was to measure PDs from small cavities in solid dielectric insulation. These defects involving single and multiple cavities were made artificially.

The tests were conducted using a computer-based PD measuring system with customized fingerprints calculated to distinguish between the different defects [25].

Discharge activity in oil-impregnated papers, which was presented in HV power transformers, was investigated using a computer-based measuring system. A number of operating conditions, including the presence of moisture, small metal particles, tracking and sparking etc., were artificially created in the laboratory. The statistics associated with four different distributions were calculated using a digital PD system [26, 27].

Other applications using computer-based measuring system to obtain PD patterns were tests on generator stator bars [26-30], insulation papers and films [31, 32]. Computer-based PD measuring systems were also applied in the on-line PD monitoring of large generators [33-35], HV power transformers [36-37], gas insulated substation [38, 39] and power cables [40-43].

1.1.5 Limitation

Discharge within an insulation system has long been associated with gradual degradation and dielectric failure. Among the established correlation between PD intensity and degradation, the maximum amplitude of PDs is the most significant quantity. Unfortunately, simple experimental results based on a few laboratory models show that the maximum discharge amplitude is not related to the time to breakdown or the amount of deterioration in the dielectric [26 27]. In addition, experiments also prove that the damaging effect of a discharge in solid dielectric depends on the nature of the defect in which it occurs. When the dimensions of the defect are microscopic, low discharge amplitudes can also result in very high energy densities that lead to speedy degradation of the dielectric [28].

In fact, the diagnosis of insulation deterioration from PD measurements is complicated by the wide range of defects. The damaging effect of a PD depends on the defect in which it occurs. The relationship between the apparent PD magnitude and the deterioration rate or life of the insulation is nonlinear. The meaningful evaluation of PD measurements in terms of the rate of degradation and remaining life is impossible in the

absence of the knowledge about defect type as well as a microscopic description of the defect.

1.2 PARTIAL DISCHARGE STATISTICAL CHARACTERISTICS

A PD is an electrical breakdown phenomenon that is confined to localized regions of the insulation material between electrodes. The field enhancement as result of localized discharge can be associated with abrupt changes in the nature of the insulating material that may be caused by voids in solid dielectrics or gas-filled spaces at dielectric-conductor or dielectric-dielectric surface. PD activity occurs in regions corresponding to occlusion in solids or bubbles formed by vaporization of a liquid. The PD phenomena has self-quenching characteristics by nature, due to the interaction between the applied and defect local field [45-47].

Although it is very difficult to establish a deterministic approach to PD theory and measurement results, the fact remains that pulsating PD phenomena are inherently stochastic processes. They exhibit significant statistical variation in terms of discharge pulse shape, pulse amplitude, and time of occurrence. The stochastic character of PD phenomena is originated from the probabilistic nature of PD processes that lead to discharge initiation and growth. For example, the field-induced emission of electrons from a surface can initiate a discharge. Such a process can only be properly described by quantum theory and is inherently probabilistic. In addition, the electron-molecule collision processes that determine the evolution of a PD are also described in terms of probabilities. Moreover, the gas ionization coefficient is derived from ionization cross sections and it represents the average behavior of many electrons with different velocities. It is related to the probability per-unit-path length that an electron will cause ionization by collision with a gas molecule [48,49]. Factors that can affect the stochastic behavior of PD include:

(1) Probability of initiatory electron injection
(2) Dynamics of dielectric surface charging
(3) Growth rate of discharge-induced cavities in liquids
(4) Rates of discharge-generated ion space charge

(5) Fluctuations in gas composition or density

(6) Presence of ionizing radiation

(7) Memory propagation associated with the influence of residuals from previous PDs

The above factors are not independent and in fact, they affect each other. The existence of memory effects implies that the PD process is non-Markov process. It has significant consequences in controlling or predicting the outcome of a PD measurement. Therefore, PD phenomena must be regarded as complex stochastic processes.

1.3 REVIEW OF PARTIAL DISCHARGE PATTERN ANALYSIS

Because of the importance of measuring the condition of insulation system of HV apparatus, many techniques have been developed for PD detection, location and evaluation throughout years. International standard on PD measurement has suggested a few important quantities to diagnose the condition of test object. A number of discharge quantities are defined in IEC Publication 270 representing the statistical information regarding PDs in a given time interval. Unfortunately, they are not able to provide information regarding discharge physical mechanisms because these quantities do not present distribution information related to discharge activities inside the insulation.

As each defect has its won particular degradation mechanism, it is important to quantify the degree of correlation between discharge distribution patterns. With rapid advancement of digital technologies, many computer-aided systems have been developed for the measurement and evaluation of PD phenomena through PD distribution patterns. These computer-based PD measuring and evaluating systems not only improve data handling and storage but also provide much more power and flexibility in data processing. Digital analysis methods enable PD physical related fingerprints to be calculated and applied in the assessment of the insulation condition of particular configurations. The selection of quantities is extremely important for PD distribution pattern analysis. However, researchers do not adequately explore more of the physically related PD distributions, enabling the extraction of discriminating features from them. Instead, they apply various data mining techniques on limited distribution patterns [25, 26, 27, 50, 51].

1.3.1 Definition

In this section, some important definitions regarding terms used in discharge pattern analysis are presented. These terms will be used frequently throughout this thesis.

Basic PD Quantity: The directly measured properties of a discharge event including PD magnitude, instantaneous voltage and ac phase position when it occurs.

Derived PD Quantity: The calculated properties of a discharge event including PD energy, quadratic value of a PD magnitude.

Integrated PD quantity: The statistics or other PD properties calculated from basic and derived PD quantity or quantities in a given time period. For example PD repetition rate, average PD magnitude, PD current, quadratic rate, and PD energy etc.

Partition window: An equally divided window of an index variable. There are (1) the phase window (figure 1.11), (2) the pulse-height window (figure 1.12), (3) the cycle window (figure 1.13), (4) the voltage difference window (figure 1.14a), the charge difference window (figure 1.14b) and the time interval window (figure 1.14c).

Partition quantity: The statistical or other PD physically related properties calculated based on each partition window.

Distribution Function: A function of partition quantity against partition window. The distribution of discharge current against ac phase window $I_\varphi(i)$ and the distribution of discharge power against PD magnitude window $P_q(i)$ are examples of distribution function. Here i is the phase or pulse-height window index respectively. (Distribution function usually refers to the propagation of PD characteristics in half cycle for PRPD and PHPD pattern analysis, due to PD behaves differently in positive and negative half cycles).

Distribution Category: A group of distribution functions with the same variable as partition window.

Feature Quantity: The statistical parameters calculated from one or more distribution functions.

1.3.2   Basic and Derived Discharge Quantity

As PD distribution patterns contain information regarding discharge process, effective diagnosis of the insulation condition depends on the quality of extracted PD fingerprints representing the characteristics of discharge physical mechanisms. Discharge fingerprints not only can assist to identify different types of PD source but also help to predict the insulation condition of equipment under test. A number of analyzing techniques have been used so far to calculate PD fingerprints and are briefly summarized herewith. Basic and derived discharge quantities are the quantities measured from each discharge:

(1) Apparent discharge magnitude q_λ (C)

(2) Discharge energy E_λ (J)

(3) Power frequency phase position φ_λ (degree)

(4) Instantaneous value of applied voltage V_λ (V)

As PD phenomena are inherently complex stochastic processes as described earlier in this chapter, the above basic quantities exhibit significant statistical variability. The assessment of the insulation condition can not be based solely on the effect of any information of individual PD.

1.3.3   Integrated Discharge Quantity

The integrated quantities are quantities being computed from the basic quantities [24]. They are used to characterize the general trend of the discharge activity over a given time period as shown in figure 1.4.
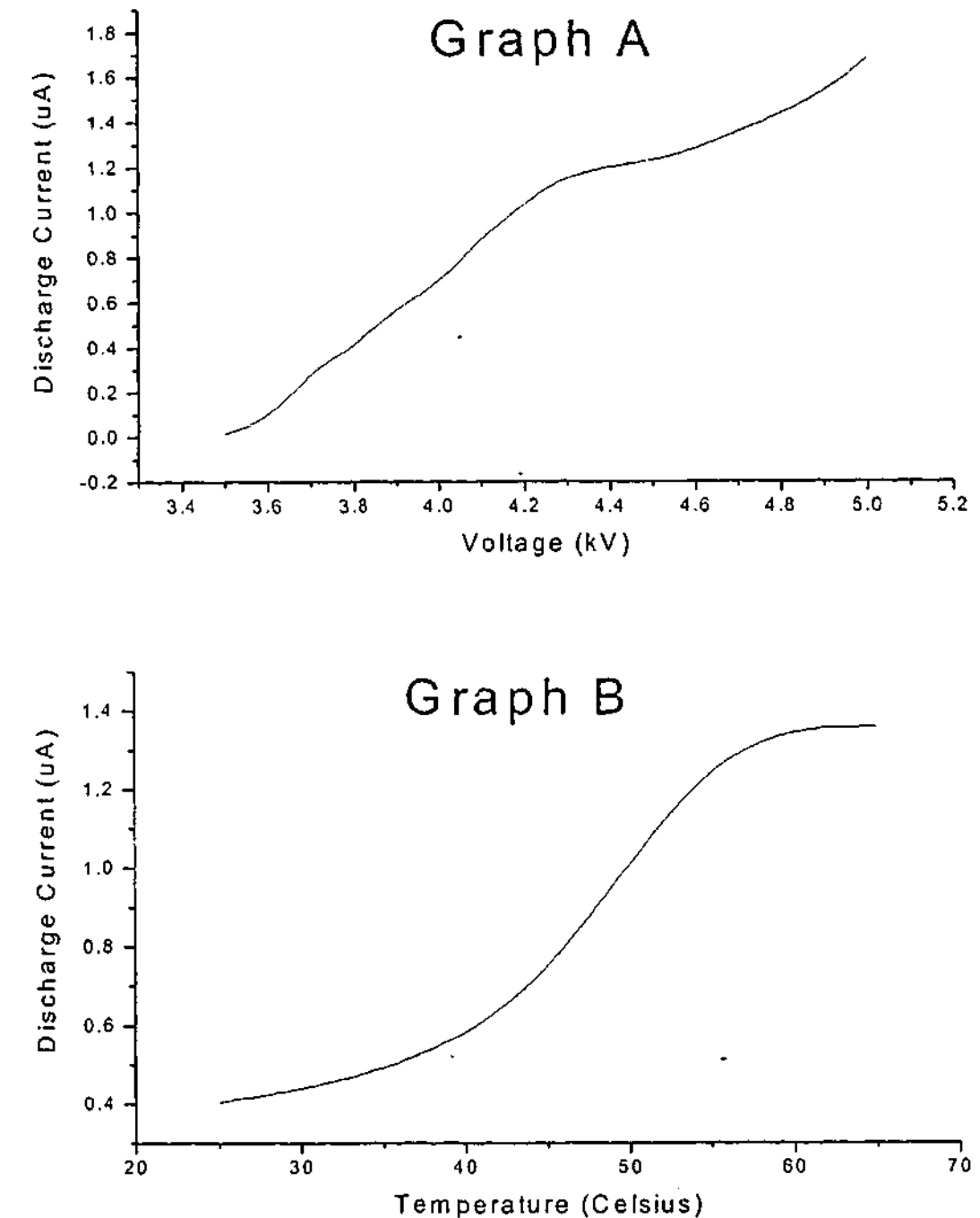
Fig. 1.4 Air corona measured from a point-to-plane arrangement with 10mm-gap space
Graph A: Discharge current varying with voltage
Graph B: Discharge current varying with temperature

The integrated quantities are recommended in the IEC Standard Publication 270 and illustrated as follows:

$$\text{PD repetition rate} = \frac{n}{T} (s^{-1}) \tag{1.1}$$

$$\text{Average PD magnitude} = \frac{1}{n} \sum_{\lambda=1}^{n} |q_\lambda| \ (C) \tag{1.2}$$

$$\text{Maximum PD magnitude} = \max(q_1, \cdots, q_n) \tag{1.3}$$

$$\text{Average PD current} = \frac{1}{T} \sum_{\lambda=1}^{n} |q_\lambda| \ (A) \tag{1.4}$$

$$\text{PD power loss} = \frac{1}{T} \sum_{\lambda=1}^{n} q_\lambda V_\lambda \ (W) \tag{1.5}$$

$$\text{PD magnitude quadratic rate} = \frac{1}{T} \sum_{\lambda=1}^{n} q_\lambda^2 \ (C^2/s) \tag{1.6}$$

where λ is an arbitrary PD event, n is the total number of PD events within the time interval T, q_λ and V_λ are the apparent charge magnitude and the instantaneous value of applied voltage respectively.

1.3.4 Distribution Function

Distribution functions are important in the application of PD source recognition as they contain information relating to the degradation mechanism of a defect. In addition to the patterns derived from voltage, PD magnitude difference and time interval of consecutive PD events, phase and PD pulse-height resolved distributions have been widely used for discharge pattern recognition. Based on these distributions, only a few distribution functions have been used to calculate statistical moments and the other statistical operators as discharge feature quantities. Distribution categories and relevant functions have been used for pattern recognition [27, 50].

(1) Distribution functions for phase resolved pattern
- PD repetition rate
- Average PD magnitude
- Maximum PD magnitude

(2) Distribution functions for pulse-height resolved pattern
- PD repetition rate
(3) Distribution functions for PD energy intensity resolved pattern
- PD repetition rate
(4) Patterns based on the voltage difference between consecutive events [52, 53]
- $\Delta V_n (\Delta V_{n-1})$
- PD repetition rate
(5) Patterns based on the time interval between consecutive events [54]
- $q_n (\Delta t_{n-1})$
- PD repetition rate

Distribution functions of category (1) – (4) have been employed in various applications of PD pattern recognition while (5) has been used in the extensive investigation of pulse-to-pulse memory effects and other discharge physically related properties.

1.3.5 Feature Quantity

Derived from distribution functions earlier discussed, a few feature quantities were proposed by Gulski and his coworkers to discriminate the distribution by selecting statistics as well as distribution shape profile in terms of three asymmetry parameters [55, 56]. The first is defined by

$$H_{qn}(\varphi) = \frac{Q_s^- / N^-}{Q_s^+ / N^+} \tag{1.7}$$

where Q_s^- and Q_s^+ are the sum of discharge amplitudes in the positive and negative half cycles; N^- and N^+ are the number of discharge events in the negative and positive half cycles respectively.

The second asymmetry quantity is defined as

$$\Phi = \frac{\varphi_{inc}^{-}}{\varphi_{inc}^{+}} \qquad (1.8)$$

where φ_{inc}^{-} and φ_{inc}^{+} are respectively the mean inception phase of occurrence on the negative and positive half cycles.

A third measure of asymmetrical behavior is given by the cross correlation factor defined as

$$CC = \frac{\sum(x_i \bullet y_i) - \sum x_i \bullet \sum y_i / n}{\sqrt{(\sum x_i^2 - (\sum x_i)^2 / n) \bullet (\sum y_i^2 - (\sum y_i)^2 / n)}} \qquad (1.9)$$

where x and y represent the two distribution variables and i is the window index of either positive or negative half cycle of a distribution. Correlation coefficient has the values ranging between –1 and +1. If one variable tends to increase as the other decreases, the correlation coefficient is negative. Conversely, if the two variables tend to increase or decrease together the correlation coefficient is positive.

In addition to the above three quantities, the phase-resolved distribution functions can be characterized according to their skewness and kurtosis that defined by

$$S_k = \sum_{\lambda=1}^{n} (x_\lambda - \mu)^3 p(x_\lambda)/\sigma^3 \qquad (1.10)$$

$$K_U = \sum_{\lambda=1}^{n} \frac{(x_\lambda - \mu)^4 p(x_\lambda)}{\sigma^4} - 3 \qquad (1.11)$$

where x_λ is a discrete value of a distribution function, μ is the mean value of the distribution, σ is the standard deviation, and $p(x_\lambda)$ is the probability for the occurrence of the value x_λ.

The skewness indicates the degree of asymmetry relative to a normal distribution. If $S_k < 0$, then distribution is skewed to the left, otherwise it is skewed to the right. The parameter K_U, on the other hand, provides an indicator for the sharpness of a distribution relative to a normal distribution. If $K_U > 0$, then the distribution is sharper than a normal distribution, and if $K_U < 0$, it is flatter than a normal distribution.

These defined feature quantities have been widely used in most cases to characterize phase resolved PD distributions. Efforts have been made to correlate these quantities with void or gap geometry and with charge induced aging resulting in physical or chemical change of the defect site. These quantities have been found varying significantly with changes in shapes of occlusions artificially made into dielectric materials placed between two parallel plate electrodes. The variation of these quantities is demonstrated in figure 1.5 to 1.8 where PD data were measured by author from a point-to-plane and a point-to-dielectric configuration respectively. The defined quantities are calculated and displayed in relevant graphs. Although the description of these quantities may be proved useful for pattern recognition in the sense that they can be correlated with conditions under which PDs are formed, they are not informative in terms of PD physical processes. From figure 1.5 to 1.8, x, y, c, Sk and Ku are defined in equation 1.7, 1.8, 1.10 and 1.11 respectively.

(a)
$x=9.21$
$y=0.86$
$c=0.487$
$Sk(+)=2.76$
$Sk(-)=0.75$
$Ku(+)=7.30$
$Ku(-)=-1.04$

(b)
$x=10.70$
$y=0.91$
$c=0.454$
$Sk(+)=3.00$
$Sk(-)=0.75$
$Ku(+)=8.78$
$Ku(-)=-1.13$

(c)
$x=8.10$
$y=0.80$
$c=0.493$
$Sk(+)=3.46$
$Sk(-)=0.54$
$Ku(+)=12.30$
$Ku(-)=-1.24$

(d)
$x=2.71$
$y=0.82$
$c=0.408$
$Sk(+)=3.58$
$Sk(-)=0.93$
$Ku(+)=13.61$
$Ku(-)=-0.79$
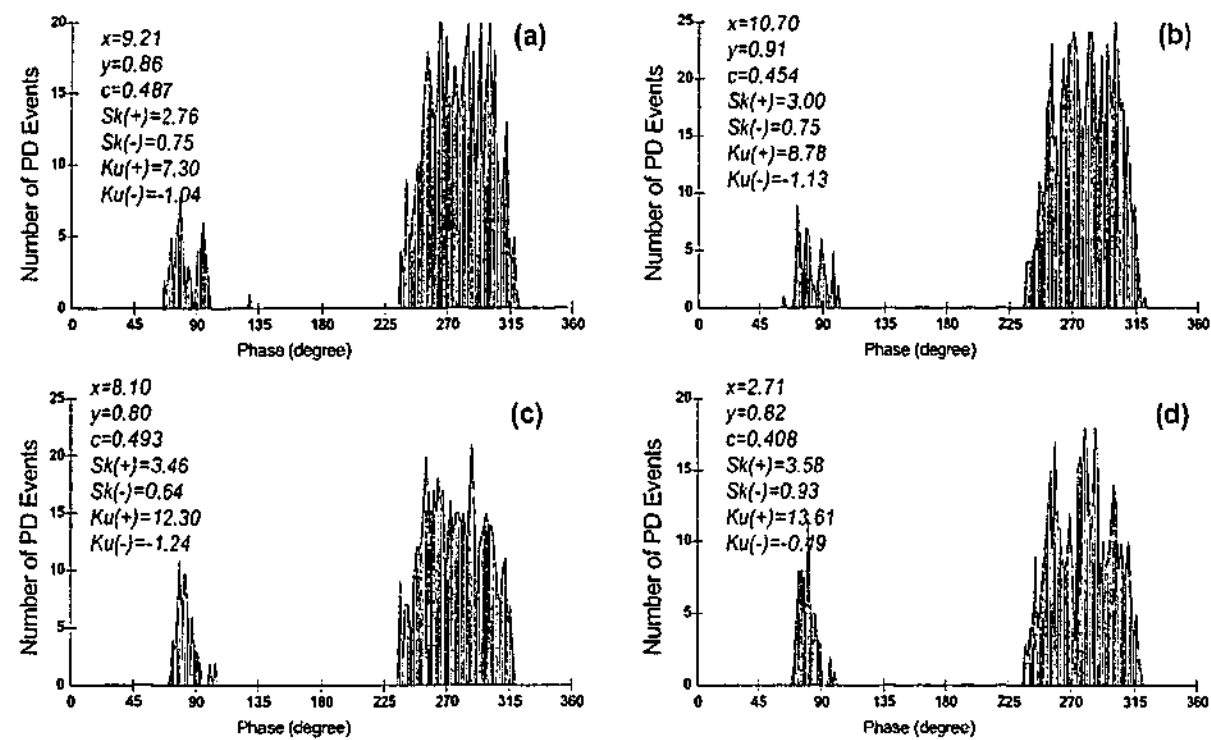
Fig. 1.5 Phase resolved PD occurrence distribution at 12mm gap of a point-to-plane dielectric. Patterns with the calculated quantities were measured after applying 5 kV voltage for
(a) 30 minutes; (b) 35 minutes; (c) 40 minutes; and (d) 45 minutes

(a)
$x=1.346$
$y=1.625$
$c=0.861$
$Sk(+)=1.250$
$Sk(-)=0.985$
$Ku(+)=0.067$
$Ku(-)=-0.635$

(b)
$x=1.608$
$y=1.833$
$c=0.747$
$Sk(+)=1.247$
$Sk(-)=0.927$
$Ku(+)=0.338$
$Ku(-)=-0.713$

(c)
$x=1.839$
$y=1.833$
$c=0.615$
$Sk(+)=1.422$
$Sk(-)=0.820$
$Ku(+)=0.788$
$Ku(-)=-0.848$

(d)
$x=1.571$
$y=1.333$
$c=0.744$
$Sk(+)=1.299$
$Sk(-)=0.952$
$Ku(+)=0.252$
$Ku(-)=-0.592$

Fig. 1.7 Phase resolved PD occurrence at 8mm gap of a point-to-dielectric dielectric. Patterns with calculated quantities were measured after applying 3 kV voltage for
(a) 16 minutes; (b) 18 minutes; (c) 20 minutes; and (d) 25 minutes

(a)
$x=0.36$
$y=0.86$
$c=0.525$
$Sk(+)=1.74$
$Sk(-)=-0.14$
$Ku(+)=1.19$
$Ku(-)=-2.00$

(b)
$x=0.38$
$y=0.91$
$c=0.517$
$Sk(+)=1.79$
$Sk(-)=-0.14$
$Ku(+)=1.49$
$Ku(-)=-1.99$

(c)
$x=0.46$
$y=0.80$
$c=0.460$
$Sk(+)=2.12$
$Sk(-)=-0.18$
$Ku(+)=2.74$
$Ku(-)=-1.99$

(d)
$x=0.48$
$y=0.82$
$c=0.426$
$Sk(+)=2.25$
$Sk(-)=-0.14$
$Ku(+)=3.36$
$Ku(-)=-1.99$

Fig. 1.6 Phase resolved average PD distribution at 12mm gap of a point-to-plane dielectric. Patterns with the calculated quantities are measured after applying 5 kV voltage for
(a) 30 minutes; (b) 35 minutes; (c) 40 minutes; and (d) 45 minutes

$x=1.346$
$y=1.625$
$c=0.861$
$Sk(+)=1.250$
$Sk(-)=0.985$
$Ku(+)=0.067$
$Ku(-)=-0.635$

$x=1.346$
$y=1.625$
$c=0.861$
$Sk(+)=1.250$
$Sk(-)=0.985$
$Ku(+)=0.067$
$Ku(-)=-0.635$

$x=1.346$
$y=1.625$
$c=0.861$
$Sk(+)=1.250$
$Sk(-)=0.985$
$Ku(+)=0.067$
$Ku(-)=-0.635$

$x=1.346$
$y=1.625$
$c=0.861$
$Sk(+)=1.250$
$Sk(-)=0.985$
$Ku(+)=0.067$
$Ku(-)=-0.635$

Fig. 1.8 Phase resolved average PD distribution at 8mm gap of a point-to-dielectric dielectric. Patterns with relevant quantities were recorded and calculated after applying 3 kV for
(a) 16 minutes; (b) 18 minutes; (c) 20 minutes; and (d) 25 minutes

The above feature quantities were computed from only a few PD distribution functions to form PD fingerprints. Based on the fingerprints having very limited correlation with discharge mechanisms, a few data mining techniques, including conventional, neural network, and fuzzy based classifiers, have been well developed to recognize PD source of different type [57]. Because of their unpredictable relationship with discharge physical processes, these distribution shape descriptors are limited in the application of PD source recognition. However, there are other quantities used to measure discharge patterns such fractal features etc. Details of these quantities are referred to appendix D.

1.4 OBJECTIVES AND CONTRIBUTIONS OF THIS THESIS

In earlier sections of this chapter, the concept of PD is introduced along with its basic equivalent circuit. Following that, up-to-date digital techniques relating to PD detection especially computer based PD detection have been briefly discussed. In the aim of explaining the objectives of this thesis, it is helpful to briefly outline a general procedure of PD source recognition as illustrated in figure 1.9. It is important to note that the entire process is controlled by a PC. The pattern recognition procedure consists of PD measurements that yield distribution profile, the computation of distribution functions, and feature quantities.

1.4.1 Objectives of the Project

It can be seen in figure 1.9 that it is hard to achieve the reliable recognition target if the distribution patterns employed in the profile do not cover enough information regarding PD physical activities. On the other hand, it is possible to achieve this goal or at least to improve the reliability if many more PD physical related feature quantities are extracted from a wider range of distribution functions. Therefore, three following objectives are set for this thesis:

(1) To establish a wide range of conditional PD distribution patterns or parameters as a solid base for current and future work on PD pattern recognition.

(2) To correlate distribution patterns with physical related PD characteristics. Hence, it is applicable to use measurable distributions and associated parameters to analyze PDs.

(3) To enhance discrimination and classification power by selecting physical related features to form quality PD fingerprints.


$$f_\varphi(i) = Np_1(\lambda \mid \varphi_\lambda \in \Delta\varphi_i)$$
$$f_q(i) = Np_1(\lambda \mid q_\lambda \in \Delta q_i)$$
$$f_T(i) = Np_1(\lambda \mid t_\lambda \in \Delta T_i)$$
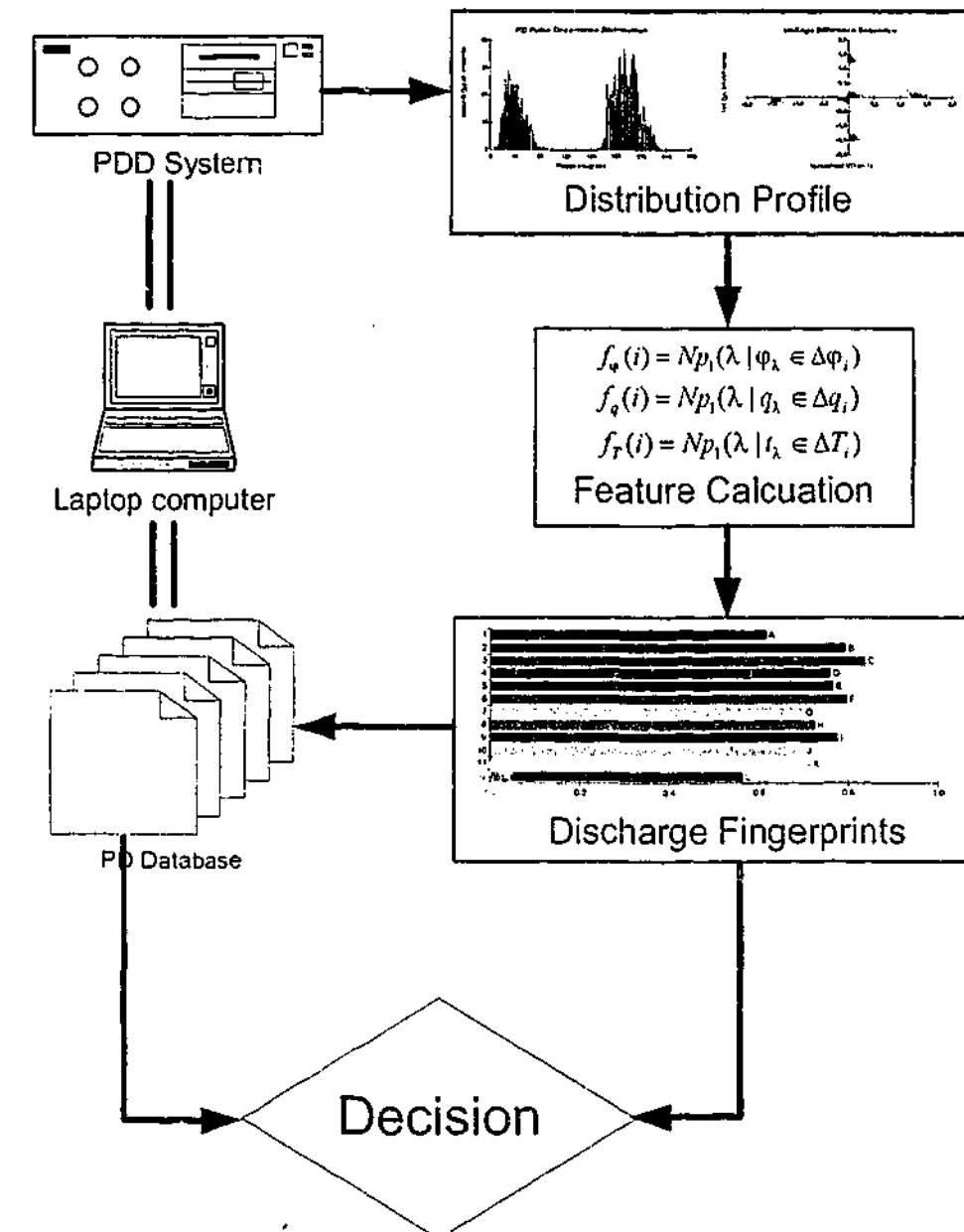
Fig. 1.9 A general PD source recognition procedure

1.4.2 Author's Main Contribution

The contribution of this project are illustrated as follows:

(1) To summarize and classify PD distribution patterns into four distribution categories including the use of some quantities defined in the IEC Publication 270 to establish distribution functions.

(2) To introduce new distribution functions and new feature quantities to analyze PD physical mechanisms as well as to classify PD source of different types.

(3) Reducing the size of PD fingerprints using a hybrid topology of neural network.

(4) To innovate a general method to find the most significant parameters regarding PD source classification using sensitivity analysis on a trained MLP neural network.

(5) To consolidate this research findings by implementing distribution functions and the extractable parameters in a PD measuring and evaluating software package.

1.5 THE MAIN CONTENTS OF THE THESIS

Chapter 1: It provides a brief background information about PD and the recently development trend on its detection and analysis. Based on this, the objectives of current project are outlined with the contributions made by author.

Chapter 2: It presents some important features about PDD system. It outlines the main features of this newly developed PD evaluation system from the system parameters setup to sophisticated analysis procedures.

Chapter 3: It studies ac phase resolved distributions and their statistics as illustrated in figure 1.10. Among six distribution functions, three are new parameters and can be treated as extension of IEC Publication 270 defined quantities. Based on conditional distribution functions, descriptive statistics of distribution functions and each phase window are employed to analyze PD characteristics. Innovated shape descriptors and other useful quantities are discussed in this chapter.
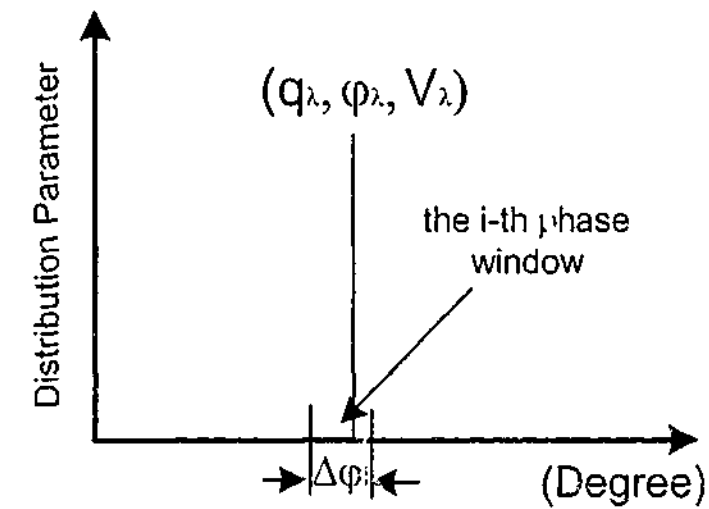
Fig. 1.10 Diagram of a discharge event $(q_\lambda, \varphi_\lambda, V_\lambda)$ in phase partition window

Chapter 4: It studies PD pulse-height restricted conditional distributions and the relevant statistics. In a similar fashion, a PD event can be classified according to its amplitude as illustrated in figure 1.11. Hence, important characteristics of discharges such as phase and voltage distributions can be analyzed based on their magnitude level. New conditional distribution functions are introduced in this chapter.
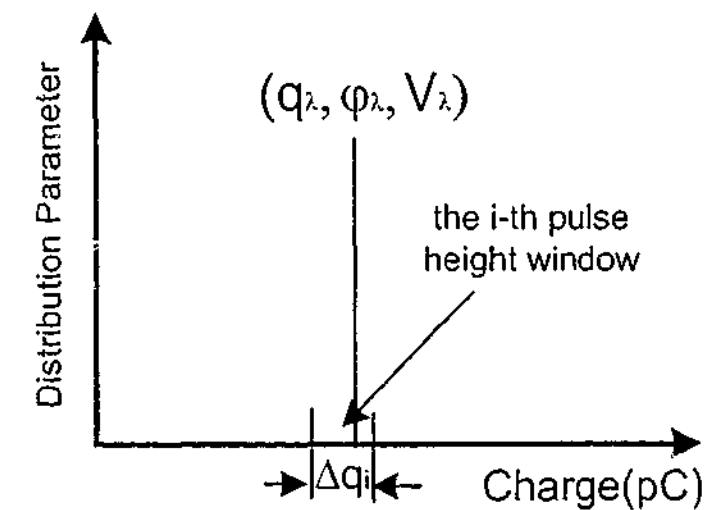
Fig. 1.11 Diagram of a discharge event $(q_\lambda, \varphi_\lambda, V_\lambda)$ in pulse-height partition window

Chapter 5: With cycle-resolved PD distributions, discharge statistical variation over a number of ac cycles is explored. Shown in figure 1.12, a PD event can be classified depending on which cycle it occurs. It is a new distribution category with six distribution functions combined with descriptive statistics to analyze discharge

phenomena. Apparently, distribution functions of this category provide useful information to the analysis of discharge pattern and they are also useful for the classification of PD source of different types.
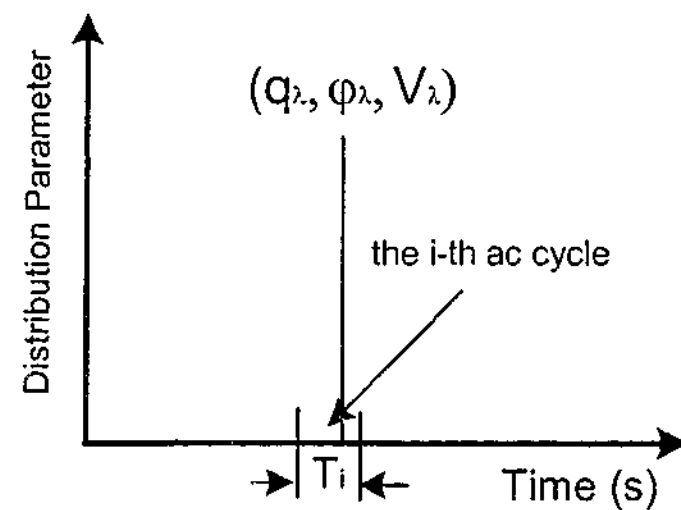
Fig. 1.12 Diagram of a discharge event $(q_\lambda, \varphi_\lambda, V_\lambda)$ in ac cycle window

Chapter 6: Difference between inter-pulse discharge properties is studied in chapter 6, as these differences are important indices that are closely related to the local stress which has significant impact on discharge initiation and growth. Statistics and other shape descriptors are extracted from those conditional distribution functions. The use of those distribution functions to study the memory effects under ac voltage is conducted as an example for discharge pattern analysis using inter-pulse distribution characteristics. As shown in figure 1.13, discharge can be analyzed by conditional (ΔV, Δq, and Δt) distribution functions.
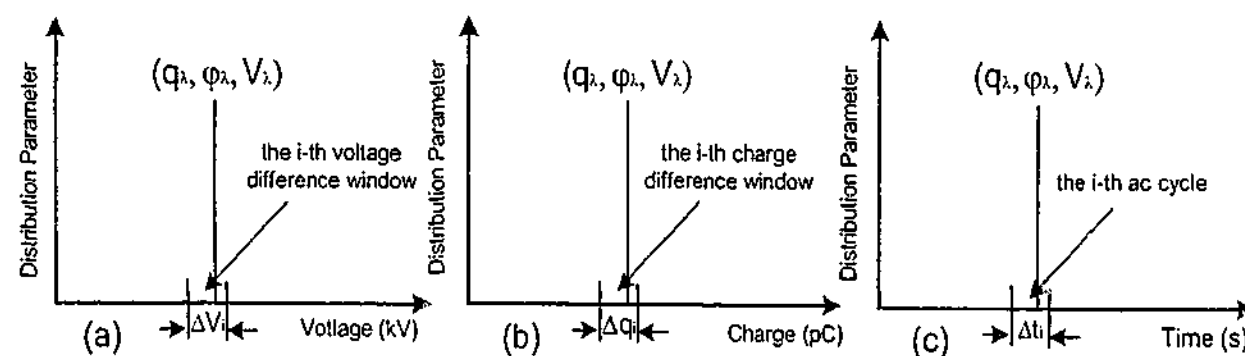
Fig. 1.13 Diagram of a PD event $(q_\lambda, \varphi_\lambda, V_\lambda)$ in consecutive partition window
(a) Voltage difference between consecutive PD events
(b) Discharge magnitude difference between consecutive PD events
(c) Time interval between consecutive PD events

Chapter 7: Extracted features from earlier chapters are put together to form PD fingerprints. Initially, PD source classification is performed with fingerprints of large size. Multilayer perceptron (MLP) neural network and its modified topologies are properly trained with these fingerprints. The results demonstrate that modified MLP has better performance. Meanwhile, compressing fingerprints of large size is another critical issue for efficient pattern recognition and speedy computation. A combined topology of a PCA connecting to a MLP has been placed for such a task with encouraging results. Finally, sensitive discharge parameters can be found by performing the sensitivity analysis on a trained MLP neural network. The results show that feature quantities extracted from phase resolved distribution functions and consecutive distribution functions contribute most of the quality or sensitive PD parameters. The findings are supported by laboratory experiment and simulation results.

Chapter 8: It contains the conclusions and recommendations for further work.

CHAPTER 2

Development of an Integrated PD Measuring and Evaluating System

Attempt has been made in this research project to characterize discharge mechanisms of different sources using four categories of distribution pattern. The distribution category is a group of distribution functions that have the same independent variable such as ac phase angle, PD magnitude, ac cycle index, and difference between PD properties of consecutive pulses. In order to effectively investigate discharge mechanisms using distribution patterns, an integrated PD measuring and evaluating system has been developed and implemented as a necessary tool for this task.

2.1 INTRODUCTION

The continuous impact of PD may reduce the remaining lifetime of high voltage (HV) equipment. The breakdown of insulation while in service may cause significant damage to power equipment and the power network to which it is connected. It has been recognized that this kind of failure is sometimes related to the occurrence and severity of PDs within insulation defects. The techniques of measuring and evaluating PDs can be used to discover insulation weakness before its leading to catastrophic failure. In order to ensure reliable operation of HV equipment, it is desirable to develop an integrated system for continuous monitoring the insulation degradation. PD diagnostic procedure normally should include display and calculation of PD intensity and activity through various patterns. It is then possible to analyze the relevant magnitude and other characteristics of the PDs.

Tremendous changes that have taken place since early 1940s in terms of the development of test equipment and testing techniques. However, the interpretation of results, as well as the enhancement of remedial actions are still in need of further development.

Computerized measuring systems have gained popularity since their introduction in the late 70's [13-15]. In early days, it was common to store and analyze the pulse height data on a main frame computer. With the dramatically improved performance of personal computer, it has become more expedient to incorporate the computer as an essential part of an overall PD measuring and analyzing system. Meanwhile, PD pattern analysis has become more important as distribution patterns may contain information about the PD origin. Recently, integrated PD distribution functions have been introduced and used in the identification of PD source of different types. Descriptive statistics are employed as compressed information to quantify distribution shape [59, 60].

The PD analyzer is an indispensable tool for insulation condition assessment due to the impact of PD influence over the lifetime. Meanwhile the recent technology advancement in electronics and computer makes the implementation of high performance yet low cost measuring instruments possible. High performance of the PD analyzer has been achieved at affordable cost and a number of successful techniques for the evaluation of PD phenomena have also been developed [61, 62].

The advancement in computer based measuring techniques has made it possible to store a large amount of PD data. Meanwhile sophisticated digital data acquisition systems not only enables fast computation of various discharge parameters during the measurement but also makes PD pattern analysis possible in real time. One major objective of using computer-based measuring system is to identify discharge patterns as indicators of the physical process involved in the insulating materials. There are many types of distribution pattern that can be used for PD source identification. If the degree of similarity and dissimilarity among various distribution patterns can be presented and included in a database, identification of defect type from observed PD patterns is possible [63, 64].

It is not the intention, neither is it possible within the scope of this thesis, to discuss all the functions designed and implemented in this new PD measuring and evaluating system. With this new system, discharge characteristics of phase resolved, pulse height

resolved, cycle resolved, and consecutive PD sequence distributions can be further analyzed with the help of advanced graphic tools. Fingerprints can also be extracted from various patterns for PD source recognition.

2.2 PDD SYSTEM DESCRIPTION

The PD test is set up according to figure 2.1. The hardware used in the system includes a coupling capacitor, a measuring impedance, a number of high pass and low pass filters, a discharge peak detector, a zero crossing detector, and a personal computer [44]. To acquire the PD basic quantities for computer analysis, some form of signal processing and digital conversion is necessary. The hardware of PDD consists of a peak-and-hold circuit and an A/D converter to digitize the PD pulse. A gating circuit is installed to start and reset the peak-and-hold circuit so that the relevant pulse is captured for digitization. According to figure 2.1, an additional circuit with a voltage divider is required to record the test voltage that is digitized with another A/D converter. To achieve real-time recording, the digitized PD basic quantities must be temporally stored into a buffer. After continuously acquiring PD data for a given period of time, PDD will send the data to a host PC through a parallel cable by request.
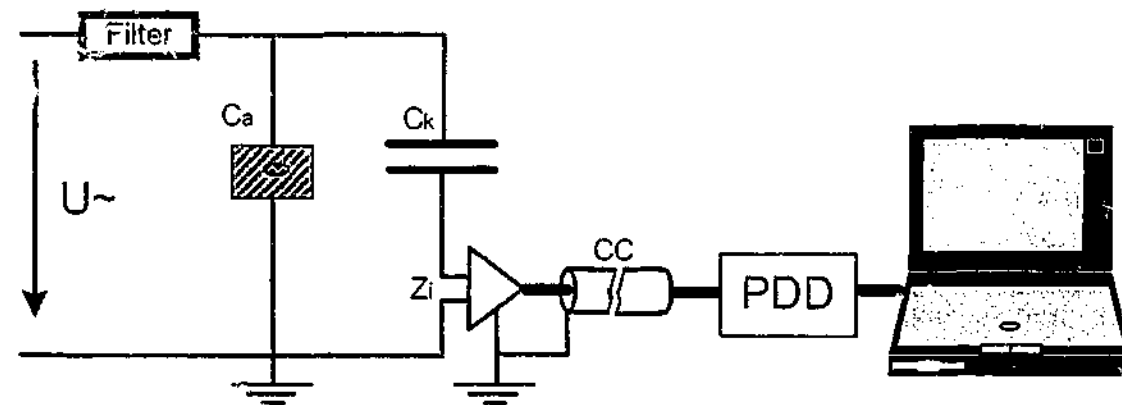
Fig. 2.1 PD measuring system
U~: High-voltage supply
CC$_a$: Connecting cable
C$_k$: Coupling capacitor
C$_a$: Test object.
Z$_i$: Input impedance
PDD: Partial discharge detector
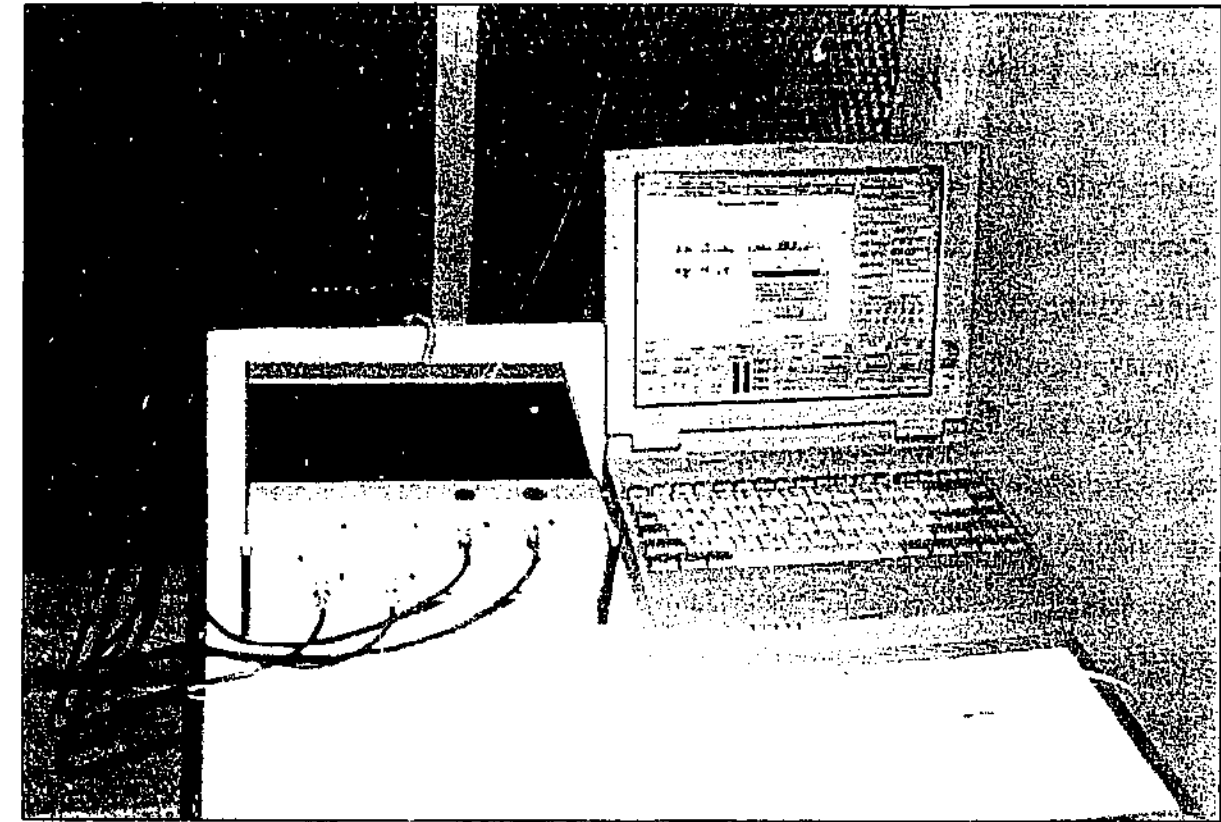
Fig. 2.2 A photo showing a PDD system installed on an in-service 80 MW hydro-generator

The information about the first peak of discharge pulse and its polarity must be correctly captured. Meanwhile, the tail of the waveform and its following oscillation may be discarded as the oscillation is caused by the characteristics of the measuring circuit. A typical PD pulse is shown in figure 2.3 where two different frequency passbands are used to process the discharge signal. The software, developed with MS Visual Studio technology is not only able to control the detector through a customized communication protocol but also to manage, transform, analyze and store PD data. This system is designed and implemented for the systematic detection and analysis of PD feature quantities through distribution patterns. PDD software consists of six major components, which are system, communication, data type, graphic control, feature calculation, and database.

The system component is used to organize system parameters for a particular test object, including which mode (manual or automatic), and the power frequency applied during the test. An operator can easily interact with such a component to change to any system parameter. The communication component has a set of communication interface routines based on hand shaking and acknowledgement. It controls the flow of all the

system commands as well as PD data including calibration information and hardware settings. The data type component holds all the details of PD data of all channels well as the setup of each gating. Zero crossing information is embedded in the PD data that can be either loaded from a previously saved file or directly measured through PDD. Graphic control component offers a wide range of display functions. The operator is able to change the style of a display by changing the relevant property in an appropriate property page. The operator can also change background and foreground color, text font and color et al. The feature calculation component is to calculate feature quantities of a selected distribution category. Some results can be calculated and displayed either in the statistical or advanced statistical panels. Other statistical results are only exported in a file with text delimited format. Database component is referred to the physically implemented database structure in a shared operational mode. It is an object-oriented database with build-in backup and restoring functions.
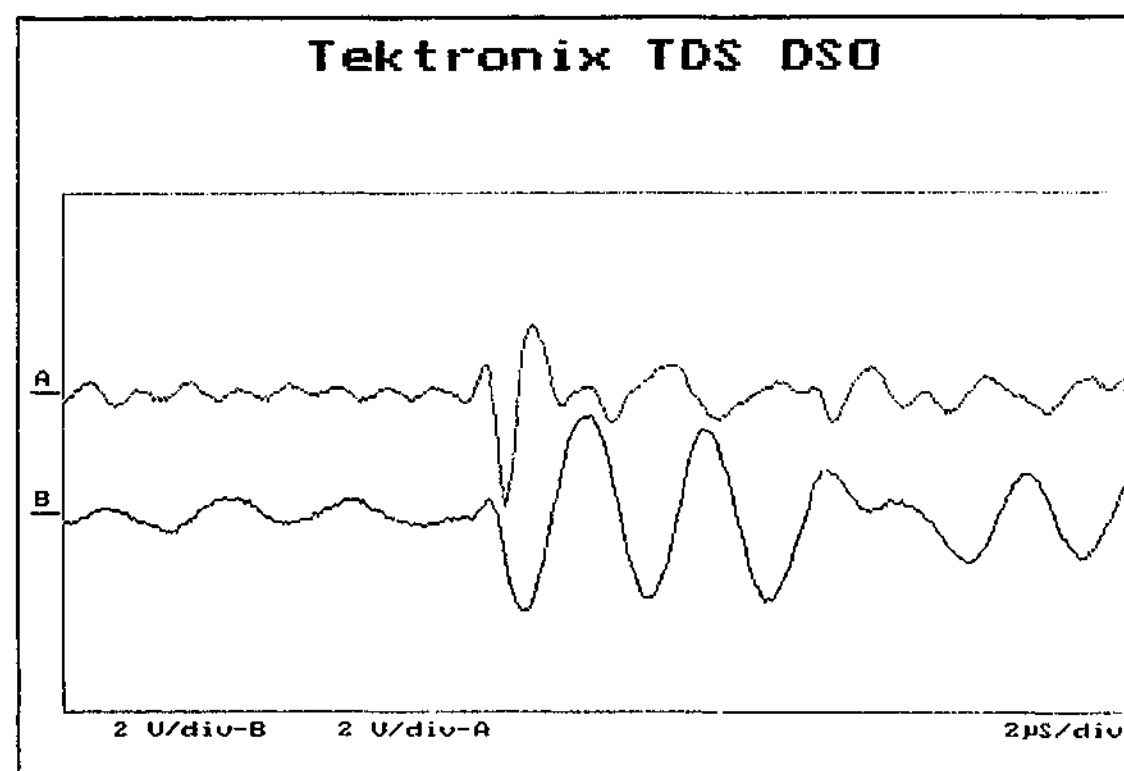

Fig. 2.3 Typical discharge waveshape measured from a 220 MW in-service turbine generator
Channel A: Frequency passband 1-5 MHz
Channel B: Frequency passband 100 kHz – 1 MHz

The partial discharge detector works as a real-time based instrumentation. The personal computer is used for controlling the hardware device, data processing, displaying, analyzing and storing. During test, PD pulses are measured according to the current

system setting. PD pattern analysis including phase resolved, pulse height resolved, frequency cycle resolved, and consecutive PD sequence analysis can be performed on-line or off-line.

2.3 PARTIAL DISCHARGE DETECTION

HV test circuits for PD measurements adopt two fundamental methods: the balanced detection method or the direct detection method. The latter one with a PDD system is adopted in this research project. During the measurement, PD pulses are detected at the terminal of measuring impedance and then fed into a signal conditioning circuit of suitable bandwidth and gain. The pulses are stretched at this point to match the instrumentation requirement as input signals. The peak value of the pulse and it's polarity are captured then digitized by the A/D convert to obtain a PD magnitude with 9 bit quantization. The overshoot of the following oscillation is a difficulty for PDD to capture the real first peak and the presence of this overshoot may result in measurement errors. Fortunately, this overshoot problem can be minimized by adjusting the appropriate value of R, L, and C of the measuring impedance and the frequency passband. The acquired PD data is temporary stored in a 256 kilobyte buffer until the completion of one set of data acquisition. The data placed in the buffer are then transferred to PC through a parallel port cable. The number of ac cycle per acquisition as well as the time interval between two adjacent acquisitions then can be easily setup as seen in figure 2.4 and 2.9. The number of discharge events can be recorded in one set of acquisition is only limited by the physical size of the buffer. After receiving PD data from the discharge detector, the software calculates and displays the summarized quantities defined in IEC Publication 270 in addition to displaying distribution patterns of selected category. The main interface of the PDD software package is illustrated in figure 2.4 with the results measured and calculated from an oil-impregnated pressboard discharge.

Apparently, the statistical results regarding to PD distribution patterns can be calculated in the host PC. Original PD data along with the hardware settings during the measurement can also be saved to the PC hard disk for later use. Analysis of PD

distribution patterns can be performed anytime when PD data are loaded into the environment either from the detector or from a saved file.
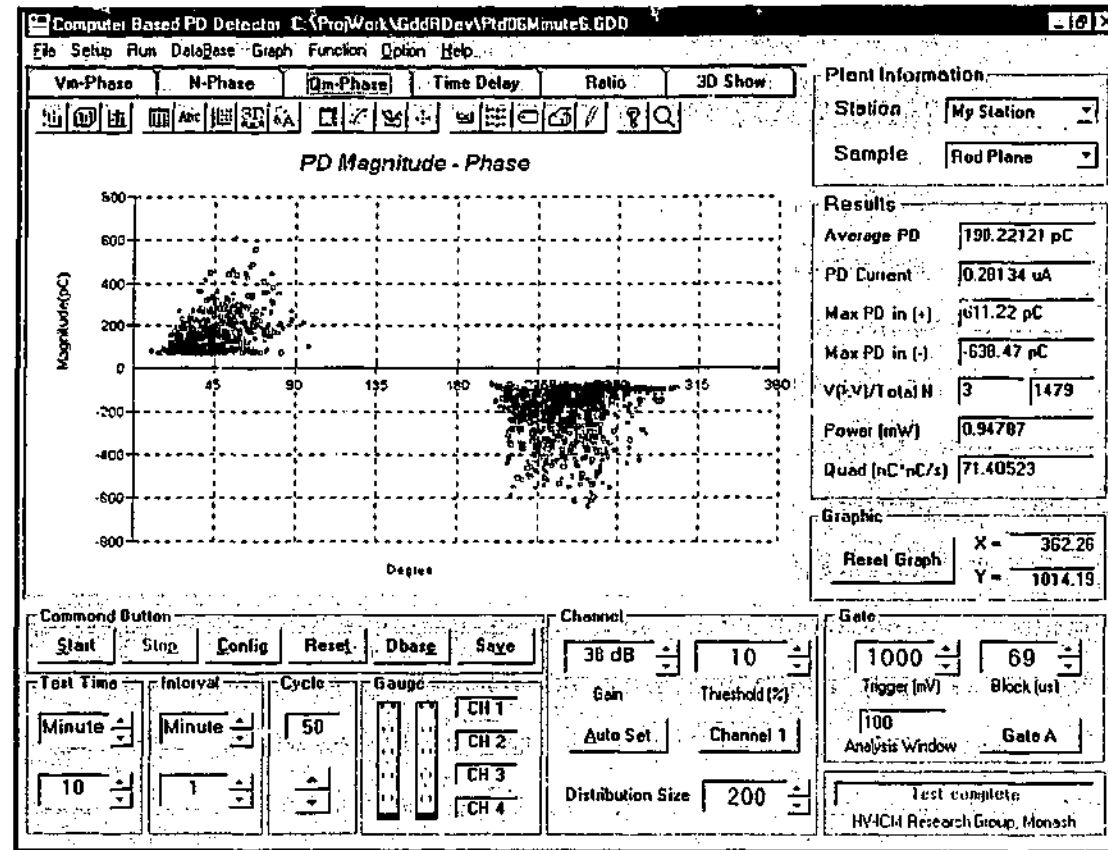
Fig. 2.4 The main interface of PDD host software

2.3.1 Discharge Physical Model

A number of methodologies have been developed to analyze patterns derived from discharge physical models. PD data obtained from the physical models illustrated in figure 2.5 are analyzed for PD source classification in this study. Model of (a), (b), and (c) are simple configurations representing the physical shape of possible defects around sharp point. Instead of producing very high field intensity around the sharp edge, model (d) and (g) produce smoothly distributed electric field. Model (e), (f), (h), and (i) are artificially made with a sharp or non-sharp nail inserted into half the thickness of the insulation layer. This group of models simulates the natural defects occurring in a generator stator bar.
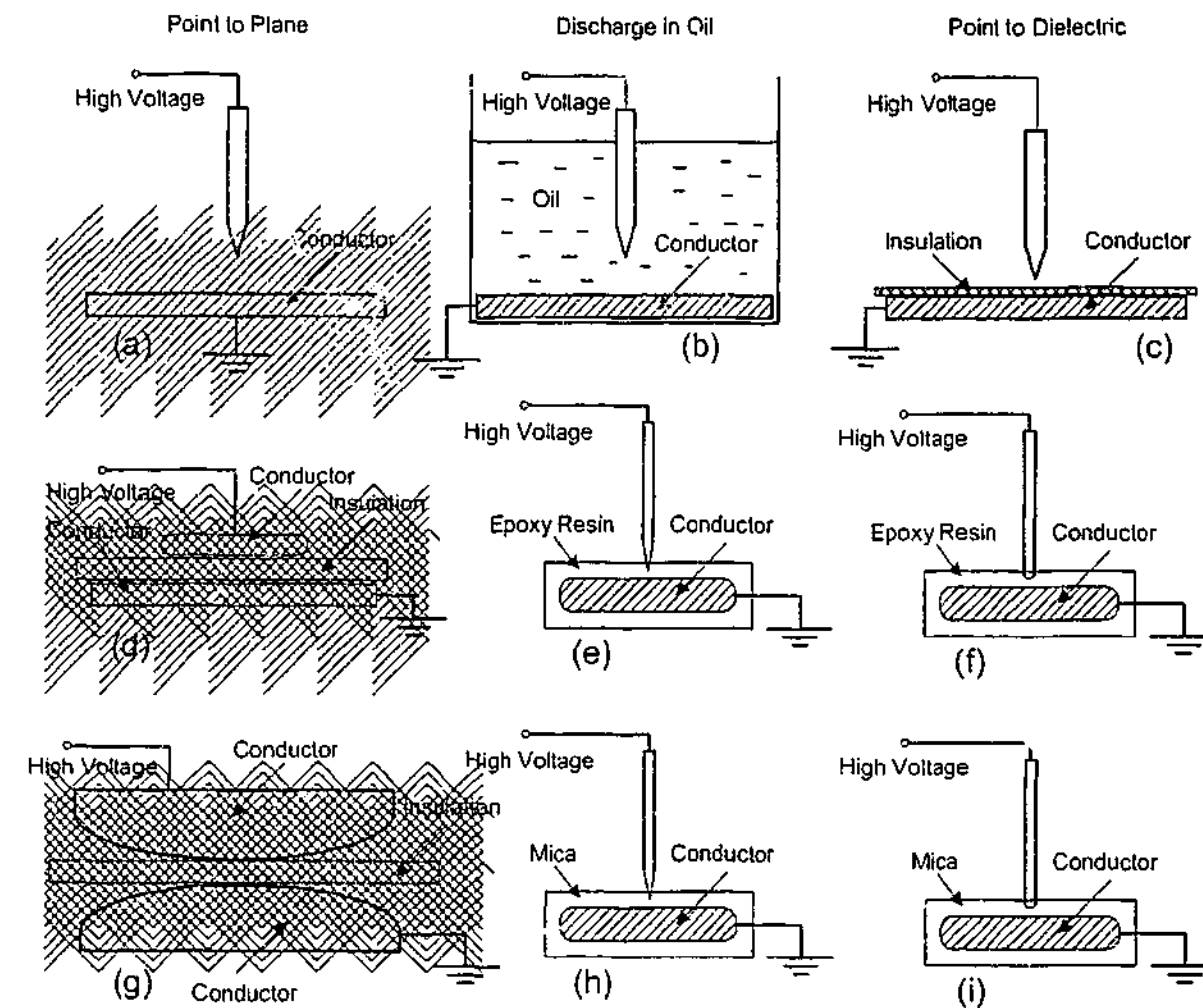
Fig. 2.5 Physical arrangements of discharge models

2.3.2 The Parallel Port Communication

In the PDD system, communication between the PD detector and the host PC is via a parallel port. The advantages of using a parallel port are (1) easy to use as every PC usually has at least one parallel port, (2) low cost. However, the parallel port must be configured to the extended capability port (ECP) with bi-directional transfer mode to communicate with the discharge detector. The parallel port configuration panel is shown in figure 2.6 in which the status of existing parallel port can be automatically detected and even tested.
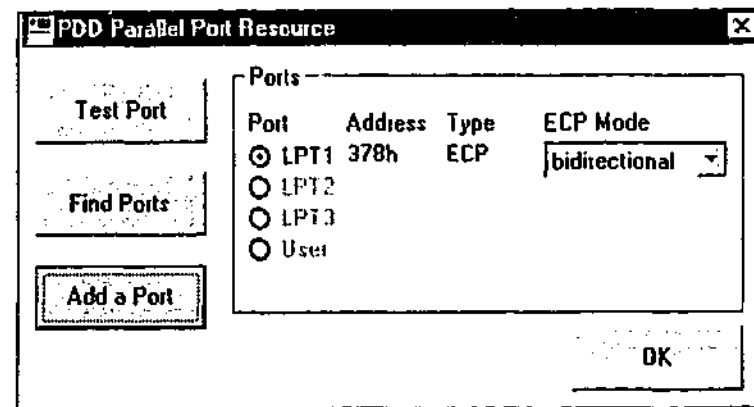
Fig. 2.6 The parallel port configuration panel

As the design of the PC evolved, several manufacturers have introduced improved versions of parallel port. While compatible with the origin design, new ports usually add new features, mainly in the improvement of operating speed. According to the measuring requirement, ECP is selected for the communication in PDD system. With ECP, PC can read or write a byte of data in one cycle of the ISA expansion bus. The transfer of data is bi-directional at ISA bus speed. In addition, ECP has a buffer to support direct memory access [65].

2.3.3 Hardware Setting Parameter

The host computer software controls the following hardware setting parameters:

(1) amplifier gain of each channel
(2) frequency pass bands of filters for each channel
(3) signal threshold level of each channel
(4) tracking window width
(5) noise triggering thresholds of each gate
(6) noise block-out time of each gate
(7) zero crossing phase shift
(8) power frequency
(9) operation status
(10) automatic setup of gains of input channels

The system parameter setup interface is shown in figure 2.7 in which various settings of each channel and gate can be easily set and reset.
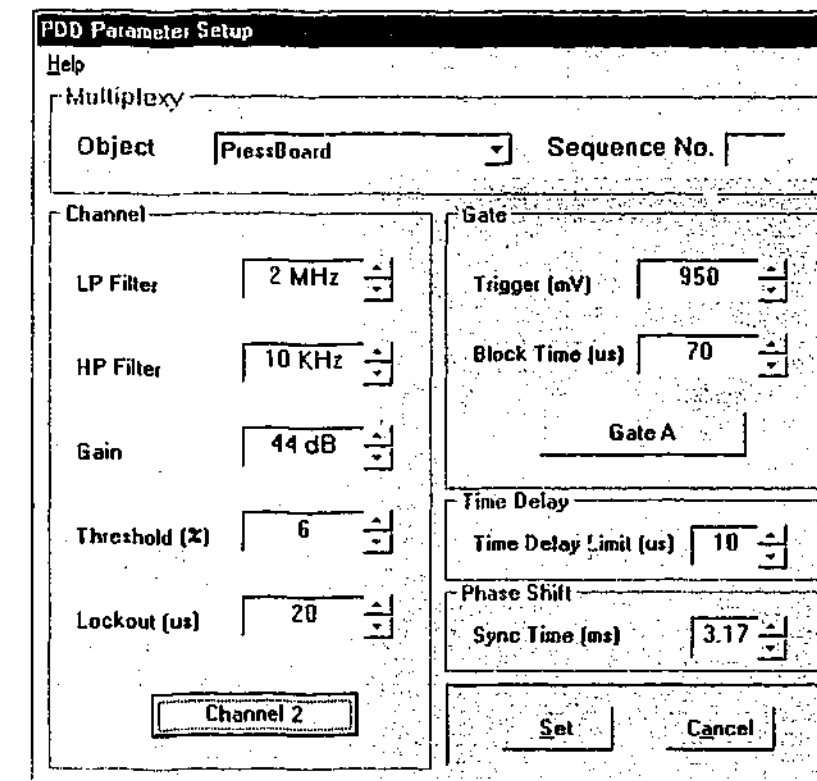
Fig. 2.7 The system parameter setup panel

2.3.4 Calibration and Operation

Having rise times of some nanoseconds to microseconds, PDs occurring within the internal insulation of HV apparatus are detected as small current pulses or voltages at the terminals of the test object. The scale factor of a PD measuring system depends strongly on the interaction between the PD coupling circuit and the test object that associated with HV circuit. Therefore, a calibration with complete measuring circuit, including the HV circuit, is indispensable before PD detection being conducted.

The conversion from PD current pulse to apparent charge magnitude is determined by the transfer characteristics of the analog measuring system. The transfer characteristics must be specified if test results are to be used for comparison and further evaluation of other PD data, such as PD power, energy etc.

The PD measuring circuit comprises a measuring impedance and a measuring instrument for wide-band or narrow-band detection. The current pulses produced by PDs are dependent upon parameters of the test circuit. The calibration can be done by using a build-in calibration module. The interface of this module is illustrated in figure 2.8.
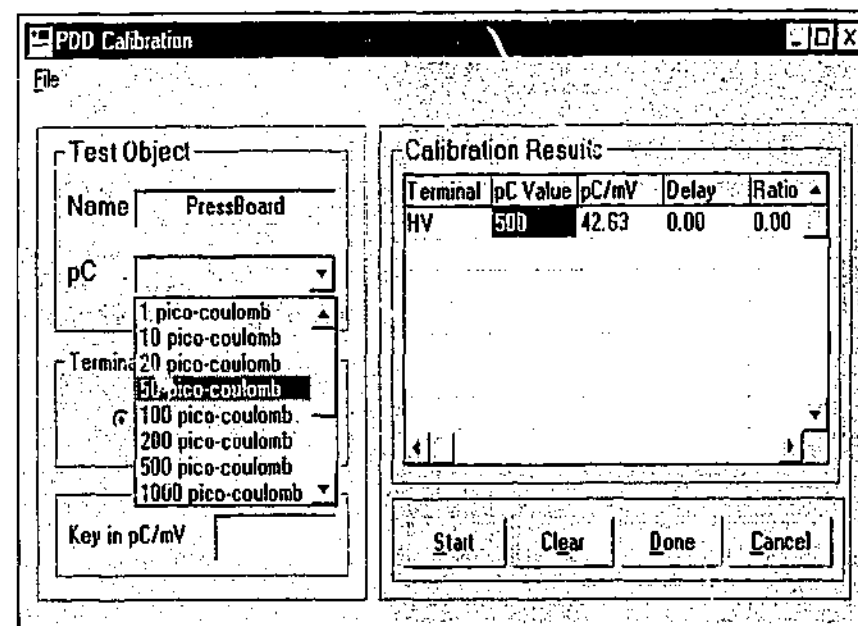
Fig. 2.8 The interface of calibration control module

The waveshape of the transient voltage delivered to the measuring instrument as a result of a discharge in C_a of figure 2.1 is determined by the characteristics of the test circuit and the amplifier. The transfer ratio is an imperial constant because the peak amplitude is proportional to the magnitude of the discharge can not generally be estimated with accuracy and must be determined experimentally. This may be done by injecting a small step pulse in series with a capacitor connected parallel to the test object. Before calibrating the system, PDD must know the pico-coulombs of injecting charge. Shown in figure 2.8, the value of injecting charge and its phase position can be selected from the drop-down combo box. Meanwhile the calibration terminal can also be selected according to which terminal calibrating pulses are injected. The calibration can be run as many times as required. The calibration results relating to the calibrated channel, along with the other settings of relevant channels, the results will be saved along with the acquired PD data.

When performing a PD test, there are two operating modes available in the system: manual and automatic. Manual mode allows an operator to run tests one at a time. Under the manual operation mode, operator needs to set cycle numbers from the main panel. The test time and the interval time buttons are inaccessible with manual operation. However under the automatic operation mode, the PDD system can be set to run a test over a period of time. Before running a test, operator needs to set test time and interval time as well as cycle numbers for each acquisition. The control functions are placed in the left-bottom side of the main panel as shown in figure 2.9.
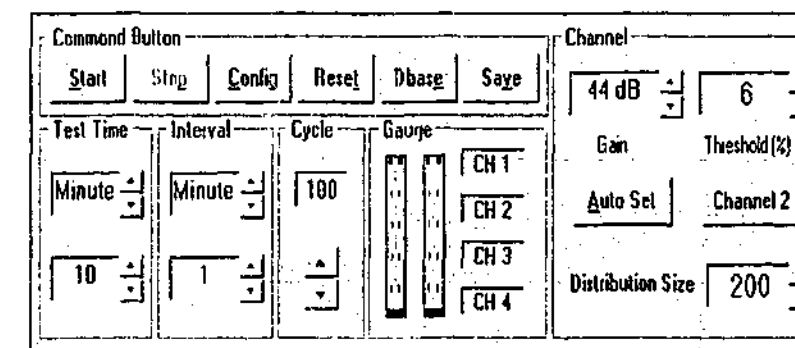
Fig. 2.9 The operating control functions placed on the main interface

2.4 DISTRIBUTION FUNCTION

Pulsating discharges are complex stochastic processes that can be investigated using the discharge distribution pattern analysis. It is understood that the important parameters to characterize PD are phase angle φ and PD amplitude q. PD distribution patterns are derived from these two basic parameters. However there are other parameters that are often used to characterize PD, such as the maximum and the average value of integrated distribution functions. It is enormously useful to reorganize PD data in many different indices for further analysis [50,51]. The description of distribution shapes can be interpreted using descriptive statistics and feature quantities.

2.4.1 Phase Resolved Distribution Function

The use of phase resolved partial discharge (PRPD) distribution functions for the recognition of PD source of different type in electrical insulation has been studied for many years. Recent research has shown that discharges can exhibit complex stochastic behavior correlating with PRPD distribution [60]. As an example, discharge power loss

can be drawn against the ac phase window, which is shown in figure 2.10.
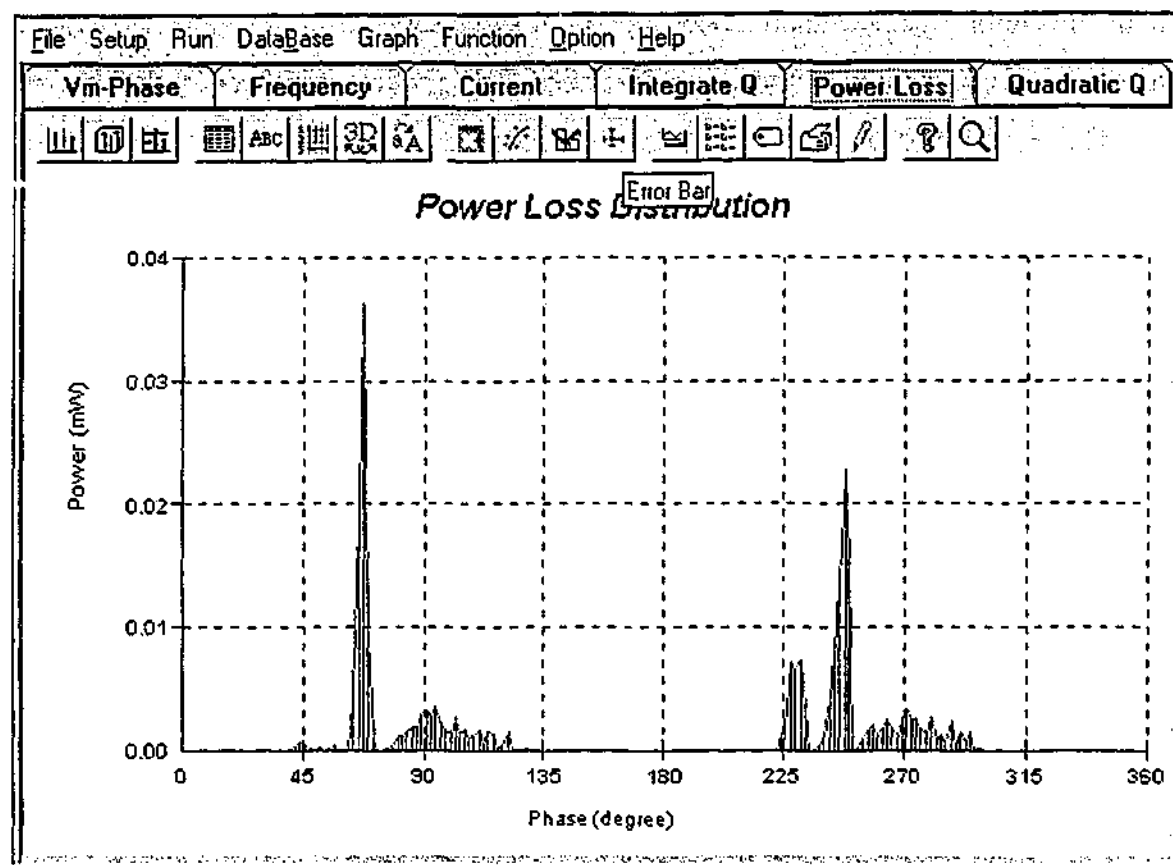
Fig. 2.10 The phase resolved power distribution function measured from a pressboard discharge

In addition to the distribution of power loss, there are other PRPD distribution functions that can be plotted and analyzed in PDD system, such as average and maximum discharge magnitude, PD occurrence, discharge current, integrated charge, and PD quadratic rate.

2.4.2 Pulse-height Resolved Distribution Function

Pulse height resolved PD (PHPD) distribution functions are useful in the assessment of insulation degradation [66]. With this approach, discharge occurrence, phase position, and applied voltage when PD occurs can be analyzed based on the level of discharge magnitude. In PHPD, distribution functions such as discharge current, and power loss can also be directly linked to the discharge amplitude level. These distribution functions are especially useful in aging testing. As an example, the distribution of power loss in PHPD category is shown in figure 2.11.
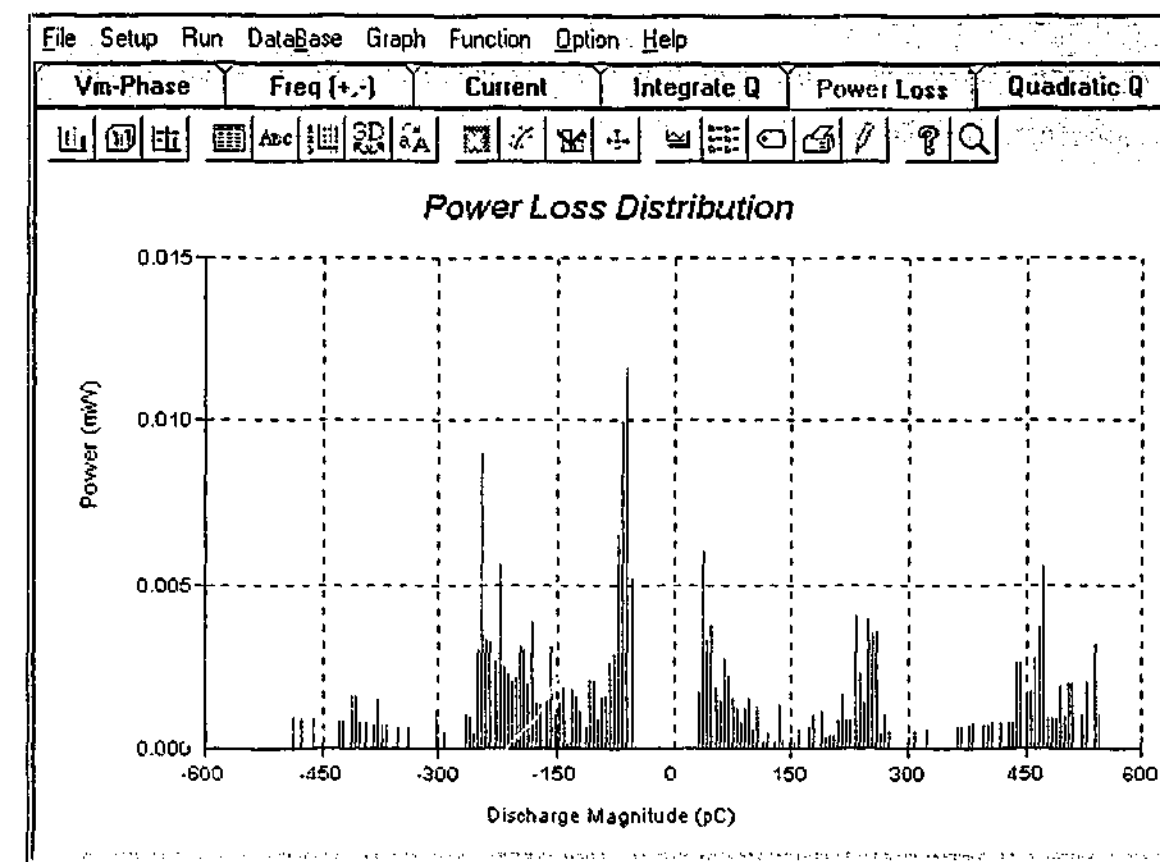
Fig. 2.11 The pulse height resolved power distribution measured from a pressboard discharge

In addition to the distribution of power loss, there are many other PHPD patterns that can be displayed and analyzed such as PD occurrence, discharge current, integrated charge, and PD quadratic rate distributions.

2.4.3 Cycle Resolved Distribution Function

Once established under periodical ac voltage, a discharge can be maintained with a voltage lower than the initial voltage required because of the existence of surface and/or space charges produced by previous PD events. Discharge disappears when the voltage dropped to the value below the minimum required voltage and appears again when voltage is above the minimum voltage. The observable discharge phenomenon such as occurrence, magnitude, and power loss may vary according to the voltage applied. Hence, it is vital to investigate discharge behavior and its statistics based on the index of ac voltage cycle. Instead of examining PD statistics, related quantities based on ac phase or pulse-height windows, cycle resolved PD (CRPD) distribution patterns, consider discharge statistics on cycle to cycle basis. The CRPD based discharge power loss

distribution is shown in figure 2.12. Apparently, useful information regarding discharge behavior based on consecutive per ac cycle can be found with CRPD pattern analysis. CRPD pattern analysis is a new application of discharge pattern analysis, which has been implemented in PDD system.
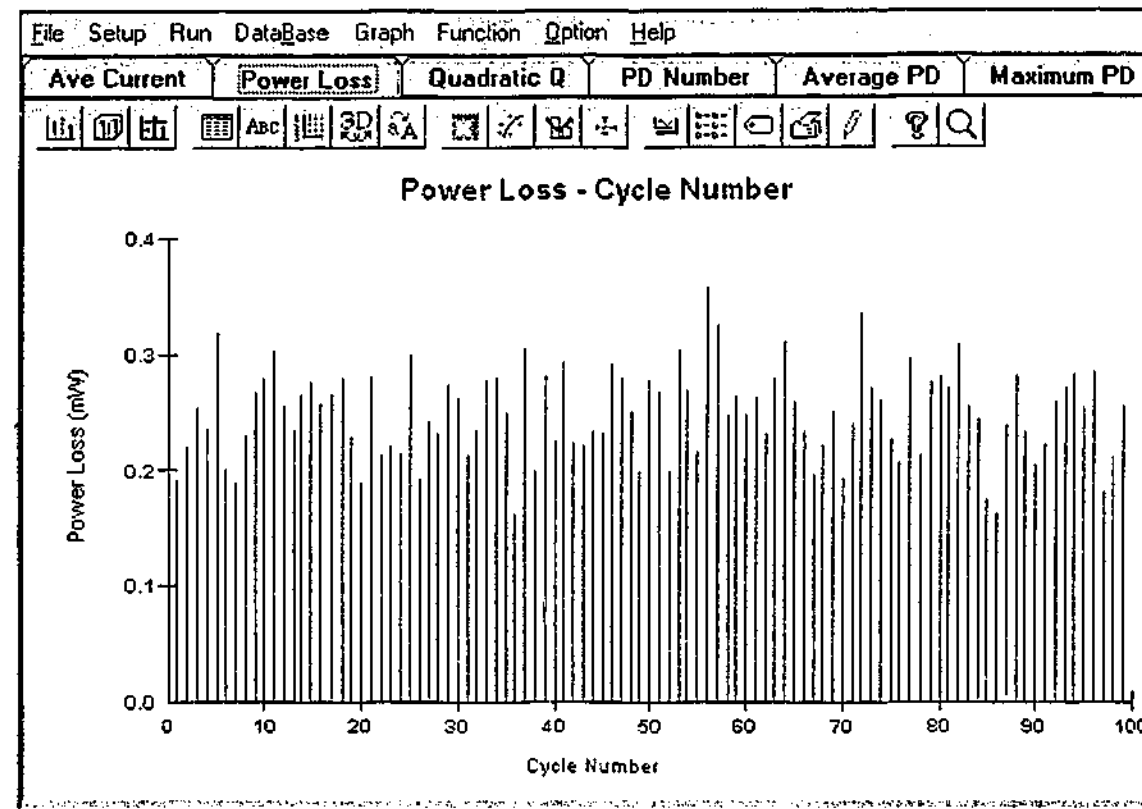

Fig. 2.12 The cycle resolved power distribution measured from the pressboard discharge

In addition, some properties of CRPD distributions can be attributed to the influence of pulse-to-pulse memory effects [59,60]. For instance, the ion space charge and metastable species between the electrodes produced by previous pulses has a significant impact on the initiation and development of subsequent pulses. Like PRPD and PHPD patterns, it is important to note that CRPD distribution properties are also associated with the test criteria and the setup of PD measuring system.

2.4.4 Consecutive PD Distribution Pattern

Due to the memory effect, discharge initiation and development is significantly affected by residuals, ions or metastable species produced by earlier PD pulses. The influence of memory effect is associated with the moving ion space charge cloud as well as the surface charge deposited on the insulation surface. The presence of these residuals has

significant impact not only on the rate of electron release but on the initiation of subsequent pulses as well. Voltage difference between consecutive pulses has been used in evaluating discharges at the voltage slightly above the inception level [52, 53]. This approach is based on the fact that the variation of the moving charge carriers and the external voltage are associated with the actual local electric field. The pattern of voltage difference distribution is shown in figure 2.13.
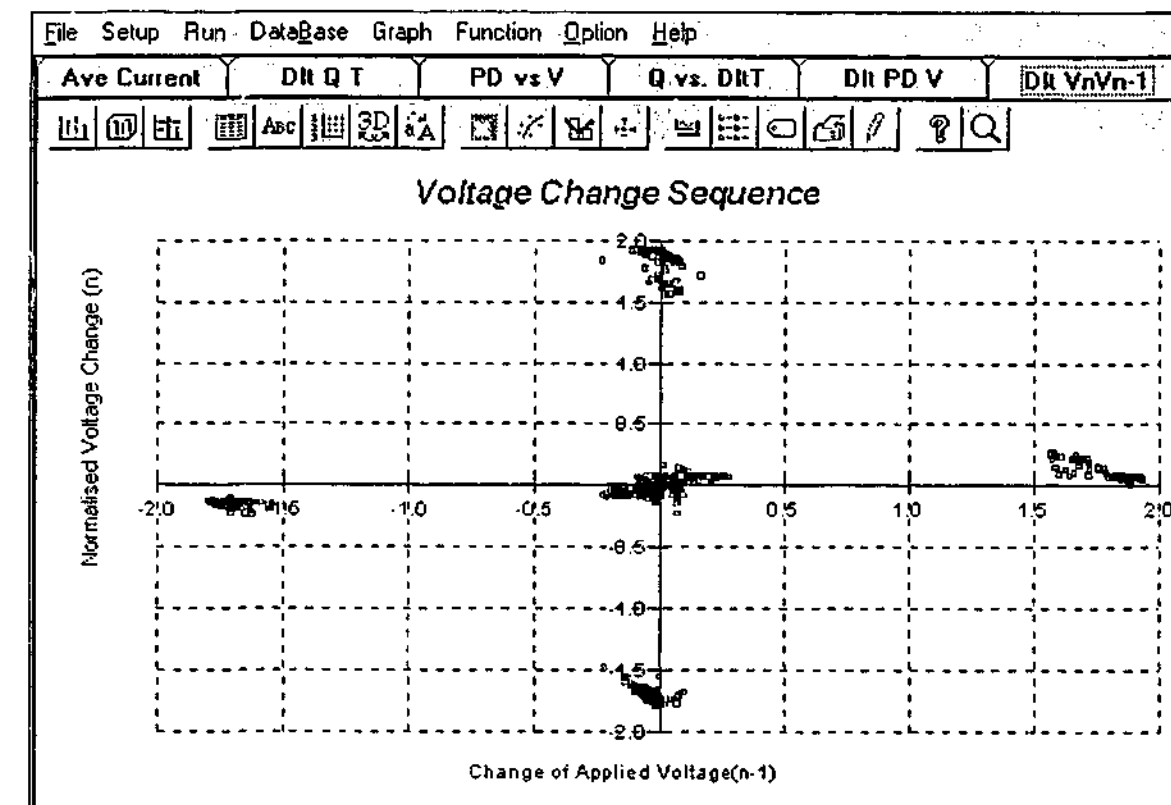
Fig. 2.13 Pattern of successive voltage difference measured from the pressboard discharge

Time interval and charge difference between consecutive PD pulses are important indices since memory effect plays a dominant role for discharge initiation and growth. Figure 2.14, 2.15 and 2.16 show mapping distributions of consecutive discharge events measured from a pressboard discharge.
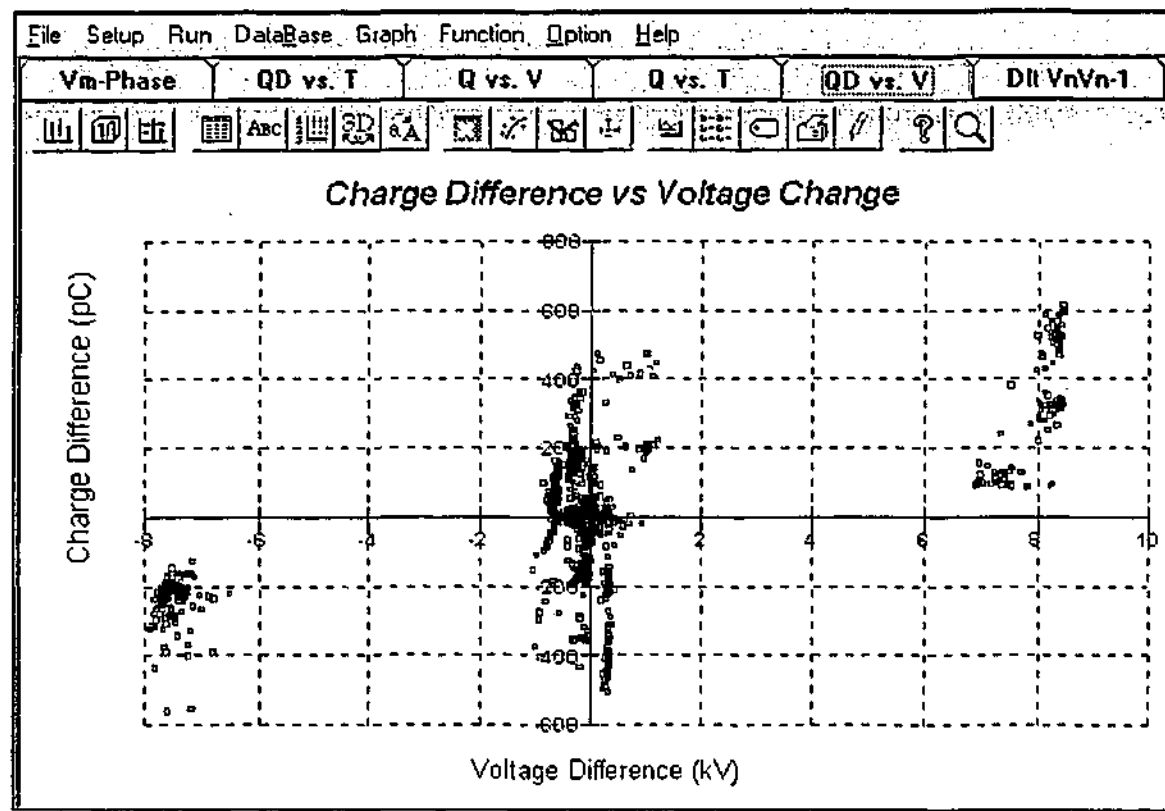
Fig. 2.14 Pattern of charge difference against voltage difference between consecutive PD events measured from the pressboard discharge
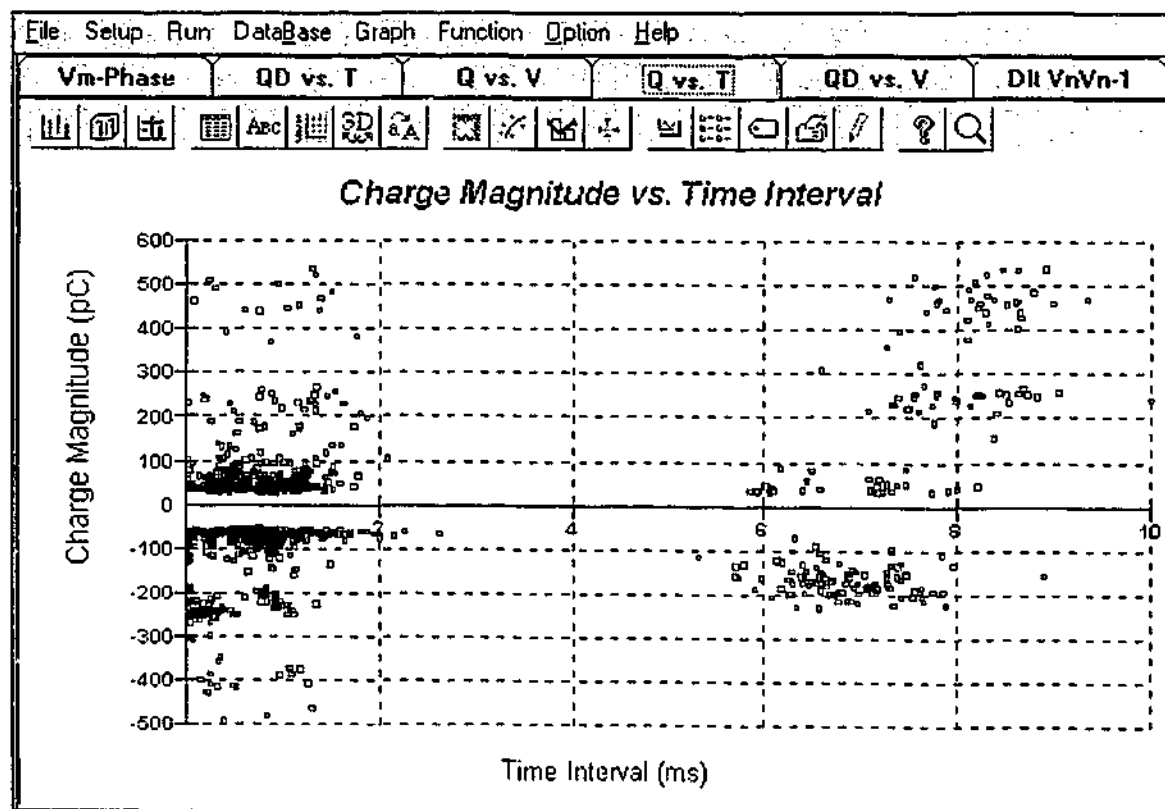
Fig. 2.15 Pattern of charge magnitude against time interval between consecutive PD events measured from the pressboard discharge
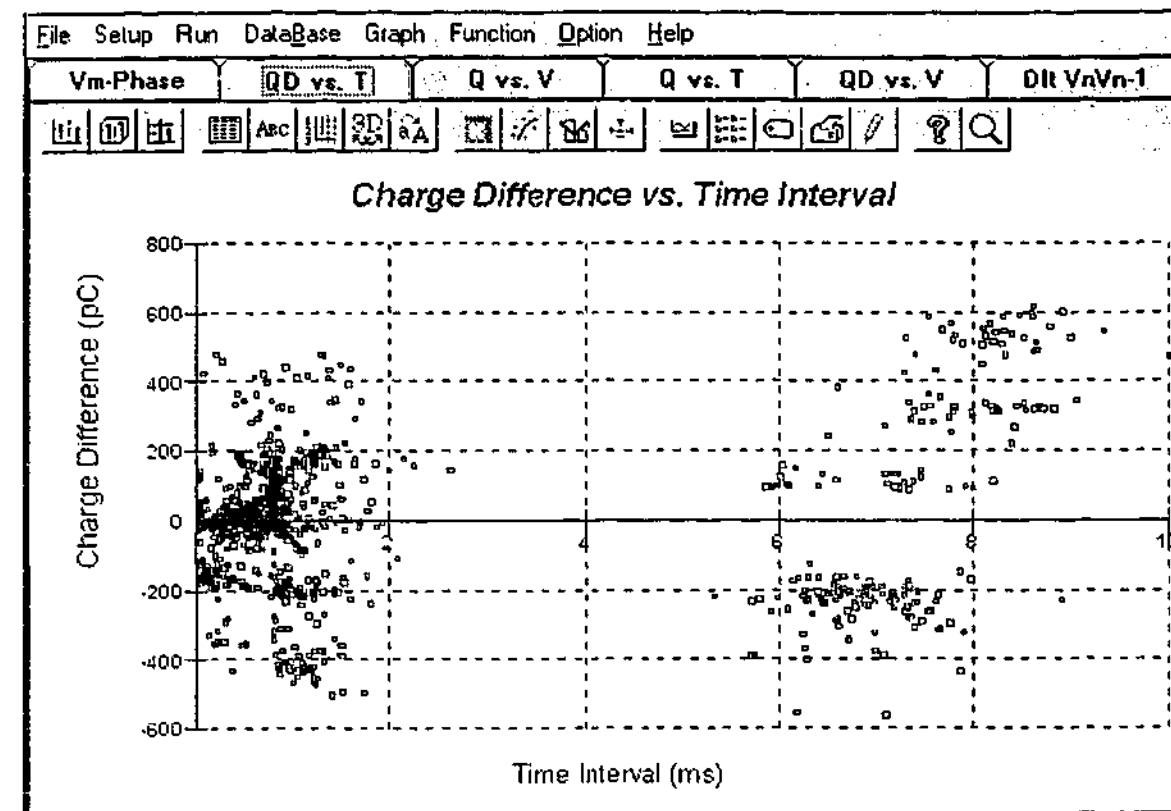
Fig. 2.16 Pattern of charge difference against time interval between consecutive PD events of measured from the pressboard discharge

2.4.5 φ-q Plane Based 3-Dimensional Distribution Pattern

In addition to above 2-dimentional mapping plots, 3-dimentional PD distribution patterns is another plotting feature implemented in PDD system. It was suggested by Satish et al 1995 that PD fingerprints can also be extracted directly from distribution of φ-q plane based discharge occurrence [58]. This approach starts directly from φ-q-n 3-dimensional distribution as shown in figure 2.17.

Besides the φ-q-n distribution pattern, PDD has other new distribution functions that can be plotted against the φ-q plane such as the integrated PD power as well as the integrated charge of different polarities et al. As an example the integrated PD power is plotted against φ-q plane shown in figure 2.18.

42

43
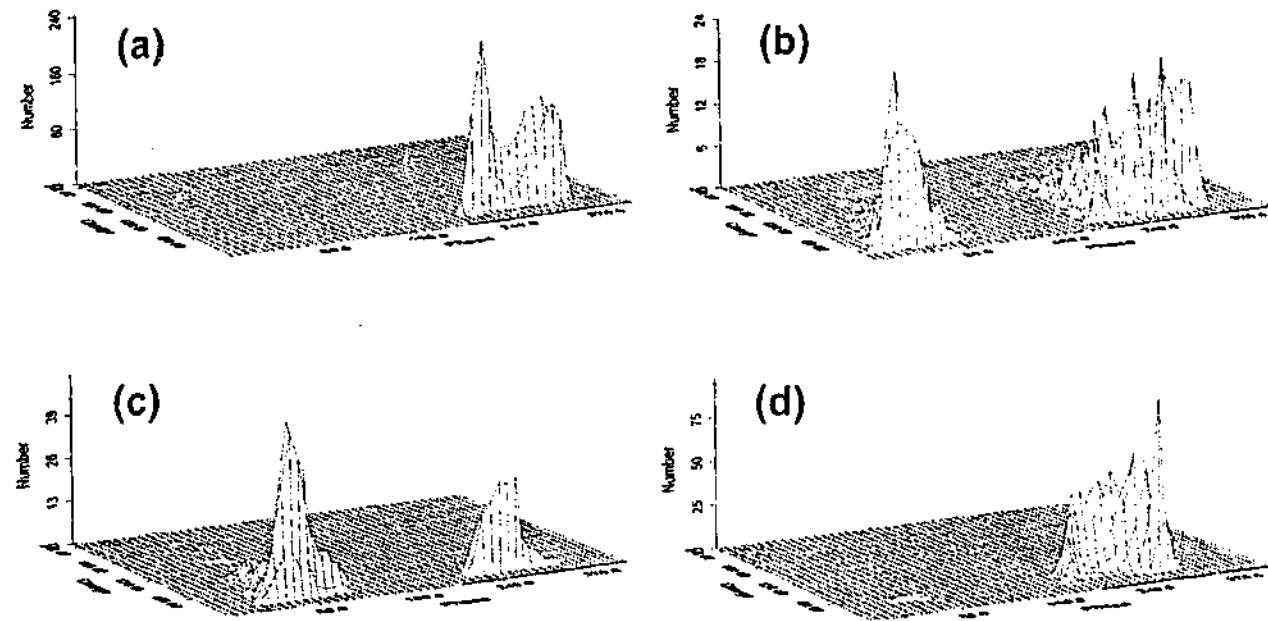
Fig. 2.17 Distribution of φ-q-occurrence measured from
(a) a point-to-plane arrangement
(b) a Point-to-dielectric arrangement
(c) a oil-impregnated pressboard sample
(d) an epoxy resin stator bar sample with an artificial defect inside
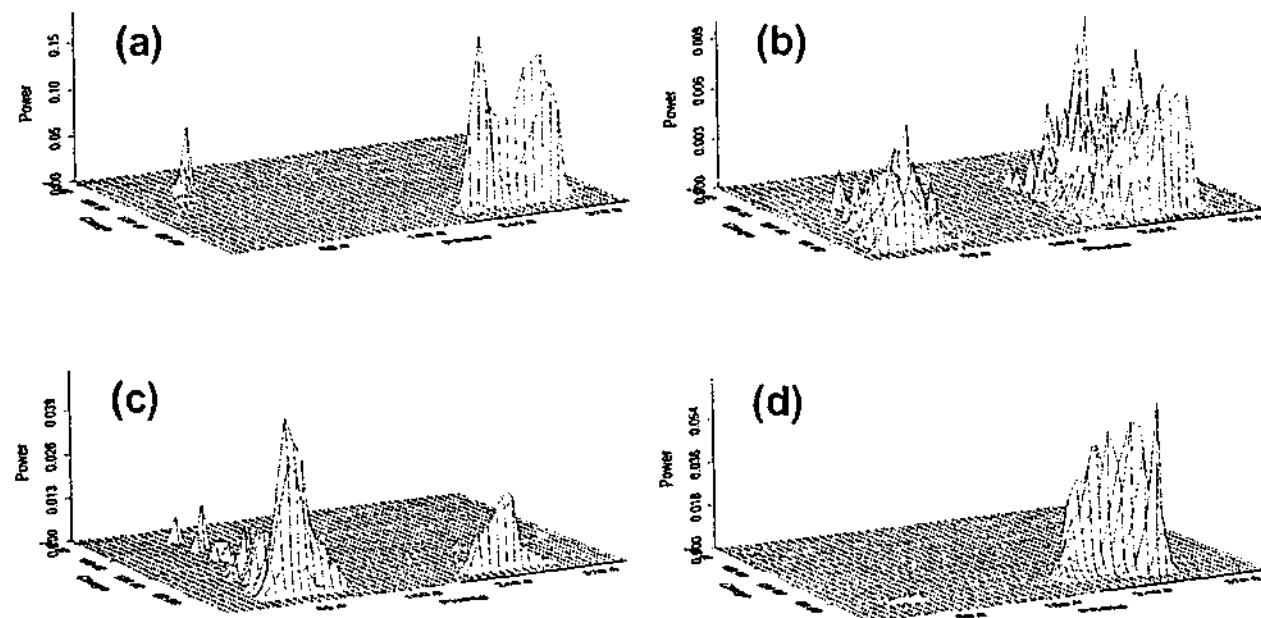
Fig. 2.18 Distribution of φ-q-power patterns measured from
(a) a point-to-plane arrangement
(b) a Point-to-dielectric arrangement
(c) a oil-impregnated pressboard sample
(d) an epoxy resin stator bar sample with an artificial defect inside

2.4.6 Distribution Pattern of ΔV-Δq-ΔT

Pulse sequence analysis becomes more and more important because many discharge physical properties are closely related to the stochastic properties between consecutive discharge pulses. Therefore, some interesting distribution functions such as occurrence, PD power, and quadratic value of PD magnitude etc. have been built in PDD system for further analysis of discharge patterns. The 3-dimentional pattern of voltage, charge and time difference between consecutive PD events of a sequence is shown in figure 2.19.
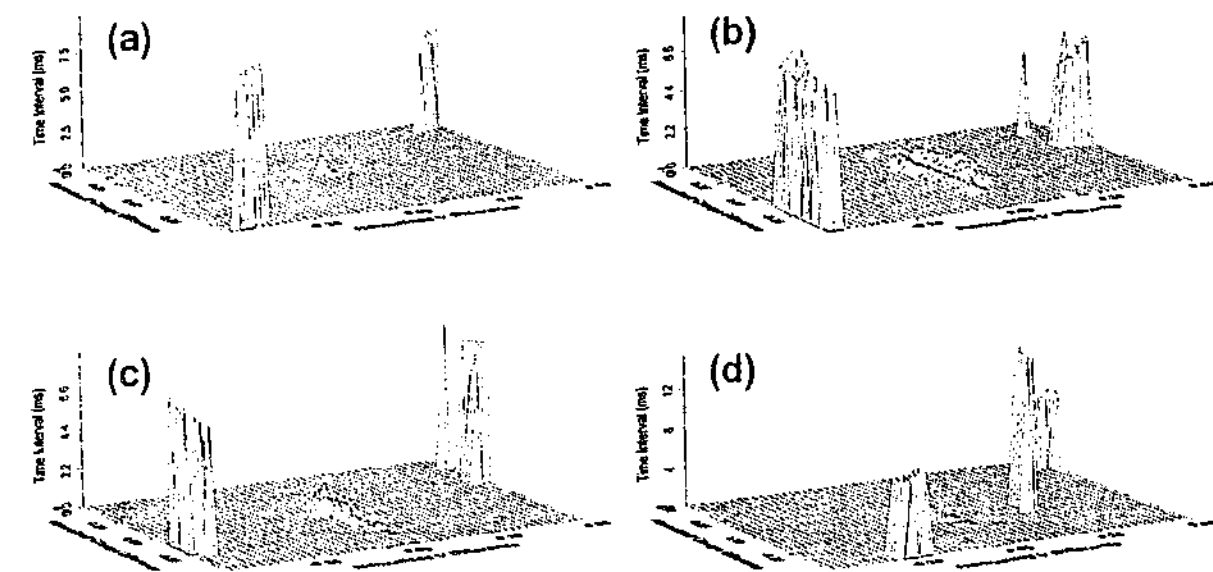
Fig. 2.19 Distributions of $\Delta\varphi$-Δq-ΔT between adjacent PD events measured from
(a) a point-to-plane arrangement
(b) a point-to-dielectric arrangement
(c) a oil-impregnated pressboard sample
(d) an epoxy resin stator bar sample with an artificial defect inside

2.5 QUANTIFICATION OF DISTRIBUTION FUNCTION

Because each defect has its own particular degradation mechanism and it is important to quantify the degree of correlation between discharge patterns [10]. Quantities such as descriptive statistics may play an important role in describing a particular distribution. Figure 2.20 shows some descriptive statistics calculated from phase and pulse-height resolved occurrence distribution functions.
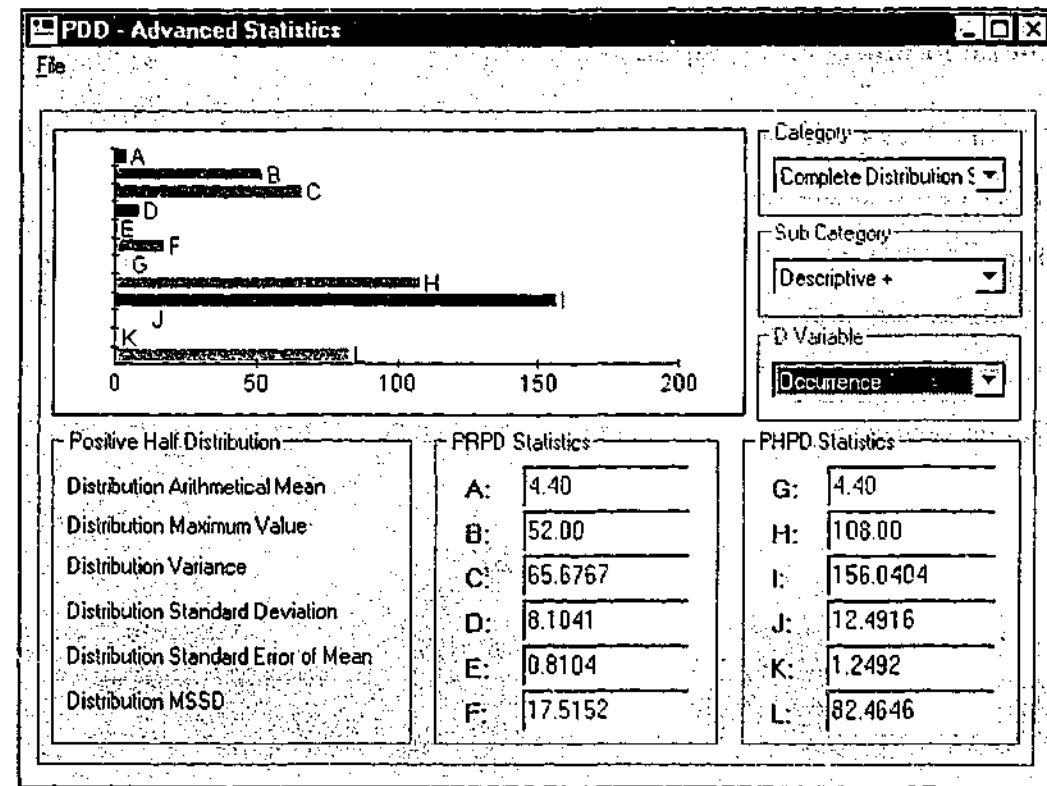
Fig. 2.20 Descriptive statistics of PD occurrence measured from the pressboard discharge

It is understandable that mechanisms of PD initiation in positive and negative half cycles will be different if the defect is not symmetrical in terms of its geometry and material composition. The asymmetries between PD behavior in the positive and negative half cycles can be quantified with the following four asymmetry parameters that can be calculated in PDD system.

The first parameter is defined as $R_\varphi \approx \dfrac{\Delta\varphi_+}{\Delta\varphi_-}$

where $\Delta\varphi_+$ and $\Delta\varphi_-$ are respectively the covering range in positive and negative discharge distributions.

The second parameter is defined by $R_{inc} = \dfrac{\varphi_{inc+}}{\varphi_{inc-}}$

where φ_{inc+} and φ_{inc-} are respectively the position of average inception for the positive and negative discharges.

The third parameter is defined by $R_M = \dfrac{\varphi_{M+}}{\varphi_{M-}}$

where φ_{M+} and φ_{M-} are the position of maximum distribution variable for the positive and negative discharges respectively.

The fourth parameter is defined by $R_h = \dfrac{h_{m+}}{h_{m-}}$

where h_{m+} and h_{m-} are the mean distribution variables for the positive and negative discharges respectively. The results are calculated in a module of PDD system shown in figure 2.21.
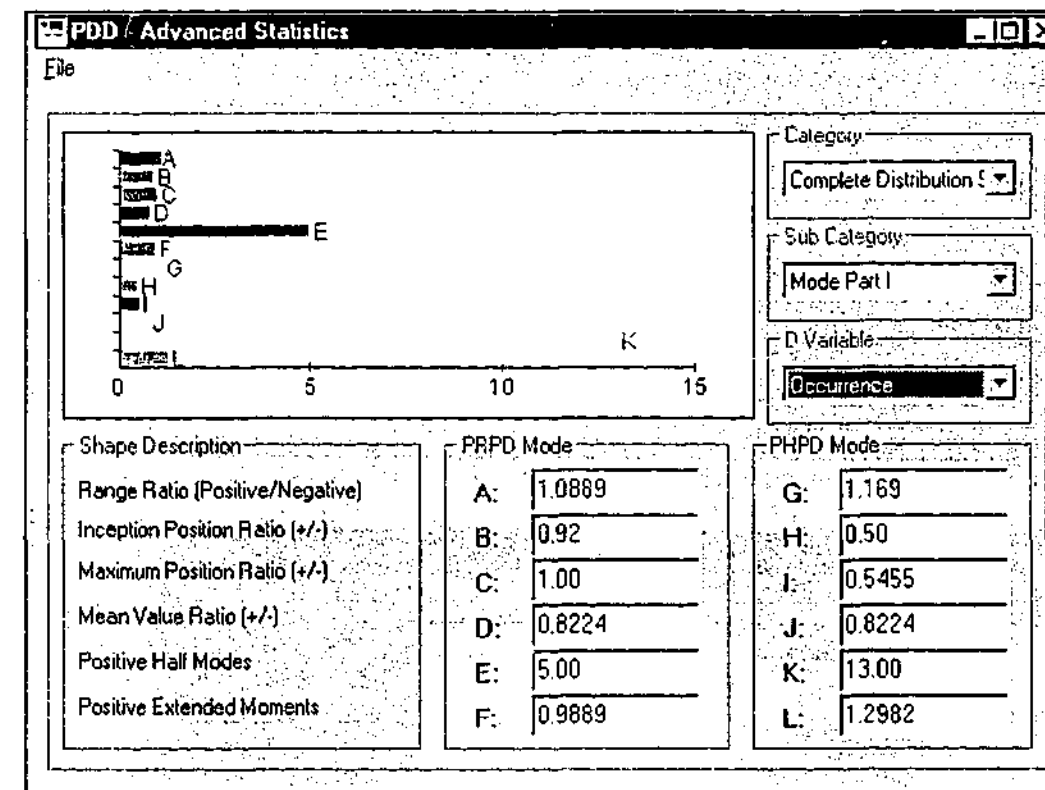
Fig. 2.21 Feature quantities describing the asymmetry of a discharge distribution calculated in a module of PDD system

In addition to the parameters described above, distributions can be quantified according to their skewness and kurtosis. Skewness indicates asymmetry of a distribution relative to a normal distribution. If skewness is negative, the distribution is skewed to the left. Otherwise the distribution is skewed to the right. The kurtosis, on the other hand, provides an indicator for the sharpness of a distribution relative to a normal distribution. If kurtosis is greater than zero, then the distribution is broader than a normal

distribution, Otherwise it is narrower. Figure 2.22 and 2.23 have shown the shape parameters calculated from a positive and negative half of a distribution respectively.
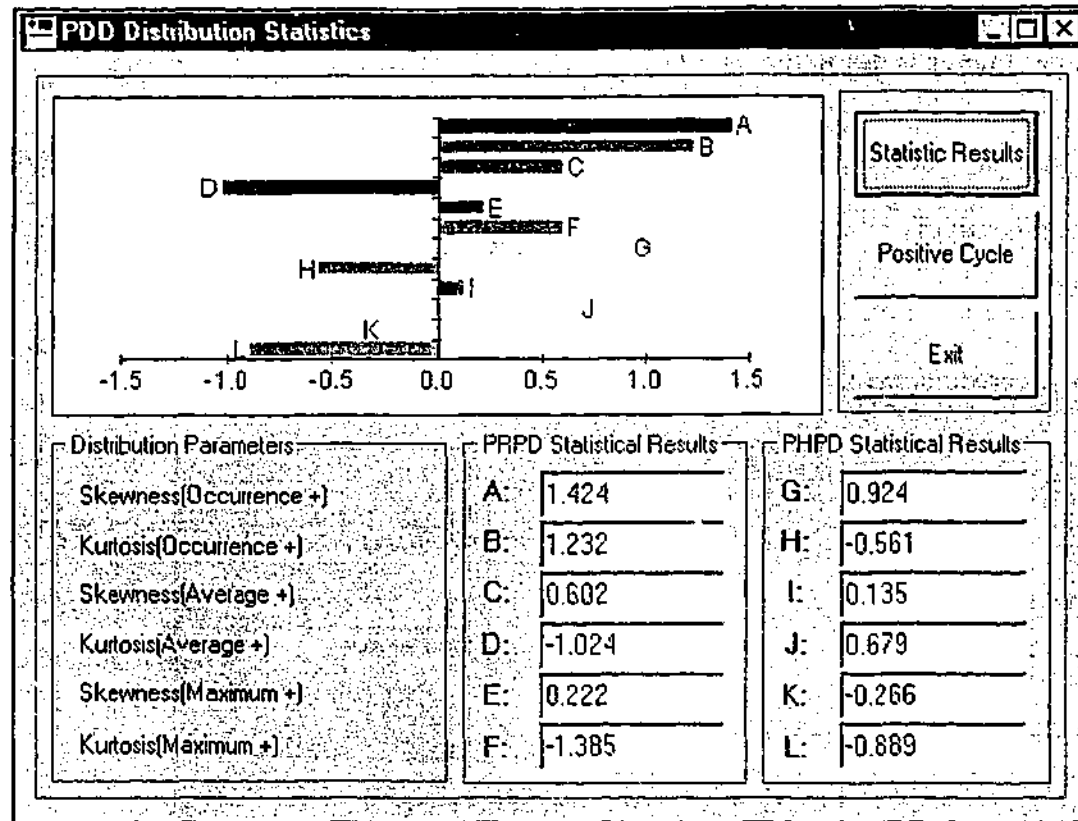
Fig. 2.22 Skewness and Kurtosis calculated from the positive pressboard discharge
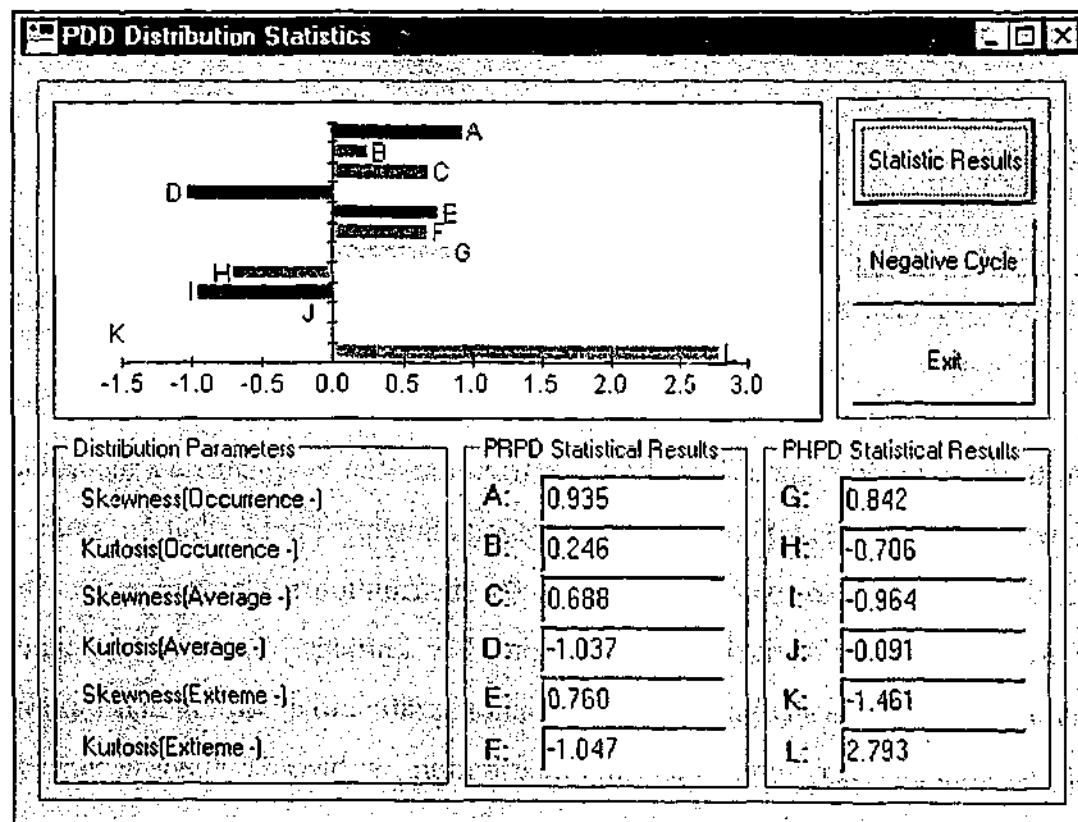
Fig. 2.23 Skewness and Kurtosis calculated from the negative pressboard discharge

2.6 IMPORTATION AND EXPORTATION PD DATA

In addition to the control and graphic functions described in previous sections, PDD system allows user to export acquired PD data to other software packages using build-in tools as indicated in figure 2.24. Meanwhile, the saved data as well as the statistical results from a database can be imported to the PDD system for analysis and evaluation. The acquired PD data not only can be saved into a PDD format file but the analysis results with different indices can be exported to a file with text-delimited format as well. Undoubtedly, these tools make the PDD system really versatile for discharge distribution pattern analysis.
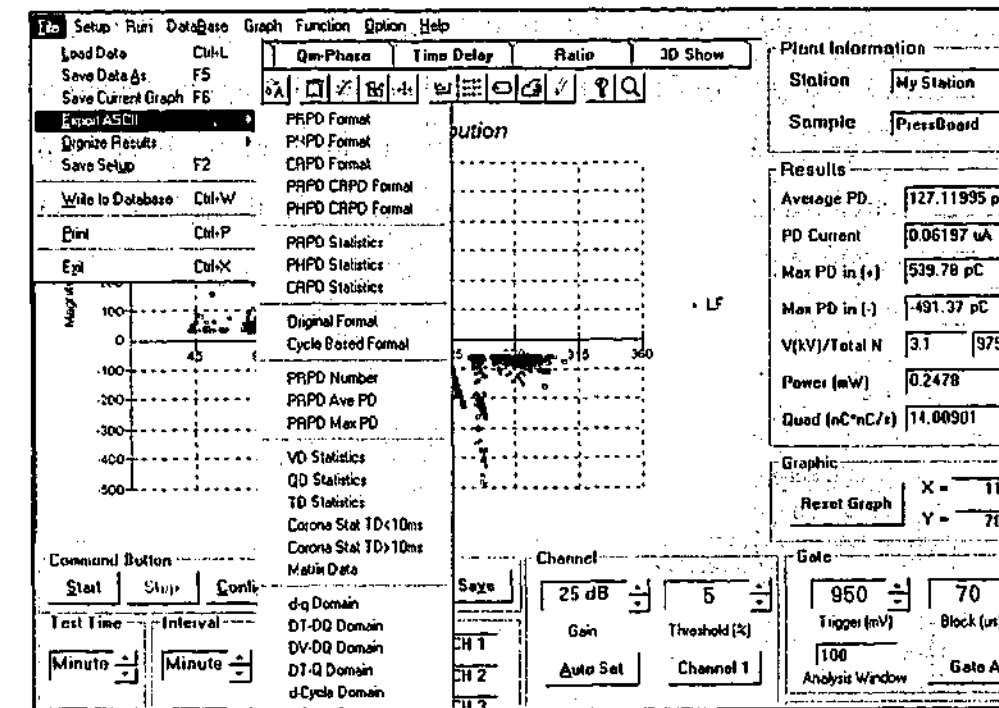
Fig. 2.24 Data import and export functions of PDD system

In addition to calculating the integral quantities defined in IEC Publication 270 and other quantities, distribution functions related to the quantities defined in IEC270 can be calculated based on each PRPD, PHPD, and CRPD window. These partition window based distribution functions provide details regarding discharge distribution against relevant partition windows. More over, feature quantities can also be calculated from these distribution functions and exported to a file with text delimited format. Calculated

from PRPD partition window, the available distribution functions for exportation are tabulated in table 2.1:

Parameter Name	Interpretation
LFCount	Number of PD events
LFAvePD	Average discharge amplitude (pC)
LFMaxPD	Maximum absolute PD amplitude (keep original polarity (pC)
LFIa	Integrated PD current (uA)
LFPower	Integrated PD power loss (mW)
LFQuad	Quadratic rate of PD amplitude (nC*nC/s)

Table 2.1 Exportable IEC270 defined parameters based on phase partition window

In addition to the distribution functions listed in above table 1, descriptive statistics describing PD distribution within PRPD partition window are also available for exportation. Figure 2.25 shows that there are totally μ events of discharge in the range of the $i th$ phase partition window. Possibly, the statistics and other derived quantities about the distribution of these PD events may provide extra information for in-depth analysis of discharge behavior under ac voltage. In short, the exportable PRPD based statistical parameters are tabulated in table 2.2.
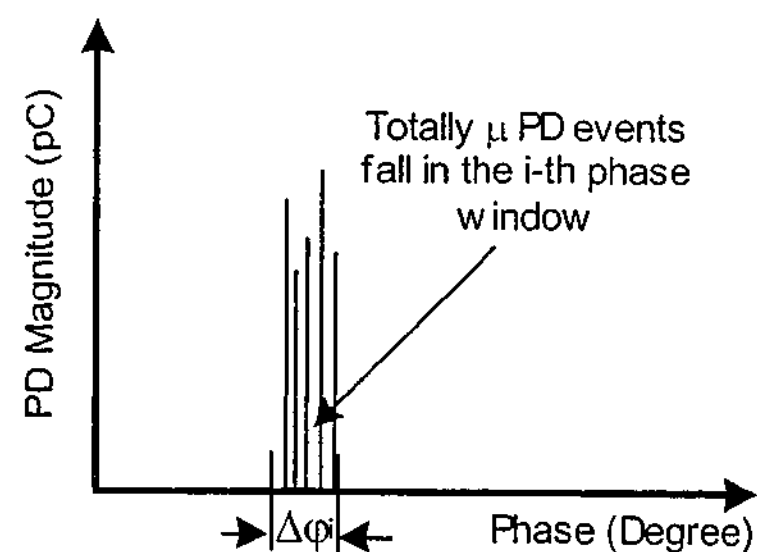
Fig. 2.25 Diagram of total μ events PD falling in the range of the $i th$ phase partition window

Parameter Name	Interpretation
Count	Total observable number of PD events
Mean	Arithmetical mean of PD amplitude
Maximum	Maximum PD amplitude
Minimum	Minimum PD amplitude
Range	PD amplitude variation range
Median	Geometrical mean of PD amplitude
Variance	Variance of PD amplitude
StdDev	Standard deviation of PD amplitude
SumOfData	Total sum of PD amplitude
SumOfSq	Total sum of squared value of PD amplitude
MSSD	Half the mean of successive squared difference of PD amplitude
Skewness	Measure of distribution symmetry
Kurtosis	Measure of distribution sharpness in relation to normal curve

Table 2.2 Exportable statistical parameters based on phase partition window

With the help of statistical information in each PRPD window, it is easy to investigate PD phenomena using PDD system. However, it may not be necessary to use of all these feature quantities at current stage to analyze PD distribution patterns. These listed quantities may be useful in future research or industry application.

As for PHPD and CRPD distributions, there are comparable statistics and other derived quantities that can be calculated for display and for exportation as well. The current available exportable parameters for PHPD and CRPD are listed in tables E.1 and E.2 as well as figure E. 1 of appendix E.

2.7 GRAPHIC TOOLS

PD distribution graphs of various distribution categories are all important for the analysis of PD distribution patterns. PDD provides a wide range of graphic tools to support "run-time" analysis. There are totally six graphical groups supporting more than fifty distribution functions. The six graphical groups are listed as follows:

(1) Phase/voltage resolved distribution pattern
(2) Pulse-height resolved distribution pattern

(3) Power frequency cycle resolved distribution pattern

(4) Voltage difference (between consecutive events) resolved distribution pattern

(5) Charge difference (between consecutive events) resolved distribution pattern

(6) Time interval (between consecutive events) resolved distribution pattern.

With the built-in graphic facilities, PDD system offers a very user-friendly environment to switch easily from one pattern to another as seen in figure 2.26.
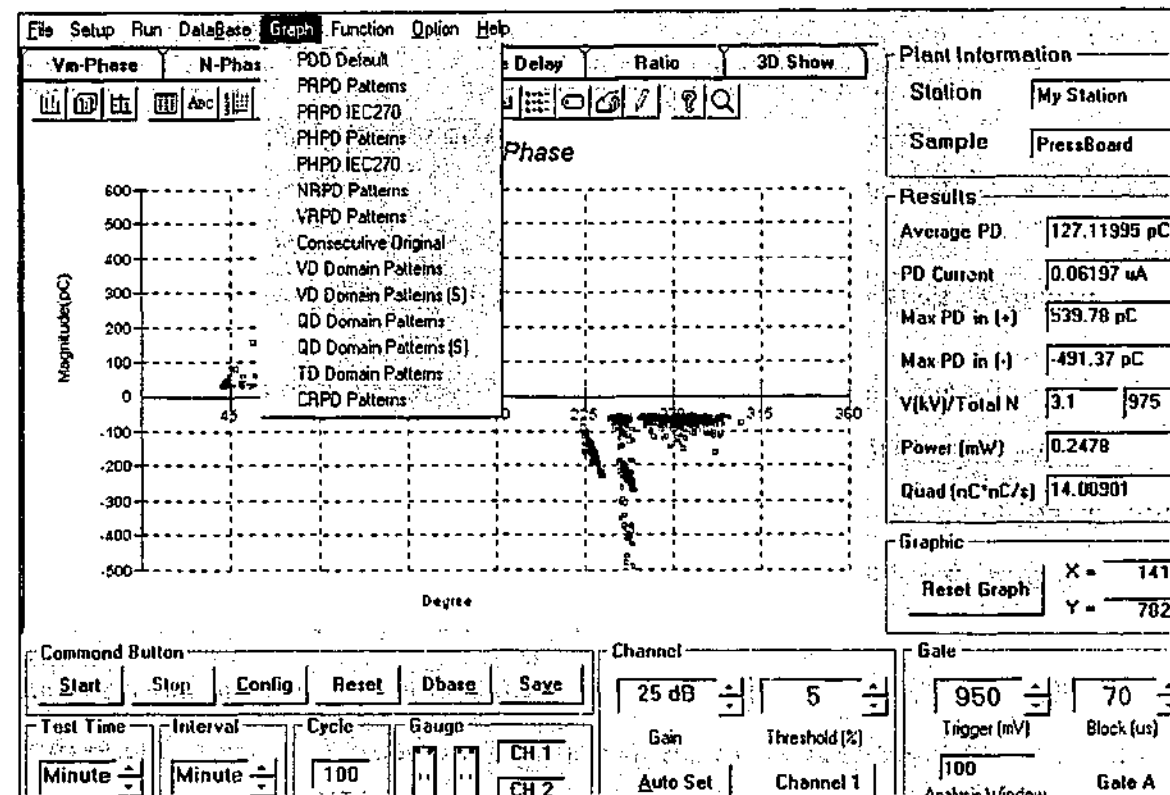
Fig. 2.26 Graphic tools for displaying and analyzing PD patterns

In addition, PDD has run-time editing and analyzing facility including zooming and positioning functionality, which allows user to scaling and analyzing PD from various patterns easily as shown in figure 2.27.
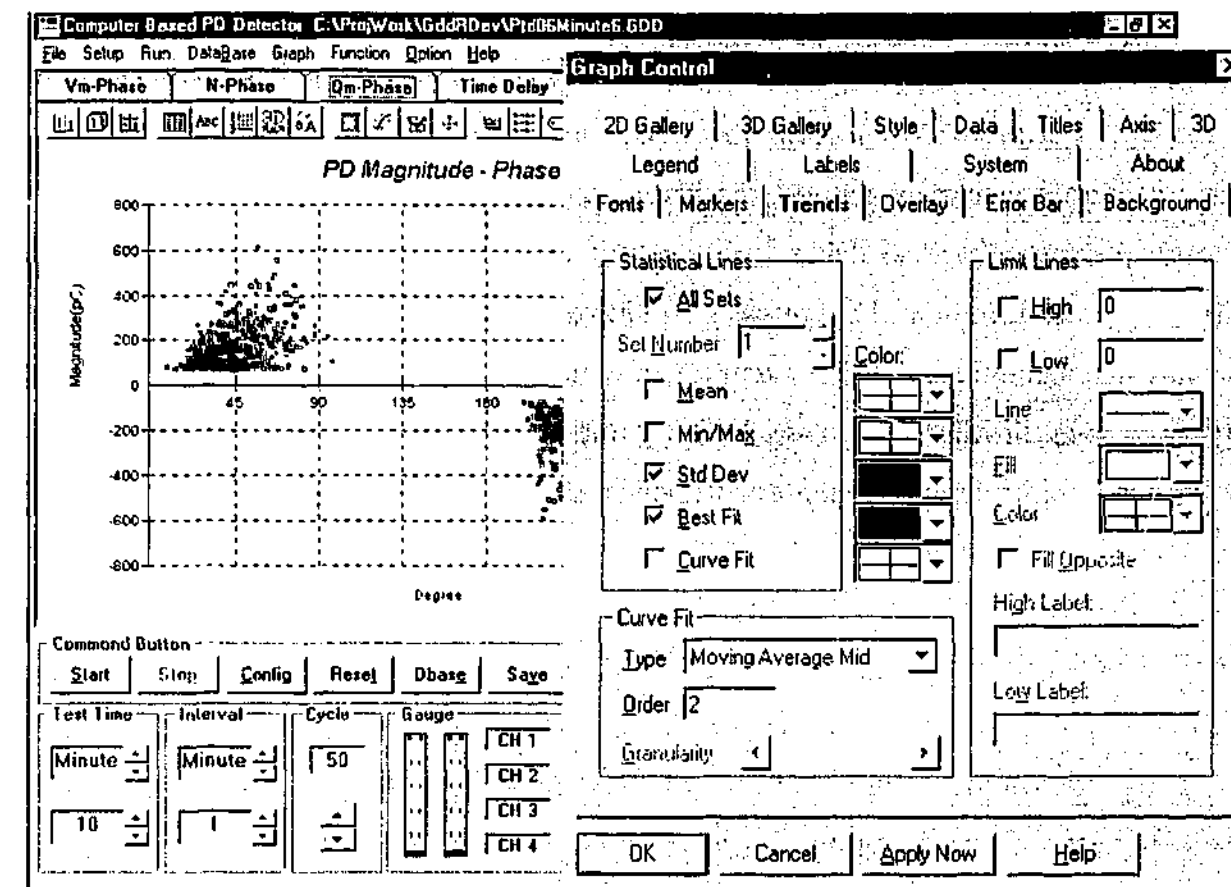
Fig. 2.27 PDD system run-time editing and analyzing tools

2.8 CONCLUDING REMARKS

PD phenomena are very complicated in fact because of the influence of memory propagation effects that make PD susceptible to nonstationary behavior [67, 68]. Therefore, it is impossible to assess the quality of an insulation system by only a few integrated quantities [24]. Only limited number of PD distribution functions has been in use in PD measuring systems up to date to analyze PD behavior. The difficulties or problems encountered in the interpretation of measured data are quite obvious because there is not enough PD activity related information extracted. However, the problems can be at least partly overcome by exploring and introducing more PD distribution functions in PD measuring system. PDD is an example of such a system. With the PDD system, a great deal of discharge information including subsequent distribution functions, can be obtained by appropriate data processing. It uses advanced digital signal processing techniques with the support of comprehensive database and analysis routines. It is a reliable system with features such as easy to install and operate. Test results are saved together with the hardware settings under which PD data are acquired.

In addition, the results can be analyzed and displayed instantly with the support of various distribution graphs and printable reports. The results are also in compliance with the IEC Publication 270 standard. Moreover, some important distribution functions such as average discharge magnitude, discharge current, and discharge power loss can be saved in the database so that further analysis can be done to determine the trend of insulation deterioration. This marks a significant improvement in PD measuring and evaluating techniques. PDD system carries out PD measurement and analysis with greater speed, flexibility and ease. Visually impressive two and three dimensional pulse distribution plots depicting their evolvement with time are obtained with little effort.

Chapter 3

New Techniques for Phase Resolved Partial Discharge Pattern Analysis

The great advances that have been made in PD measuring technology can be attributed to the development of PD pulse analysis technique that has taken place over more than half of a century. Along with the improvement of cumulative PD pulse count measuring techniques, one of the important techniques, called phase resolved PD (PRPD) analysis, has been introduced in mid 70's. In the PRPD approach, the entire ac cycle is equally divided into 200 phase partition windows containing the statistics of interest. PD distribution in the $i-1^{th}$ and i^{th} partition windows is illustrated in figure 3.1. Partition quantities may be calculated based on discharge distribution in each partition window in order to quantify discharge activities in the partition window. The propagation of PD properties along the partition window can be represented in PRPD distribution functions.
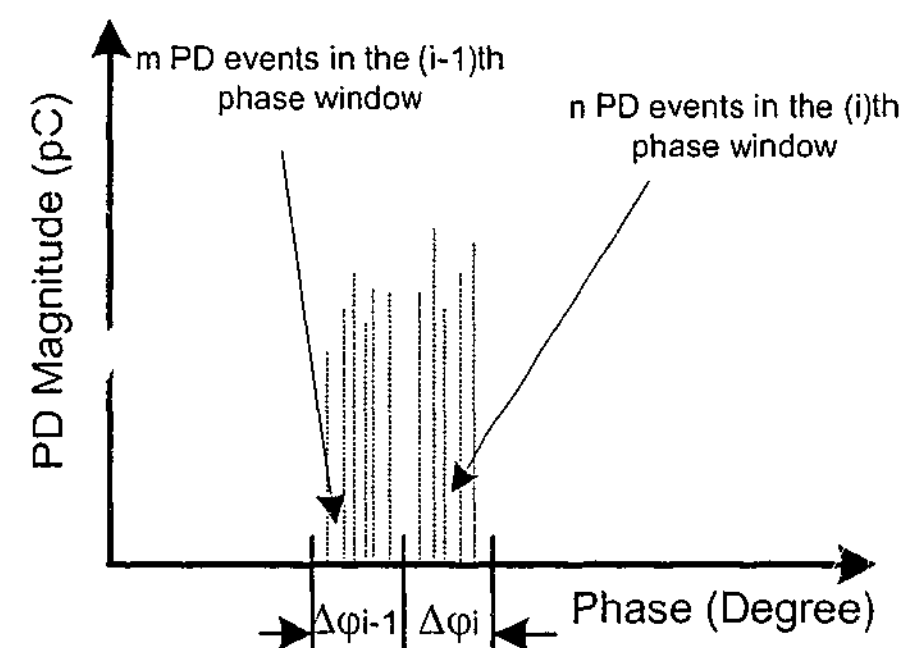

Fig. 3.1 Discharge distribution in the $i-1^{th}$ and i^{th} phase windows

3.1   REVIEW OF PRPD ANALYSIS TECHNIQUES

Phase resolved partial discharge (PRPD) patterns have been studied for many years. The experience has found that PRPD distributions are susceptible to the degree of geometrical asymmetry of electrodes undergoing discharge [2, 47]. To date, research in this direction has revealed that discharges can exhibit complex stochastic behavior in which phase-to-phase memory effects have significant impact on PRPD distribution [69]. Under ac voltage, the probability of a discharge event at a particular ac phase position depends on the properties of the defect such as the insulation material surrounding the defect, the location and geometry of the defect etc.

3.1.1   Phase of Occurrence

There has been considerable interest in using PRPD distribution pattern to assess the quality of electrical insulation system under ac electrical stress [26, 27, 44, 50, 56]. It can be observed from PRPD patterns that once the local field strength increases and exceeds the inception level, the probability for PD initiation increases as well. When a PD occurs, local field strength drops due to the ion residuals produced by earlier pulses. The so-called memory effects are associated with those residuals. It has been proved that some important properties of pulsating PD phenomena can be revealed by the observation of PRPD distribution functions that are defect dependent. In fact, the characteristics of PRPD distribution functions reveal the memory propagation behavior under ac voltage.

Among the conventional PRPD distribution functions, the most popular one is the distribution of phase of occurrence. The distribution function of PD occurrence along with the partition window is an important property relating to the discharge mechanism of a defect. Discharge pulse repetition rate is the total number of measured PD pulses in an equally divided ac phase range. With the measuring system of figure 2.1, it is noteworthy that only pulses above the threshold are collected. Therefore, the settings of measuring system have serious impact on the acquired distribution functions. The statistical nature of PD phenomena can be taken into account by considering the

frequency of PD events occurring during the test period. The distribution functions of different types of defect source are in figure 3.2.
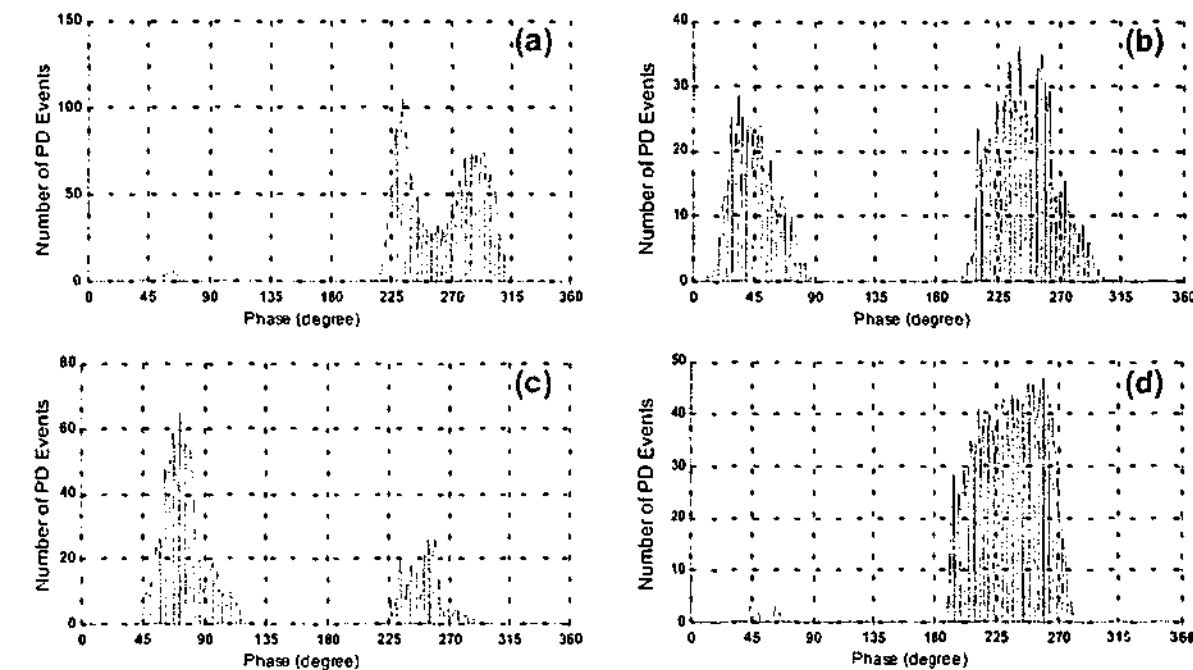
Fig. 3.2 PD Phase of occurrence distribution functions measured from
(a) a point-to-plane corona
(b) a point-to-dielectric discharge
(c) an oil-impregnated pressboard discharge
(d) an epoxy resin stator bar with an artificial defect inside

3.1.2   Distribution of Average PD Amplitude

The distribution of average discharge amplitude along PRPD partition window is an important distribution property that has been used in many applications to classify discharge source of different types. It is a measure of average intensity of discharge pulse magnitude along the partition window, which describes part of the natural distinctiveness of the defect itself. The distribution functions of average PD amplitude of different types of discharge source are illustrated in the following figure 3.3. Obviously, the difference can be visually recognized between the shown patterns.
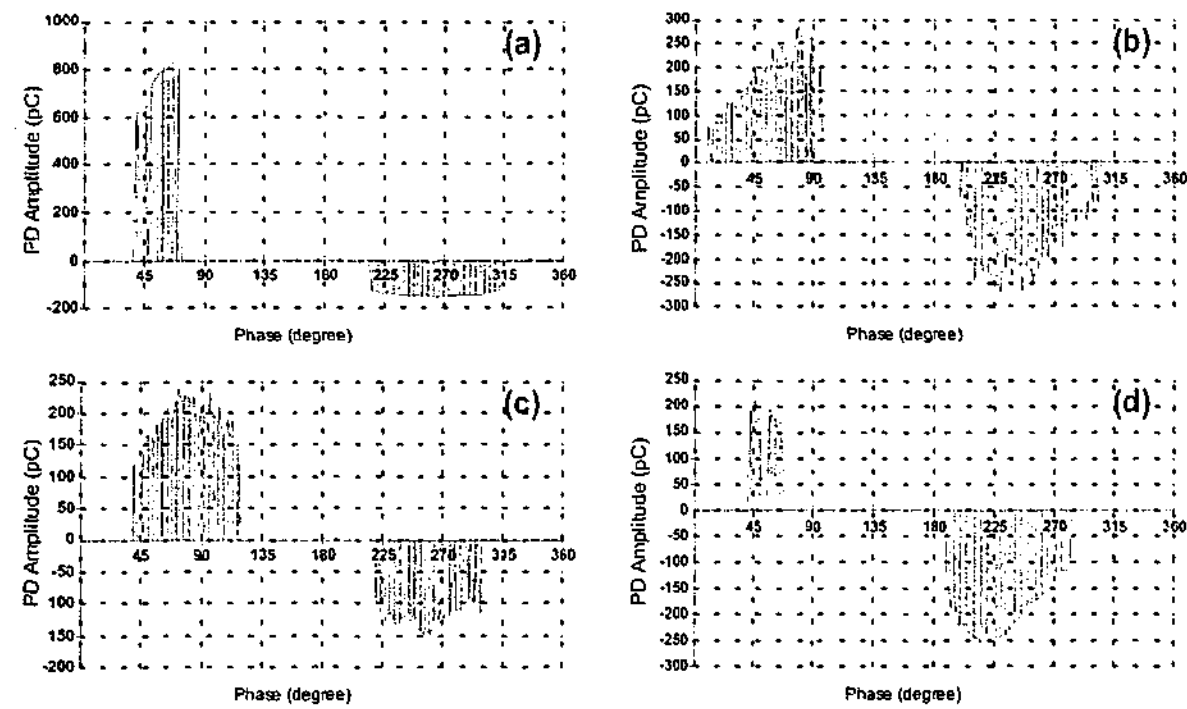
Fig. 3.3 Distribution functions of discharge average amplitude measured from
(a) a point-to-plane corona
(b) a point-to-dielectric discharge
(c) an oil-impregnated pressboard discharge
(d) an epoxy resin stator bar with an artificial defect inside

3.1.3 Distribution of Maximum PD Amplitude

In practice, it is important to monitor the maximum PD amplitude over a period of time. With PRPD approach, it is feasible to arrange the distribution function of the maximum PD amplitude along the partition window in which the maximum PD amplitude appearing at particular phase position in a given time can be observed. Like the distribution function of average PD amplitude, the distribution function of maximum PD amplitude has also been widely used to provide quantification to form discharge fingerprints. The importance of this distribution is illustrated by taking an example. The maximum distribution functions measured from different types of defect are shown in the following figure 3.4 in which a visual comparison among the four different types of discharge can be easily conducted.
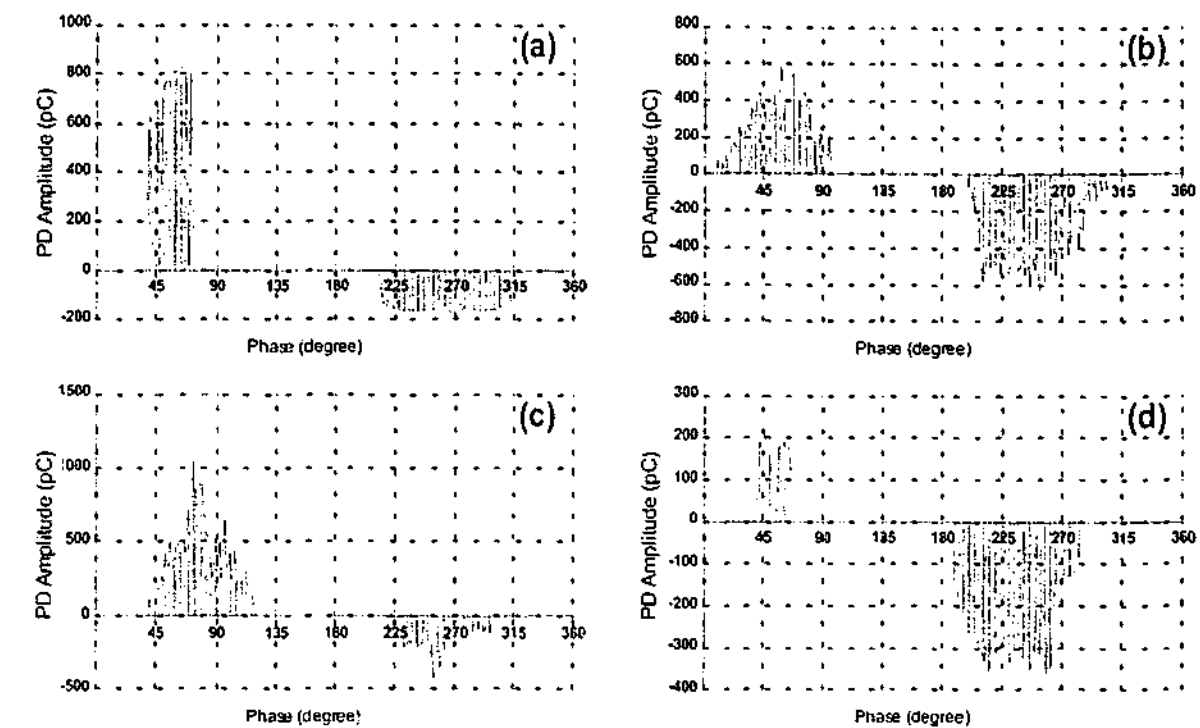
Fig. 3.4 Distribution functions of discharge maximum amplitude measured from
(a) a point-to-plane corona
(b) a point-to-dielectric discharge
(c) an oil-impregnated pressboard discharge
(d) an epoxy resin stator bar with an artificial defect inside

3.1.4 Distribution of Discharge Current

The distribution of discharge current along the partition window is actually a measure of the distribution of accumulated charge along the partition window. It reveals the distribution information about accumulated discharge intensity along ac voltage phase during the measurement time interval. Compared with the phase of occurrence, average, and maximum PD distribution functions, the PD current distribution function provides a specific correlation between accumulated charge and the phase partition window. Undoubtedly, the distribution function helps to characterize the stochastic properties about the nature of the defect under test. The discharge current within a partition window is related to the total PD events occurring in that partition window. It can be calculated as the sum of apparent charge divided by the measurement time interval. In conjunction with distribution functions of occurrence, mean and maximum PD amplitude, the PD current distribution function is implemented in the PDD system. The current distribution functions for different types of defect are shown in figure 3.5.
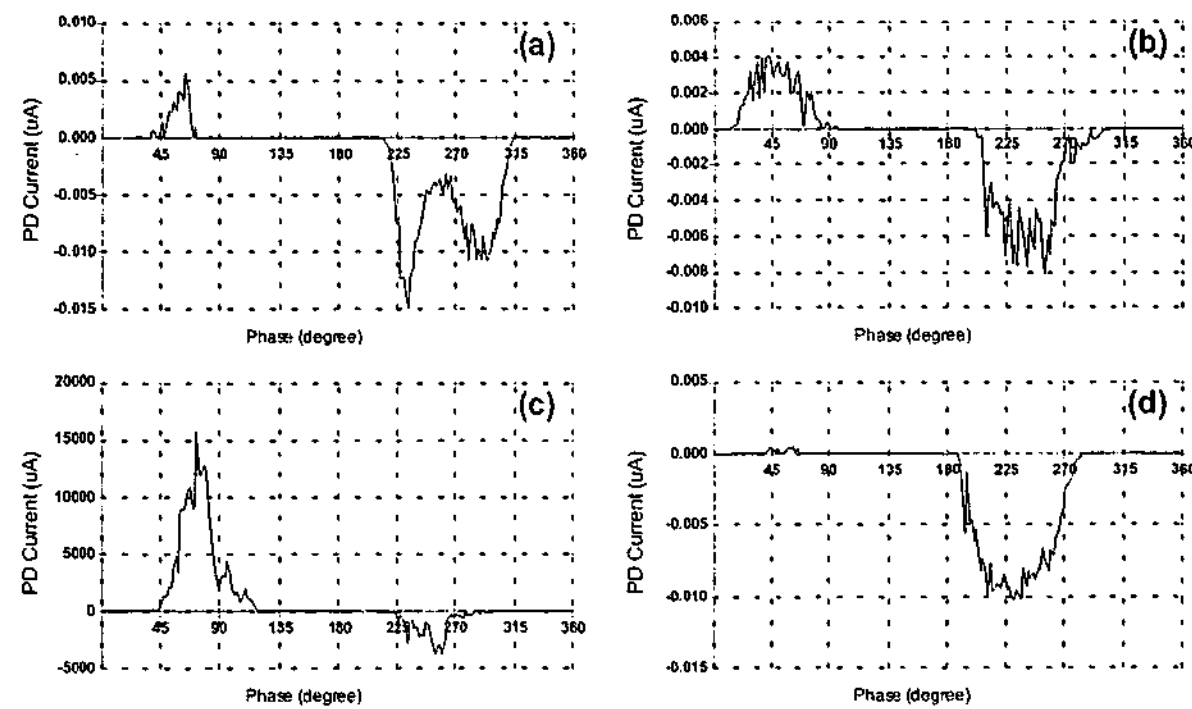
Fig. 3.5 Distribution functions of discharge current measured from
(a) a point-to-plane corona
(b) a point-to-dielectric discharge
(c) an oil-impregnated pressboard discharge
(d) an epoxy resin stator bar with an artificial defect inside

In summary, distribution functions of PRPD category that have been used so far by other researchers in the study of PD physical mechanisms as well as PD pattern recognition are:

- PRPD distribution functions discussed in section 3.1.1 were measured and used for the investigation of discharge stochastic phenomena (Bartnikas, Van Brunt, Niemeyer, Heitz, Fruth et al.). Discharge mechanisms were investigated with particular emphasis on the statistical characteristics of PD pulse signals. Their physical interpretation has been supported by simplified mathematical models and simulations.
- Distribution functions of PRPD category (from 3.1.1 to 3.1.3) provide feature quantities to assess the insulation degradation at various aging stages. The discharge induced aging process in dielectric voids were evaluated to a certain degree by these quantities. Based on feature quantities extracted from PRPD distribution functions, the defects of various origins were classified when using a computer based pattern

recognition system. Obviously, the classification needs the support of a backend database (Kreuger, Okamoto, Gulski et al.).

- Distribution functions of PRPD patterns have been successfully used for the evaluation of insulation condition of HV equipment such as rotating machines, power transformers, GIS, and power cables etc. The assessment was conducted on the equipment either in or out of service (Gulski, Stone et al.).
- In conjunction with the discharge pulse sequence analysis, PRPD distribution functions were sometimes used in the investigation of electrical treeing phenomena. (Hoof, Patsch, Suwarno et al.).

3.2 PRPD DISTRIBUTION FUNCTION

Distribution function is an important new concept defined in the first chapter of this thesis. For PRPD pattern analysis, many feature quantities are calculated from distribution functions as parameters of PD fingerprints. It is necessary to provide general mathematical expressions regarding distribution functions used in pattern analysis and to implement them in PDD system.

Discharge phase of occurrence is an important distribution function describing the probability of PD events along PRPD partition window. If $p_1(\lambda|\varphi_\lambda \in \Delta\varphi_i)$ is the probability that a PD event λ occurred at ac phase φ_λ and $\varphi_\lambda = \Delta\varphi_i = \varphi_{i-1} - \varphi_i$, the PD occurrence distribution function in the ith partition window may be defined as:

$$f_\varphi(i) = N \bullet p_1(\lambda|\varphi_\lambda \in \Delta\varphi_i) \qquad (3.1)$$

where N is the total number of PD events acquired in a measurement and i is the equally divided PRPD partition window index. Average distribution function describes the distribution of average PD amplitude. It is defined as:

$$A_\varphi(i) = \frac{\sum(q_\lambda|\varphi_\lambda \in \Delta\varphi_i)}{N \bullet p_1(\lambda|\varphi_\lambda \in \Delta\varphi_i)} \qquad (3.2)$$

where $p_1(\lambda \mid \varphi_\lambda \in \Delta\varphi_i) > 0$ otherwise $A_\varphi(i) = 0$, and $q_\lambda \mid \varphi_\lambda \in \Delta\varphi_i$ is the PD amplitude at discharge event λ under the given condition that PD phase is in the ith PRPD partition window $\Delta\varphi_i = \varphi_{i+1} - \varphi_i$. Maximum distribution function represents the distribution of maximum PD amplitude along the phase partition window. It is defined as:

$$M_\varphi(i) = \max(q_\lambda \mid \varphi_\lambda \in \Delta\varphi_i), \text{ when } q_\lambda > 0 \qquad (3.3a)$$

$$\text{or } M_\varphi(i) = \min(q_\lambda \mid \varphi_\lambda \in \Delta\varphi_i), \text{ when } q_\lambda < 0 \qquad (3.3b)$$

PRPD cu⋯ ⋯ ⋯ ⋯nction stands for the distribution of PD current and defined as:

$$I_\varphi(i) = \frac{\sum \cdots}{t} \cdots \Delta\varphi_i) \qquad (3.4)$$

where t is the time interval used for acquiring the PD data and q_λ is the amplitude of PD pulse. PRPD power loss distribution function exhibits the distribution of PD pulse power based on phase partition window and defined as:

$$P_\varphi(i) = \frac{\sum(q_\lambda \bullet V_\lambda \mid \varphi_\lambda \in \Delta\varphi_i)}{t} \qquad (3.5)$$

In the similar fashion, PRPD distribution function of quadratic rate of PD amplitude is defined as:

$$Q_\varphi(i) = \frac{\sum(q_\lambda^2 \mid \varphi_\lambda \in \Delta\varphi_i)}{t} \qquad (3.6)$$

where t is the time interval used for acquiring the PD data and q_λ is the amplitude of PD pulse.

3.3 NEW PRPD DISTRIBUTION FUNCTION

Unlike distribution functions described in section 3.2, the distribution function of PD power loss and quadratic rate are calculated based on their partition quantities. With the aid of the PDD system, more characteristics of PD phenomena can be observed from these new distribution functions.

3.3.1 PD Power Distribution Function

Discharge power is a measure of the energy dispassion in a given time period inside the test sample. The calculation of PD power within a phase partition window is restricted by the total PD events occurred in that partition window. The partition quantity of PD power loss can be calculated as the sum of pulse energy in the partition window divided by the measurement time interval. According to equation 3.5, the distribution functions of PD power are implemented in PDD system as shown in figure 3.6.
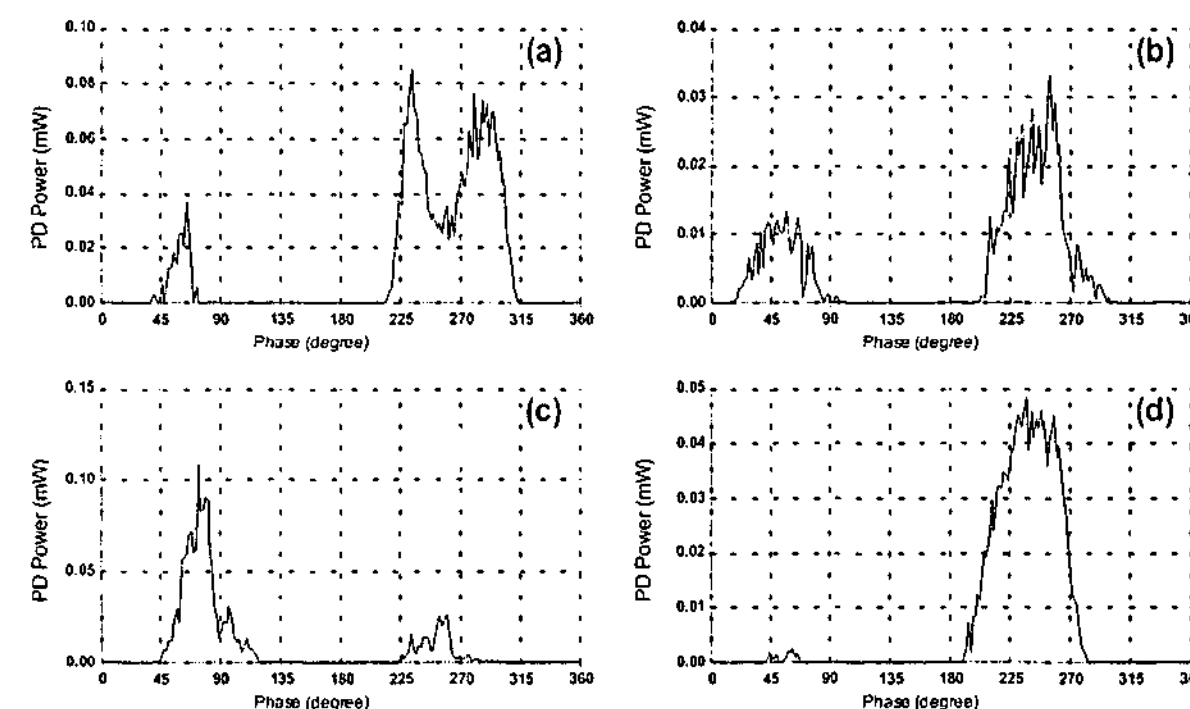

Fig. 3.6 Distribution functions of discharge power loss measured from
(a) a point-to-plane corona
(b) a point-to-dielectric discharge
(c) an oil-impregnated pressboard discharge
(d) an epoxy resin stator bar with an artificial defect inside

3.3.2 Distribution Function of PD Quadratic Rate

The distribution function of quadratic rate is a distinctive measure to observe the distribution of PD amplitude in the phase partition window because the aggregation assigns greater weight to the larger discharge pulses. The PD quadratic rate in each phase partition window can be calculated as the sum of the squares of the individual discharge magnitudes in the range of the partition window divided by that time interval as illustrated in equation 3.6. The distribution functions of discharge quadratic rate are illustrated in figure F.1 of appendix F.

3.4 STATISTICAL ANALYSIS

The stochastic behavior of PD pulses under ac voltage has been widely investigated [69]. The results reveal significant phase-to-phase memory propagation in a relatively simple configuration. The use of PRPD distribution functions for identification of defects in electrical insulation has been considered for many years [70, 71]. Efforts have also been made to derive PRPD distribution functions using computer based measurement and evaluation techniques. Using the recently developed PDD system is a promising way to measure and evaluate discharge stochastic property variation against phase partition window. The PDD system calculates PRPD distribution functions that representing memory effects regarding PD activities inside the defects. It helps to observe the dependence of the discharge characteristics at particular phase position.

In PRPD pattern analysis, distribution functions are PD partition quantities varying against the phase partition windows. The calculated distribution functions are used to associate with discharge physical mechanisms. Statistical analysis can be performed on each phase partition window as well as both positive and negative half cycles. Feature quantities are statistics calculated from positive and negative half cycle distribution functions separately. Obviously, distribution functions of a discharge may assist in understanding the discharge physical process inside the insulation. Meanwhile feature quantities of a discharge are compressed information representing the distribution profiles of discharge activities along phase partition windows. In addition, the distribution of discharge properties in a phase partition window, such as PD amplitude,

exhibits some important properties of the defect itself. Detailed analysis performed on phase partition windows may help to improve the understanding of the mechanism of discharge process. More over, the investigation of the statistics of PD distribution functions and the phase partition windows may disclose some useful information about discharge physical mechanism under ac voltage.

3.4.1 Feature Quantity

For the purpose of discriminating patterns of different defect sources, distribution functions such as the arithmetical mean and maximum of PD magnitude, PD current and power loss, are calculated in every PRPD partition window. In order to quantify the degree of symmetry between positive and negative half distributions, feature quantities are separately calculated for the positive and negative half cycles. PD distributions in a half cycle can be represented by their statistics. As an example, the arithmetical mean of PD magnitude and the standard deviation of PD magnitude distribution can be calculated using PDD system for both positive and negative half cycles as shown in figures 3.7(b) and 3.7(c) respectively.

Obviously, the values of the mean and standard deviation are useful to quantify the central tendency and dispersion of PD magnitude distribution over a half cycle. However, other distribution shape descriptors such as skewness and kurtosis can also be calculated for the positive and negative PD distributions respectively. The equation 1.10 and 1.11 are used to calculate these statistics and the calculation algorithms are developed and implemented in the PDD system. For example, the skewness and kurtosis of the 12 PRPD distribution functions are presented in conjunction with the bar chart graphs that are useful for initial visual comparison. As an example, the results for the positive half cycle are shown in figure 3.8 while negative results are shown in figure 3.9.
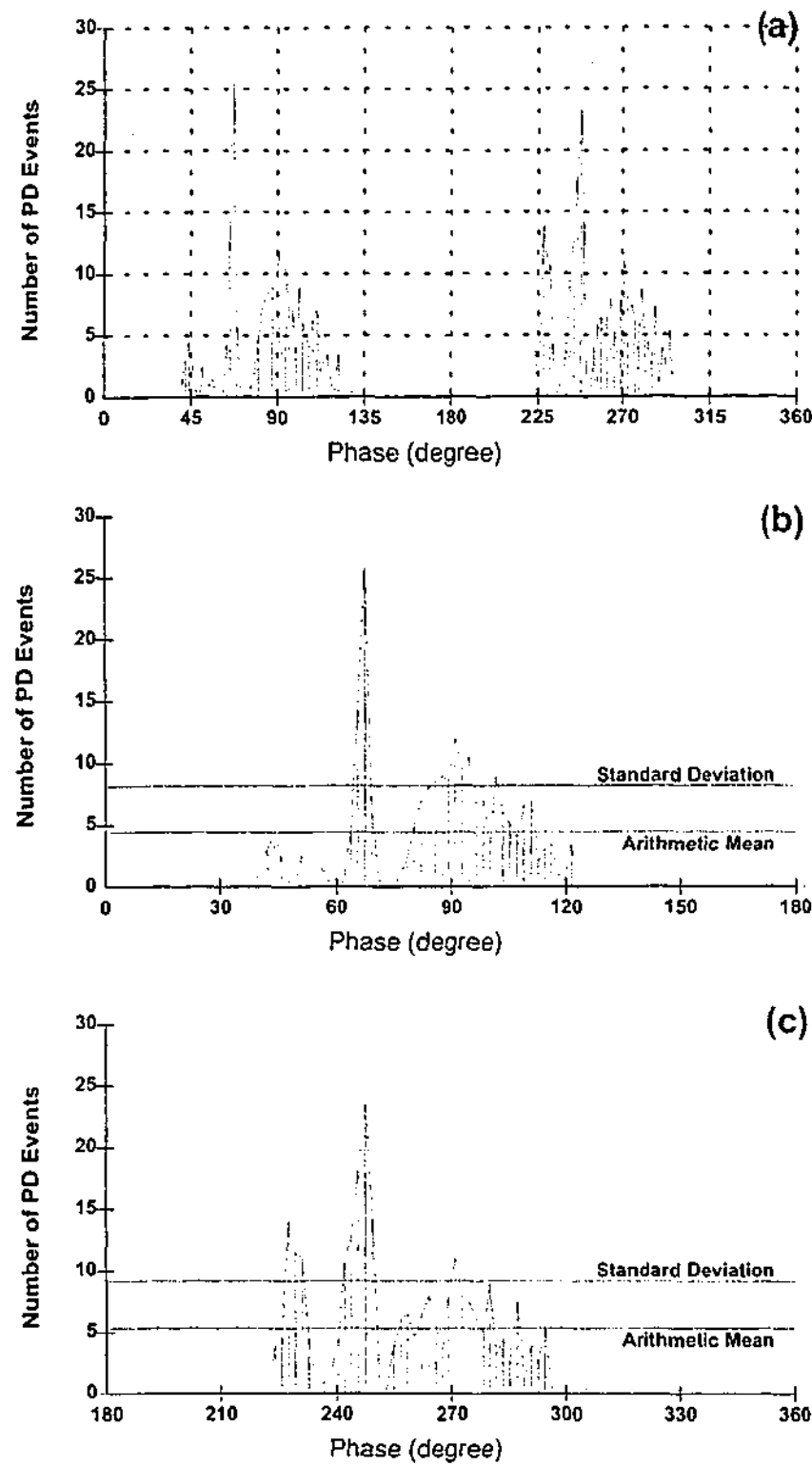
Fig. 3.7 Analysis of discharge occurrence measured from pressboard discharge
(a) A complete phase of occurrence distribution
(b) The positive half distribution function with its standard deviation and mean
(c) The negative half distribution function with its standard deviation and mean
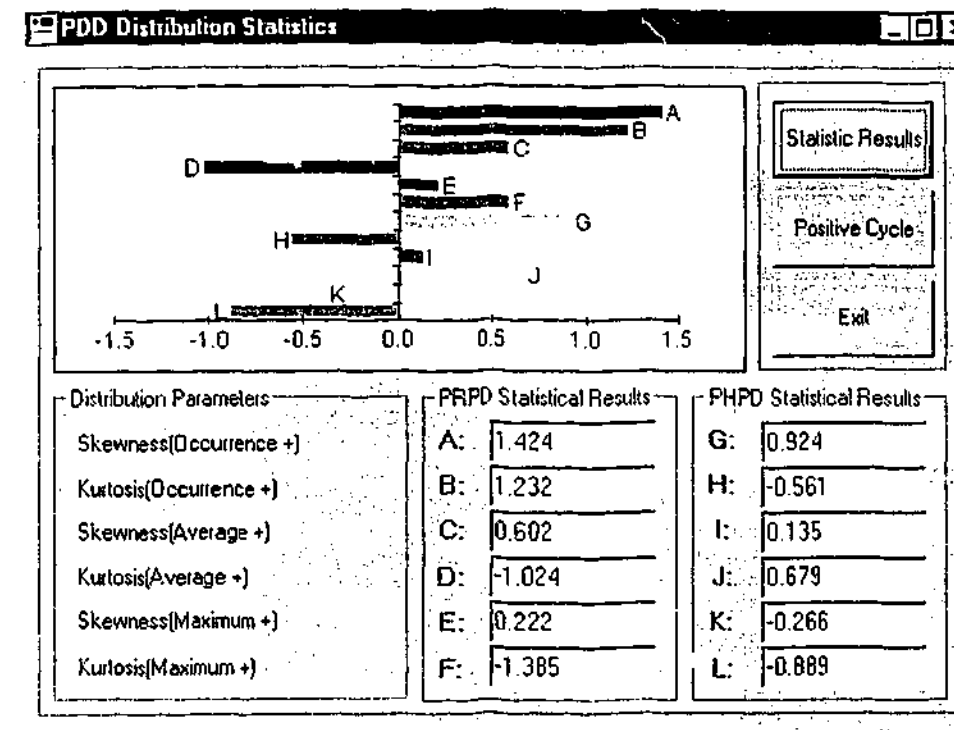
Fig. 3.8 Skewness and kurtosis of distribution functions in the positive half
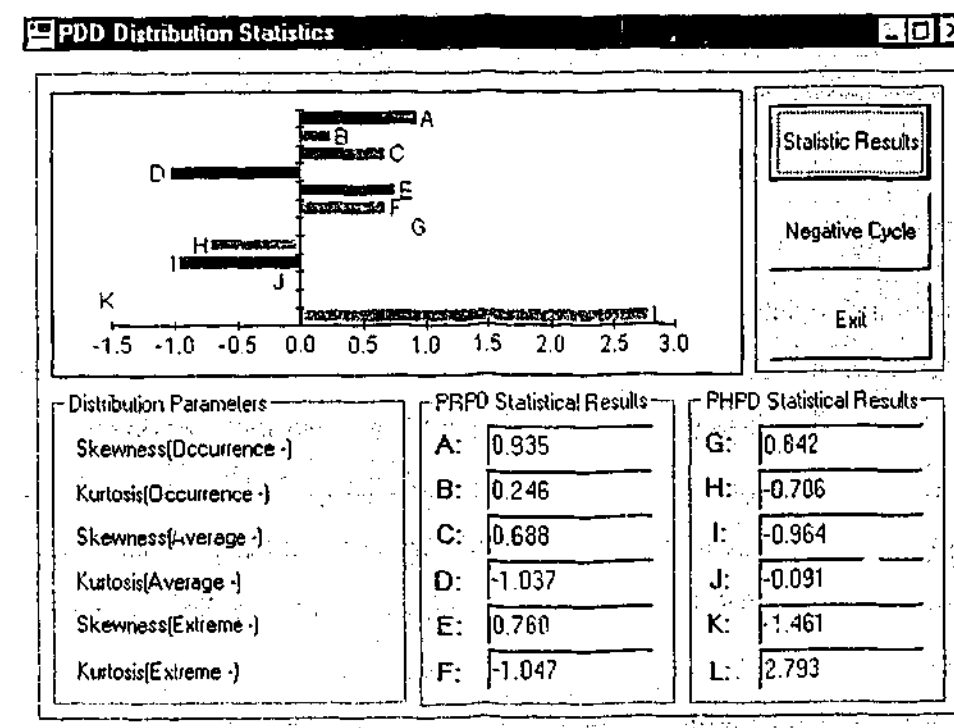
Fig. 3.9 Skewness and kurtosis of distribution functions in the negative half

In addition to the skewness and kurtosis, correlation coefficients between positive and negative half distributions can be calculated as a measure for the degree of symmetry between the positive and negative half distributions. The routine for calculating the

correlation coefficients is based on equation 1.9 and it is implemented in PDD system as shown in figure 3.10.
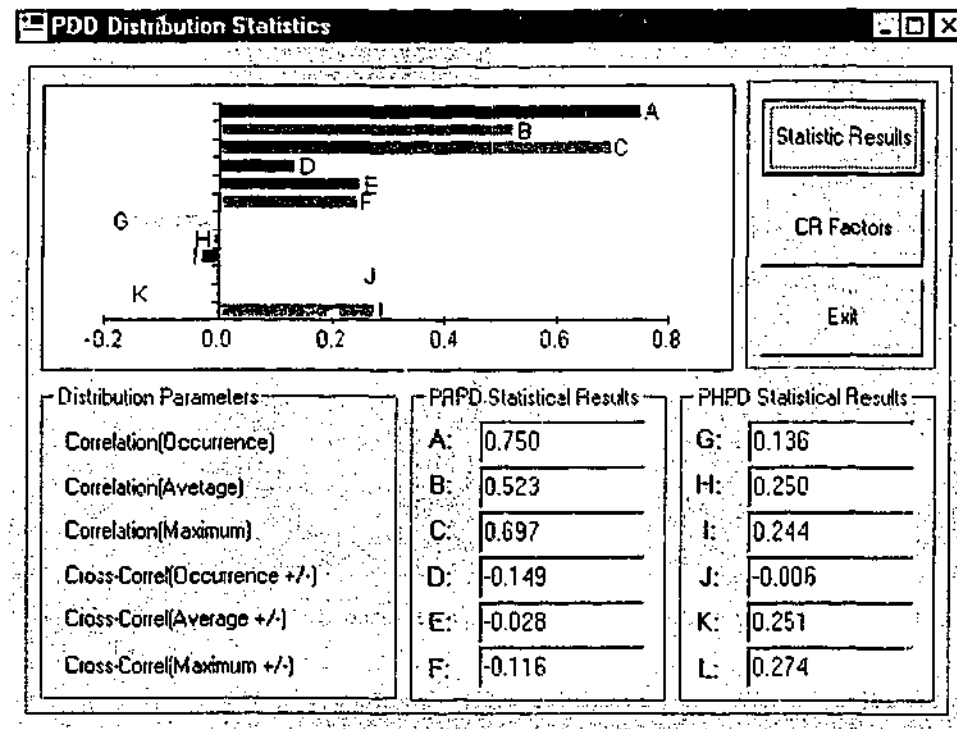
Fig. 3.10 Correlation coefficients between positive and negative halves of PRPD distribution functions

3.4.2 Other PRPD Statistics

Feature quantities calculated from distribution functions of PD occurrence, average and maximum amplitude, current, power, and quadratic rate provide a set of broad information about discharge distribution along the phase partition window. The calculated feature quantities represent the PD propagation along the ac phase. These feature quantities are combined with those calculated from distribution functions of other categories to form a general PD fingerprints. In addition, study on the statistics of phase partition window based PD distribution may provide extra information about discharge stochastic properties since phase dependent distribution are closely associated with discharge physical process. Some other interesting statistics such as mean, range and standard deviation of PD magnitude distribution can be calculated from each divided PRPD window. The variation of these partition quantities against PRPD partition windows is shown in figure 3.11 where results from dry and oil-impregnated pressboard discharges are compared. Both pressboard samples have the thickness of

3mm and measured under the same voltage of 4.2 kV. Partition quantities that describe PD distribution shape within each PRPD partition window, are calculated. The variation of these shape descriptors against PRPD partition windows is illustrated in figure 3.12.
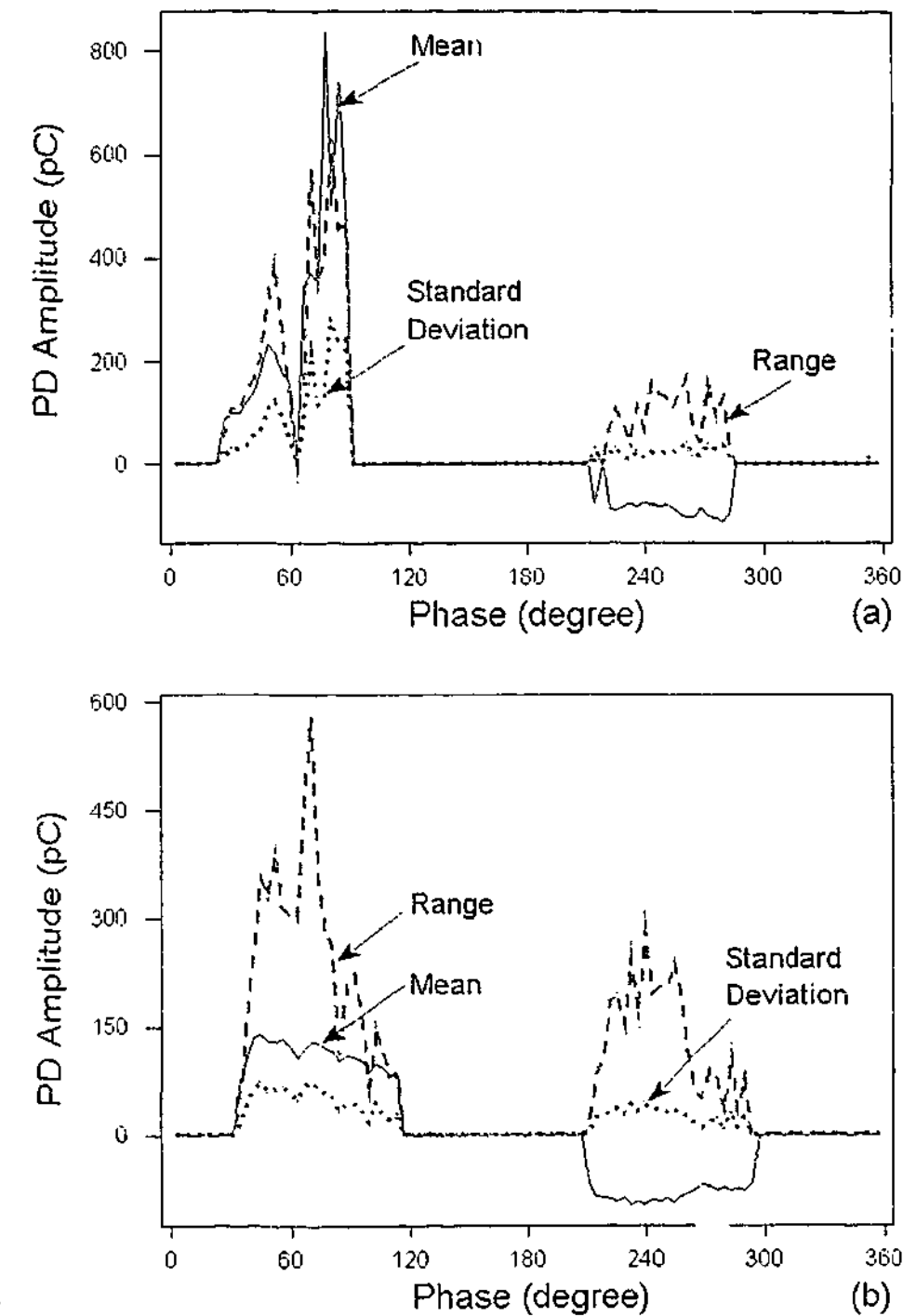

Fig. 3.11 Dispersion measures of PD amplitude along phase partition windows
(a) Results from a dry pressboard sample
(b) Results from an oil-impregnated pressboard vs. phase window

It is observed that positive PD distributions of the dry pressboard have more variation in magnitude than those of the oil-impregnated pressboard discharges. Meanwhile the

dispersion of negative PD is quite similar in both dried and oil-impregnated pressboards. The distribution of skewness and kurtosis of both types of pressboard describes the difference between dry and oil impregnated pressboard in terms of distribution shape of PD amplitude in divided phase windows.
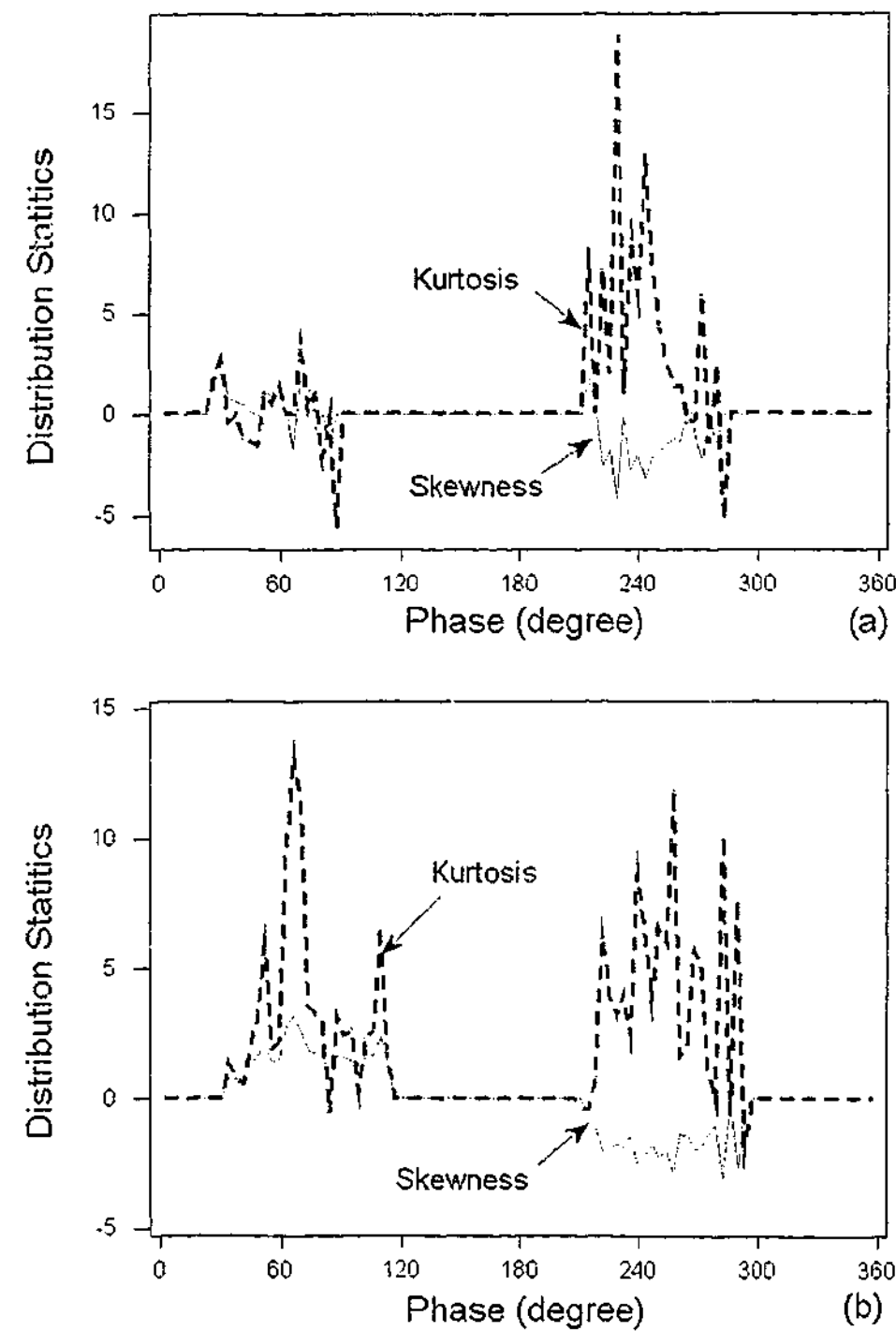

Fig. 3.12 Skewness and Kurtosis of PD distribution in phase partition windows
(a) Results from a dry pressboard sample
(b) Results from an oil-impregnated pressboard vs. phase window

3.5 RELATIONSHIP BETWEEN PRPD DISTRIBUTION FUNCTIONS

Discharge characteristics can be further explored by investigating the correlation between statistics of PRPD partition window. It is understood that the PRPD occurrence distribution function reflects the probability of discharge initiation and development in the entire ac phase range. Therefore, the PRPD window based occurrence can be utilized as an independent variable to study the variations of other statistics. The relationship between of the partition quantities and PD occurrence is interested in this chapter and further analysis is conducted in order to learn more discharge stochastic properties. It is a novel approach to analyze the PD propagation along ac phase using the partition window based statistics and their correlation with the PD occurrence. Obviously, calculated feature quantities are associated with the number of PD occurrence in PRPD partition window. The relationships may be examined from plot 3.13 to 3.16 where results are measured from different sources of defect type.
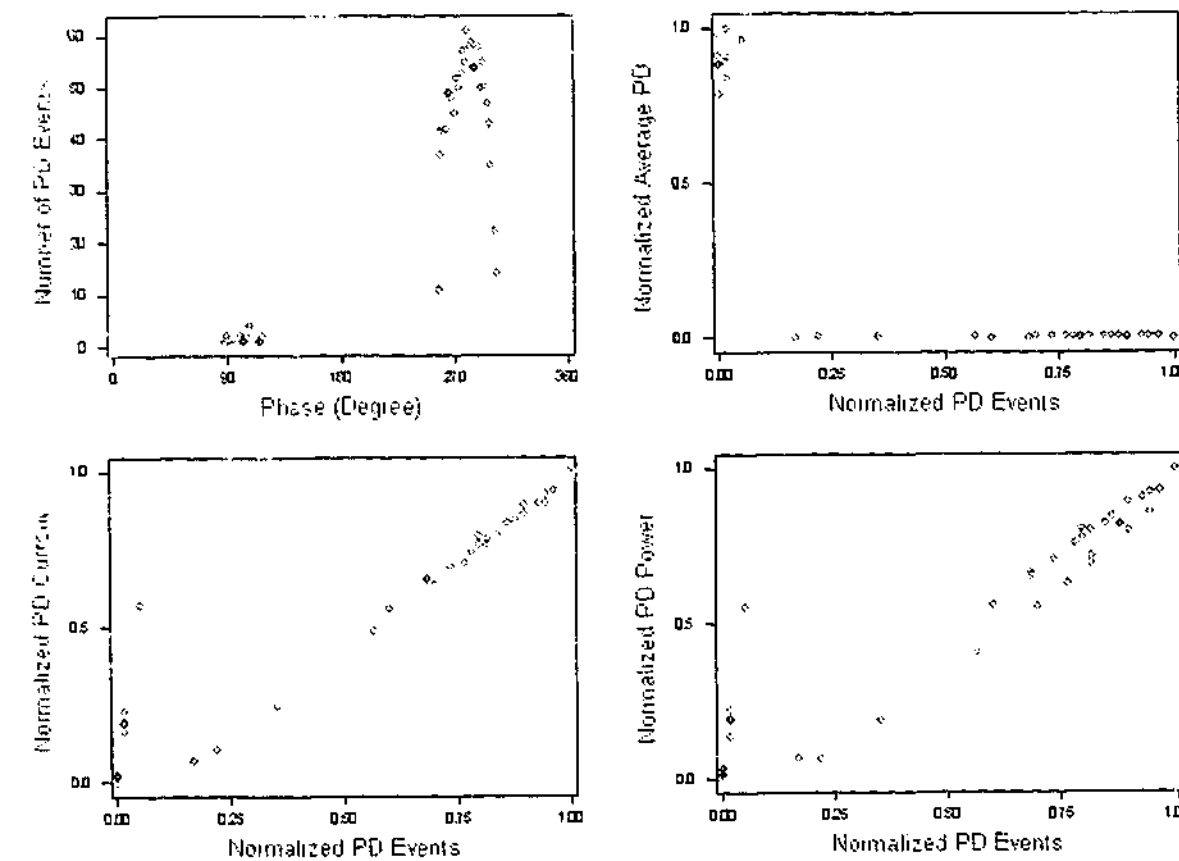

Fig. 3.13 Correlation between other statistics and occurrence of the point-to-plane corona
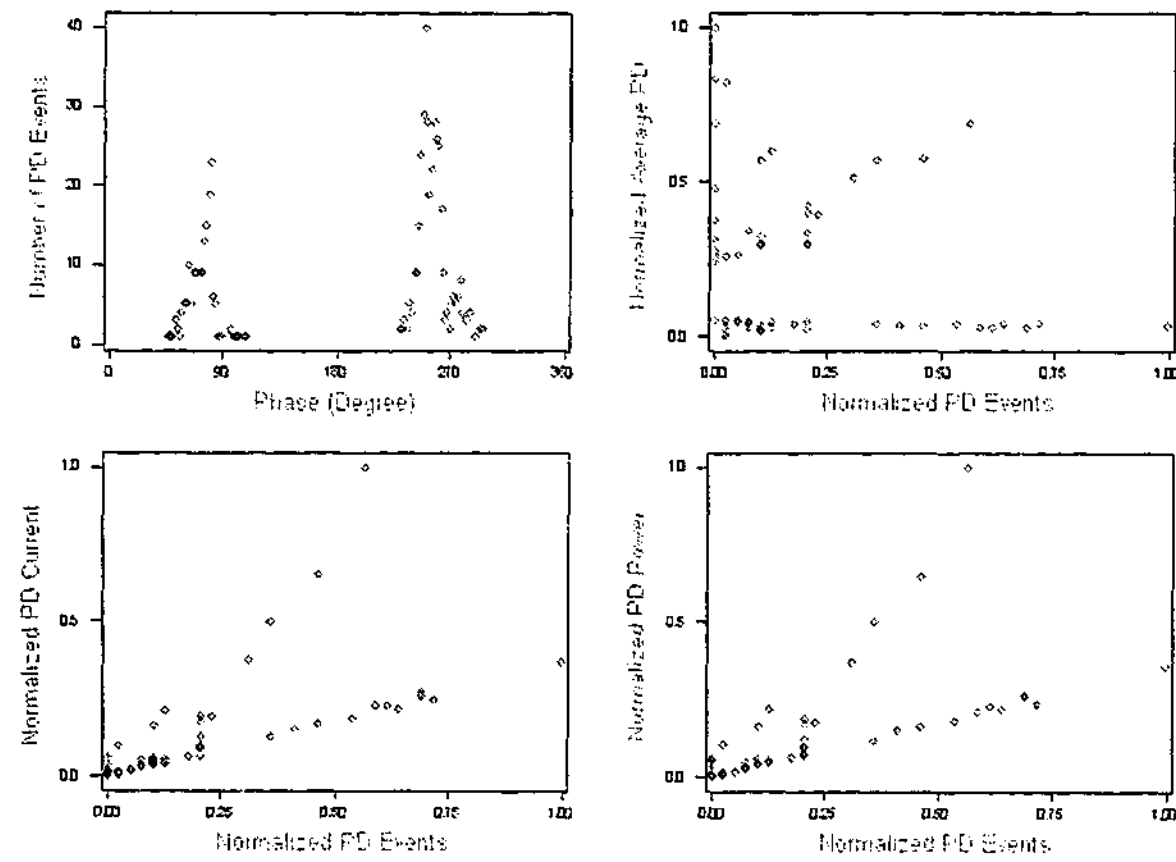
Fig. 3.14 Correlation between other statistics and occurrence of the dry pressboard discharge
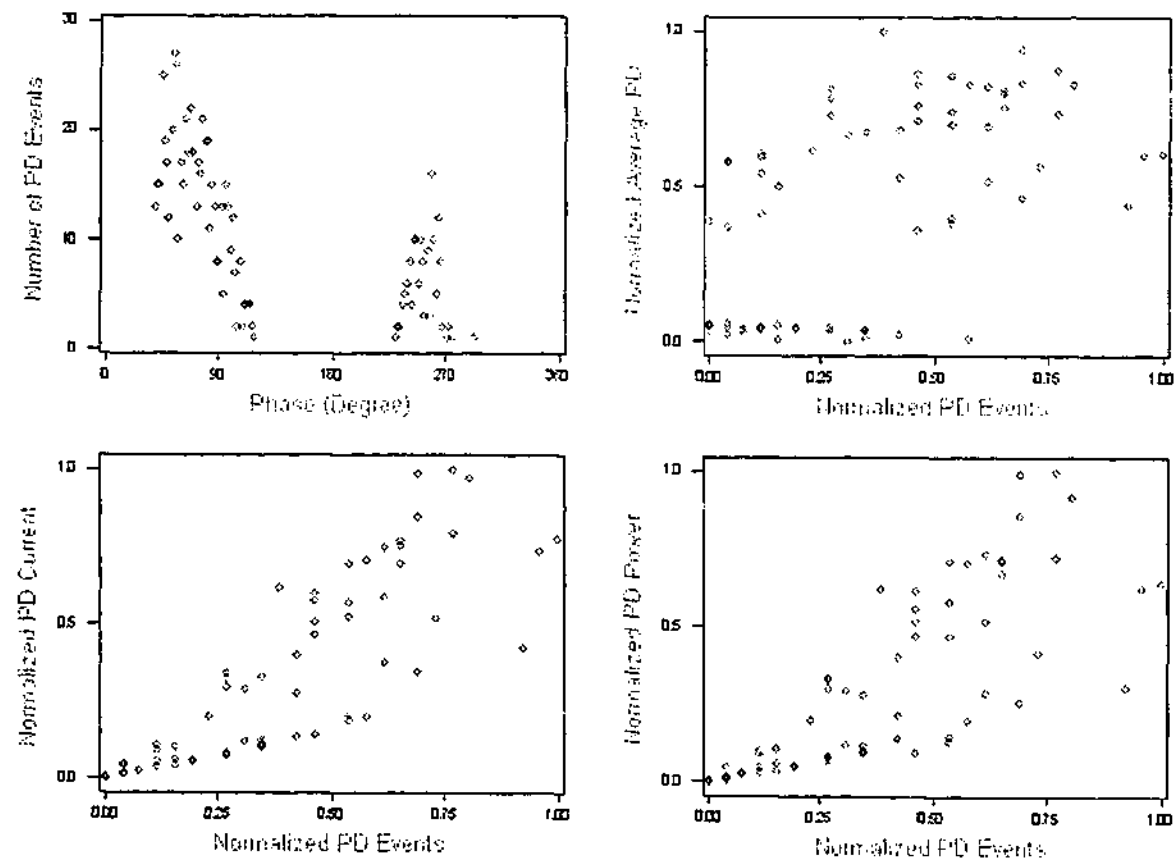
Fig. 3.15 Correlation between other statistics and occurrence of the mylar-film discharge
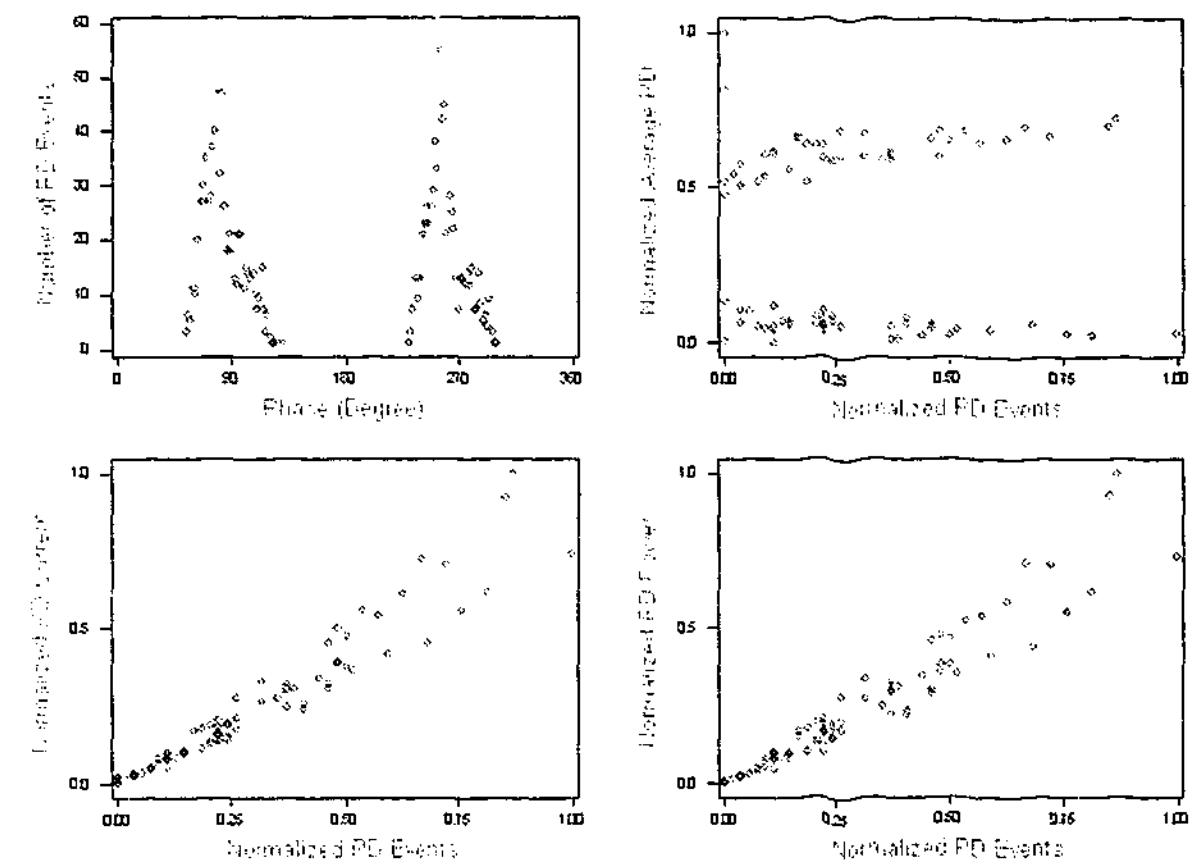
Fig. 3.16 Correlation between other statistics and occurrence of the oiled pressboard discharge

As seen from the above figures, based on PRPD occurrence distribution function, the distribution functions of PD power, average and accumulated charges are different for different defects. Further investigation on PRPD statistics can be performed by observing how these statistics tend to change when test criteria are changed. By comparing the patterns between figure 3.18 and 3.19, it is found that corona discharge is easily separated from pressboard discharge. The reason for such a difference is that negative corona discharges are quite stable in magnitude while pressboard discharges have a high proportional variability in magnitude and have a relative symmetrical distribution between positive and negative discharges. On the other hand, positive and negative corona distribution functions are asymmetrical in terms of magnitude and repetition rate. Therefore, in PRPD partition windows, the tangent of accumulated discharges to the number of events in both positive and negative halves are significantly different. The differences can be clearly seen in figure 3.18. Meanwhile, for the pressboard sample, it is not suitable to use such a tangent line to separate positive and negative discharges due to the physical characteristics of pressboard discharges.
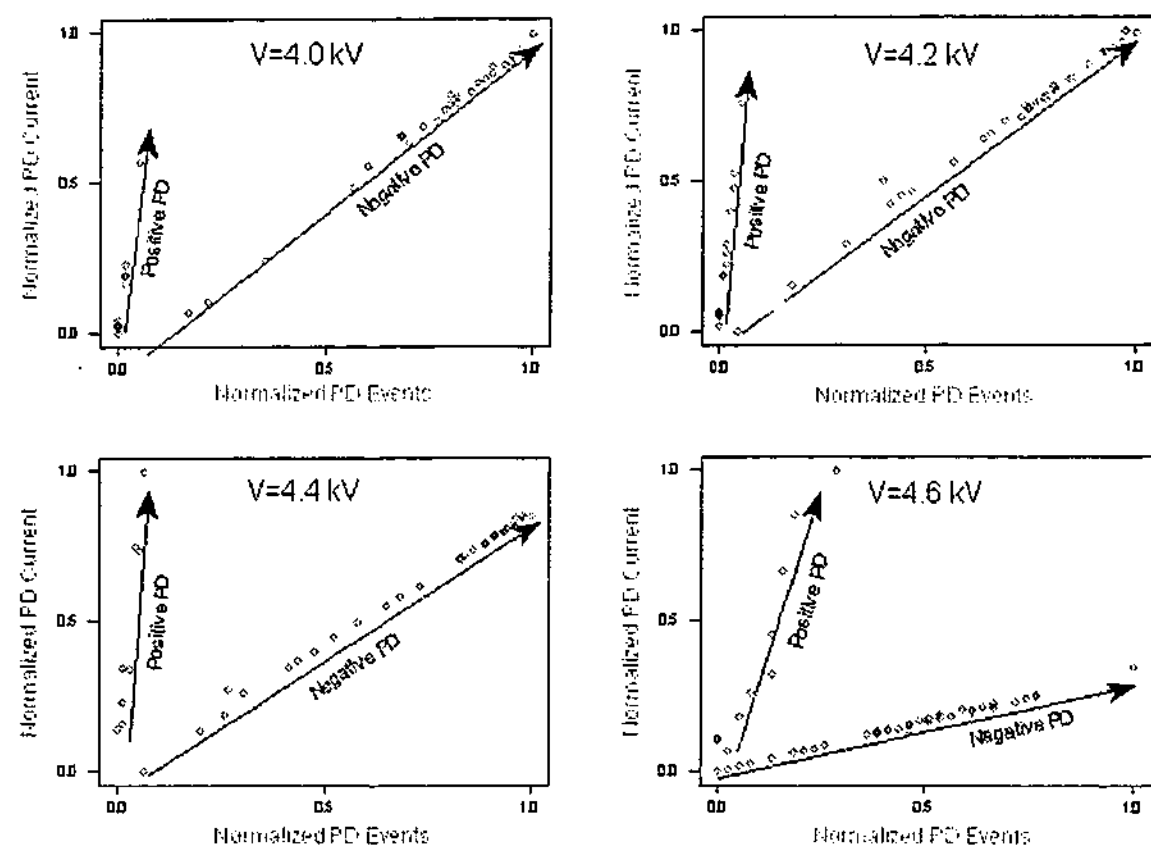
Fig. 3.17 Corona phase partition current vs. partition occurrence
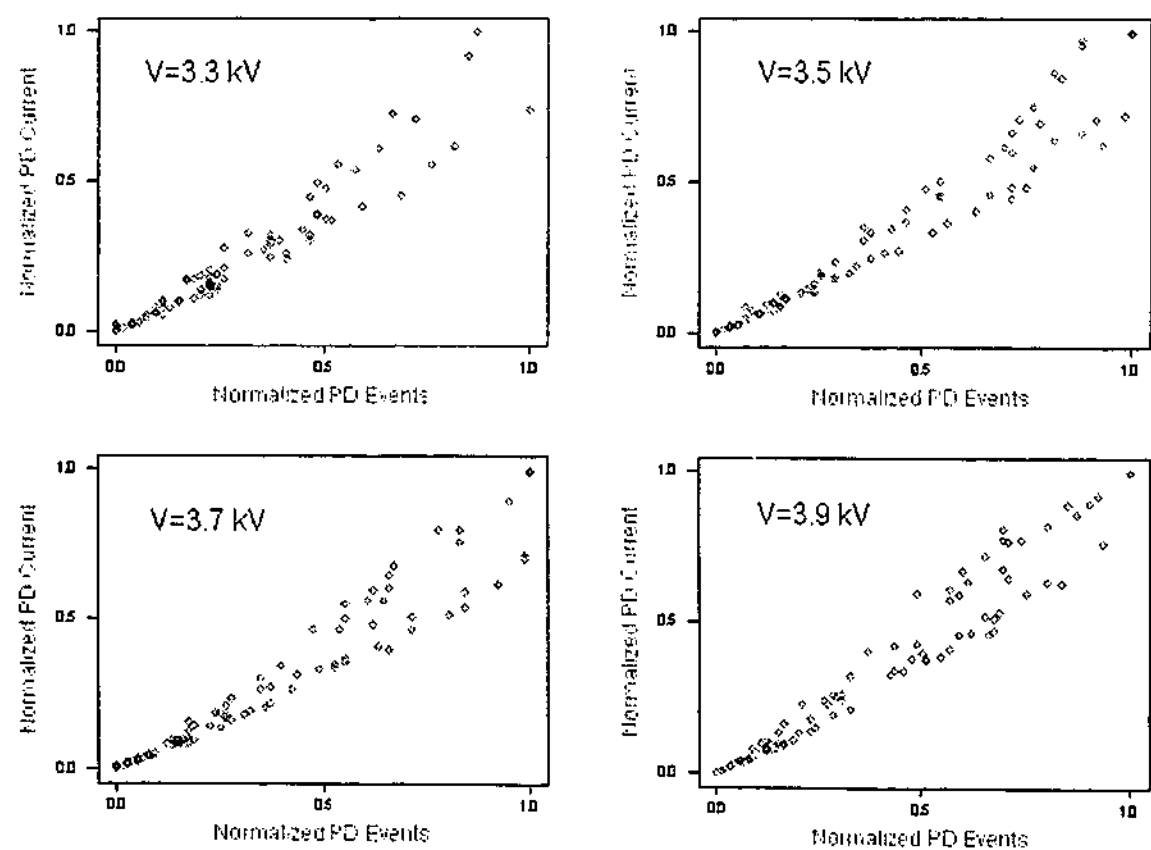
Fig. 3.18 Oil-impregnated pressboard discharge phase partition current vs. partition occurrence
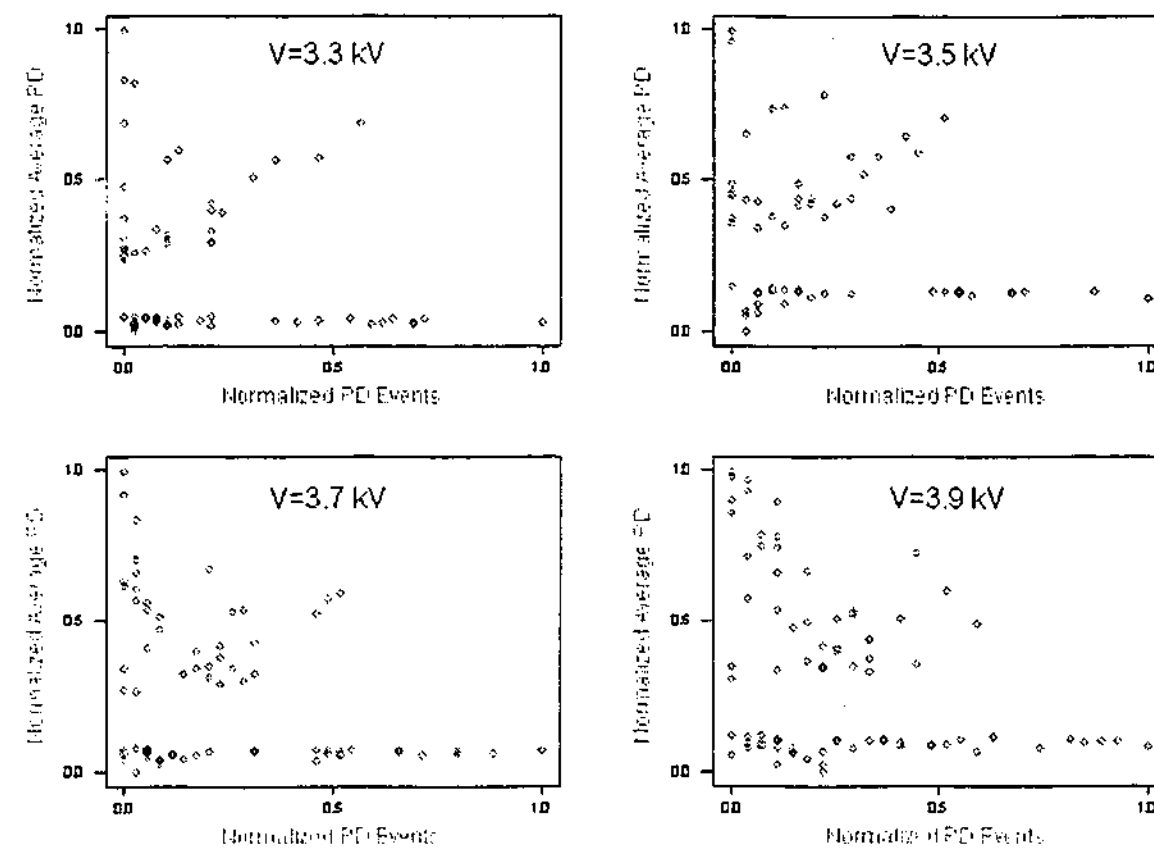
Fig. 3.19 Dry pressboard discharge partition average PD vs. partition occurrence
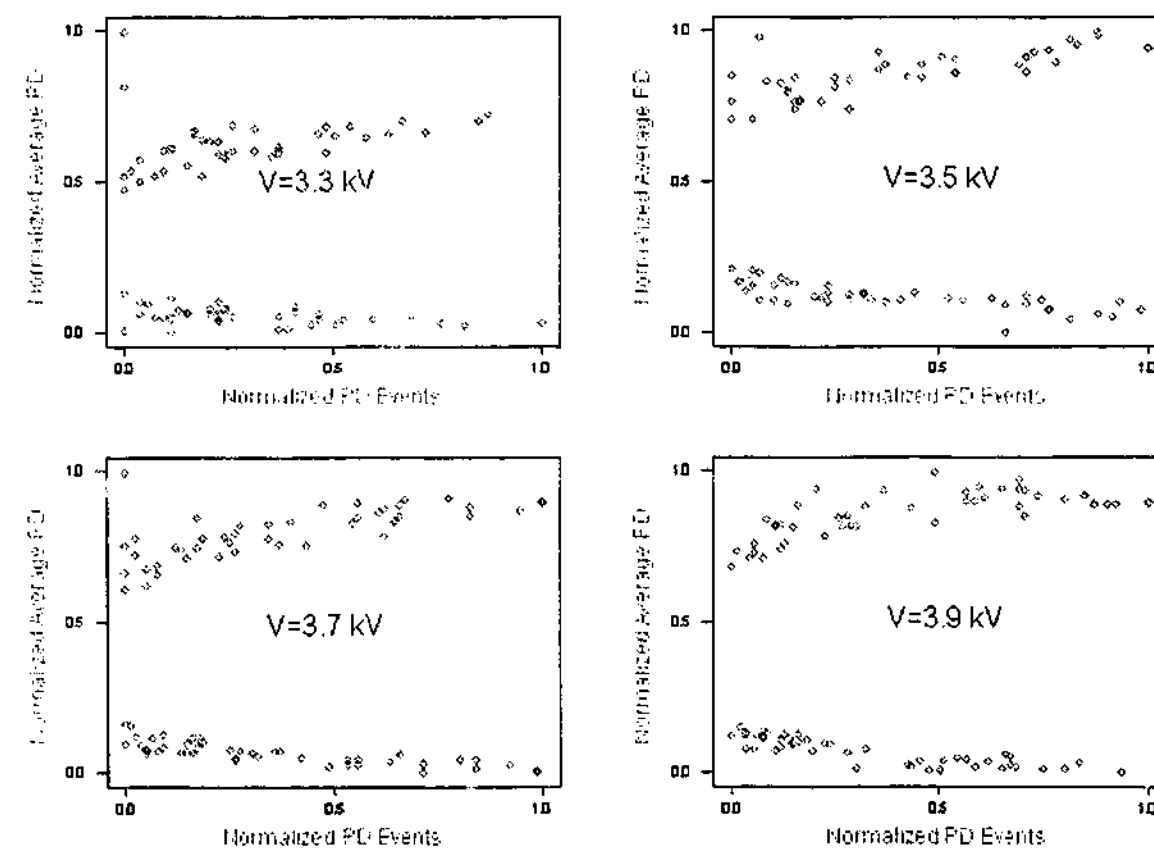
Fig. 3.20 Oil-impregnated pressboard discharge partition average PD vs. partition occurrence

It is possible to characterize oil-impregnated pressboard discharges from the dry pressboard discharges using distribution functions. It has been found in figure 3.19 and 3.20 that the average PD amplitude in PRPD partition windows is quite different for these two discharges. Though in each PRPD partition window, discharges from the oil-impregnated pressboard have a wider range in magnitude, the average magnitude is quite smooth with the increase of the number of PD events. For the dry pressboard, the average discharge magnitude in relation to the number of PD is spread around especially for the positive discharges. With the help of marginal histograms, the mapping of the partition window based statistics in relation to the number of PD events can be visually examined. The mapping diagrams are easily extracted as fingerprints to classify different type of discharge as indicated in figure 3.21.
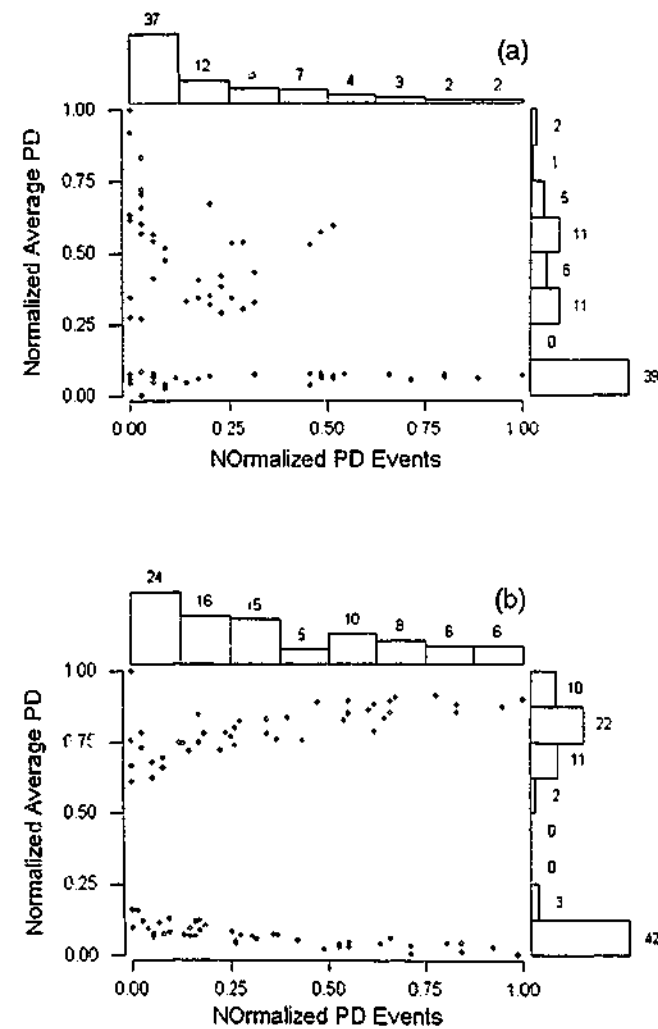

Fig. 3.21 Partition average PD magnitude vs. partition PD occurrence
(a) Dry pressboard (b) Oil-impregnated pressboard

3.6 DOMINANT PARTITION WINDOW ANALYSIS

The dominant partition windows (DPWs) in PRPD distributions may be defined as the PRPD partition windows containing one or more for the largest PD quantities in terms of discharge activity, accumulated charge, and power loss etc. Apparently, DPWs are the most important windows in PRPD distributions. Therefore DPWs can be specially treated and calculated from PRPD distribution functions to characterize a defect because PRPD distribution functions are defect dependent. An observed interesting phenomenon is the phase location of DPWs in both positive and negative half cycles. In PRPD distribution functions, the three important definitions regarding DPWs are listed below:

- The dominant partition window with the largest PD occurrence – DPWn
- The dominant partition window with the largest accumulated PD – DPWq
- The dominant partition window with the largest PD power loss - DPWp

It may be observed that the DPWs may be overlapped in a phase partition window or located in different phase partition window depending on the type of defect and the test criteria.

3.6.1 Partition Window with the Largest PD Occurrence

It has been experienced that phase resolved PD distributions are found susceptible to the degree of geometrically asymmetry of electrodes undergoing discharge. In the current investigation, PRPD distribution functions are summarized and some discharge descriptive statistics are used to interpret the PD distribution along the partition window. PRPD partition window having the most active discharge occurrence is of interest in this investigation due to the phase and pulse-height restricted discharge occurrence being defect dependent. The most active PRPD window is particularly useful to analyze multiple defect discharge samples.

As phase of occurrence distribution exhibits some important properties of defect itself, a detailed analysis performed on PRPD window may be helpful to reveal part of the mechanism of discharge process. The study on PD distribution and particularly on the

statistics of PD distribution within an individual PRPD partition window may uncover some useful information about discharge physical mechanism under ac voltage. As seen in figure 3.11, the dispersion of discharge amplitude is significantly different between discharges from dry and oil-impregnated pressboard samples. Meanwhile PD distribution in individual PRPD window measured from both types of pressboard samples clearly indicates the difference. It may be concluded that PRPD distributions have a complicated ac phase dependence.

Among the dominant partition windows introduced, DPWn is the one selected for further investigation as illustrated in figure 3.22. The position of the dominant partition window may also reveal some information related to the discharge activities in a multiple defect environment.
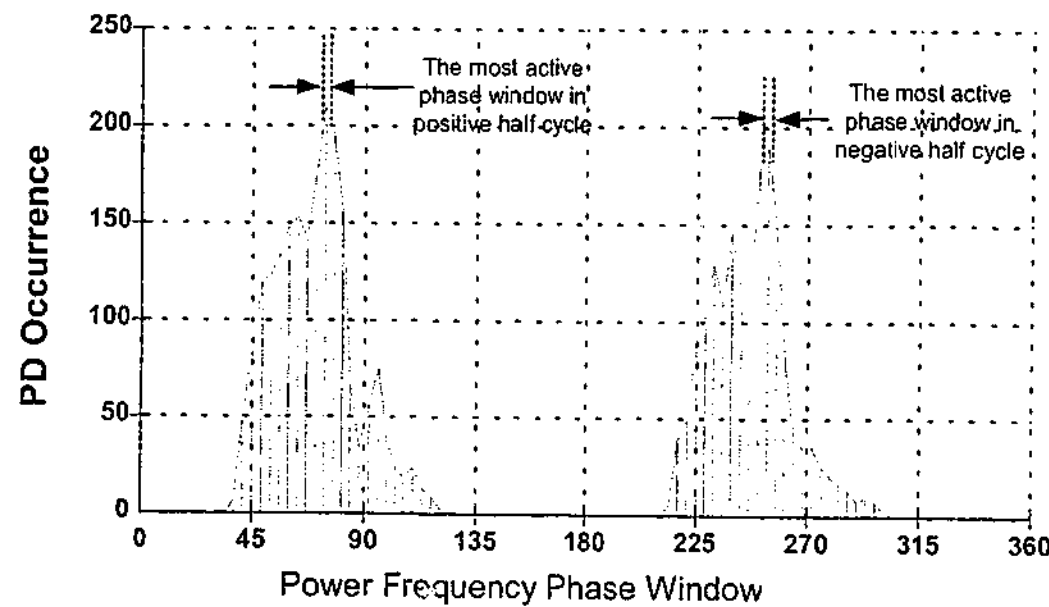
Fig. 3.22 DPWn in positive and negative half cycle

Detailed statistical analysis is performed on DPWn in both positive and negative half cycles. As indicated in figure 3.22, the corresponding descriptive statistics together with a swing range of both arithmetic and geometry mean with 95% confidence applied are shown in figure 3.23(a) and (b) respectively.
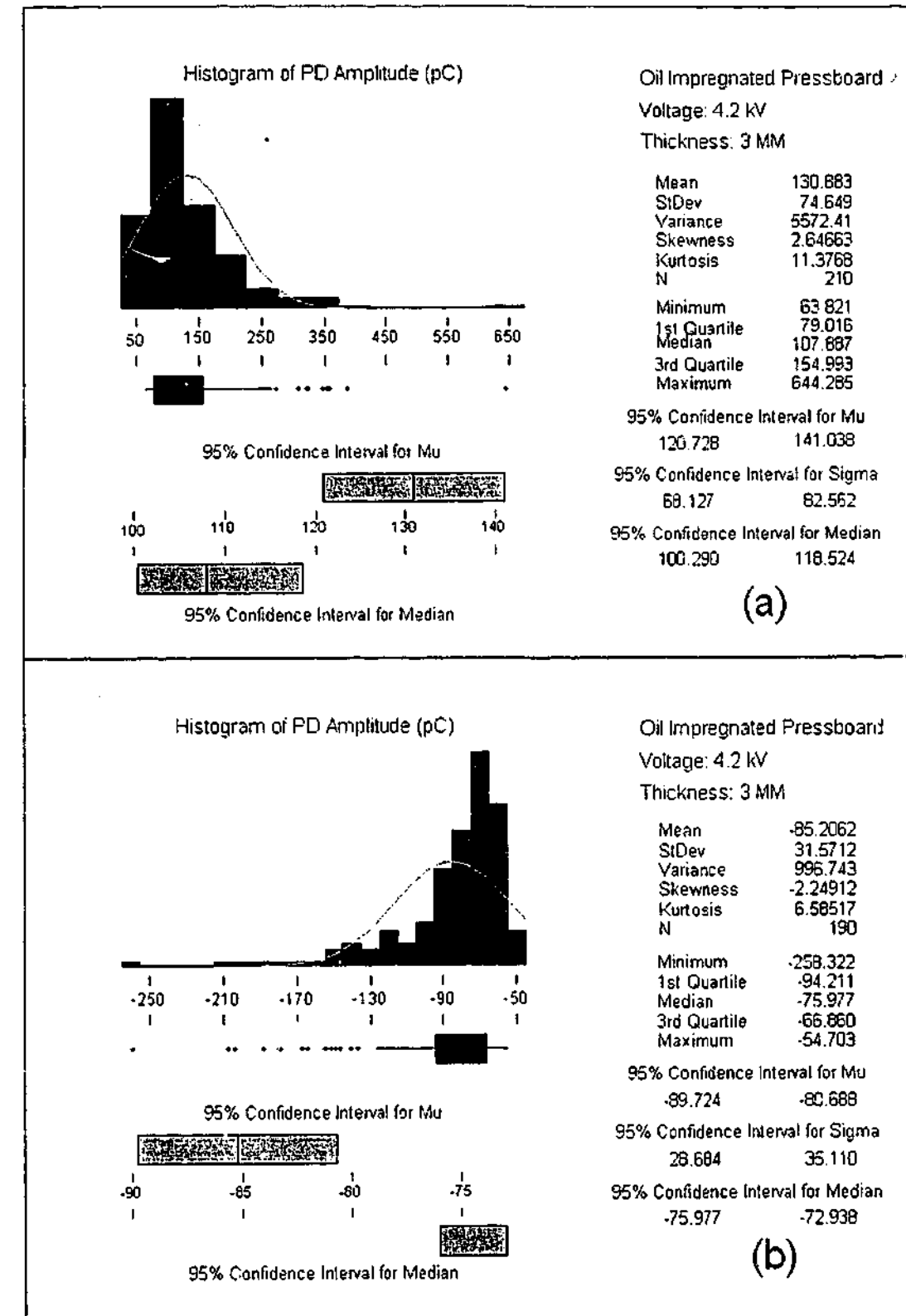
Figure 3.23 Descriptive statistics of DPWn illustrated in figure 10
(a) Distribution of PD within the most active phase partition window in positive half cycle
(b) Distribution of PD within the most active phase partition window in negative half cycle

Under ac voltage, the location and the distribution of PD amplitude within the most active PRPD partition window are dependent on discharge mechanism. The measured results of DPWn from dried and oil-impregnated pressboard samples can be found in figure 3.24 where the DPWn in both positive and negative half cycles are illustrated.
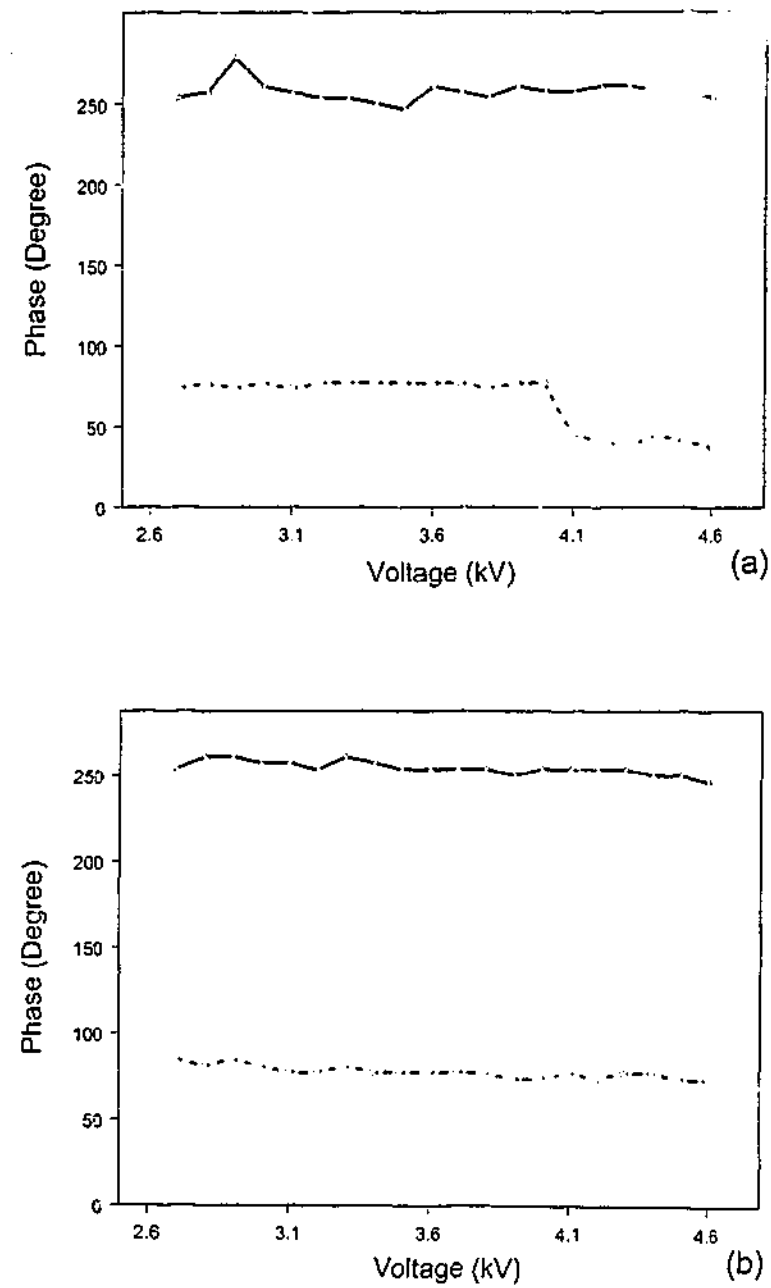
Figure 3.24 Location of DPWn in positive and negative half cycle vary with voltage
Solid line: Positive half cycle   Dashed Line: Negative half cycle
(a) Discharges measured from a dry pressboard sample
(b) Discharges measured from an oil-impregnated pressboard sample

3.6.2   Partition Window with the Largest Accumulated Charge

Since PRPD distributions are defect dependent, some important properties regarding the discharge mechanism can be characterized with the DPWq. The phase location of DPWq against the change of voltage in positive and negative half cycles can be observed from the pressboard discharges shown in figure 3.25.
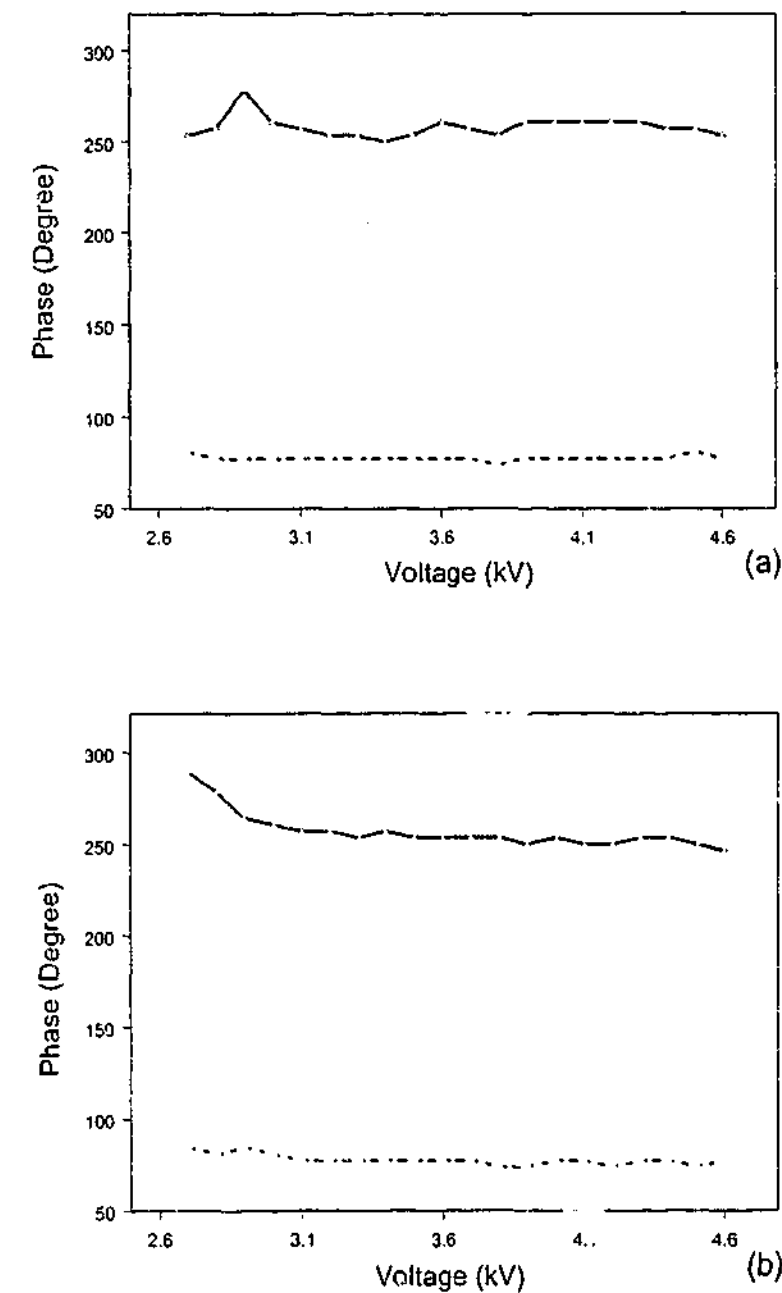
Figure 3.25 Location of DPWq in positive and negative half cycle vary with voltage
Solid line: Positive half cycle   Dashed Line: Negative half cycle
(a) Discharges measured from a dry pressboard sample
(b) Discharges measured from an oil-impregnated pressboard sample

3.6.3 Partition Window with the Largest PD Power

Along with DPWn and DPWq, DPWp has important features about the discharge power loss. The measured results from the pressboard samples are shown in figure 3.26.
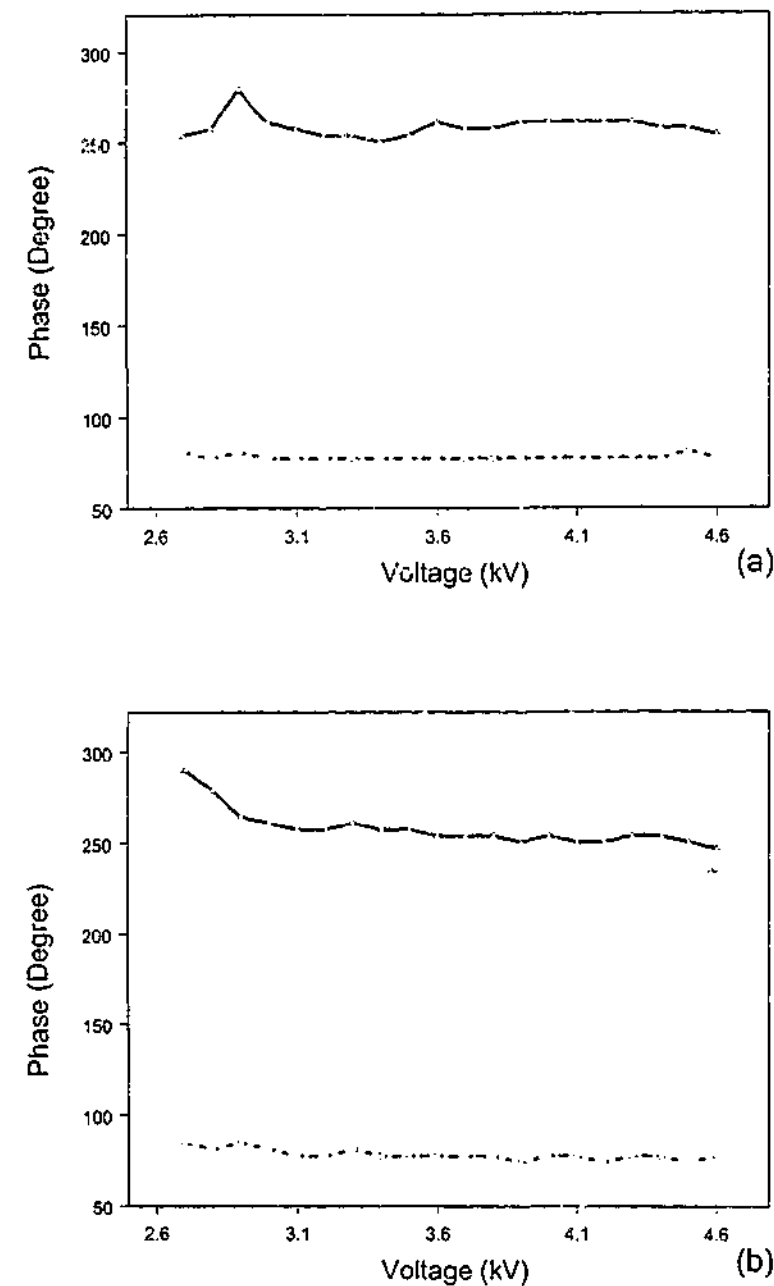
Fig. 3.26 Location of DPWp in positive and negative half cycle vary with voltage
Solid line: Positive half cycle   Dashed Line: Negative half cycle
(a) Discharges measured from a dry pressboard sample
(b) Discharges measured from an oil-impregnated pressboard sample

It can be observed that DPWq and DPWp are very similar both in positive and negative half cycles. The DPWn of both positive and negative half cycle are illustrated in figure 3.27 where the measurement results from pressboard are presented for comparison. It is quite obvious that for the oil-impregnated pressboard, the symmetry of positive and negative half cycle is better than that of the dry pressboard. In the positive half cycle, the DPWn of the oil-impregnated pressboard is sustainable with the increase of voltage. The initial volatility is due to the voltage being not high enough to produce stable phase position of DPWn. As can be observed from figure 3.27(a), that the DPWn observed from the pattern of dry pressboard drops suddenly after the voltage reaching to 4 kV. In contrast, the most active phase partition window observed from the pattern of oil-impregnated pressboard has a relative stable position.

The arithmetic mean and its dispersion of discharge amplitude in DPWn of both positive and negative half cycles are calculated with the increase of voltage. The results from the pressboard samples are shown in figure 3.28 and 3.29 respectively. The distinguishable features can be observed in these figures. Obviously, the statistics measured from the dry pressboard has a peak over the test voltage and this phenomenon is associated with the sudden change of DPWn position when voltage increased to above 4 kV. As seen in figure 3.28(a), discharge activities gradually build up in the DPWn with an increase of the voltage to a certain level. On the other hand, discharge activity of the DPWn drops back when the voltage further increased. The results from the quantitative analysis of DPWn can be used to distinguish dry and oil pressboard without much effort. The quantitative results of DPWn as illustrated in figure 3.28 and 3.29, are valuable to associate measurable distribution patterns with the discharge physical mechanisms.
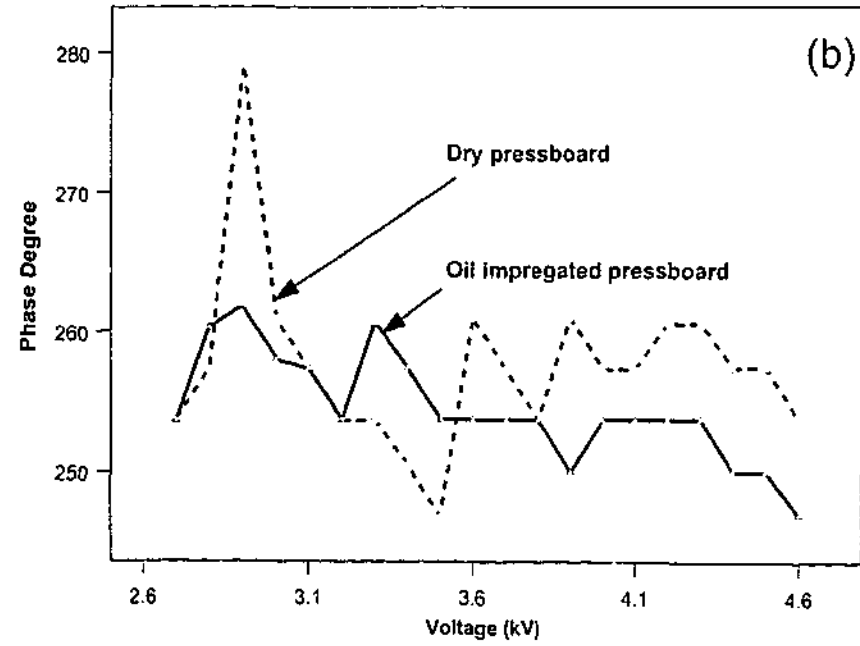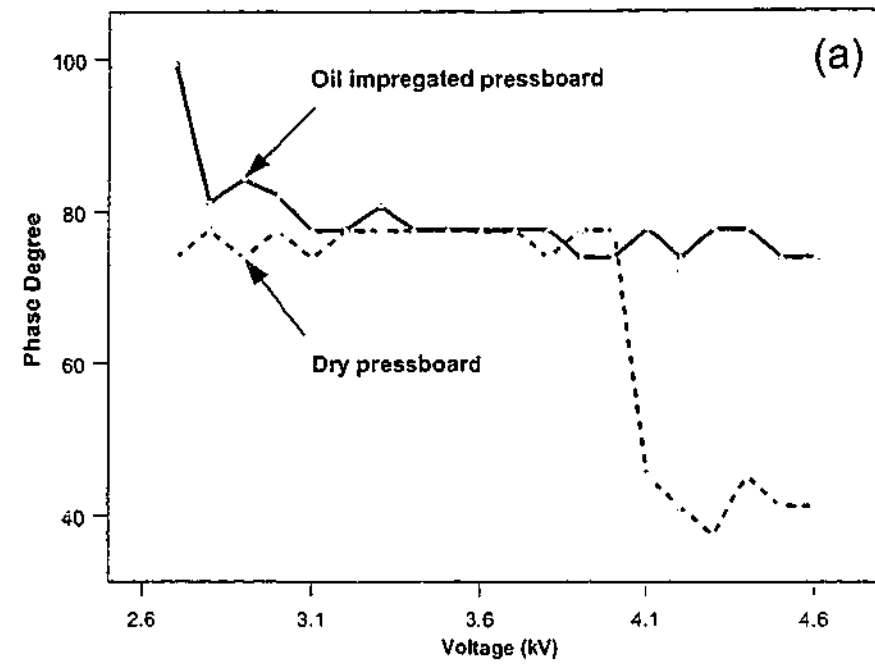
Figure 3.27 The most active phase partition window in a phase restricted distribution vs. ac voltage
(a) Phase position in the positive half cycle
(b) Phase position in the negative half cycle
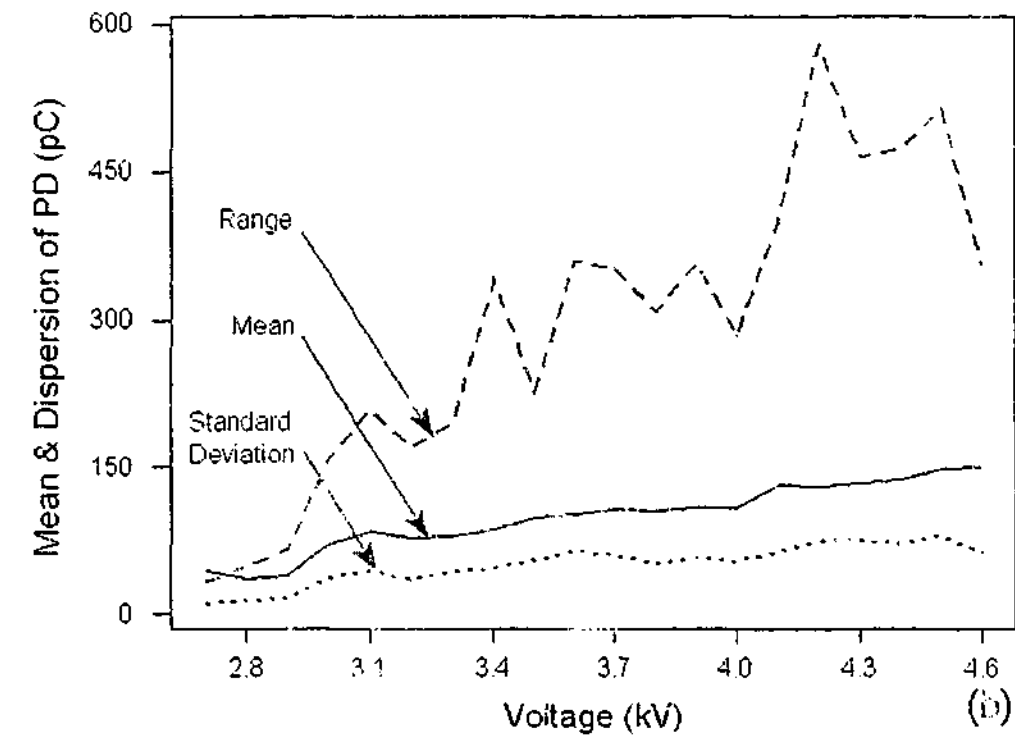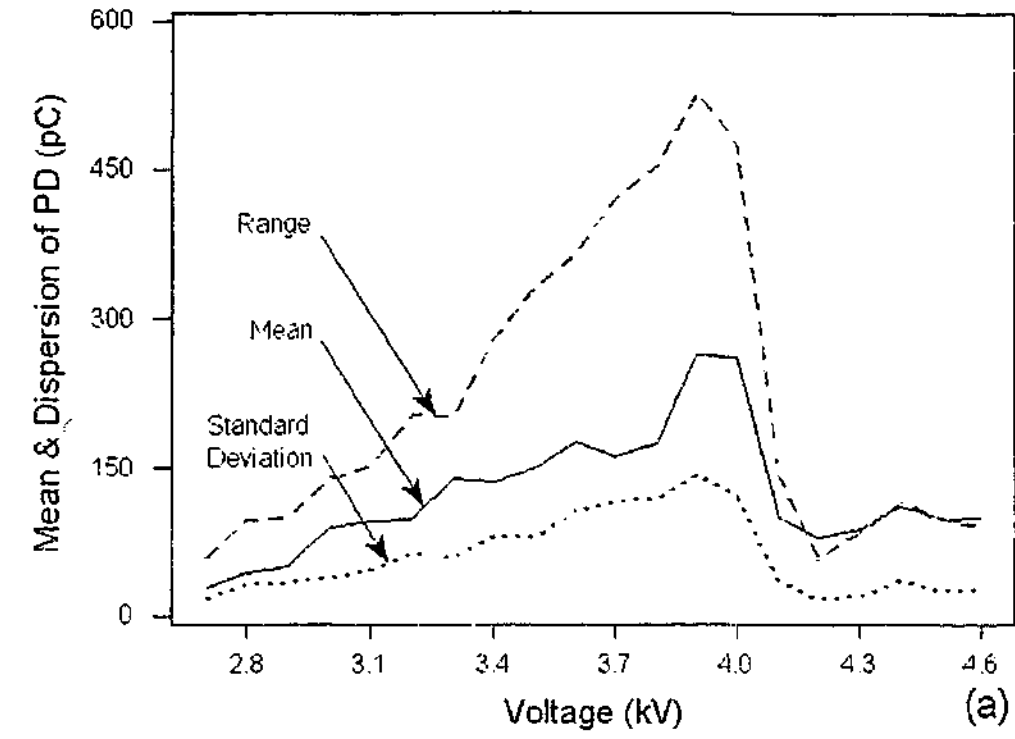
Figure 3.28 Arithmetic mean and dispersion of positive PDs in DPWn vary with voltage
(a) Results from a dry pressboard sample
(b) Results from an oil-impregnated pressboard sample
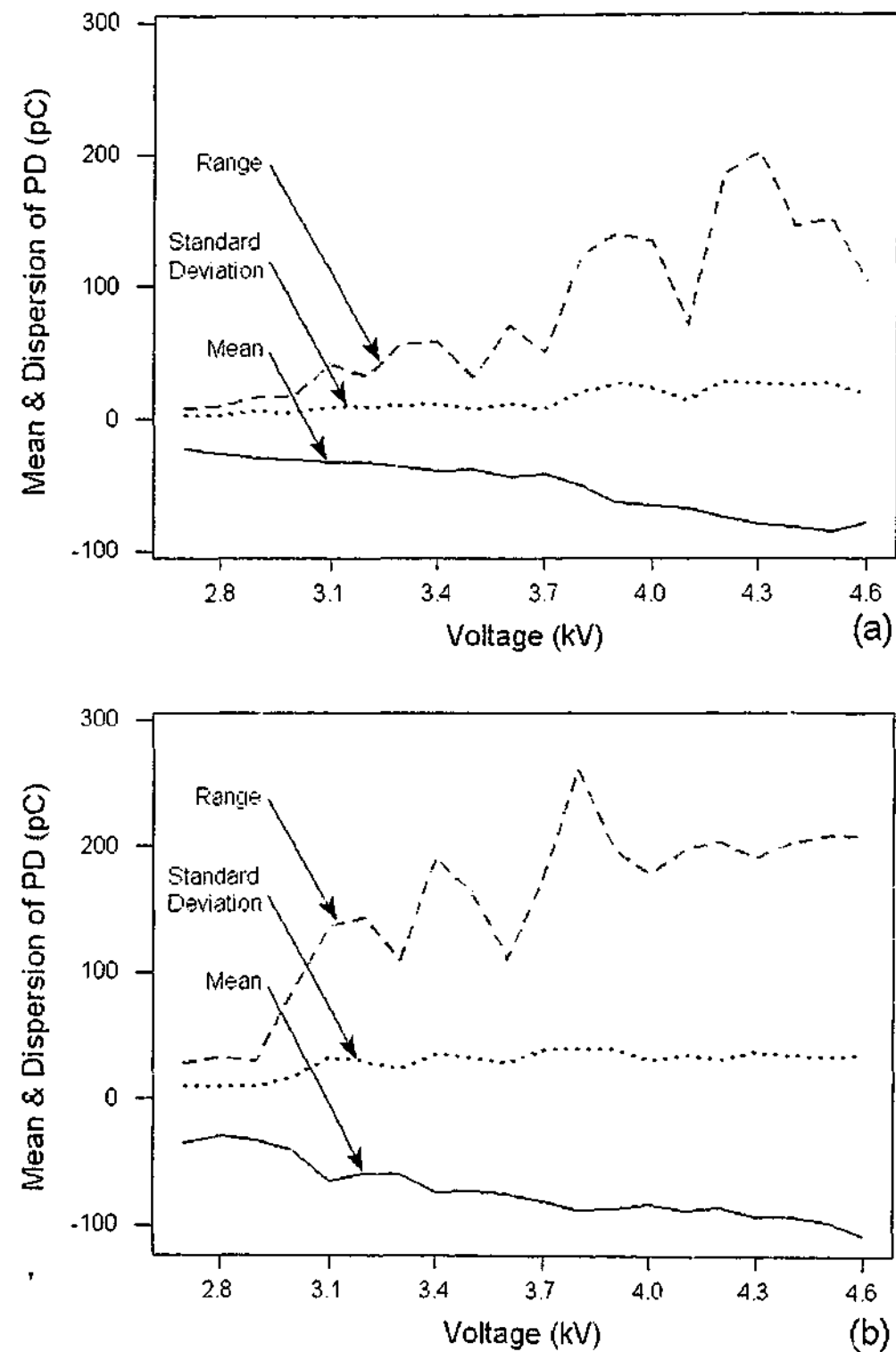
Figure 3.29 Arithmetic mean and dispersion of negative PDs in DPWn vary with voltage
(a) Results from a dry pressboard sample
(b) Results from an oil-impregnated pressboard sample

86

3.7 CONCLUDING REMARKS

With PRPD analysis, distribution functions are derived in relation to the sinusoidal applied voltage and PRPD partition quantities are also calculated over the phase partition window. In this chapter, conventional PRPD distribution functions are summarized in conjunction with the introduction of novel PRPD distribution functions such as PD power loss $P_\varphi(i)$ and quadratic rate $Q_\varphi(i)$, where i is the index of PRPD window. Within PDD system, PRPD feature quantities of various distribution functions and other discharge statistics are calculated. The distribution functions are very complicated and they are correlated with the PD occurrence distribution function. Feature quantities that calculated from PRPD patterns can be directly exported to form part of the PD fingerprints used in chapter 7.

In addition, PRPD distribution function can be applied to analyze discharge phenomena. As an example illustrated in this chapter, the pressboard discharge samples that contain multiple defect voids are used for PRPD analysis. Usually, the difficulty is encountered when more than one defect appeared in the sample especially when their inception levels are close. In fact, it is difficult to analyze the multiple discharge phenomena from only conventional PRPD distribution patterns though PRPD distribution functions can help to quantity PD activity under ac voltage. However, a novel method to tackle this problem is to use the dominant partition window analysis. DPWn provides information regarding the most active PD occurrence at or around particular ac phase. Meanwhile DPWq and DPWp provide ac phase positions where the largest accumulated charge and power occur. For pressboard discharges, the results show the variation of DPWs against applied voltage, the latter being the major factor in initiating a new discharge and causing deterioration in existing defects. Figure 3.28(a) shows that a sudden shift of DPWn occurred in the negative half cycle of the dry pressboard discharge. It probably initiates a new discharge at around 4 kV in the highly water contaminated pressboard. Meanwhile this new discharge initiation phenomenon can not be found in either DPWq or DPWp diagrams because the accumulated charge and the power dissipated from the new initiated discharge are not in the dominant position.

Though PRPD distribution functions and their derived feature quantities are useful to analyze discharges, they do not contain sufficient information to describe details of discharge physical processes [74, 75]. For example, it is found that some PRPD feature quantities vary significantly with changes in the location and geometry of a defect void [76, 77]. Therefore, there is still a demand to make use of other distribution functions where new independent variables are employed instead of phase partition window to analyze discharge and to calculate new feature quantities.

Chapter 4

New Techniques for Pulse-height Resolved Partial Discharge Pattern Analysis

In chapter 3, distribution functions of PRPD distribution category are investigated in some detail with the introduction of new distribution functions. PRPD partition window based statistical analysis is use to study the relationship between other distribution functions and the occurrence distribution function. Also the dominant window analysis method has been introduced and performed on samples of pressboard discharges. In this chapter, discharge functions of pulse-height distribution category will be studied.

With pulse-height PD (PHPD) pattern analysis, the entire resolution space (9 bit) is equally divided into 200 pulse-height partition windows in which partition statistics are calculated. PD distributions in the $i-1^{th}$ and i^{th} pulse-height partition window are illustrated in figure 4.1. Partition quantities of applied voltage and phase angle are calculated based on pulse distribution in the PHPD partition window. The feature quantities can be calculated from distribution functions and compressed distribution information exported to a file with text-delimited format for further analysis.
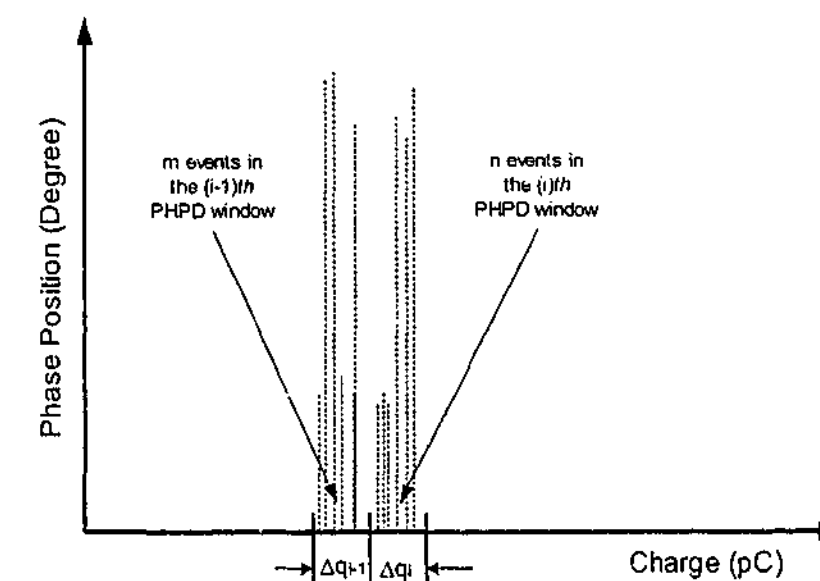

Fig. 4.1 Discharge phase angle distribution in the $i-1^{th}$ and i^{th} pulse-height windows

4.1 REVIEW OF PHPD PATTERN ANALYSIS

Like many of the great advances made in the PD measuring technology, the stochastic analysis of PHPD distributions has been used to provide information on the evolution of PD phenomena. Along with the improvement of cumulative PD pulse-counting measuring techniques, a pulse-height analyzer was initially designed for corona discharge studies [22]. Pulse height distribution was found to be useful for the analysis of the relationship between induced apparent charge and other PD related statistics.

Likewise, PHPD pattern analysis is based on the fact that pulsating discharges are complex stochastic processes and PD pulse-height is an important variable. It actually is one of the most important techniques employed in the evaluation of the insulation system. With PHPD pattern analysis, some encouraging results have been obtained in the study of PD degradation processes during aging [85- 87]. The advantage of such an approach is that distributions of partition quantity are directly associated with the magnitude of discharge pulses.

The primary concern for PD source recognition is the effectiveness and the significance of derived quantities used to assess the condition of the insulation system. Among the techniques for PD pattern recognition, those resorting to the stochastic analysis of pulse-height and phase resolved distributions are being investigated in order to extract information regarding the types of defects as well as their correlation with the insulation aging and the estimated remnant life of insulating systems.

Among distribution functions of various categories, the stochastic analysis of pulse-height PD (PHPD) distribution functions has been investigated in order to find information on the evolution of PD phenomena during the aging process. The distribution function of discharge events as a function of discharge amplitude partition window has been widely used to analyze discharges. PD data are processed based on the two and five parameter Weibull functions. A technique combined with a non-parametric regression and a mixed Weibull function model has also been used to detect the presence of simultaneous multi-PD phenomena [85].

The Weibull probability function has been applied to the occurrence pulse-height distribution in order to separate multi-PD sources [78-80]. It shows that different PD sources can be identified on the basis of the shape parameters of the Weibull distribution, but the two-parameter Weibull function is limited on multi-PD source identification. The shortcoming has been partly overcome by employing the 5-parameter Weibull function, which allows the separation of PD source in multi-PD testing environment under certain circumstances. The results show that PHPD occurrence measured on a single type of defect generally fits straight lines in the Weibull plot. For more than one type of defect, one or more curvatures can possibly be observed [93-96].

4.2 PHPD DISTRIBUTION FUNCTION

Similar to PRPD pattern analysis, there are many pulse-height distribution functions that are important and worthwhile to observe in detail. The distribution functions of interest are PD occurrence, average and maximum voltage, PD current, power and quadratic rate etc.

Discharge occurrence is an important distribution function describing the probability of PD events on PHPD partition window. If $p_1(\lambda \mid q_\lambda \in \Delta q_i)$ is the probability that a PD event λ having amplitude q_λ between q_i and $q_i + dq_i$, the PD occurrence distribution function in the i*th* window may be defined as:

$$f_q(i) = N \bullet p_1(\lambda \mid q_\lambda \in \Delta q_i) \qquad (4.1)$$

where N is the total number of PD events acquired in a measurement and i is the PHPD partition window index.

PHPD average distribution function describes the distribution of average applied voltage when a PD occurs. It is defined as:

$$A_q(i) = \frac{\sum(V_\lambda \mid q_\lambda \in \Delta q_i)}{N \bullet p_1(\lambda \mid q_\lambda \in \Delta q_i)} \qquad (4.2)$$

where $p_1(\lambda \mid q_\lambda \in \Delta q_i) > 0$ otherwise $A_q(i) = 0$, and $V_\lambda \mid q_\lambda \in \Delta q_i$ is the voltage when a discharge event λ occurs under the given condition that PD amplitude is in the ith PHPD partition window $\Delta q_i = q_{i+1} - q_i$.

PHPD maximum distribution function represents the distribution of the absolute value of applied voltage when a PD occurs. It is defined as:

$$M_q(i) = \max(V_\lambda \mid q_\lambda \in \Delta q_i), \text{ when } q_\lambda > 0 \qquad (4.3a)$$

or

$$M_q(i) = \min(V_\lambda \mid q_\lambda \in \Delta q_i), \text{ when } q_\lambda < 0 \qquad (4.3b)$$

PHPD current distribution function stands for the distribution of PD current and is defined as:

$$I_q(i) = \frac{\sum(q_\lambda \mid q_\lambda \in \Delta q_i)}{t} \qquad (4.4)$$

where t is the total time for acquiring the PD data.

PHPD power loss distribution function exhibits the distribution of PD current and is defined as:

$$P_q(i) = \frac{\sum(q_\lambda \bullet V_\lambda \mid q_\lambda \in \Delta q_i)}{t} \qquad (4.5)$$

The last PHPD distribution function implemented in PDD system to analyze PHPD distributions is the PD amplitude quadratic rate and it is defined as:

$$Q_q(i) = \frac{\sum(q_\lambda{}^2 \mid q_\lambda \in \Delta q_i)}{t} \qquad (4.6)$$

4.3 OCCURRENCE DISTRIBUTION FUNCTION

The distribution function of PHPD occurrence is the most popular one used in pattern analysis because it provides information about how PD events are distributed on different PD magnitude level with or without considering pulse polarity. The statistical nature of PD phenomena can be taken into account by observing such a distribution of PD activities. The distribution functions of PHPD occurrence measured from different types of defect are shown in figure 4.2 in which distribution of PD activities in both positive and negative halves can be visually compared. Obviously, with the help of figure 4.2, the degree of asymmetry of PD activities can be easily examined and even quantified if appropriate algorithms are applied.
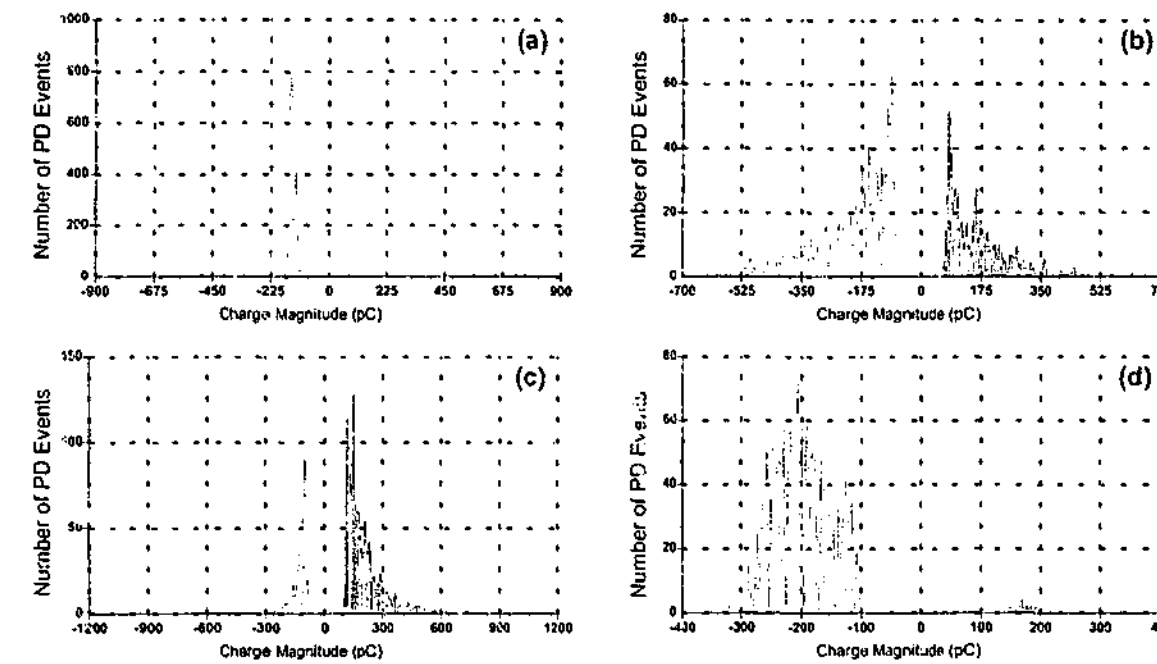
Fig. 4.2 Pulse-height of occurrence distribution functions (with polarity) measured from
(a) a point-to-plane corona
(b) a point-to-dielectric discharge
(c) an oil-impregnated pressboard discharge
(d) an epoxy resin stator bar with an artificial defect inside

Regardless of the polarity, the distribution functions of PD activity at different PD amplitude can also be drawn on the host PC screen of PDD system as shown in figure 4.3. The degree of symmetry between positive and negative halves can not be investigated in this case. With this approach, the interest is restricted to learning the distribution of PD activity at different PD amplitude.

At the time of writing, the type of occurrence pattern, not considering pulse polarity, has been widely used in PD pattern analysis as well as in diagnosing insulation condition of HV apparatus by other researchers [88-91]. The distribution that considers pulse polarity is a new distribution function in which the positive and negative pulses of a measurement are treated separately. One clear benefit for using such a distribution is its self-evident feature that demonstrates PD activities of both polarities. It is also useful to calculate PHPD feature quantities from this kind of pattern. For example, a correlation coefficient may be calculated between a PRPD distribution function and the corresponding PHPD distribution function. Both types of pulse-height of occurrence distribution functions are implemented in PDD system.
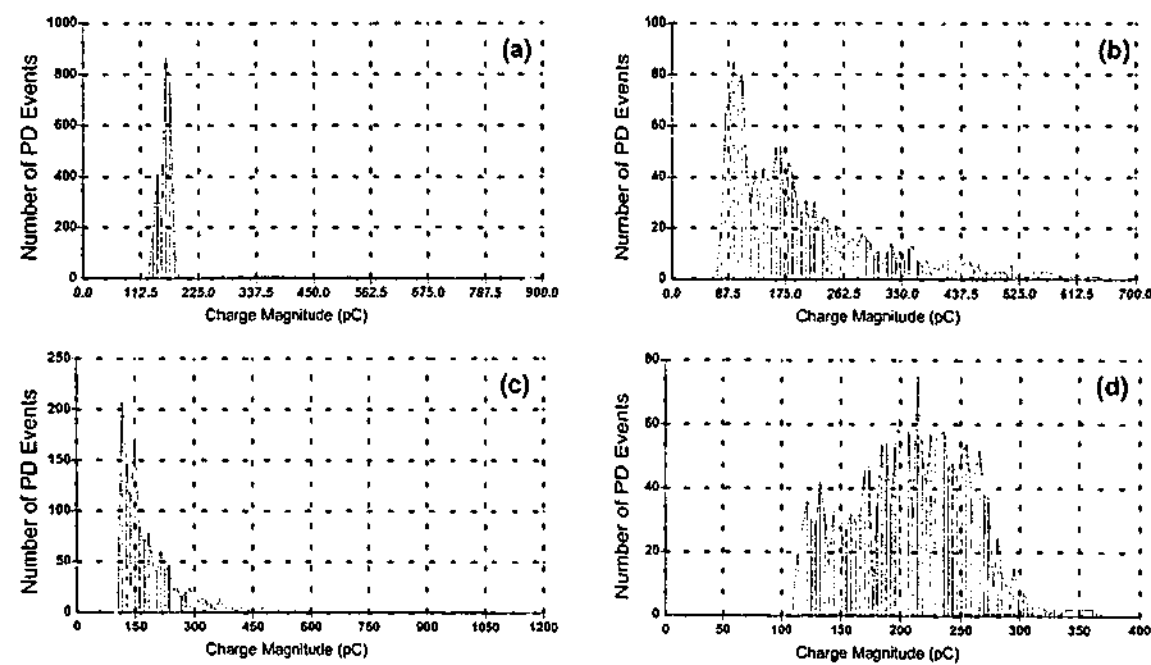

Fig. 4.3 Pulse-height of occurrence distribution functions (without polarity) measured from
(a) a point-to-plane corona
(b) a point-to-dielectric discharge
(c) an oil-impregnated pressboard discharge
(d) an epoxy resin stator bar with an artificial defect inside

4.4 NEW PHPD DISTRIBUTION FUNCTION

The distribution function of pulse-height-of-occurrence is informative because it contains information in regard to discharge physical mechanism [21, 22]. Further processing the distribution function data may help to quantify the degree of insulation degradation as well as identify the type of discharges.

However, it may not be possible to obtain enough information about the discharge physical process if PD amplitude of occurrence is the only distribution function being considered. In addition to the occurrence distribution function, more distribution information regarding the nature of discharge may be disclosed if other distribution functions are included in the study. In the PDD system, distribution functions of average and maximum applied voltage as well as relevant phase location are implemented for PD pattern analysis.

4.4.1 Average Voltage Distribution Function

Discharge initiation and development will occur in a weak spot of insulation because of external voltage. Therefore, it is meaningful to analyze the distribution of average applied voltage at different PD magnitudes. Geometrically, the distribution is related to the discharge physical process inside insulation defect because it provides statistical information relating to the average voltage when PD occurs in a partition window representing PD magnitude level and its polarity. Apparently, this distribution is not independent. It is actually related to the distribution of pulse-height of occurrence (see above). After both distributions are studied together, more information can be extracted to represent discharge physical process. Figure 4.4 has shown the distribution functions of applied voltage measured from different types of defect.
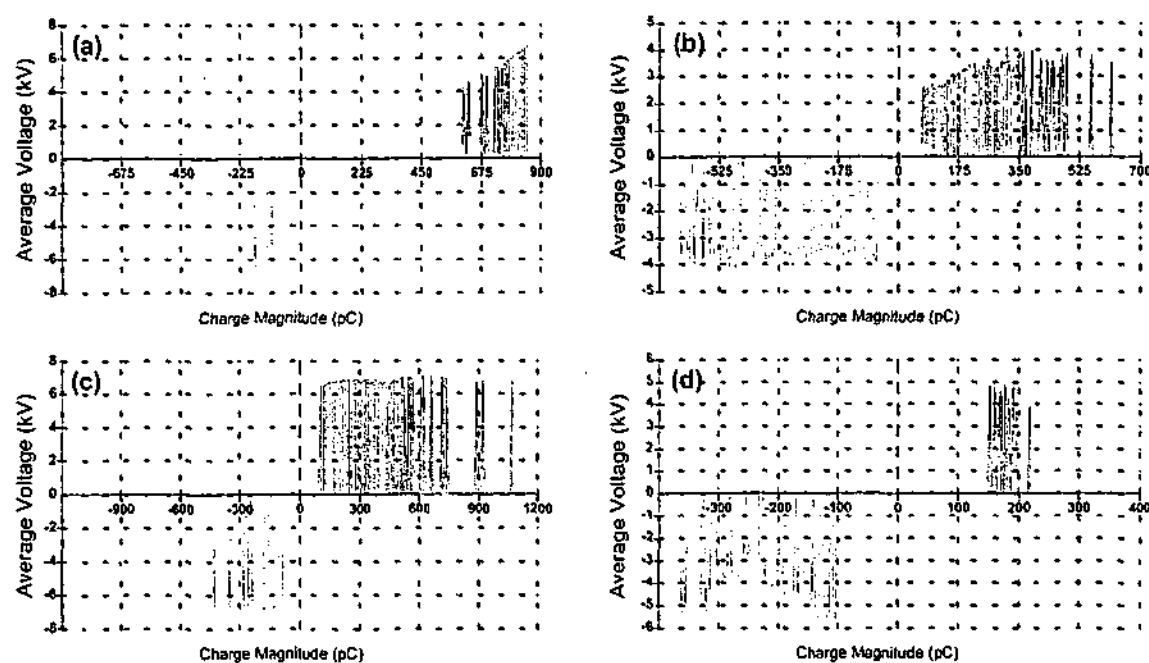
Fig. 4.4 Average voltage distribution functions measured from
(a) a point-to-plane corona
(b) a point-to-dielectric discharge
(c) an oil-impregnated pressboard discharge
(d) an epoxy resin stator bar with an artificial defect inside

4.4.2 Maximum Voltage Distribution Function

Statistically, it is of utmost importantance to find a discharge that has the maximum amplitude under the same applied voltage during the test period. Conversely, it is also important to learn the maximum applied voltage causing a discharge event having the same magnitude. Therefore, the maximum voltage distribution function is a measure for PD pattern analysis. The maximum voltage distribution functions of different types of defect are illustrated in figure 4.5. It demonstrates patterns measured from point-to-plane and point-to-dielectric discharges as well as discharges measured from an oil-impregnated pressboard sample and a turbine generator stator bar with an artificial defect.
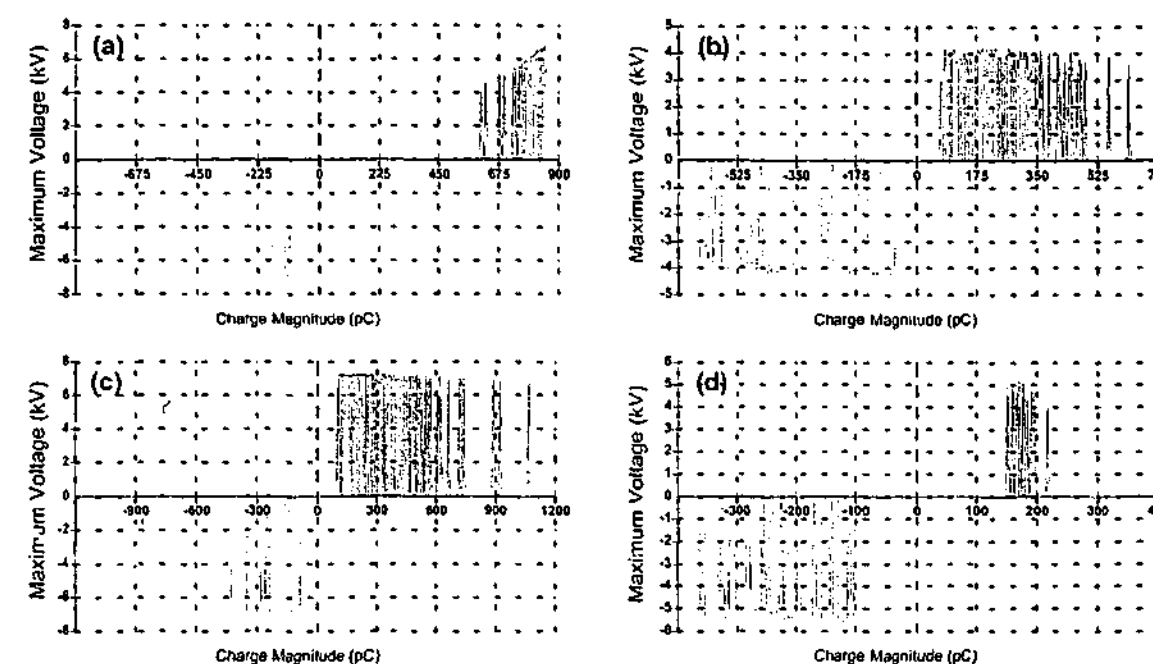
Fig. 4.5 Distribution functions of maximum voltage measured from
(a) a point-to-plane corona
(b) a point-to-dielectric discharge
(c) an oil-impregnated pressboard discharge
(d) an epoxy resin stator bar with an artificial defect inside

4.4.3 Distribution Function of Discharge Current

The importance of average and maximum voltage distribution functions has been previously discussed. Another important distribution function to characterize PD physical process is the distribution of accumulated charge at different PD magnitude. The PD current is actually directly related to the accumulated charge. The partition quantity of discharge current within a partition window is calculated as the sum of individual charge occurring in the partition window during a reference time interval divided by the time interval, as seen in equation 4.5. The distribution functions of discharge current measured from different types of defect are depicted in the following figure 4.6. Obviously, it is a measure of the allocation of accumulated discharge against the partition window representing PD magnitude and polarity.
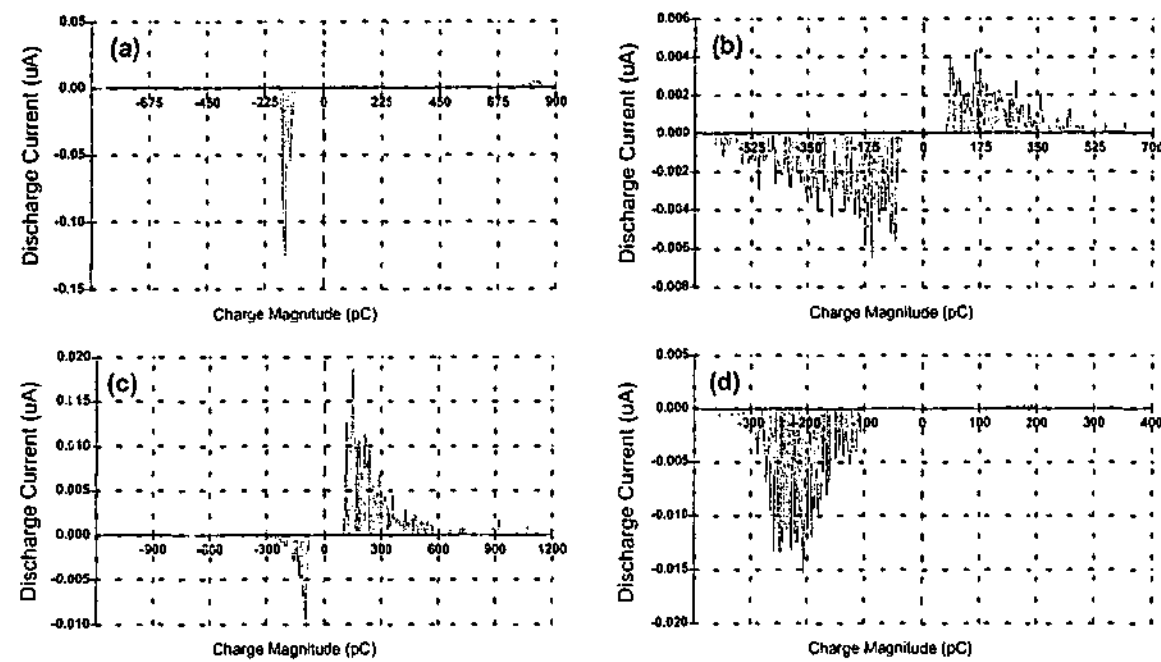
Fig. 4.6 Distribution functions of discharge current measured from
(a) a point-to-plane corona
(b) a point-to-dielectric discharge
(c) an oil-impregnated pressboard discharge
(d) an epoxy resin stator bar with an artificial defect inside

4.4.4 Distribution Function of Discharge Power

Like occurrence, average and maximum voltage distribution functions, distribution function of discharge power loss denotes the energy impact of the insulation defect. It is an important measure to characterize PD physical mechanism because the basic PD pulse energy contains information not only related to the PD amplitude but also related to the voltage under which discharge occurs. The PD power in a partition window can be calculated as the sum of individual PD energy that occurred in the partition window divided by the reference time interval. The detail of the calculation can be referred to equation 4.6. The distribution function is implemented in the PDD system to analyze PD phenomena as well as to extract feature quantities for PD pattern recognition. The distribution functions of PD power measured from various defects are shown in figure 4.7. In addition, this distribution function provides unique information relating to PD energy impact on the insulation system under test. It may be used in conjunction with other PHPD distribution functions or even distribution functions of other distribution categories.
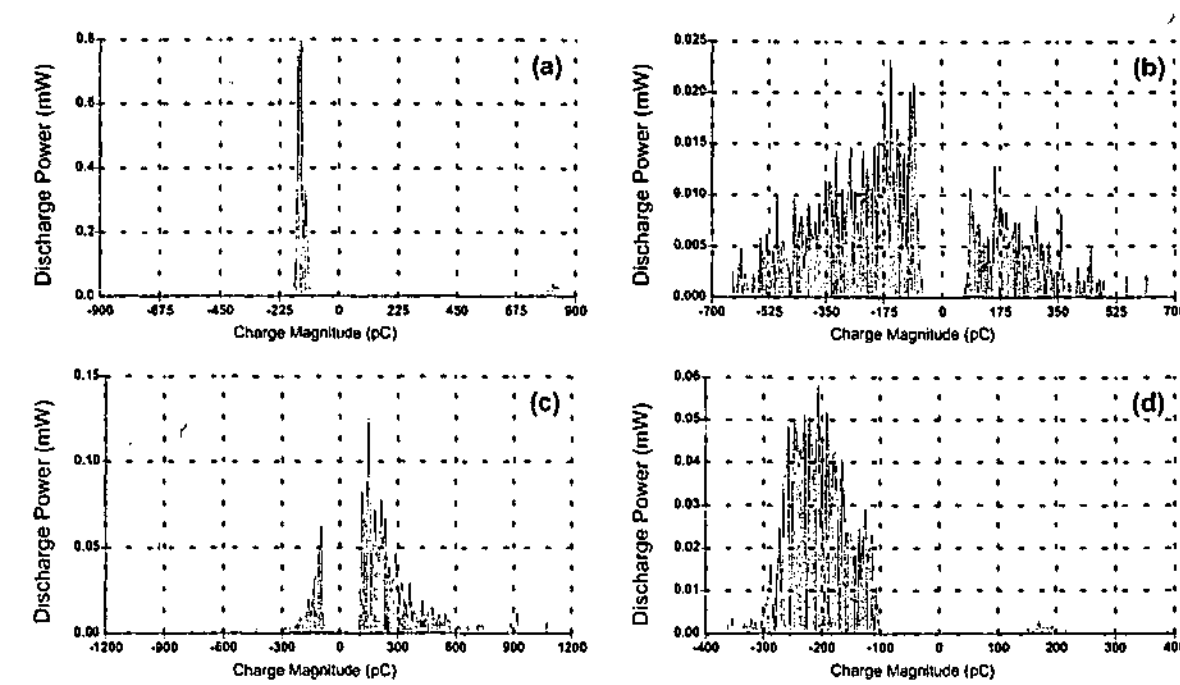
Fig. 4.7 Distribution functions of discharge power measured from
(a) a point-to-plane corona
(b) a point-to-dielectric discharge
(c) an oil-impregnated pressboard discharge
(d) an epoxy resin stator bar with an artificial defect inside

4.4.5 Distribution Function of PD Quadratic Rate

Quadratic rate is a PD quantity defined in the standard of IEC Publication 270. It is calculated by the sum of squared PD amplitude divided by the time interval used to acquire PD data. This squared aggregation assigns greater weight to the larger discharge pulse and it results in the differentiation between pulses of different magnitude. The original concept defined in IEC Publication 270 is modified and extended in this thesis by treating PD amplitude quadratic rate as a distribution function.

The distribution function of PD amplitude quadratic rate provides more detailed information about discharge amplitude distributions as it assigns a squared aggregate to discriminate pulses with different amplitudes. Obviously, this is another measure to allocate PD distributions due to the nature of this squared aggregate. The partition quantity of quadratic rate can be calculated as the sum of the squares of the individual PD magnitude that occurred in the partition window divided by the time interval. The detailed calculation can be found in equation 4.7, which is implemented in the PDD

system. The distribution functions of PD amplitude quadratic rate measured from various types of defect are illustrated in figure F. 2 of appendix F for different types of discharge sources.

4.5 PHPD PATTERN ANALYSIS

It is well understood that each PD source is different in terms of its geometry, location in the insulation, type of dielectric, type of gas in the void, gas pressure and temperature etc. The stochastic nature of PD can be characterized by the time behavior of the discharge process. Variations may occur in both discharge magnitude and triggering time during test. This temporal behavior is caused partly by statistical variations in the discharge phenomenon itself and partly by the changes at the discharge site. To describe the characteristics of a discharge, many distribution functions have been introduced over the years. To understand the ac phase and voltage distribution in relation to discharge amplitude, phase and voltage distributions acquired from a point-to-plane arrangement are plotted from figure 4.8 to 4.12 respectively. The distance between electrodes was set to 10mm. For PD patterns measured from a point-to-plane arrangement in air, the range and standard deviation of phase distribution in partition window of negative PD have little change when the applied voltage slightly increased as shown in figure 4.8 and 4.9. Meanwhile the range and standard deviation of phase distribution in the positive PD partition window have significant changes compared with the phase distribution in the negative partition window. The result reveals that negative corona discharges are insensitive to the applied voltage (in certain range). The magnitude of negative PD is also very stable. In addition, it can be observed that negative discharges are small in magnitude while positive discharges are large in magnitude. With the help of these new distribution functions, discharge phenomena of a point-to-plane in air can be summarized and the results are in line with earlier findings that negative corona varies little in magnitude [Trichel (1939)]. Figure 4.10 and 4.11 are distributions of the voltage range and standard deviation. It can be observed that the distributions of voltage range and standard deviation behave in the similar fashion as the phase distributions do.

Figure 4.12 to 4.15 have shown distribution functions measured from the same point-to-plane arrangement but in oil. The distribution functions of phase range and standard deviation are shown in 4.12 and 4.13 in which the applied voltage is increased from 11 to 14 kV in equal steps. It can be observed that the distribution symmetry between positive and negative discharges is improved dramatically. The distributions are subject to the increase of applied voltage but the change is very complicated to describe. However, with the PDD system, feature quantities can be calculated from distribution functions with ease and extracted as part of PD fingerprints. The distribution functions of voltage range and standard deviation are illustrated in figure 4.14 and 4.15.
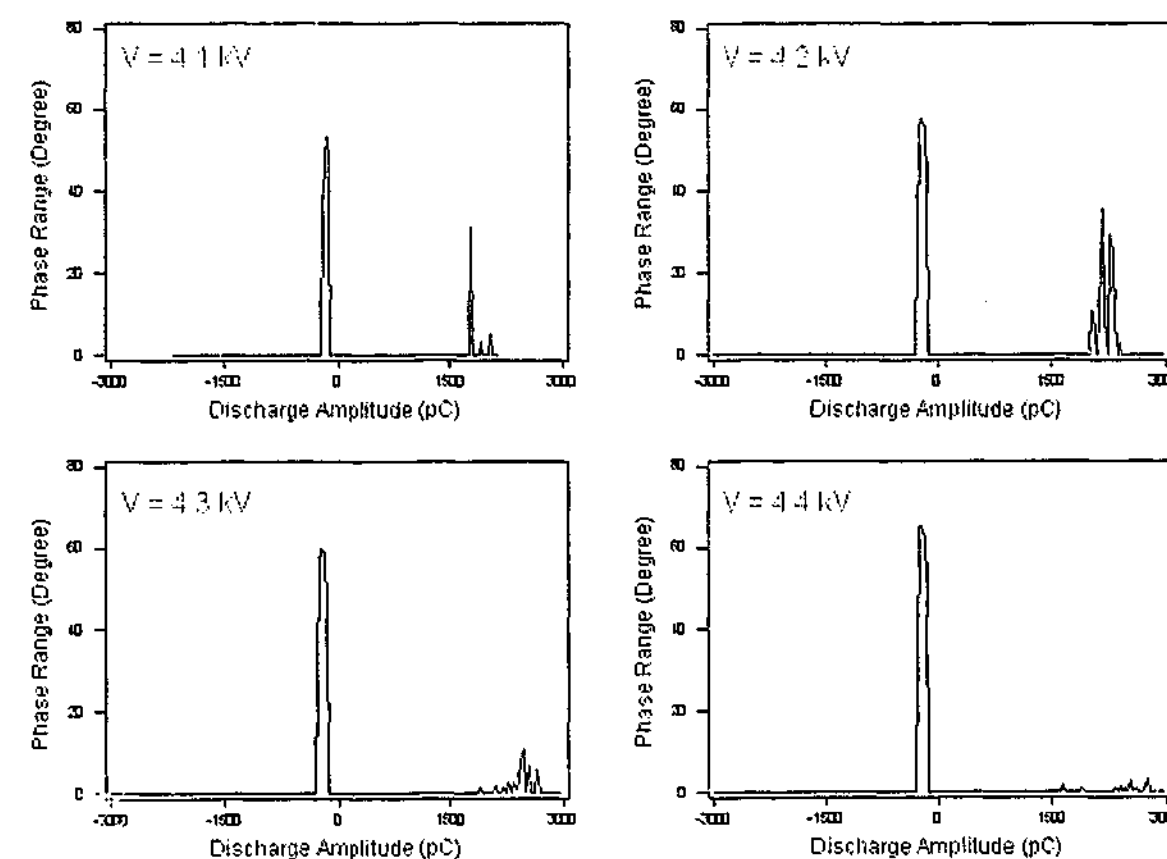
Fig. 4.8   Distribution functions of phase range measured from air coronas
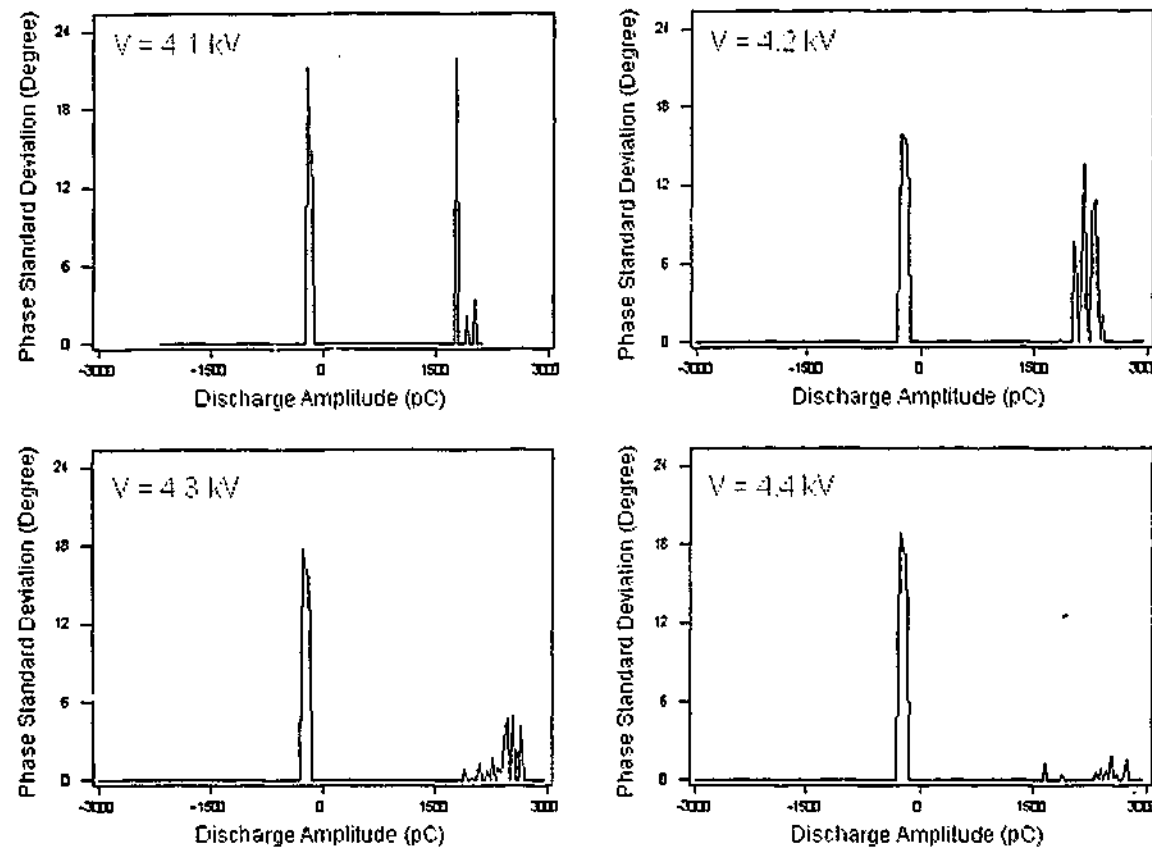
Fig. 4.9 Distribution functions of phase standard deviation measured from air coronas
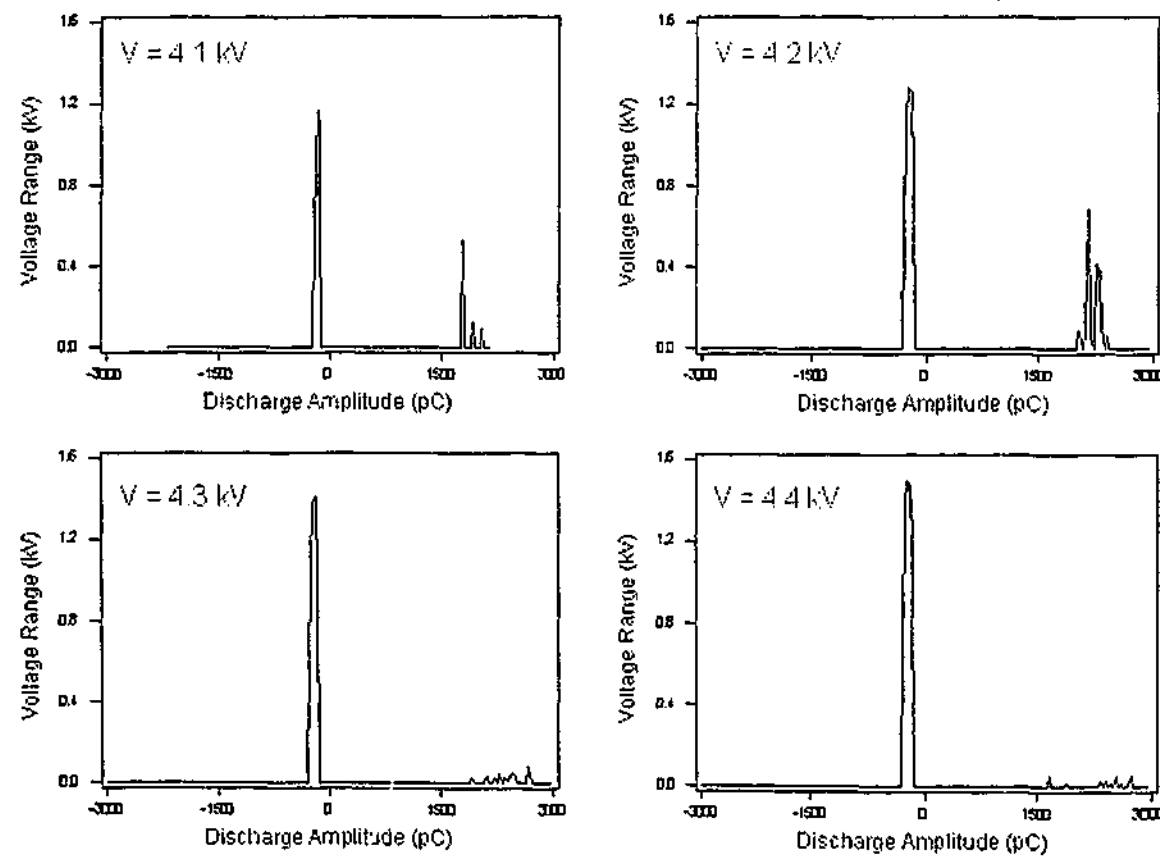
Fig. 4.11 Distribution functions of voltage standard deviation measured from air coronas


Fig. 4.10 Distribution functions of voltage range measured from air coronas
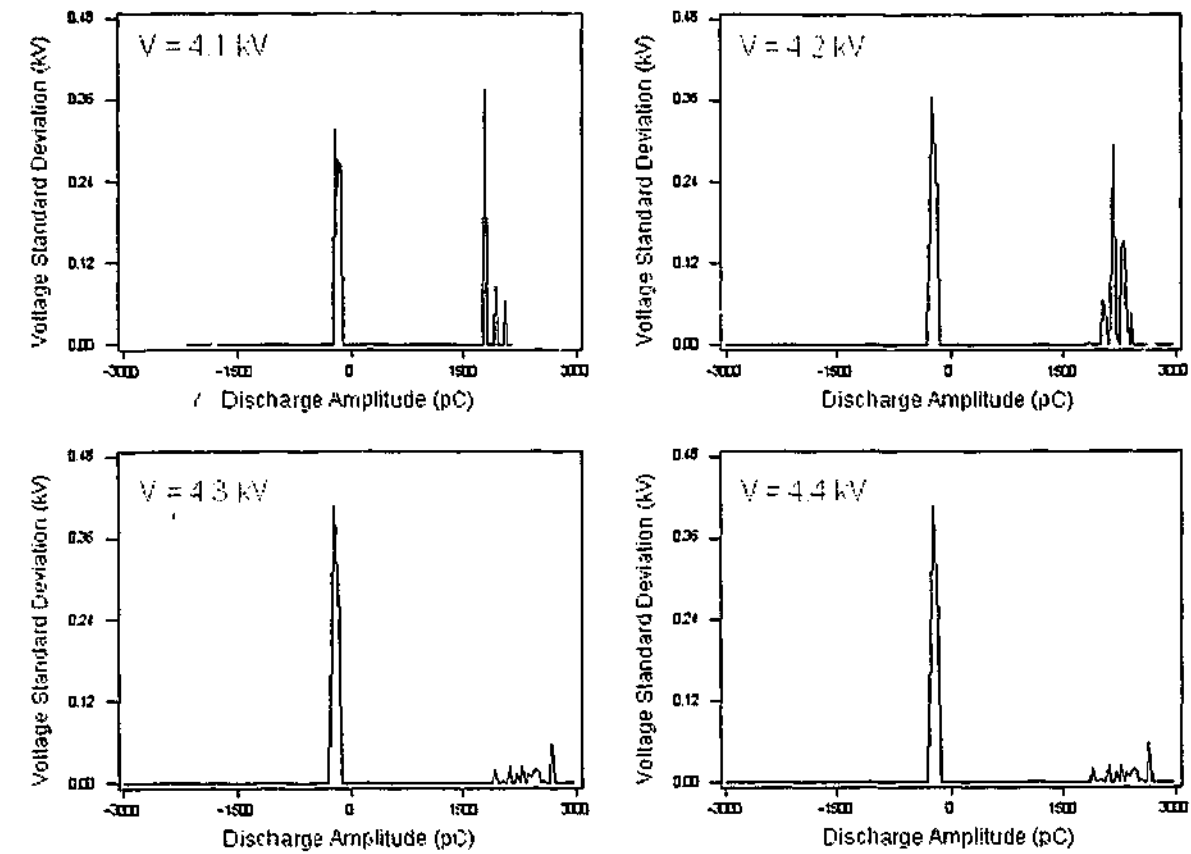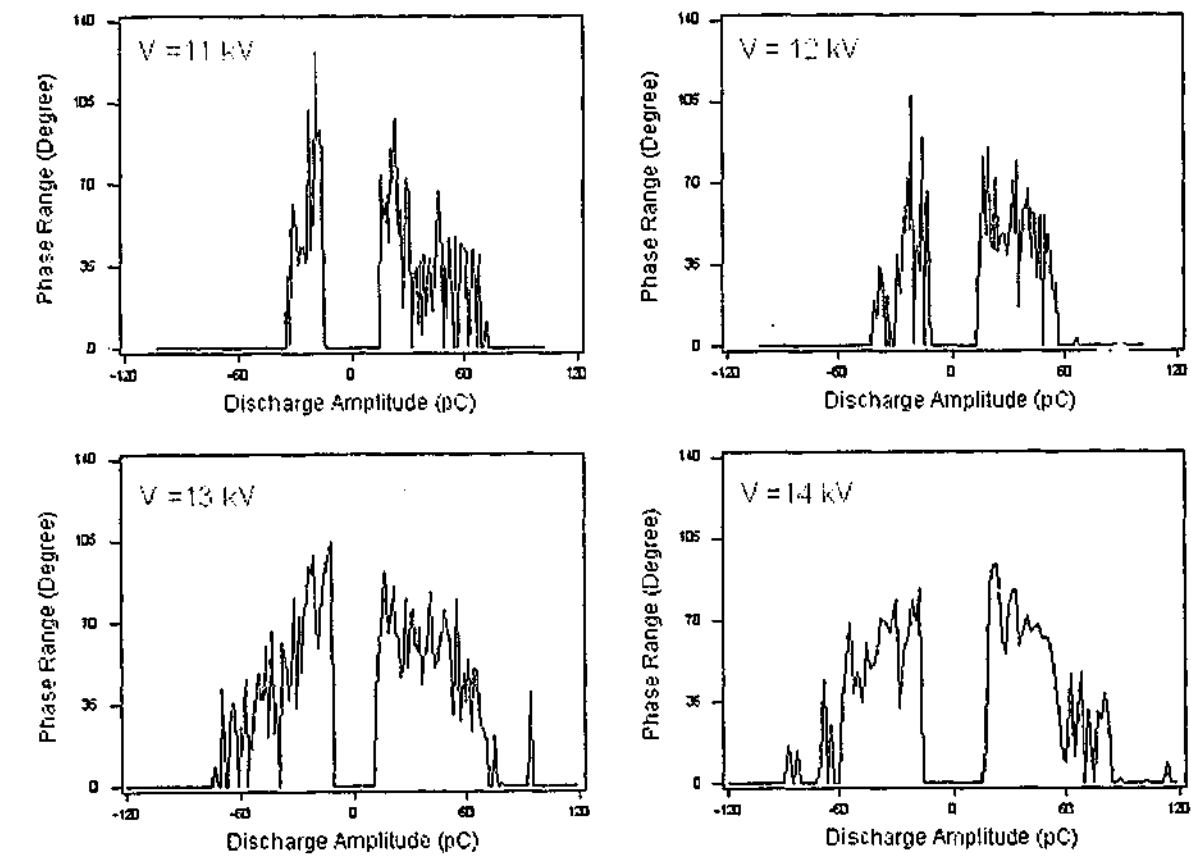

Fig. 4.12 Distribution functions of phase range measured from point-to-plane discharges in oil
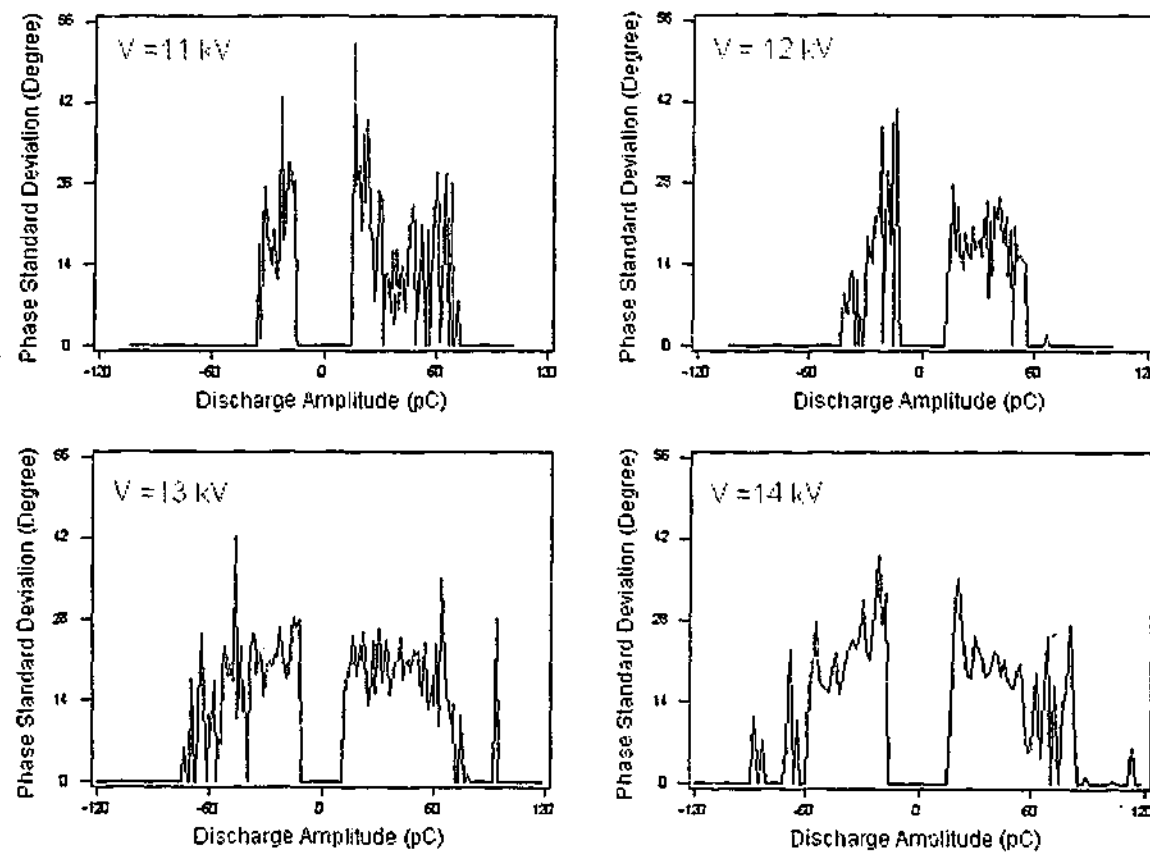
Fig. 4.13 Distribution functions of phase standard deviation measured from point-to-plane discharges in oil
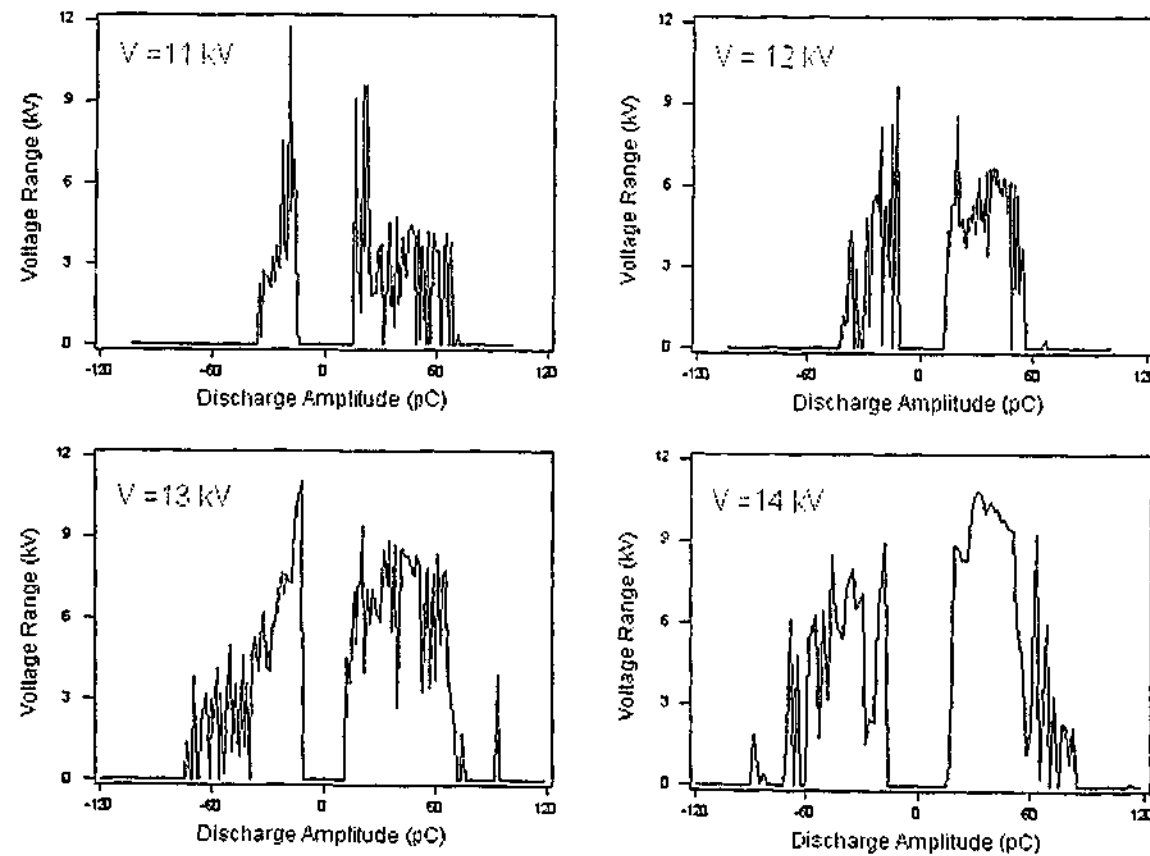
Fig. 4.14 Distribution functions of voltage range measured from point-to-plane discharges in oil
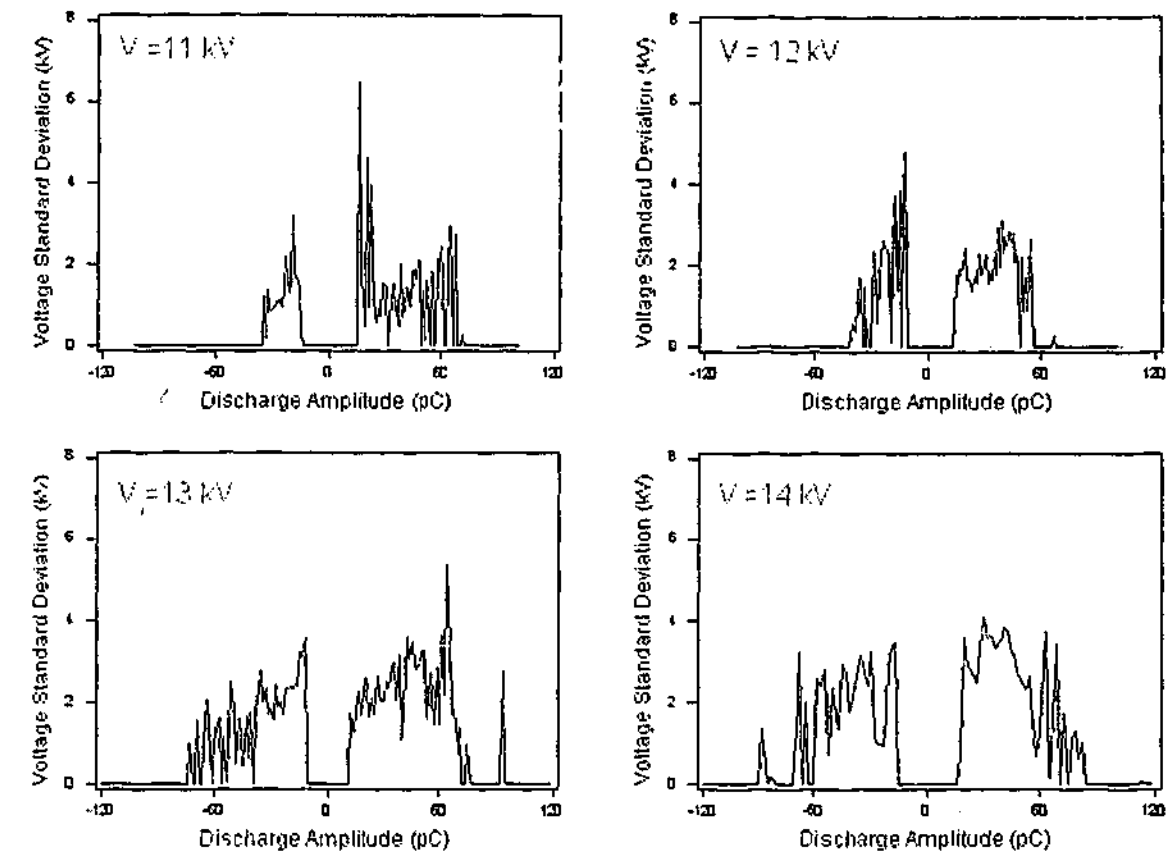
Fig. 4.15 Distribution functions of voltage standard deviation measured from point-to-plane discharges in oil

The distribution functions of phase range and standard deviation measured from both dry and oil-impregnated pressboard discharges are shown from figure 4.16 to 4.23. First of all, patterns are shown varying with the change of applied voltage. It is observed that for both pressboard discharges, the distribution range of PD amplitude is increased as the increase of applied voltage. Visual comparison of the phase range distribution between the dry and the oil-impregnated pressboard discharges can be done by examining (1) the stability of the distribution when voltage increases and (2) the degree of distribution symmetry between positive and negative discharges.

Phase range distribution functions of both pressboard discharges have very similar stability. However, they change with the increase of applied voltage. Meanwhile, it can be observed that the degree of distribution symmetry between positive and negative discharges is improved as the voltage increases. However, it is observed the maximum phase range appears having an increasing trend as the increase of applied voltage.

The correlation between positive and negative discharge distributions can also be quantified to describe the degree of the distribution symmetry. The calculated correlation coefficients provide information regarding the distribution symmetry as they are closely related to electrode configuration, defect geometry, location and insulation material etc. The correlation coefficients are calculated from various distribution functions including the distribution functions of phase and voltage range as well as their standard deviation. In similar fashion, the stability of distribution functions can be quantified by calculating the descriptive statistics under different test criteria. The statistics represent discharge activities at different magnitudes when the applied voltage is increased. These distribution functions are implemented in the PDD system with which feature quantities can also be calculated as feature vectors. PD fingerprints are established from feature quantities calculated from various distribution categories including PHPD distribution category.
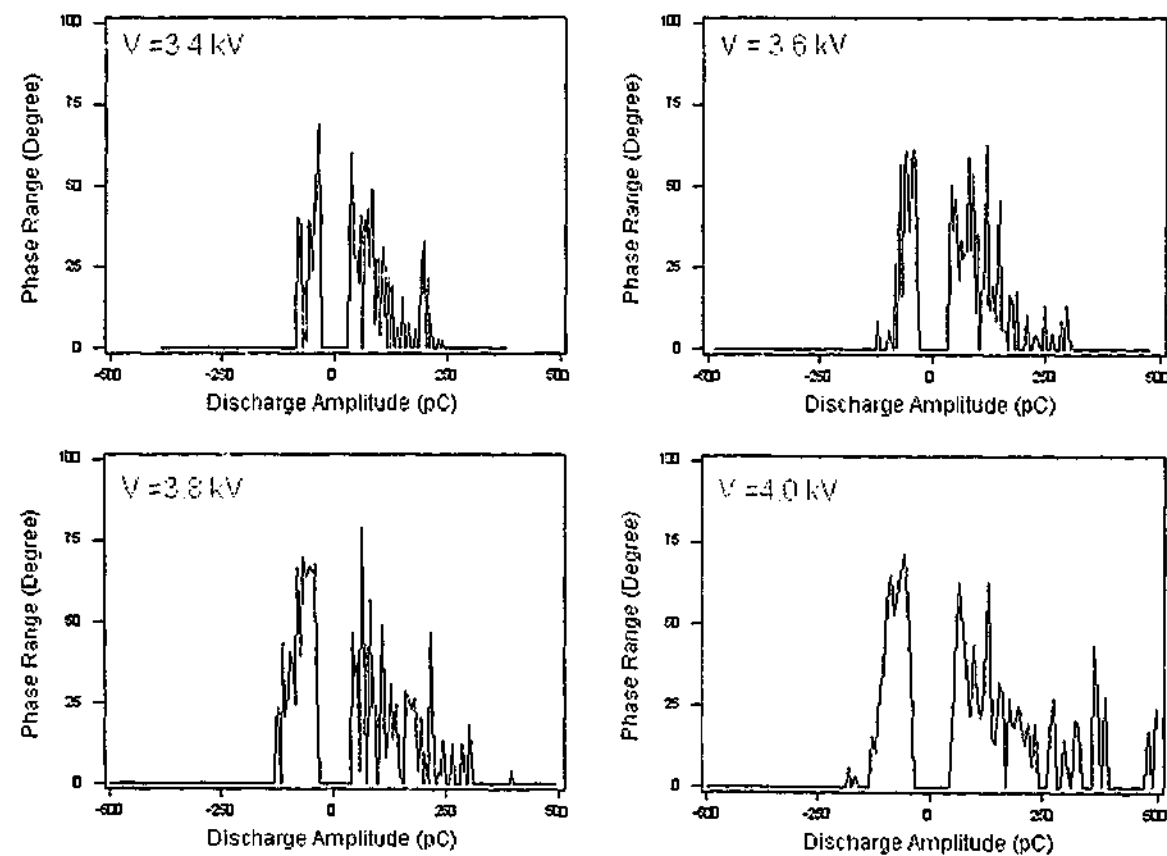
Fig. 4.16 Distribution functions of phase range measured from dry pressboard discharges
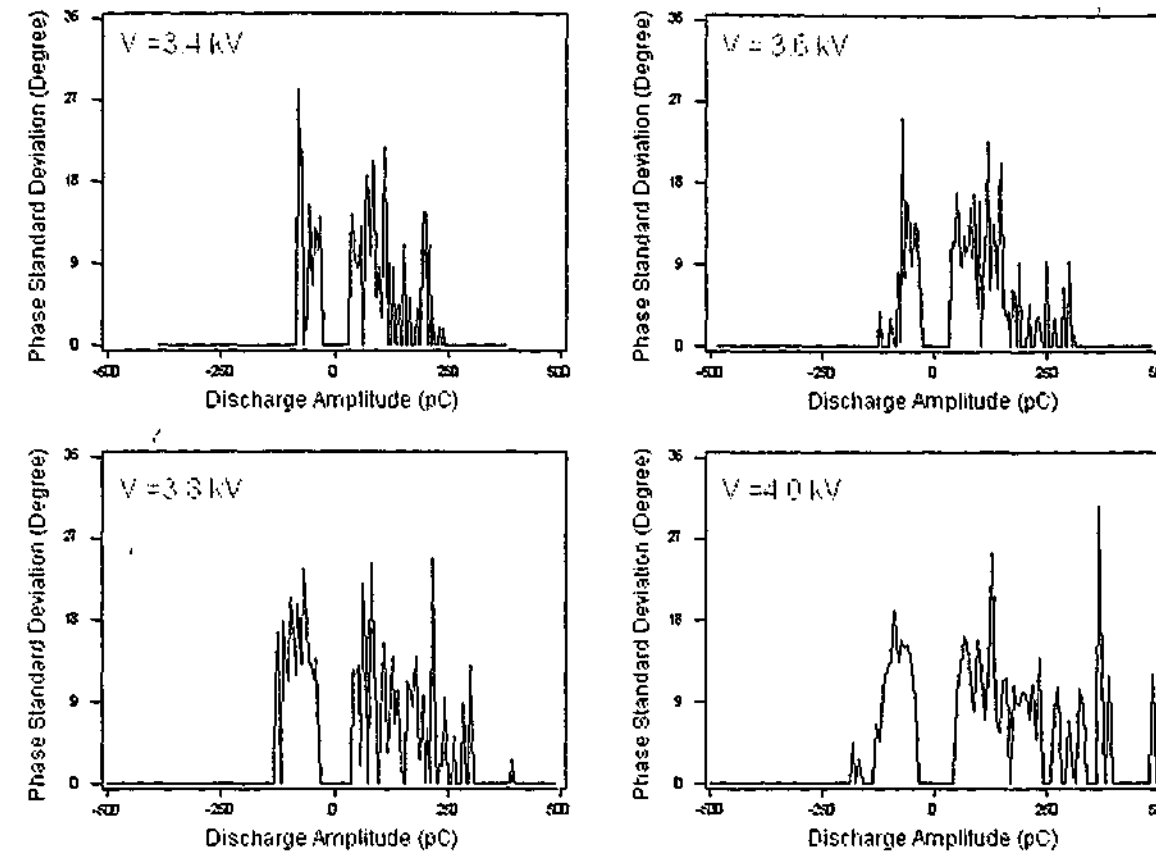
Fig. 4.17 Distribution functions of phase standard deviation measured from dry pressboard discharges
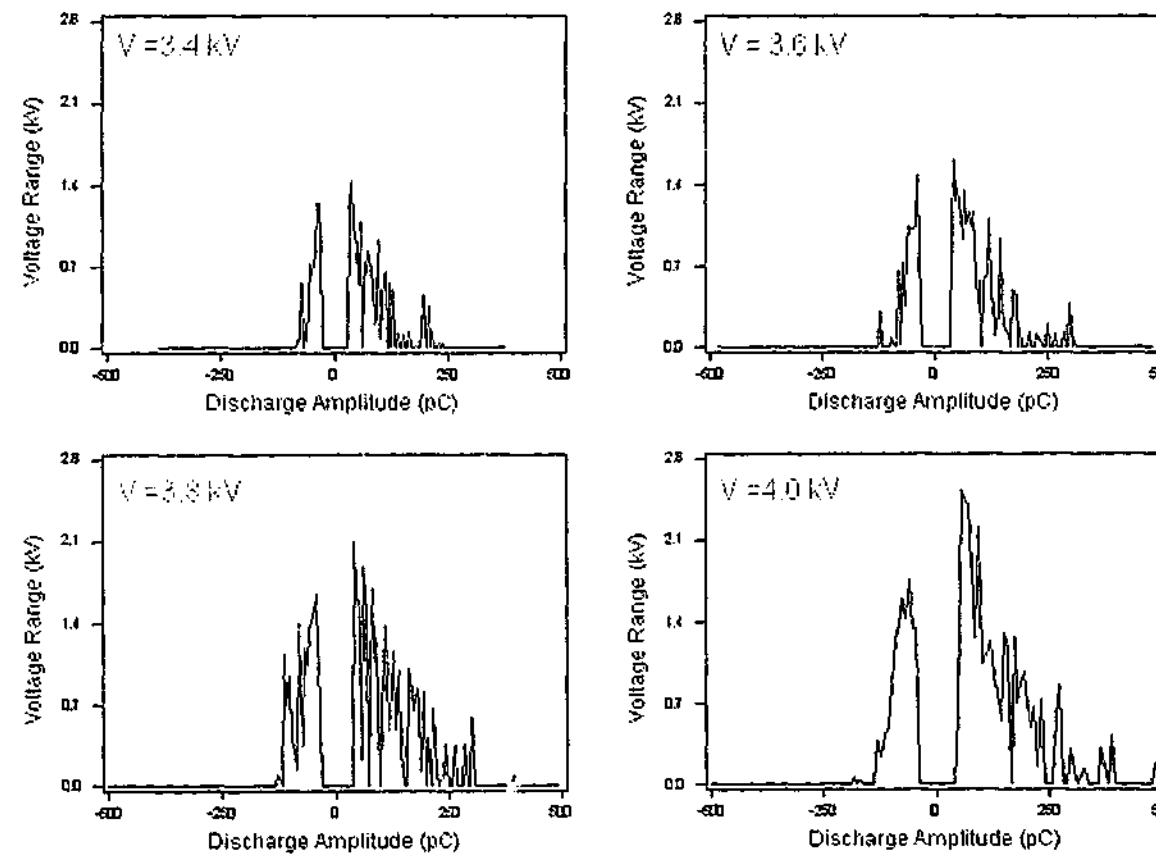
Fig. 4.18 Distribution functions of voltage range measured from dry pressboard discharges
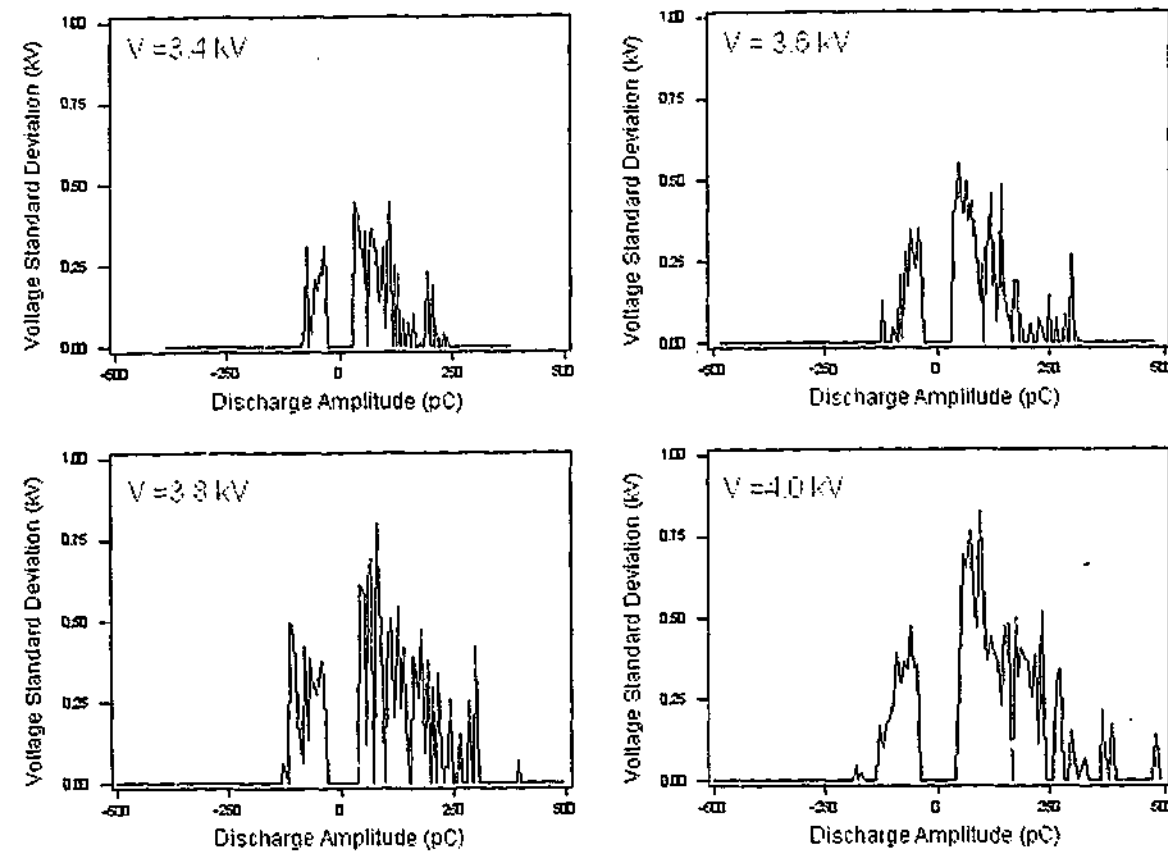
Fig. 4.19 Distribution functions of voltage standard deviation measured from dry pressboard discharges
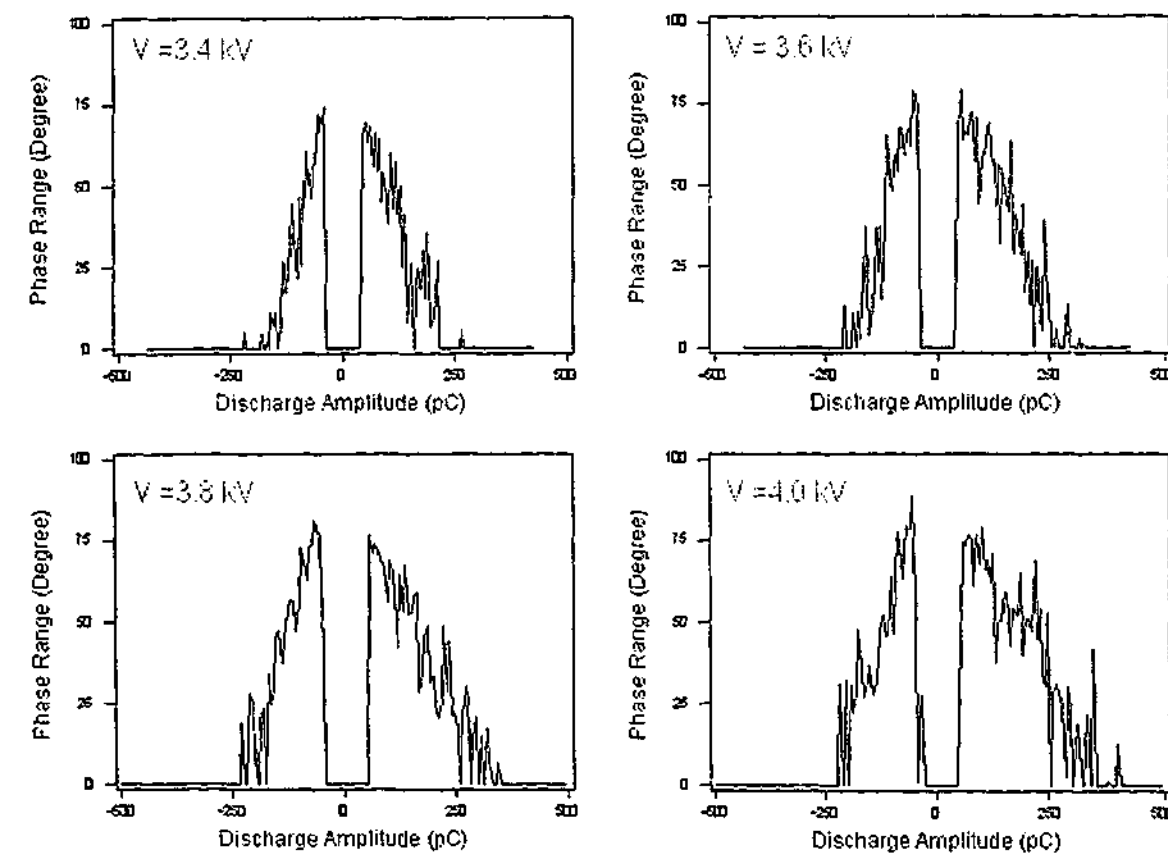

Fig. 4.20 Distribution functions of phase range measured from oil-impregnated pressboard discharges
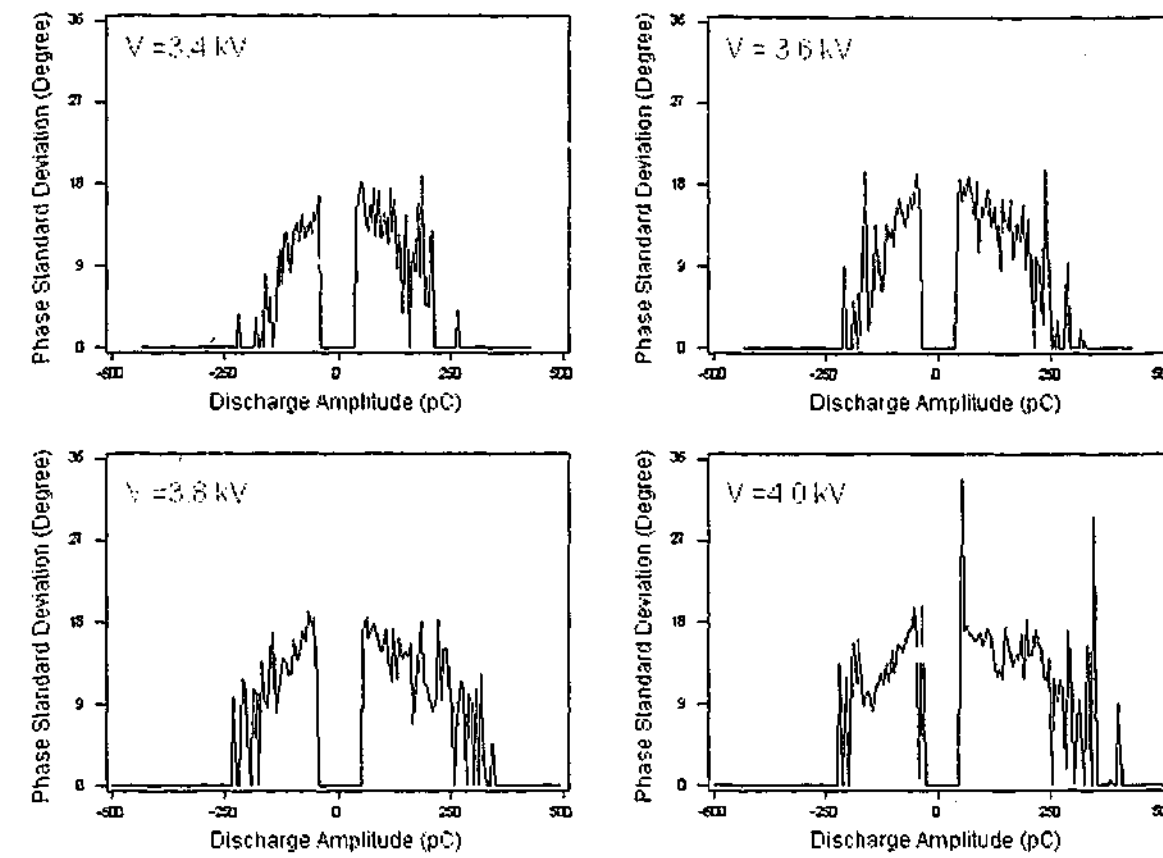
Fig. 4.21 Distribution functions of phase standard deviation measured from oil-impregnated pressboard discharges
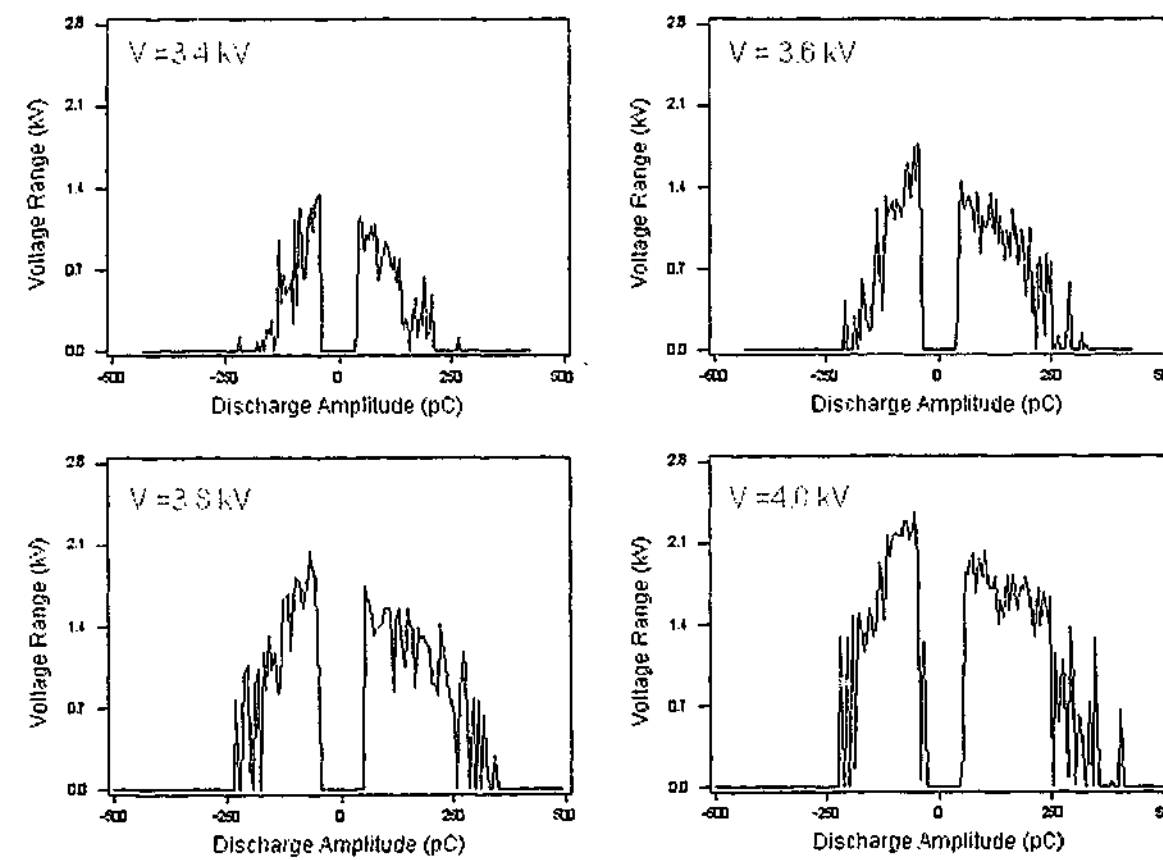

Fig. 4.22 Distribution functions of voltage range measured from oil-impregnated pressboard discharges
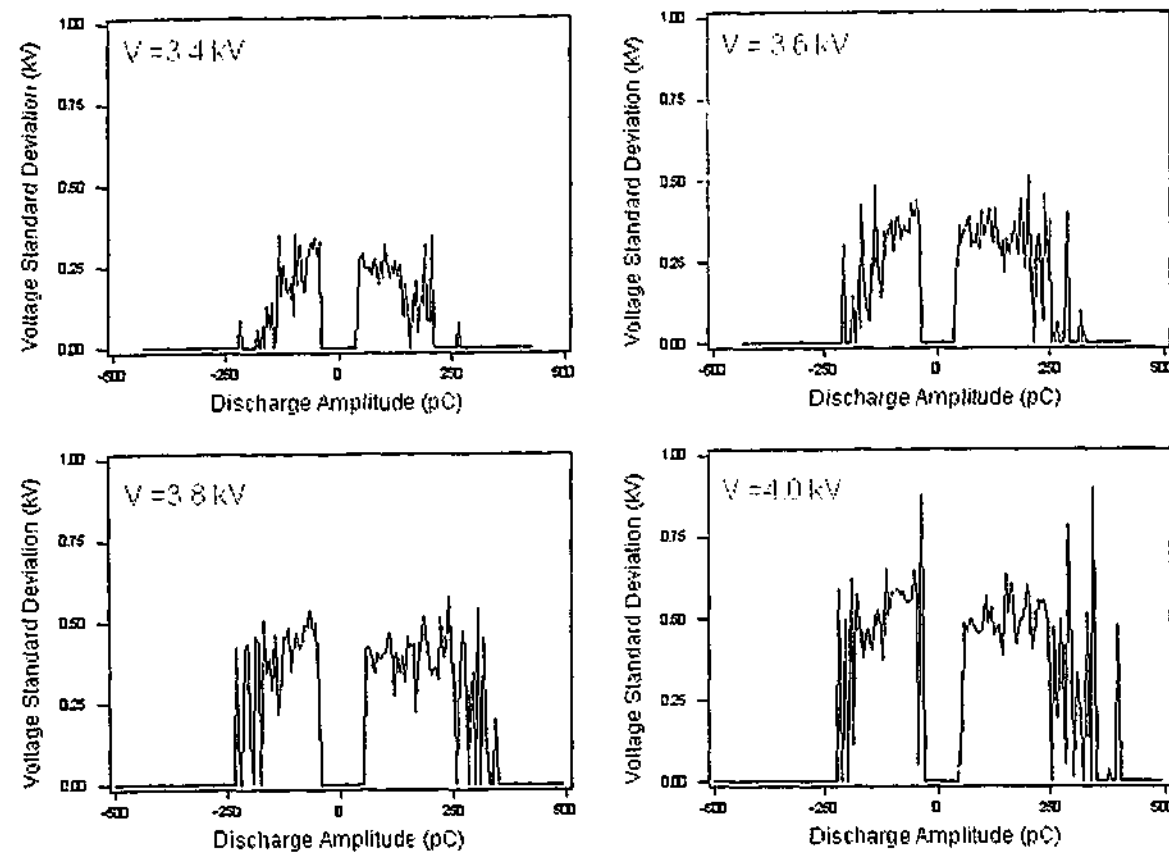
Fig. 4.23 Distribution functions of voltage standard deviation measured from oil-impregnated pressboard discharges

4.6 THE CORRELATION COEFFICIENTS

The procedure of calculating correlation coefficient (CC) between two distributions is implemented in the PDD system to determine whether two ranges of data are moving together. In this case it can be used to describe whether large values of one half-cycle data are associated with values of the other. The formula is defined in equation 1.9 and it has the value range between -1 and $+1$. If both variables tend to increase or decrease together, the correlation coefficient is positive. Otherwise, it is negative.

4.6.1 Correlation between Positive and Negative Half of a Distribution Function

The correlation coefficients being investigated in this section are related to PHPD distribution functions. The correlation coefficients describe the degree of symmetry between positive and negative discharges of a distribution function. There are six PHPD distribution functions being plotted and the corresponding feature quantities are also calculated to quantify a distribution function. The six distribution functions are PD

occurrence, average and maximum voltage, PD current and power, and PD amplitude quadratic rate. As discussed earlier, the practical application of PD pattern recognition requires the consideration of the stability of the distribution function of interest. Correlation coefficients are feature quantities used to stand for the relationship of positive and negative discharge distributions.
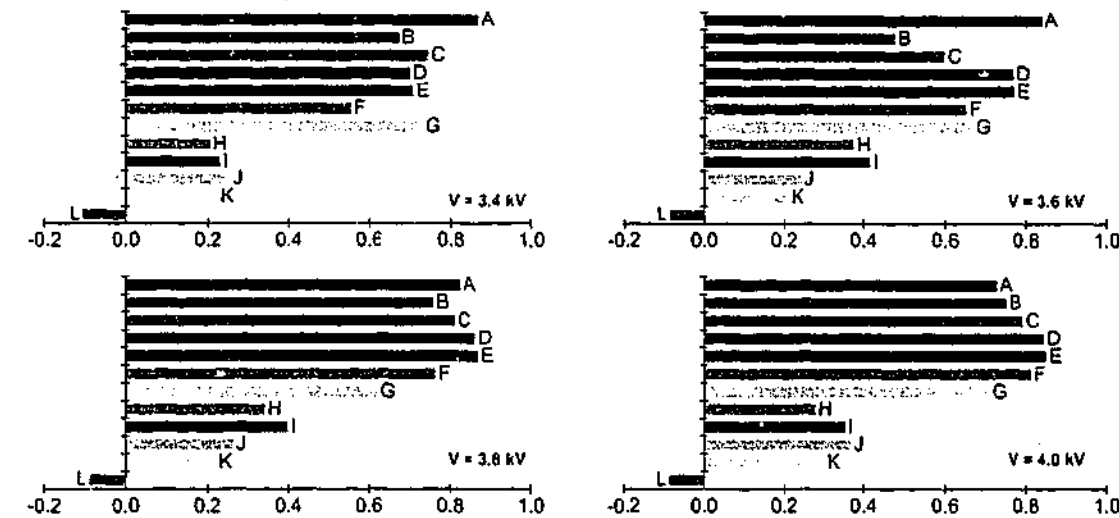
Fig. 4.24 Correlation coefficients between PHPD positive and negative distribution functions obtained from dry pressboard discharges
A – F: Correlation coefficients between PRPD positive and negative half distributions
G: PD occurrence   H: Average voltage I: Maximum voltage
J: PD current   K: PD power   L: PD amplitude quadratic rate

Fortunately, the functions of calculating these feature quantities are implemented in the PDD system. Correlation coefficients of the above six distribution functions are calculated in a statistical module. The calculated correlation coefficients are accompanied by a bar chart as shown in figures 4.24 and 4.25. Figure 4.24 presents the results measured from the dry pressboard discharges while figure 4.25 illustrates the results measured from the oil-impregnated pressboard discharges. In both figures, the bars from A to F are corresponding results calculated from PRPD distribution functions. The bars from G to L are those calculated from the described six PHPD distribution functions. The correlation between positive and negative discharges appears to have a statistical variation but in a marginal range.
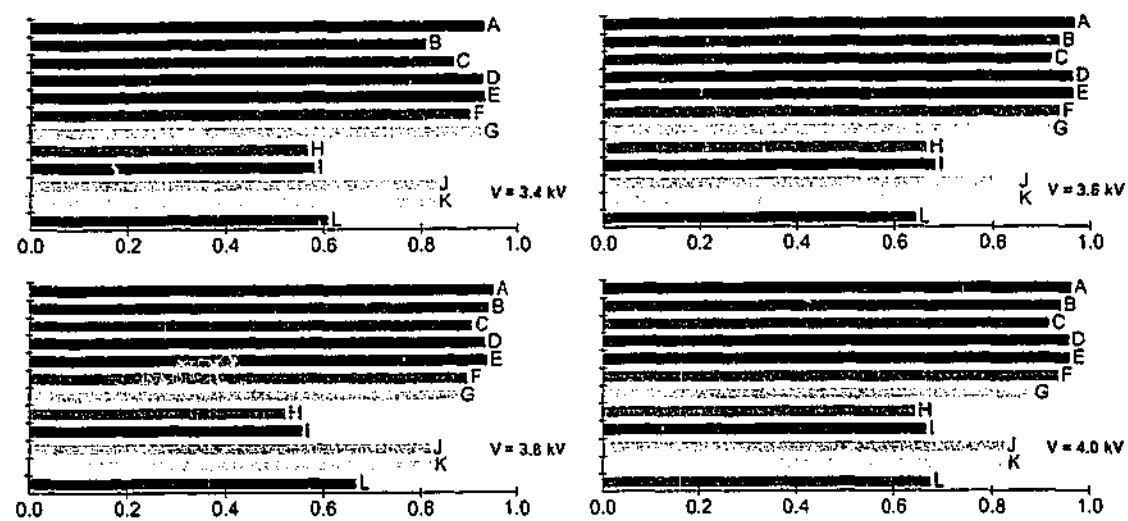
Fig. 4.25 Correlation coefficients between PHPD positive and negative distribution functions obtained from oil-impregnated pressboard discharges
A – F: Correlation coefficients between PRPD positive and negative half distributions
G: PD occurrence   H: Average voltage I: Maximum voltage
J: PD current   K: PD power   L: PD amplitude quadratic rate

4.6.2 Correlation between PRPD and PHPD Distribution Functions

In addition being used for quantifying the distribution symmetry between the positive and negative discharges, correlation coefficients can also be employed to describe the relationship of two corresponding half distributions between PRPD and PHPD distributions. In the case of the PD occurrence distribution, the X is the PRPD occurrence distribution function of either positive or negative discharges and Y is the PHPD occurrence distribution of the corresponding half distribution. A correlation coefficient can be calculated to quantify the relationship between X and Y. Figure 4.26 presents the results measured from the dry pressboard discharges while figure 4.27 shows the results measured from the oil-impregnated pressboard discharges. The bars from A to F are results calculated from positive distribution functions while the bars from G to L are those calculated from negative distribution functions.
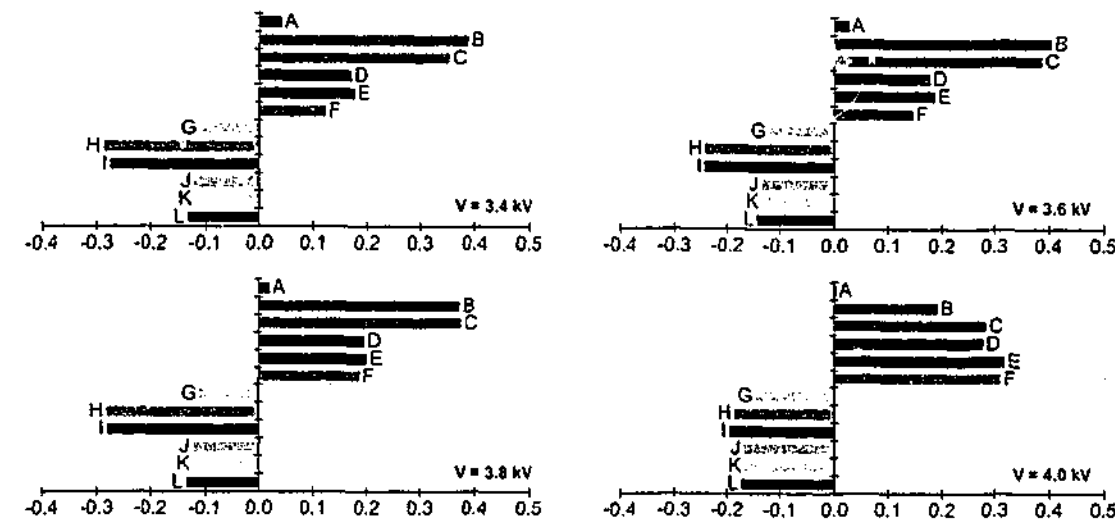
Fig. 4.26 Correlation coefficients between corresponding half of PRPD and PHPD distribution functions obtained from dry pressboard discharges
Positive distribution functions:
    A: Occurrence   B: Average   C: Maximum
    D: PD current   E: PD power   F: PD amplitude quadratic rate
Negative distribution functions:
    G: Occurrence   H: Average   I: Maximum
    J: PD current   K: PD power   L: PD amplitude quadratic rate
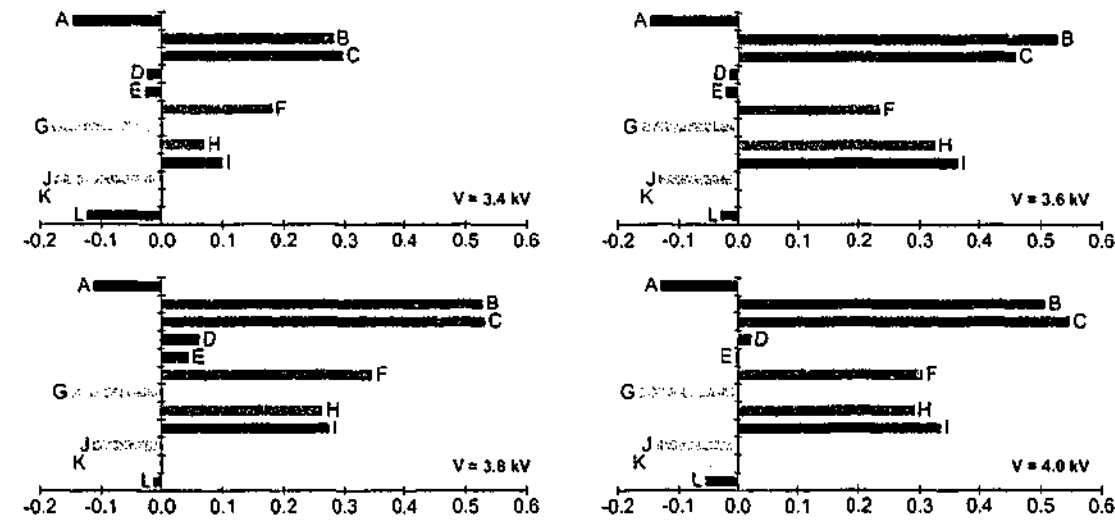
Fig. 4.27 Correlation coefficients between corresponding half of PRPD and PHPD distribution functions obtained from oil-impregnated pressboard PDs
Positive distribution functions:
    A: Occurrence   B: Average   C: Maximum
    D: PD current   E: PD power   F: PD amplitude quadratic rate
Negative distribution functions:
    G: Occurrence   H: Average   I: Maximum
    J: PD current   K: PD power   L: PD amplitude quadratic rate

The statistical variation of discharge patterns can be evaluated using correlation coefficients to assess the change of PD distribution with changes in criteria such as applied voltage, temperature, and test sample configuration etc. Figure 4.28 demonstrates the variation of correlation coefficients between PRPD and PHPD corresponding distribution functions measured from dry pressboard discharges. For example, the average correlation coefficients between PRPD average PD distribution function and PHPD average voltage distribution function are calculated. The variation represents the change of PD distribution functions as applied voltage increases. This is important information for PD pattern recognition because neural network weights can be successfully trained to adopt the variations between distribution functions when test criteria changes.
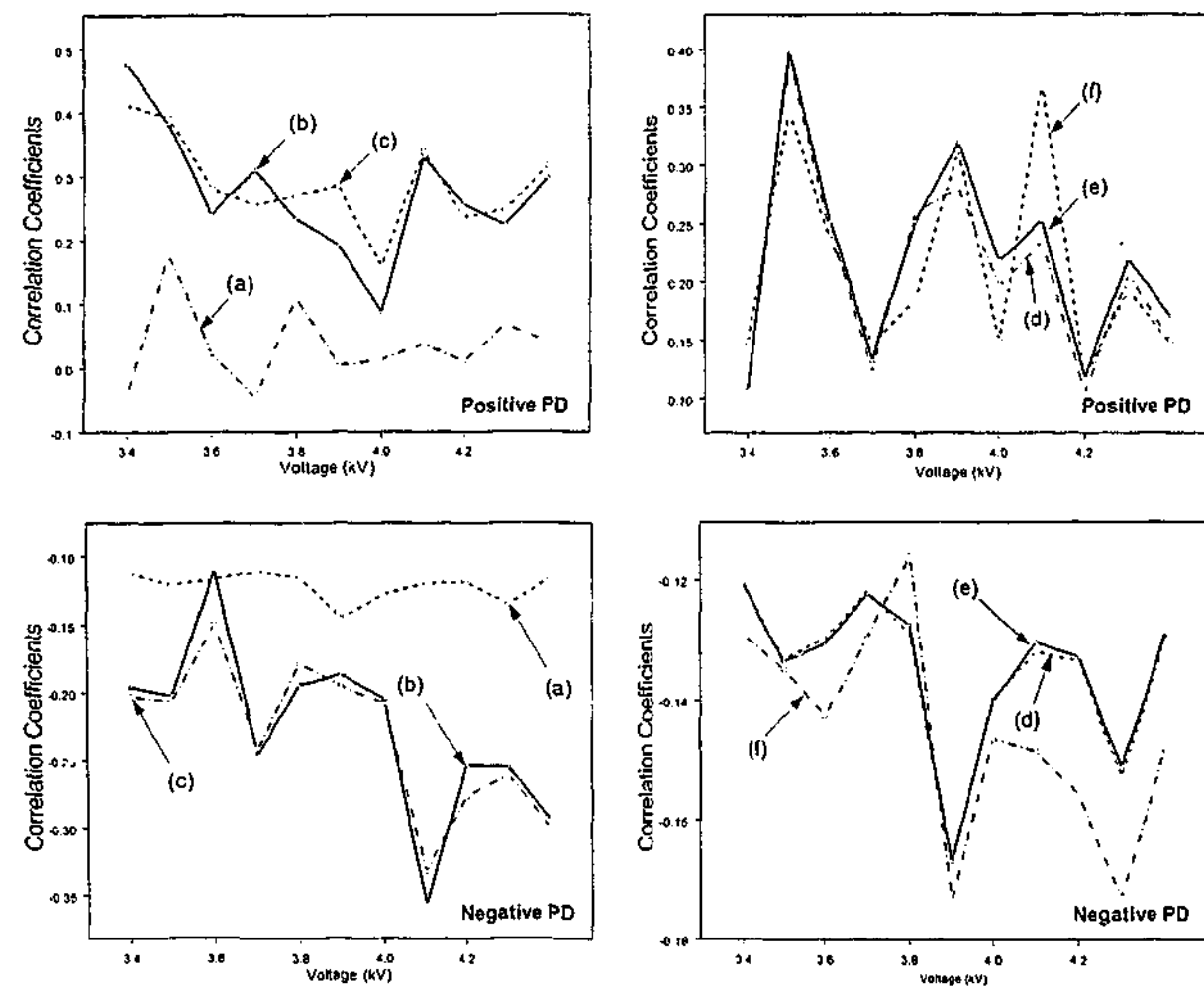
Fig. 4.28 Correlation coefficients calculated between PRPD and PHPD distribution functions that measured from dry pressboard discharges.
(a) PD occurrence   (b) average   (c) maximum
(d) PD current   (e) PD power   (f) PD amplitude quadratic rate

The variation of PHPD distribution functions can be evaluated using correlation coefficients to assess the change of PD distributions with the changes in the test criteria , such as applied voltage, temperature, and test sample configuration etc. In figure 4.30, the variation of correlation coefficients against the increase of applied voltage is shown. The corresponding distribution functions are measured from oil-impregnated pressboard discharges. As an example, the maximum correlation coefficient referred to in curve C in figure 4.29, is calculated for PRPD maximum PD distribution function and PHPD maximum voltage distribution function. These quantified PD distribution variations are extremely useful for the recognition of PD sources of different types. For PD pattern recognition purpose, it is required to (1) distinguish patterns from different defects (2) find the similarities in patterns of the same defect.
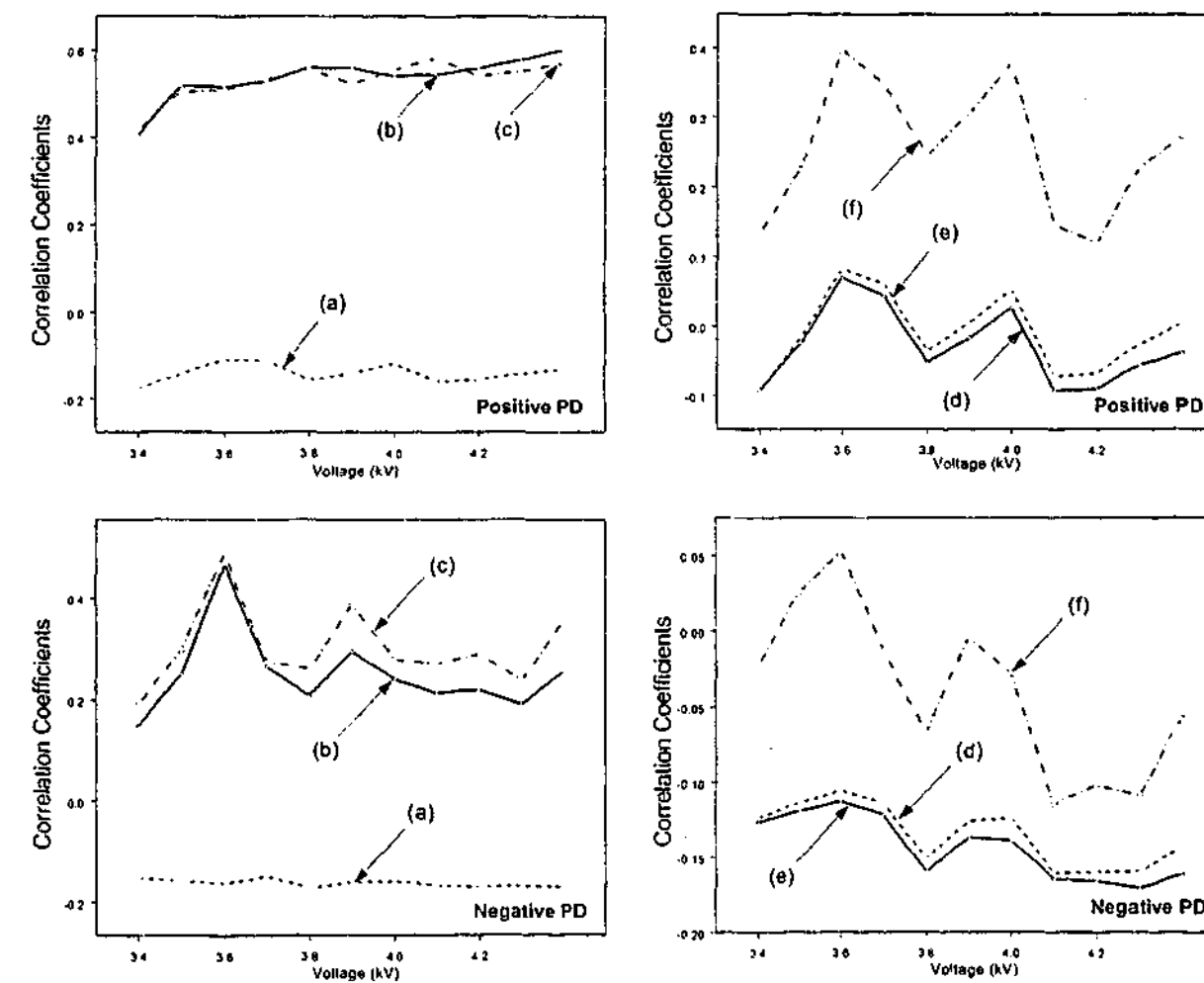

Fig. 4.29 Correlation coefficients calculated between PRPD and PHPD distribution functions that measured from oil-impregnated pressboard discharges.
(a) PD occurrence   (b) average   (c) maximum
(d) PD current   (e) PD power   (f) PD amplitude quadratic rate

4.7 CONCLUDING REMARKS

PHPD distribution functions provide details related to the discharge physical process. As explained, distribution functions of occurrence, average and maximum voltage, PD current and power and PD amplitude quadratic rate can be derived from PHPD partition windows. Obviously, each of these distribution functions is not independent and in fact, they are correlated with each other. Each of them has a unique picture to reflect part of discharge activities inside the insulation defect and provides unique distribution information about the nature of discharge. The PDD system calculates descriptive statistics regarding voltage and phase distribution functions and, in addition, gives graphical support for these distribution functions. Partition and feature quantities computed from discharge distributions are useful for further discharge evaluation as well as for PD pattern recognition.

Further more, these distribution functions are correlated with the corresponding PRPD distribution functions. The correlation coefficients between them provide another important measure for the classification of different types of defect. With tne PHPD pattern analysis approach, extra care must be taken because the PHPD partition window may vary significantly with the threshold setting. In addition to the impact of threshold setting, this PHPD pattern analysis also requires advanced techniques in noise control especially when collecting data on site.

Finally, as for the insulation aging diagnosis, the PHPD phase and voltage distribution functions are very useful. In conjunction with distribution functions of other distribution categories, they are indispensable to characterize discharge physical process. Feature quantities calculated from PHPD phase and voltage distribution functions are extracted to form PD fingerprints which are used to classify different types of defects.

Chapter 5

Cycle Resolved Distribution Function – A New Technique for Partial Discharge Analysis

In chapter 3 and 4, phase and pulse-height resolved PD distribution functions are used to analyze discharge distributions. In this chapter, ac cycle resolved PD (CRPD) distribution functions are introduced to analyze discharge activities under repeated ac voltage. The relationships between CRPD and PRPD as well as between CRPD and PHPD distribution functions are discussed. It will be demonstrated that CRPD distribution functions are useful tools to investigate discharge phenomena when they are used in conjunction with PRPD and PHPD distribution functions. Particularly, PD inception and extinction properties can be explored in detail CRPD distributions.

5.1 INTRODUCTION

PD distribution functions contain many important discharge properties in regard to discharge initiation and development. In ac tests, a periodical voltage is applied to the test object, causing the discharge to appear and disappear at certain ac phase positions. Similar to PRPD and PHPD patterns, cycle resolved distribution pattern (CRPD) can be used to assess the properties of discharge under ac condition due to its dependency on the periodically changing external stress.

The use of the PDD system to assess the insulation condition of test object has been explained in earlier chapters. The results obtained from PRPD and PHPD patterns provide details of discharge distributions in relation to ac phase position and discharge magnitude. However, PRPD and PHPD distribution functions do not present discharge distributions in relation to the ac cycle number.

In this chapter, CRPD distribution functions obtained from different types of defect are investigated in certain detail. The CRPD distribution functions as well as their possible

applications are also discussed. As an example, statistical properties of negative Trichel-pulse corona are carefully studied using modified CRPD distribution functions. It is demonstrated that cycle based partition quantities such as discharge mean and its standard deviation are strongly correlated with the distribution function of PD occurrence. The study found that the distribution function of PD occurrence over a number of continuous ac cycles may regarded as a sensitive indicator to investigate the physical mechanism of discharge initiation and growth. The quantified interdependence relationship makes the CRPD distribution functions useful for discharge pattern analysis. The results could contribute to the development of a new insulation diagnostic system.

5.2 MATHEMATICAL MODELLING

Like PRPD and PHPD distributions, there should be many valuable distribution functions derived when cycle number is the independent variable. In particular, it is interesting to consider new CRPD distribution functions such as PD occurrence, average and extreme variables, PD current, PD power loss and PD quadratic rate for PD pattern analysis.

Discharge occurrence in ac period partition window is a partition quantity related to the probability of PD events during a cycle period T_i. If $p_1(\lambda \mid t_\lambda \in \Delta T_i)$ is the probability of a PD event λ which appears at time t_λ, and is measured within the ith cycle period, the PD occurrence distribution function in the ith partition window is defined as:

$$f_T(i) = N \bullet p_1(\lambda \mid t_\lambda \in \Delta T_i) \tag{5.1}$$

where N is the total number of PD events in a complete acquisition and i is the ac cycle partition window index.

The average distribution function describes the distribution of average PD amplitude in an ac cycle partition window is defined as:

$$A_T(i) = \frac{\sum (q_\lambda \mid t_\lambda \in \Delta T_i)}{N \bullet p_1(\lambda \mid t_\lambda \in \Delta T_i)} \tag{5.2}$$

where $p_1(\lambda \mid t_\lambda \in \Delta T_i) > 0$ otherwise $A_T(i) = 0$, and $q_\lambda \mid t_\lambda \in \Delta T_i$ is the charge amplitude when occurring in the ith CRPD partition window.

CRPD maximum distribution function represents the distribution of maximum absolute PD amplitude along cycle partition window. It is defined as:

$$M_T(i) = \{q_\lambda \mid \max(abs(q_\lambda)), t_\lambda \in \Delta T_i\} \tag{5.3}$$

where $abs(q_\lambda)$ is the absolute value of discharge magnitude measured in the ith cycle partition window.

The CRPD current distribution function stands for the distribution of accumulated discharges along cycle partition window and is defined as:

$$I_T(i) = \frac{\sum (q_\lambda \mid t_\lambda \in \Delta T_i)}{t} \tag{5.4}$$

where t is the test time interval for acquiring the total PD data and q_λ is the magnitude of PD pulse measured in the ith cycle partition window.

CRPD power loss distribution function exhibits the distribution of discharge power loss along cycle partition window and is defined as:

$$P_T(i) = \frac{\sum (q_\lambda \bullet V_\lambda \mid t_\lambda \in \Delta T_i)}{t} \tag{5.5}$$

The last distribution function introduced in this chapter to investigate PD distributions is the quadratic rate distribution function. It is defined as:

$$Q_T(i) = \frac{\sum (q_\lambda^2 \,|\, t_\lambda \in \Delta T_i)}{t} \tag{5.6}$$

where t is the test time and q_λ is the magnitude of PD pulse amplitude measured in the ith cycle partition window.

5.3   CYCLE RESOLVED PD DISTRIBUITON FUNCTION

The use of cycle resolved PD (CRPD) distribution functions to analyze discharge is a new approach with which ac cycle based discharge properties and their relationship under the periodically changing external stress are observed. The results shown in this chapter demonstrate that CRPD distribution functions are practically useful to investigate discharge physical mechanisms as well as to monitor insulation degradation.

5.3.1   Discharge Occurrence

In PRPD and PHPD approaches, there has been considerable interest in using PD occurrence distribution functions to assess the quality of electrical insulation system under ac electrical stress. In CRPD approach, it is found that the number of PD events varies from cycle to cycle due to the stochastic behavior of discharge. In addition, the number of PD events in each cycle will be treated in late of this chapter as a reference to examine other cycle based discharge distribution functions.

As seen in figure 5.1, distribution functions of different defects are plotted together for comparison. Obviously, the difference is not as clear as the relevant PRPD and PHPD occurrence distribution functions. According to figure 5.1, the ranges of discharge events for different types of defect are (a): 30, (b): 10, (c): 9 and (d): 15. Obviously, air corona has the largest variation of discharge event number among the four defects under investigate. The phenomenon of varying discharge event per cycle indicates that the form and decay if discharge pulses under conditions independent of the ac voltage across the gap.
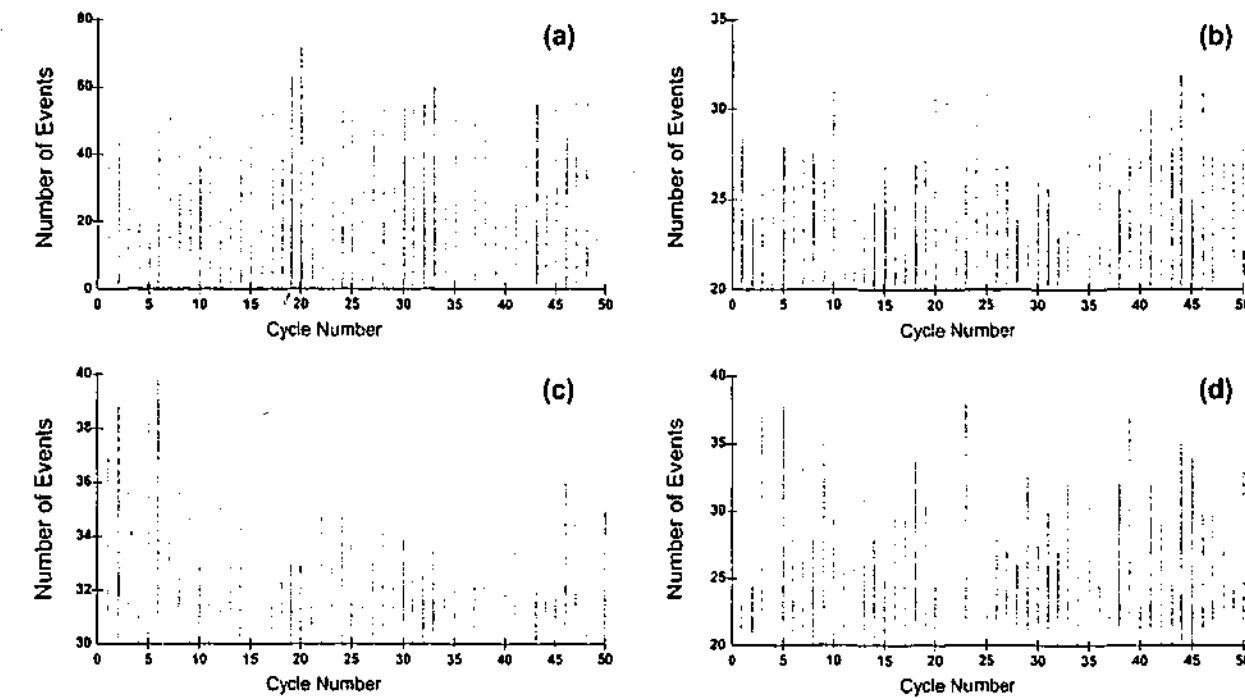
Fig. 5.1 Cycle resolved discharge occurrence distribution functions acquired from
(a)   a point-to-plane arrangement
(b)   an oil-impregnated pressboard sample
(c)   an epoxy resin stator bar
(d)   a point-to-dielectric arrangement

5.3.2   Average Discharge Amplitude

The distribution functions of average PD amplitude in each cycle are another measure to characterize discharges. As an example, figure 5.2 shows the distribution function of average PD amplitude of different types of defect. In particular, after being applied with the distribution mean and standard deviation, the central tendency of PD amplitude distribution along the continuous ac cycle is shown in figure 5.3 where Mu is the mean value of average PD amplitude and Stdev stands for the standard deviation.

It has been shown from figure 5.2 that the average PD amplitude varies from cycle to cycle. The distribution of discharge occurrence and the variation range are different for different types of defect. The standard deviation ranges of different types of defect during a continuous fifty cycles period are shown in figure 5.3. This helpful tool is implemented in the PDD system in order to provide quick visual check on the stability of the discharge activity over a number of cycles.
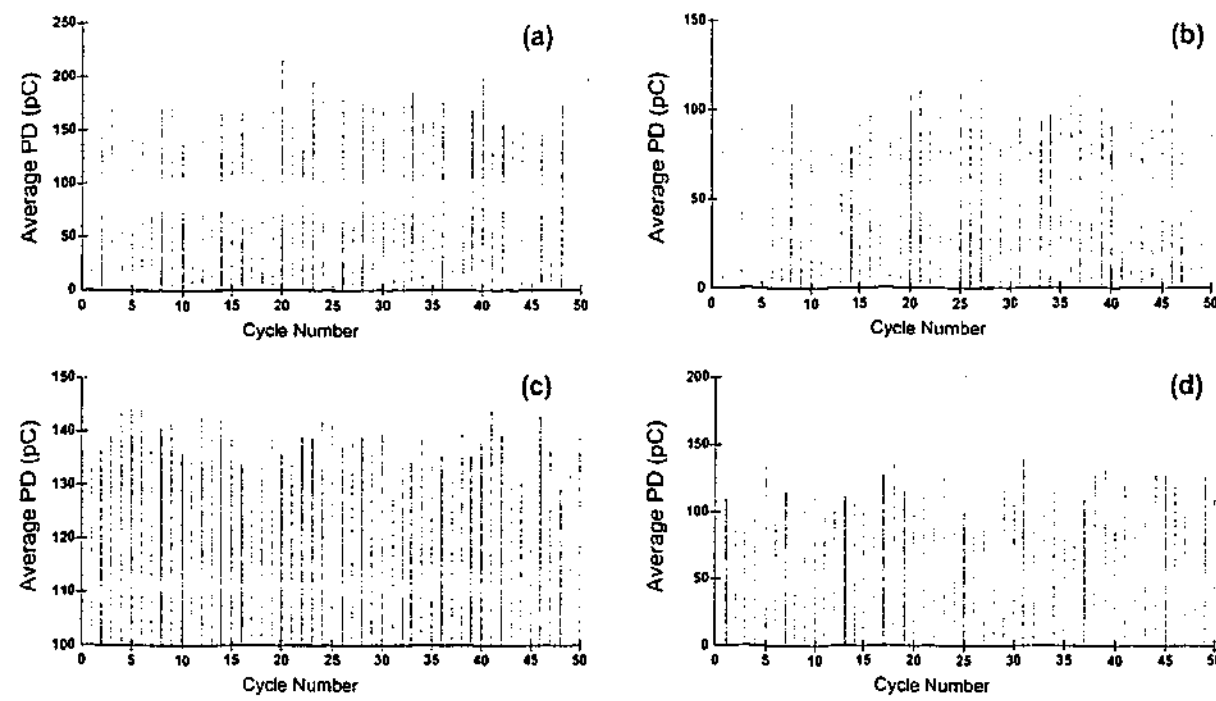
Fig. 5.2 Cycle resolved average discharge amplitude distribution functions measured from
(a) a point-to-plane arrangement
(b) an oil-impregnated pressboard sample
(c) an epoxy resin stator bar
(d) a point-to-dielectric arrangement
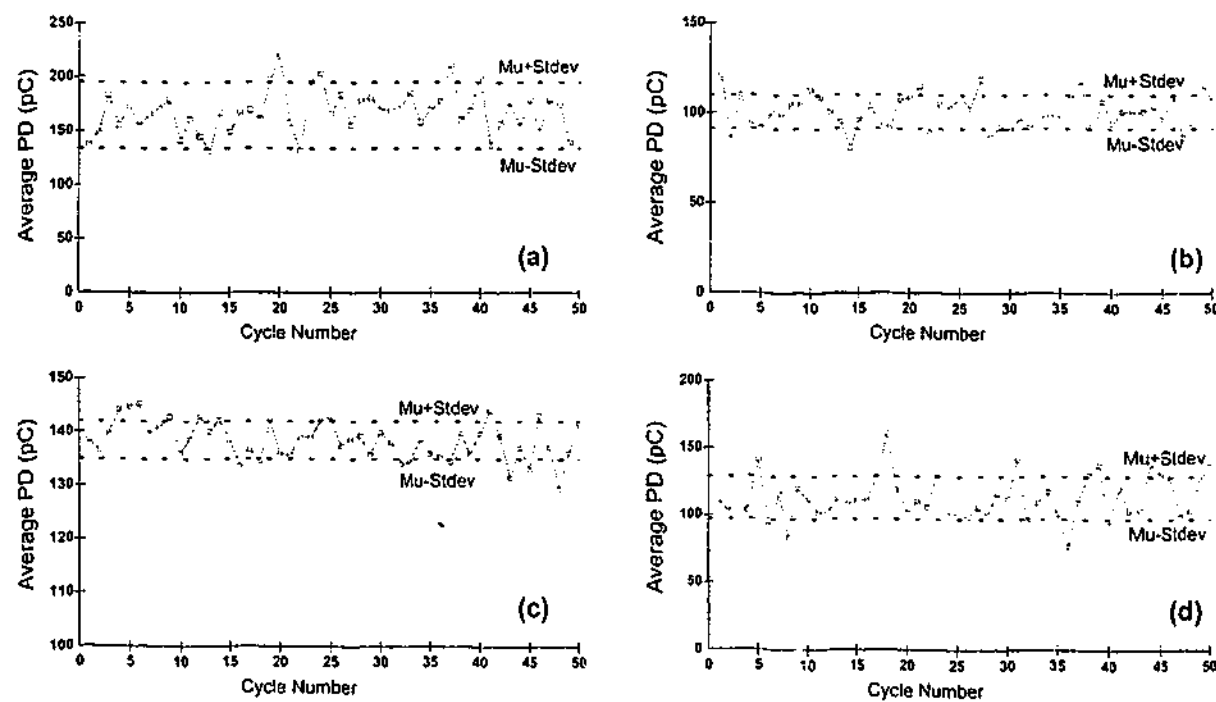
Fig. 5.3 CRPD average PD amplitude with the range of standard deviation measured from
(a) a point-to-plane arrangement
(b) an oil-impregnated pressboard sample
(c) an epoxy resin stator bar
(d) a point-to-dielectric arrangement

5.3.3 Maximum Discharge Amplitude

The maximum PD amplitude indicates the quantity of maximum PD amplitude and its polarity (positive or negative half cycle) in each cycle. This is a useful distribution function to analyze discharge as well as to provide distribution information for PD pattern recognition. The maximum distribution functions of various defects are shown in figure 5.4. With this distribution function, the polarity of the maximum discharge can be easily found in the distribution pattern.
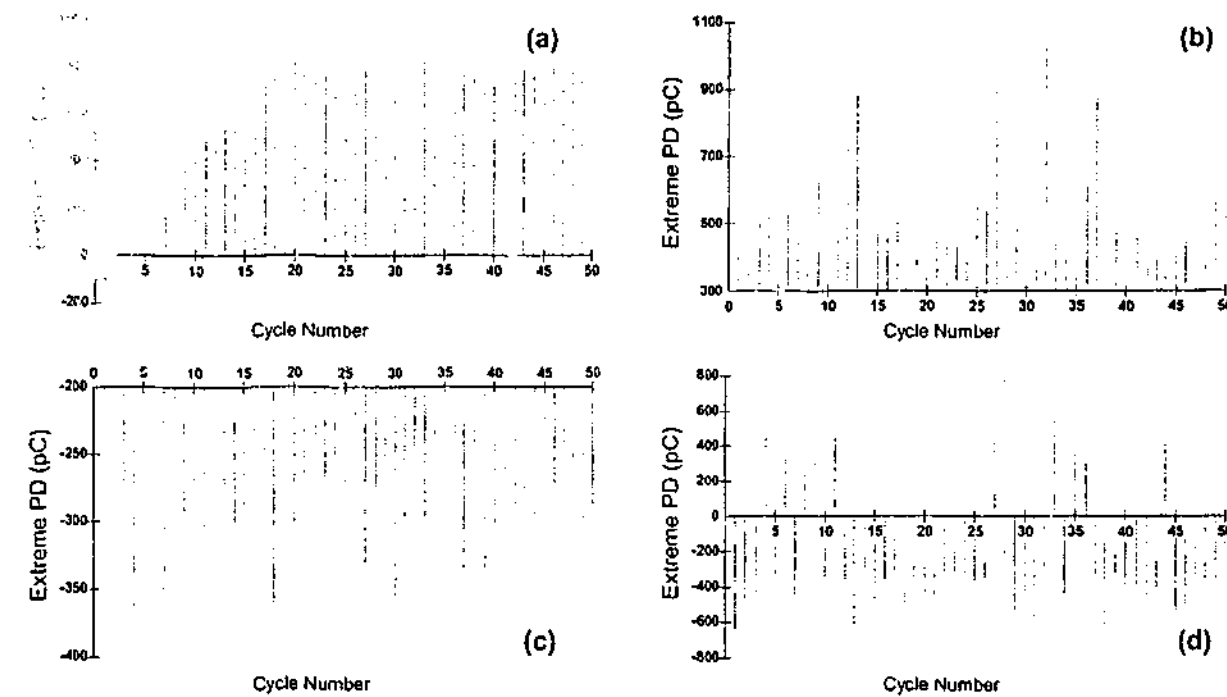
Fig. 5.4 Cycle resolved maximum discharge distribution functions measured from
(a) a point-to-plane arrangement
(b) an oil-impregnated pressboard sample
(c) an epoxy resin stator bar
(d) a point-to-dielectric arrangement

5.3.4 Discharge Current

According to equation 5.4, the distribution function discharge current reflects the distribution of accumulated discharges along cycle partition window. The distribution of accumulated PD from cycle to cycle has demonstrated important discharge characteristics as shown in figure 5.5 in which distribution functions for different types of defect are illustrated.
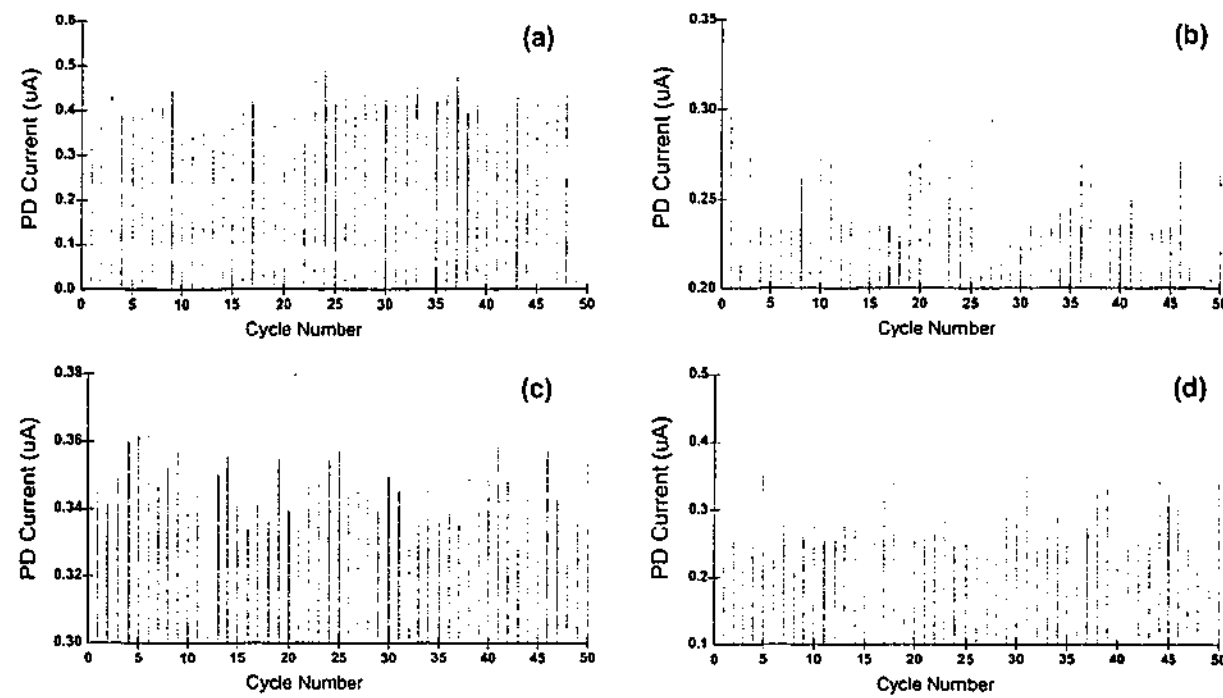
Fig. 5.5 Cycle resolved discharge current distribution functions measured from
(a) a point-to-plane arrangement
(b) an oil-impregnated pressboard sample
(c) an epoxy resin stator bar
(d) a point-to-dielectric arrangement

5.3.5 Discharge Power Loss

The distribution function of PD power loss contains not only the information for the magnitude of PD but also the instantaneous voltage under which PD occurs. Distribution function of discharge power is a measure of the PD pulse power distributed along the cycle partition window. The discharge power loss within a cycle partition window is calculated as the sum of individual discharge pulse energy then divided by the cycle period. The distributions of discharge power are shown in figure 5.6.

It has been shown in figure 5.6 that discharge power loss varies against the cycle partition window. Obviously, the distribution functions of discharge power acquired from various defects can be visually compared. In addition the feature quantities of these distribution functions can be extracted to form PD fingerprints. The power distribution functions for different types of defect during the continuous fifty cycles are different in terms of the intensity and the variation range as seen in figure 5.6.
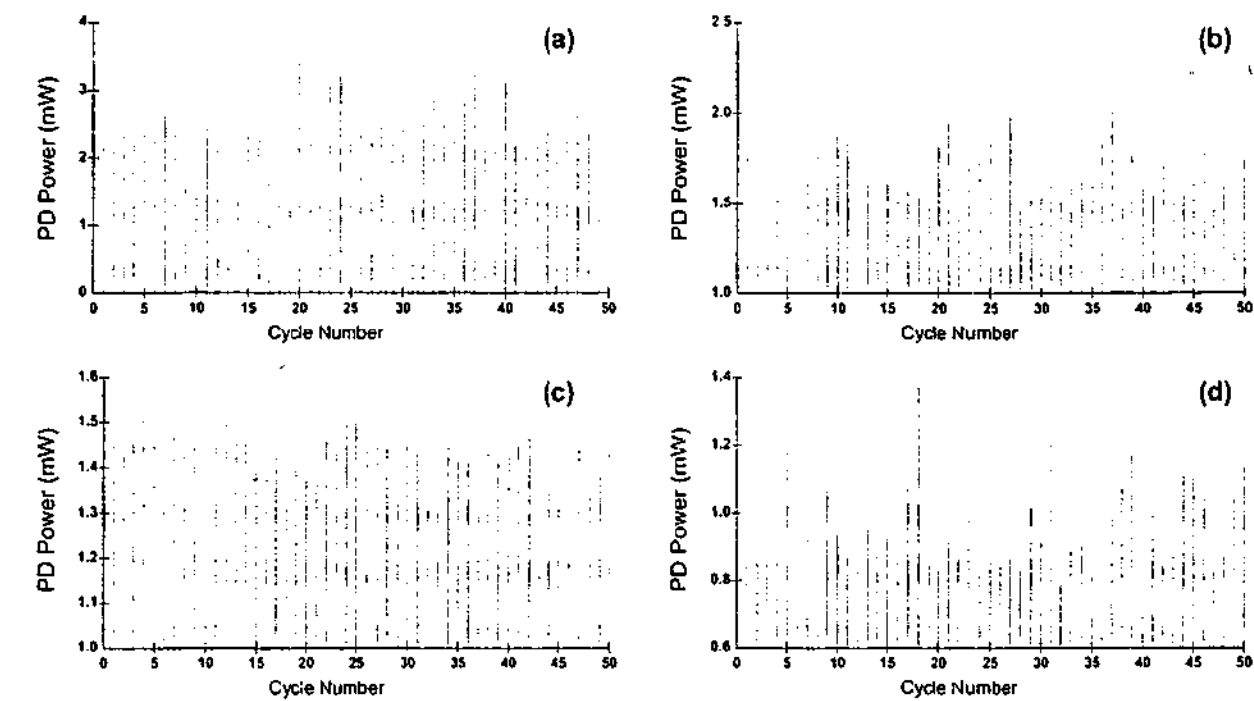
Fig. 5.6 Cycle resolved discharge power distribution functions measured from
(a) a point-to-plane arrangement
(b) an oil-impregnated pressboard sample
(c) an epoxy resin stator bar
(d) a point-to-dielectric arrangement

5.3.6 Quadratic Rate of Discharge Amplitude

Distribution function of quadratic rate is a distinctive property for dispersion discharge magnitude because the squared aggregate assigns greater weight to the larger discharge pulses. With the help of this distribution function, it makes possible detailed analysis on accumulated discharge amplitude over the cycle partition window. According to equation 5.6, the distribution function of quadratic rate is calculated as the sum of the squares of the individual discharge magnitudes in a cycle partition window and then divided by the cycle period as illustrated in figure F.3 of appendix F.

Compared with the average PD distribution functions in figure 5.2, it is found that quadratic distribution functions shown in figure F.3 of appendix F have more distribution variation, particularly for defect type (b), (c) and (d).

5.4 RELATIONSHIP WITH PRPD AND PHPD DISTRIBUTIONS

As seen from figure 5.1 to 5.6 and figure F.3 of appendix F that distribution functions show discharge activity over the continuously acquired ac cycle period. It should be remembered that these types of discharges were also analyzed using PRPD and PHPD distribution functions. It is interesting and useful to explore cycle based discharge distributions in conjunction with either phase or pulse-height partition windows. With this approach, discharge distribution functions can be partitioned on the basis of a 2-D plane made of either phase and cycle partition windows or pulse-height and cycle partition windows. Discharge power distribution function of PRPD and CRPD is demonstrated in figure 5.7(a) while the distribution function of PHPD and CRPD is illustrated in 5.7(b). PD data are measured from a point-to-dielectric arrangement. The RMS value of applied ac voltage was 3 kV and the phase window per distribution was 1.8 degrees or 0.03142 radians. Pulse-height window is partitioned in accordance with the resolution space. It is seen for this relatively simple configuration that the data on the conditional distributions show a very complicated dependence in terms of ac phase, PD amplitude as well as the ac cycle number.
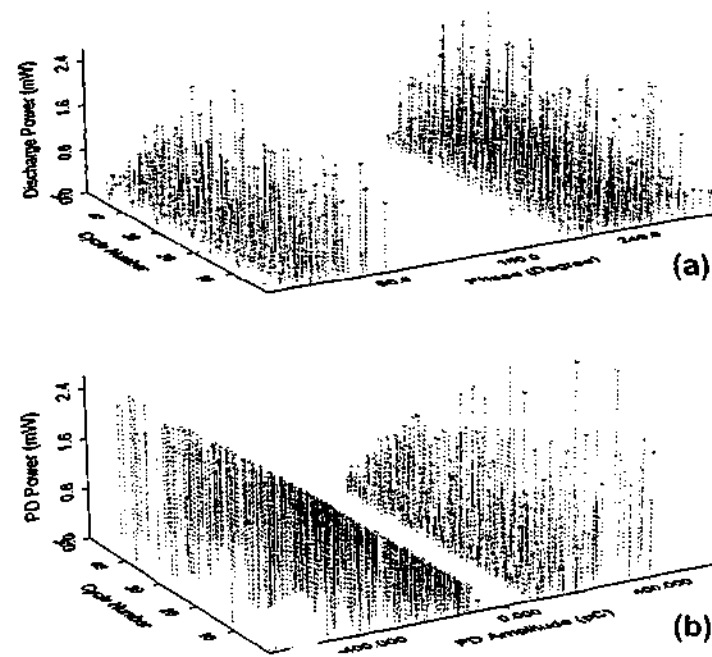

Fig. 5.7 Distributions of discharge power measured from a point-to-dielectric arrangement
(a) PD power – ac cycle window – phase window
(b) PD power – ac cycle window – pulse-height window

5.5 ANALYSIS OF CORONA USING CRPD DISTRIBUTIONS

Corona discharges in a point to plane arrangement result from electron avalanche under an inhomogeneous field. Air is a mixture of gases, primarily nitrogen and oxygen. The neutral molecules are ionized by electron impacts driven by the ac electrical field. Many great advances have been made in measuring and investigating corona discharge and it can be attributed to the development of PD pulse analysis techniques that have taken place over more than half a century [9, 45, 46, 60, 92]. With the dramatically improved performance of personal computers, it has become more expedient to incorporate the computer as an essential part of an overall PD measuring and evaluating system. PD analysis using distribution functions has become more and more popular as distribution functions may contain information about the deterioration of insulation material and even the type of defect. Recently, a few distribution functions have been introduced and applied to the recognition of PD sources of different type [62,75]. Statistical tools were employed to extracted information in relation to the shapes resulting from various distribution functions. In ac criteria, pulsating discharge phenomena caused by applied sinusoidal voltage, which makes the field at the highly stressed needle electrode varying continuously in both amplitude and polarity. In this section, cycle-based partition quantities are calculated in order to study the distribution characteristics of discharges under ac voltage. Being stochastic in nature, the discharge behaves differently from cycle to cycle. The distribution of PD occurrence over a number of continuous ac cycles provides important information relating to pulse-to-pulse and even cycle-to-cycle memory effects. Compared with phase and pulse height resolved distribution functions, CRPD distribution functions provide complimentary PD distribution information under ac criteria.
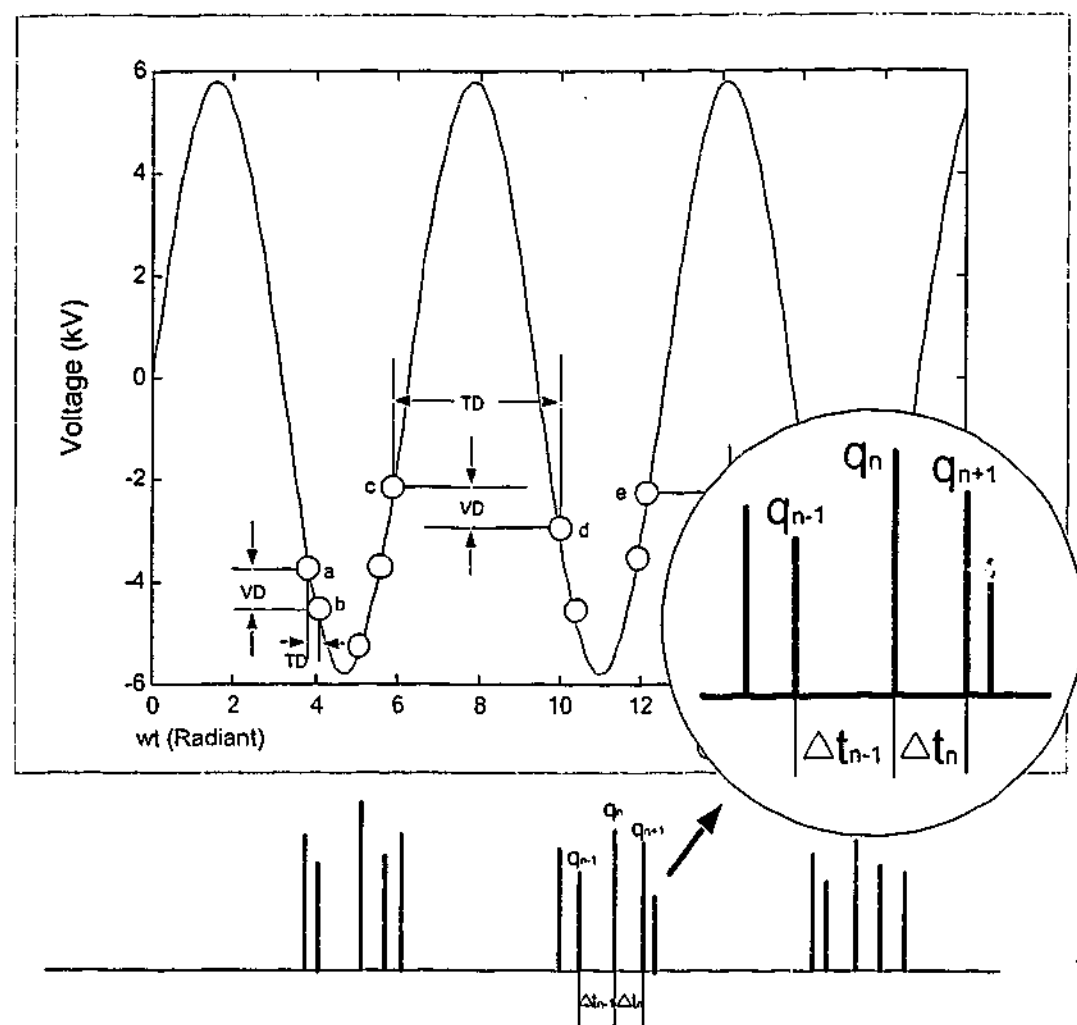
Fig. 5.8 Diagram of Trichel-pulse phenomenon measured from a point-to-plane arrangement. Δtn and Δtn-1 are pulse separation time between relevant series numbers of discharge event.
VD: Voltage difference   TD: Time difference

When Trichel pulses occur, the memory effect is due to the motion of negative-ion space charges. Depending on the arrangement of the sample and the testing criteria, the gap transit time of a space charge is much smaller than the time interval between PD extinction and inception of the subsequent cycle as illustrated in figure 5.8. The partition quantities of PD events within a cycle period and the corresponding cycle based distribution functions may led to the findings of some interesting properties of Trichel pulse phenomena.

Discharges can exhibit complex stochastic behavior in which memory effects have significant impacts on discharge pulse distributions. Under ac voltages, the probability of a discharge event at particular phase position as well as the pulse distribution within

one or a number of continuous ac cycles depend on the properties of the defect such as the geometry of void as well as the external field.

5.5.1 Corona Inception and Extinction Properties

The initial electron release that may be contributing to the PD inception at the beginning of each cycle is due to the field-induced ionization of molecules [4, 15, 47]. The process itself, under the testing criteria, is inherently probabilistic that leads to discharge initiation and growth. The cycle-based inception discharge amplitude and voltage over the continuous 50 cycles are illustrated in figure 5.9.

Apparently, memory effects have a considerable impact on a sequence of discharge within a cycle. The initial condition of each cycle is dependent upon a primary electron being presented close to the needle electrode. Such electrons may be generated by field-induced emission or by collision between molecules. It can be observed from the plots of figure 5.9 that the inception voltage is much more stable than the extinction voltage. Meanwhile discharge amplitudes of both inception and extinction events exhibit a range of statistical variation. The observable phenomena may be explained by the fact that induced ion space charges and metastable particles from the last PD event of the previous cycle have little impact on the initialization and development of the inception PD event.
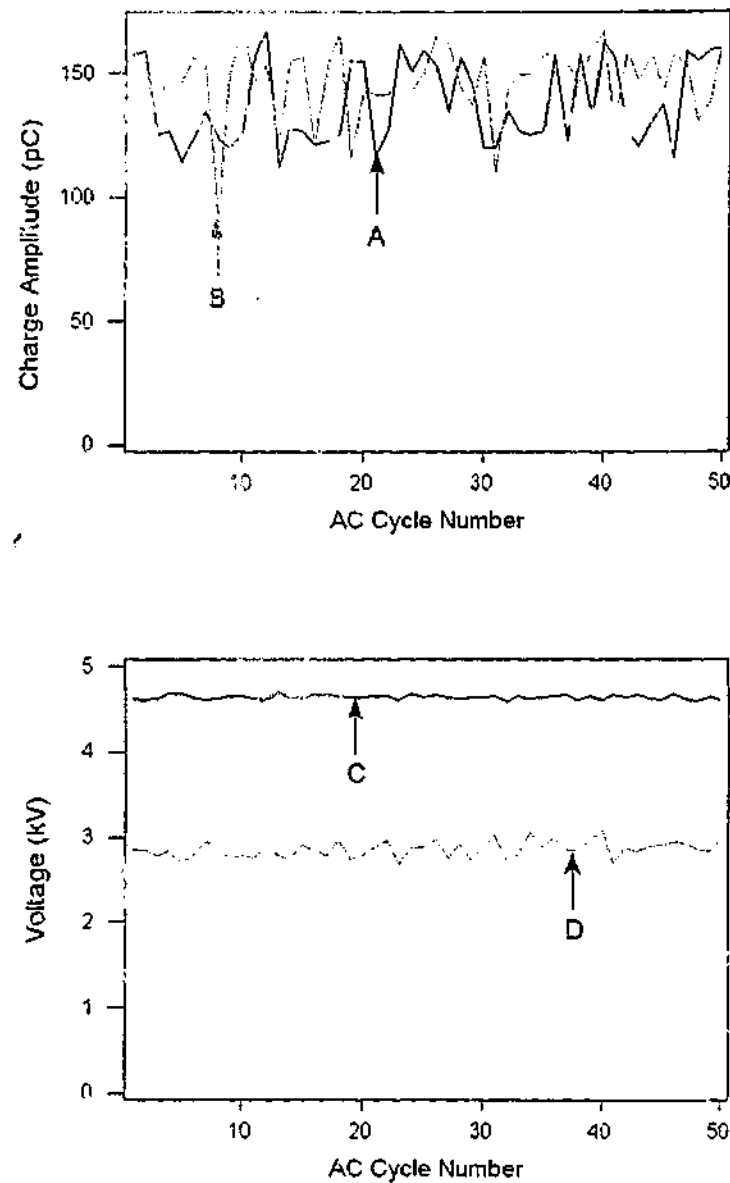
Fig. 5.9 CRPD inception and extinction parameters
A: Inception discharge amplitude
B: Extinction discharge amplitude
C: Inception voltage
D: Extinction voltage

The descriptive statistics of inception and extinction discharge amplitude are shown in figure 5.10, together with the swing range of mean, standard deviation, and median calculated at 95% confidence interval. The results indicate that the mean of inception charge amplitude is 137.5 pC, which is approximately 5.8 pC smaller than that of the extinction charge amplitude. In addition, the entire spreading of the inception charge amplitudes is about 4.07 pC smaller than that of the extinction. The range of inception

discharge is spread more widely than that of extinction discharge after applying 95% confidence level. It implies that the memory effects have stronger impact on the extinction discharge amplitude.
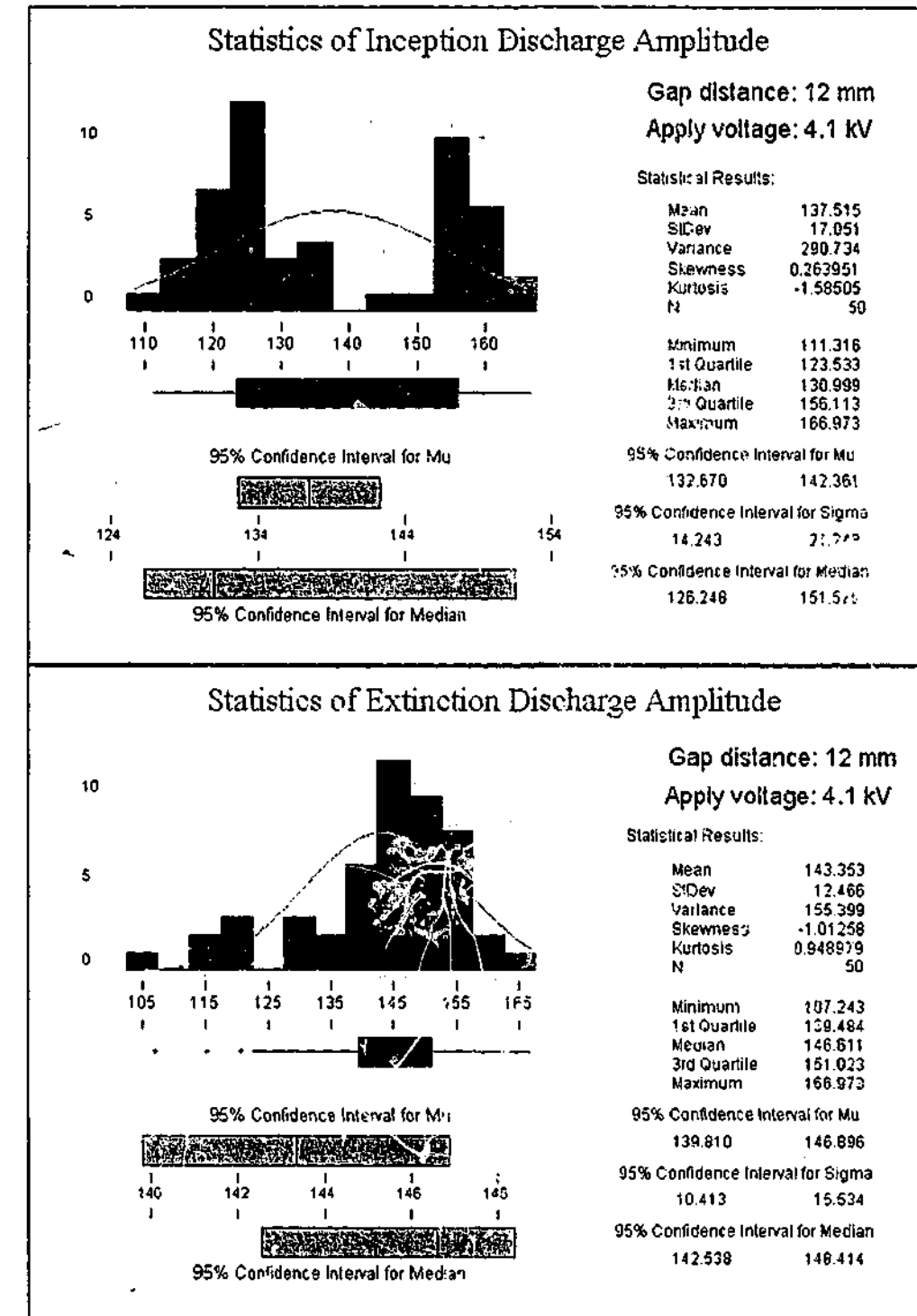
Fig 5.10 Statistics of inception and extinction discharge amplitude
(Note results calculated without considering PD polarity)

Undoubtedly, some properties of the CRPD distribution functions can be attributed to the influence of pulse-to-pulse memory effects. The ion space charge and metastable species between the gap generated from previous pulses and, especially the most recent pulse has a significant impact on the initiation and development of subsequent pulses. In addition, some statistical properties of CRPD distribution functions will be proved late in this chapter that they are associated with the influence of the test voltage. Indeed, properties of CRPD distribution functions are related to test criteria such as gap distance and background radiation etc.

Experiments have found that if the gap spacing is increased to a certain distance, the discharge characteristic for the point-to-plane arrangement changes because the presence of the surface charge becomes less important. Actually, the mechanisms of discharge initiation on the positive and negative half cycles will be different if the discharge gap is not symmetrical in its geometry. The electron release mechanisms might correspond to field emission from the metal surface on the positive and negative half cycles. As a result, the positive discharge ceases entirely, and the negative discharge takes on the appearance of a sequence of Trichel pulses. As shown in figure 5.11, the mean inception voltage is 5.566 kV compared to 4.873 kV of the extinction voltage mean. The first discharge of each cycle occurs once the local field strength exceeds the inception level, which generates ions and metastable species. Therefore, the occurrence of the following discharge events is under the influence of the remaining ions and metastable species produced by previous events. As a consequence, the memory effects have a significant impact on the extinction voltage. The calculated statistical results shown in figure 5.11 indicate that inception voltage is more stable than the extinction voltage. This is due to the remaining space ions generated during negative half cycles being cleared away in the following positive half cycle.
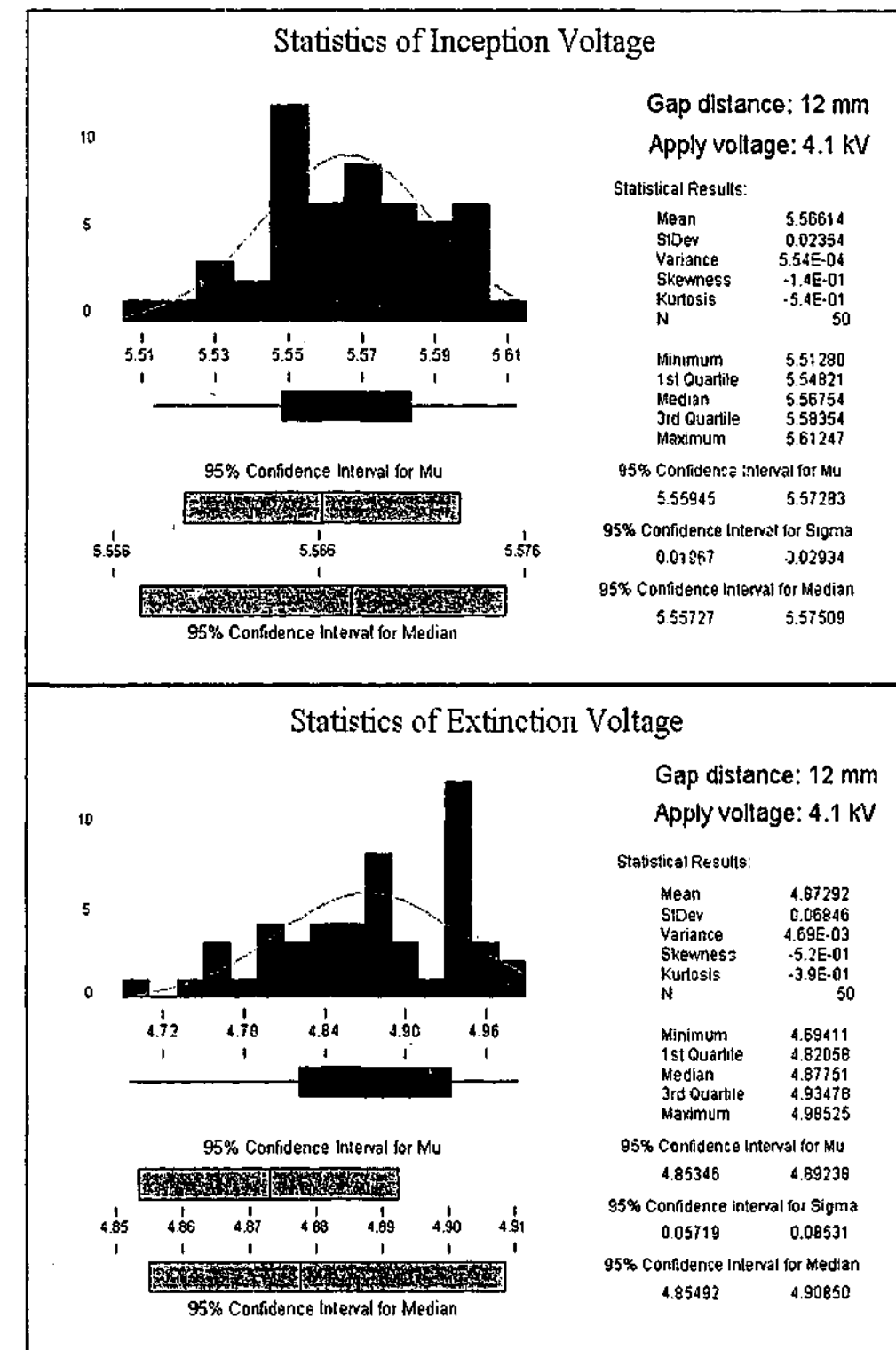
Fig 5.11 Statistics of inception and extinction voltage

5.5.2 Cycle Resolved Discharge Statistics

Cycle based distribution functions such as occurrence, mean, range, standard deviation, standard deviation of mean and mean of successive squared differences are shown in figure 5.12.
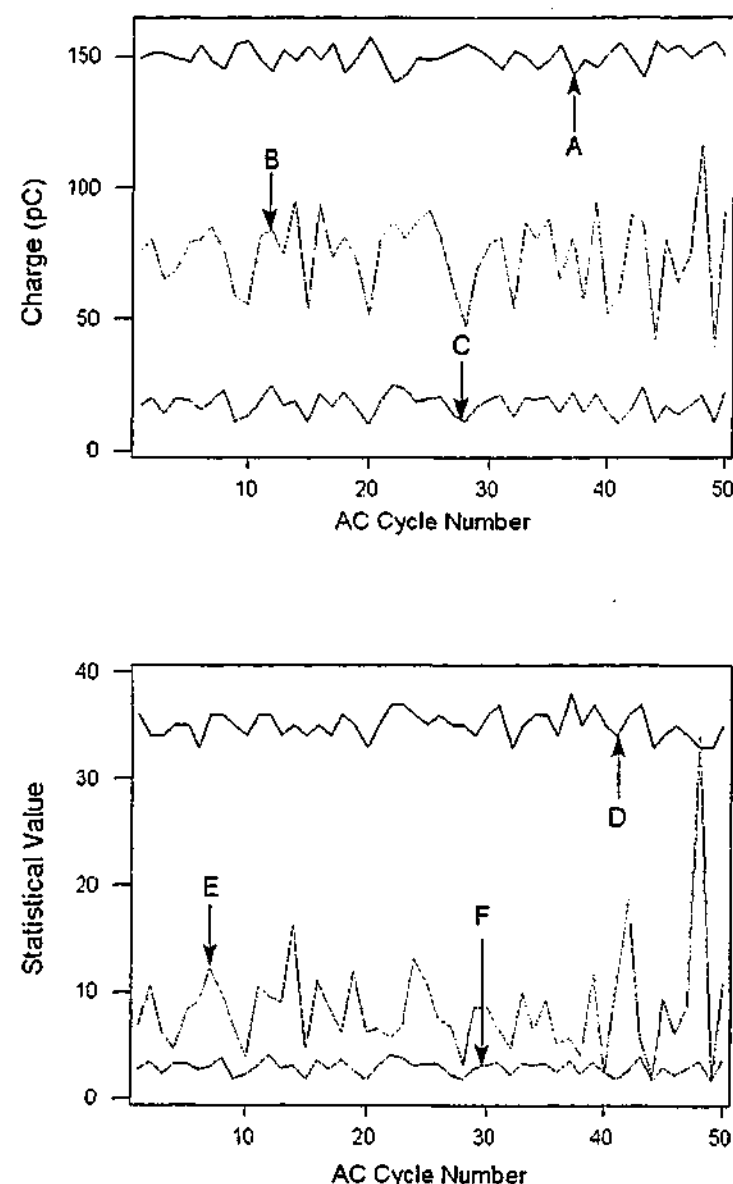
Fig 5.12 Distribution functions of selected statistics in CRPD category
A: Mean PD amplitude   B: PD amplitude range
C: PD amplitude standard division   D: PD occurrence
E: PD amplitude MSSD   F: PD amplitude standard error of mean

The process mechanisms of Trichel pulses can be revealed by the statistical correlation between cycle based discharge occurrence and other cycle partition quantities. The central tendency of some cycle partition quantities, shown in figures 5.13 and 5.14, demonstrate the correlation between the partition quantities and the number of discharge events occurring in a cycle. As illustrated in figure 5.13, the statistics of cycle based PD amplitude distributions are closely related to the number of PD events in the cycle. It is demonstrated in the figure 5.13 that the central tendency of the PD mean amplitude

distributions is statistically decreased as the discharge events, increase while the maximum PD amplitude is not related to the number of PD events in a cycle. The observed phenomena agree with the earlier findings [46].
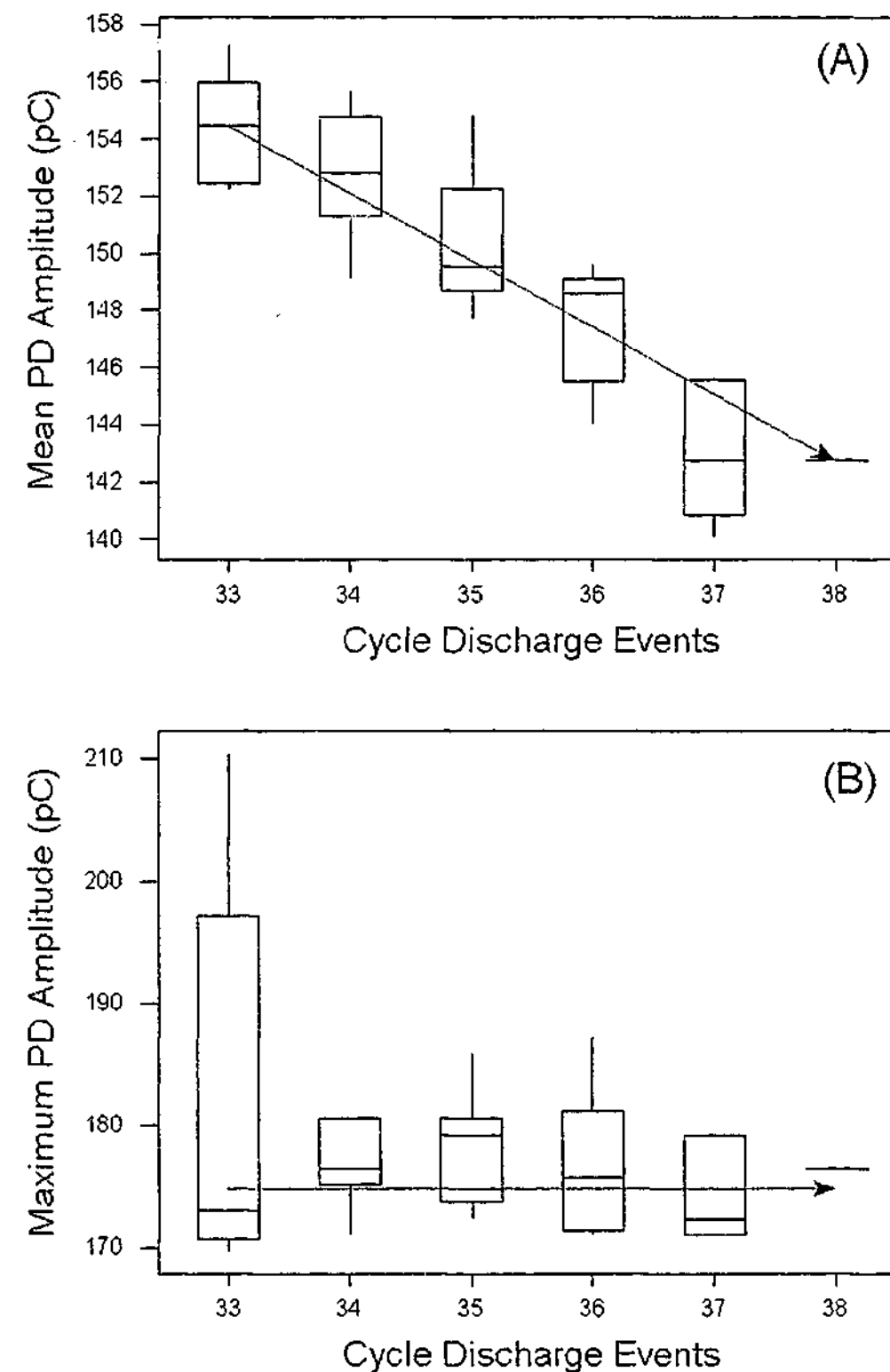

Fig 5.13 Cycle-based absolute PD magnitude vs. the number PD events measured at 4.1 kV
(A): Mean amplitude, (B): Maximum amplitude

The reason behind the phenomena is that the initial growth of a PD depends largely on the local field strength. The amplitudes of PD are sensitive to the small reductions in the field at the point electrode such as the presence of induced space charges within the gap. In addition, the process of discharge initiation and development is also dependent on the drift velocity of space charges and their distribution around the sharp point. The dependence of time separation on PD amplitude in a sequence is yet determined by the competing effects of negative-ion space charges from the previous pulses in reducing the electric field around the point electrode. Statistically, the larger the pulses, the more will be the negative ions produced and the longer will be the time to the next pulse resulting in less PD occurrence.

Under test criteria, other important characteristics of Trichel pulse can also be found in the correlation between the variation of PD amplitude and the number of PD events in a cycle. The amplitude variation can also be attributed by the time varying metastable particles and ion densities generated by previous PD events. As shown in figure 5.14, the central tendency of amplitude variance is also related to the number of PD events. MSSD stands for the half mean of successive squared differences of consecutive PD amplitude within a cycle and it is an important measure of discharge amplitude variation in a consecutive sequence within a cycle. With N denoted as the total number of PD events in an arbitrary cycle and q_n is the nth PD event with amplitude of q_n, the MSSD is defined:

$$MSSD = \frac{\sum_{n=2}^{N} (q_n - q_{n-1})^2}{2(N-1)}, \qquad N > 1 \qquad (5.7)$$

It has been shown in figure 5.14 that the central tendency of MSSD distribution is not related to the number of cycle discharge events. This is due to the statistical nature of Trichel pulse itself. The difference between the amplitude of a PD event and the amplitude of its adjacent event is not associated with the number of discharge events in a cycle. In fact, it depends on the time interval distribution within a cycle. Therefore, the central tendency of MSSD demonstrates that it is independent of the number of PD events under the test criteria. Figure 5.14 shows that the distribution of these cycle

statistics follows certain rules when compared with the distribution of PD occurrence because of the nature of the mechanisms of Trichel pulses themselves.
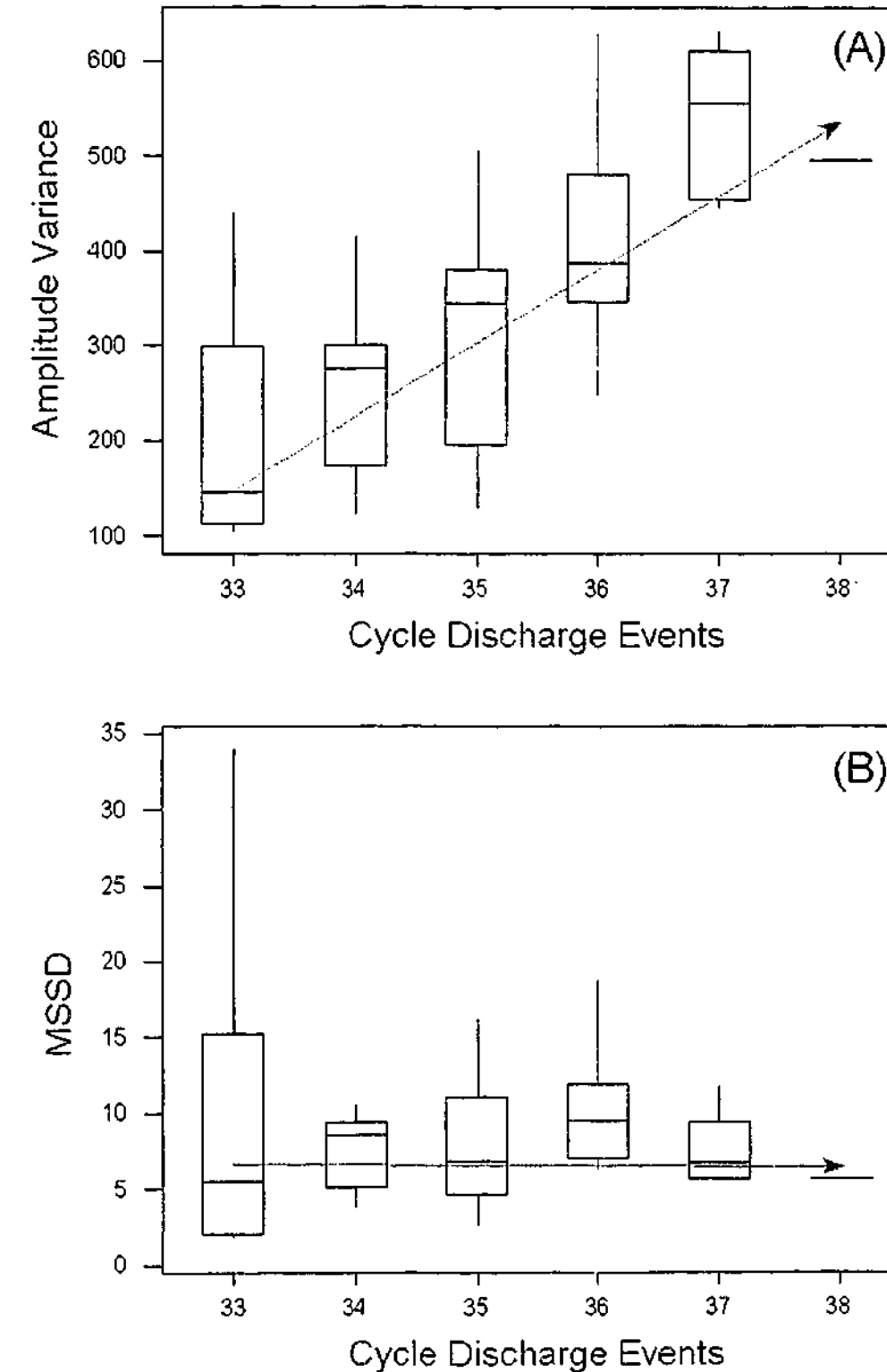

Fig 5.14 Cycle-based PD amplitude statistics vs. the number PD events measured at 4.1 kV
(A): Amplitude variance. (B): Amplitude MSSD.

PD analysis using cycle based distribution function is a new and useful approach to investigate discharge phenomena as it relates to the discharge activities under periodically changing field stress. Due to the complexity of discharge process, it is practical useful to quantify the degree of relationships among cycle based statistical variables. The correlation coefficient is a useful indicator that quantifies the relationship between two distributions. It has been used in previous chapters to quantify the correlation between PRPD and PHPD distribution functions. If one distribution function tends to increase as the other decreases, the correlation coefficient is negative. Conversely, if the two distribution functions tend to increase or decrease together the correlation coefficient is positive. Based on the continuous cycle partition window index, the correlation coefficients between a number of distribution functions are calculated and tabulated in table 5.1.

	Mean	Range	StdDev	MSSD
Range	0.580			
StdDev	0.859	0.800		
MSSD	0.078	0.745	0.318	
PD Events	0.837	0.443	0.675	-0.024

Table 5.1 Correlation coefficients between cycle based statistics at 4.1 kV

In figure 5.15, the correlation coefficients between the occurrence and discharge amplitude mean, range, standard deviation and the MSSD are calculated. The calculated correlation coefficients are plotted against the change of applied voltage. Note that polarities of discharge amplitude are taken into account in calculating these correlation coefficients.
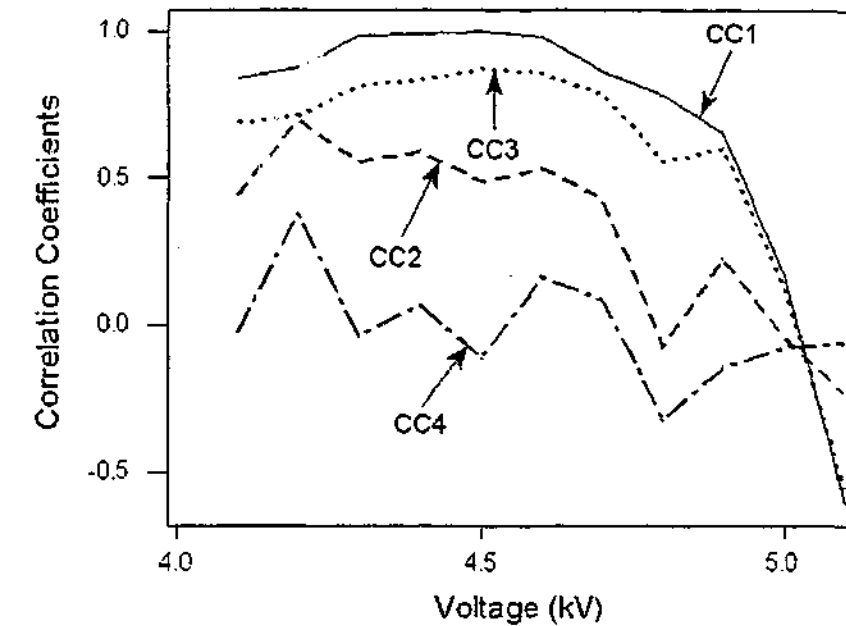
Fig 5.15 Correlation coefficients between selected statistics and the number of PD events
CC1: Mean of PD amplitudes.
CC2: Range of PD amplitudes.
CC3: Standard deviation of PD amplitudes.
CC4: MSSD of PD amplitudes.

It may be summarized from the observation based on figure 5.15 that (1) Both CC1 and CC3 are relatively stable within 4.1- 4.6 kV and then decrease rapidly when voltage further increased. The variation of CC1 and CC3 indicates that within the applied voltage range, cycles having more PD events contain higher amplitude mean and standard deviations. (2) CC2 generally follows the trend of CC3 and illustrates that the range of PD amplitude distribution becomes wider when more events occurred within a cycle. In other words, the distribution of amplitude range moves toward the opposite direction when voltage increases, meaning that when the number of PD event increases in a cycle, the PD amplitude range of the cycle decreases. (3) CC4 oscillates with a large swing of 0.4 and then becomes negative when the voltage is increased. It implies that the distribution of PD amplitude's MSSD may not be correlated with the distribution of PD occurrence. It may be affected by other factors such as the change of ion density around the sharp point electrode and the variation of background radiation etc [47, 48].

5.6 CONCLUDING REMARKS

CRPD distribution functions provide discharge activity information based on the ac voltage cycle. They are new distribution functions and implemented in the PDD system. With the help of CRPD distribution function, the PDD system can explore discharge distribution information not only on the basis of ac phase and pulse-height partition windows but also on the time basis. In addition to the basic introduction of CRPD distribution functions, properties of negative air corona are investigated as an example of the application of CRPD distribution functions for PD pattern analysis. Some important statistical characteristics of Trichel pulse are observed from CRPD distribution functions and they can be extracted to form PD fingerprints.

Experimental results of negative Trichel-pulse discharge are studied by analyzing cycle-resolved distribution functions. The statistical parameters of PD inception and the extinction within fifty continuous cycles are calculated for comparison. The results imply that the physical conditions between inception and extinction events at discharge initiation and growth stages are significantly different. The reason behind such a phenomenon is the impact of memory effects between subsequent discharge pulses. It has been observed that some cycle statistics are closely related to the number of PD occurrence. No doubt, under ac criteria, the periodical changing field is the primary cause of the discharges. A PD occurs when the electric strength within an insulation region exceeds the local inception level. With CRPD distribution functions, it is found that the distribution of PD occurrence over a number of continuous ac cycles is a sensitive indicator reflecting some important characteristics of discharge process. The observed correlation coefficients are investigated with the change of applied voltage. The experimental results demonstrate that the calculated correlation coefficients tend to decrease when the voltage is increased, as shown in figure 5.15. The results presented are in agreement with earlier findings, for instance, for a cycle with more discharge events, there is a shorter time separation between pulses, statistically resulting in higher discharge amplitude.

Chapter 6

New Techniques for Analyzing Consecutive Partial Discharge Patterns

In previous chapters, discharge distribution functions of various distribution categories are studied. It is found that PD pulses in a sequence are not independent but correlated. As for discharge pattern recognition, feature quantities can be extracted from statistics of various distribution functions. In this chapter, new techniques for pulse sequence analysis using consecutive PD distribution functions are presented.

6.1 OVERVIEW OF PULSE SEQUENCE ANALYSIS

The traditional approach to the measurement of PD in insulating systems is to determine a PD level or mean PD value. This has a certain convenience in simplicity because one only needs to report a single number for a given set of conditions. It is well known that PD phenomena which occur both in the presence and absence of solid dielectrics are inherently stochastic processes that can exhibit significant statistical variability in such characteristics as pulse shape, pulse amplitude, and times of occurrence [46, 54].

Pulse sequence analysis is used to measure the stochastic properties of PD. The method establishes new distributions that reveal correlation among successive pulse amplitudes and pulse time separations. Application of the method to an investigation of sustained negative-corona pulses in air shows the existence of strong correlation between pulse amplitudes and subsequent pulse time intervals and between amplitudes of successive pulses as well [59]. It is found that the observed correlation is consistent with Trichel-pulse formation. Under ac voltage, the stochastic behavior in a point-to-dielectric air gap has been studied from direct measurements of various conditional and unconditional distributions. The results reveal significant pulse-to-pulse and phase-to-phase memory propagation at all gap spacing. The observed memory effects are considered to be important in controlling the initiation and growth probabilities of PD pulses at any given phase of the applied voltage. The investigation for such a point-to-

dielectric arrangement was carried out by van Brunt et al. It is found that the larger the amount of charge produced by PD events in the previous positive half cycle, the sooner will be the most probable occurrence of PD events in the next negative half cycle.

The significance of memory propagation in controlling the stochastic behavior of PD phenomena was demonstrated by determination of various conditional amplitude and phase of occurrence distributions for both measured and simulated discharge pulses. PD data measured from various conditional distributions provide additional statistical information that can be used to optimize PD pattern recognition schemes. PD data on conditional distributions that give an indication of memory effects may provide the additional information needed for reliable pattern recognition.

In general, the effects of memory propagation are inherent to nearly all PD processes [60, 67]. The unconditional PD amplitude and phase distributions are sensitive to relatively small physical or chemical changes in the discharge gap, which might result from interaction of the discharge with a surface. The sensitivity to non-stationary PD behavior is much less evident in conditional distributions. This is reasonable since conditional distributions exhibit less statistical variability.

The diagnostic PD characteristics using voltage difference analysis (VDA) was originated by Patsch and Hoof in 1993 [100, 101]. It is suggested that after the initiation of an electrical tree, the generation and further growth of the hollow tree channels are accompanied by PDs. A PD usually occurs when the local electric field in a certain region exceeds within the electrode gap the local electric strength of the material. The locally confined electrical breakdown involves an avalanche of electrons whereby the separation and movement of charges lead to an opposing electric filed that reduces the local field below the value necessary to sustain the avalanche [102]. It is suggested that the external voltage difference between consecutive discharge pulses is a physically meaningful parameter for PD source identification. This approach is based on the local distribution of ions and metastable species, produced by precedent events, is governed by the physical configuration of the defect. Therefore, the correlation between successive discharges should contain information relating to type of defect. Distribution

patterns of voltage difference so far used by Patsch and Hoof are displayed in figure 6.1 and 6.2. It is assumed that the ith pulse within a sequence of PD is neither the first nor the last event of the sequence. The forward and backward voltage differences associated with the ith pulse can be defined as:

$$\Delta V_i = V_{i+1} - V_i \qquad (6.1a)$$

$$\Delta V_{i-1} = V_i - V_{i-1} \qquad (6.1b)$$

where V_{i-1}, V_i, V_{i+1} is the instantaneous voltage of the $i-1^{th}$, i^{th}, and $i+1^{th}$ PD event respectively.
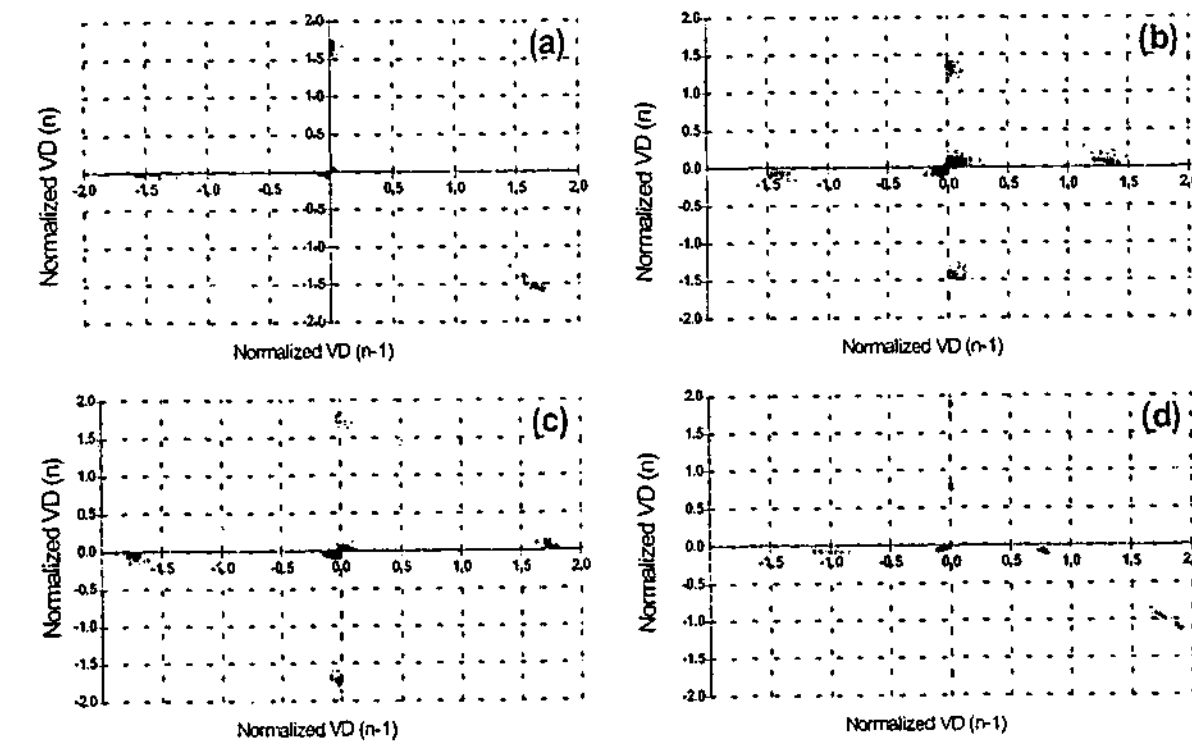

Fig. 6.1 VD distribution patterns of consecutive discharge events measured from
(a) a point-to-plane arrangement
(b) a point-to-dielectric arrangement
(c) an oil-impregnated pressboard sample
(d) an epoxy resin stator bar sample with an artificial defect inside

location, geometry, field orientation, and type of gas, gas pressure, as well as the permittivity of bulk dielectric [106-110]. Specifically, the induced charge can be divided into two components: (1) component q_μ is directly related to the space charge in a void and (2) component q_p represents the charge associated with the change in dielectric polarization. Hence, it is appropriate to investigate the discharge patterns that composed of different format in terms of discharge magnitude, voltage and time separation between consecutive PD events.

The results of earlier work have demonstrated that pulsating discharge is a stochastic process in which memory effects play an important role. The correlation between PD amplitude and time separation from the precedent pulses, particularly the latest one, has been extensively studied for ac voltage. Therefore, it is important to investigate the properties of a PD sequence using consecutive PD patterns.

Fig. 6.2 VD resolved distribution functions of PD occurrence measured from
(e) a point-to-plane arrangement
(f) a point-to-dielectric arrangement
(g) an oil-impregnated pressboard sample
(h) an epoxy resin stator bar sample with an artificial defect inside

Using these functions in conjunction with the distribution function of phase of occurrence (described in chapter 3), PD source identification was successfully presented [Patsch and Hoof]. However, there is limitation with this approach because the voltage difference model is based on the assumption that local inception field was constant. Therefore, the applied voltage should not be too much above the inception level. This prevents the accelerated physical and chemical changes inside the defect. To overcome this limitation, more patterns regarding consecutive PD properties are needed.

6.2 NEW SUBSEQUENT DISCHARGE PATTERN

The pulse-to-pulse sequence analysis is based on the fact that PD events in a sequence are correlated due to the impact from the remaining residuals produced by previous PD events. To understand the physical basis of PD transients, Pedersen etc. [103-105] studied the fundamental theory of induced charge in an ellipsoidal void. Having adopted a dipole representation, the influence of void parameters upon the induced charge has also been studied. It indicates that the induced charge is dependent on void


Fig. 6.3 Patterns of QD versus VD in a discharge sequence measured from
(a) a point-to-plane arrangement
(b) a point-to-dielectric arrangement
(c) an oil-impregnated pressboard sample
(d) an epoxy resin stator bar sample with an artificial defect inside
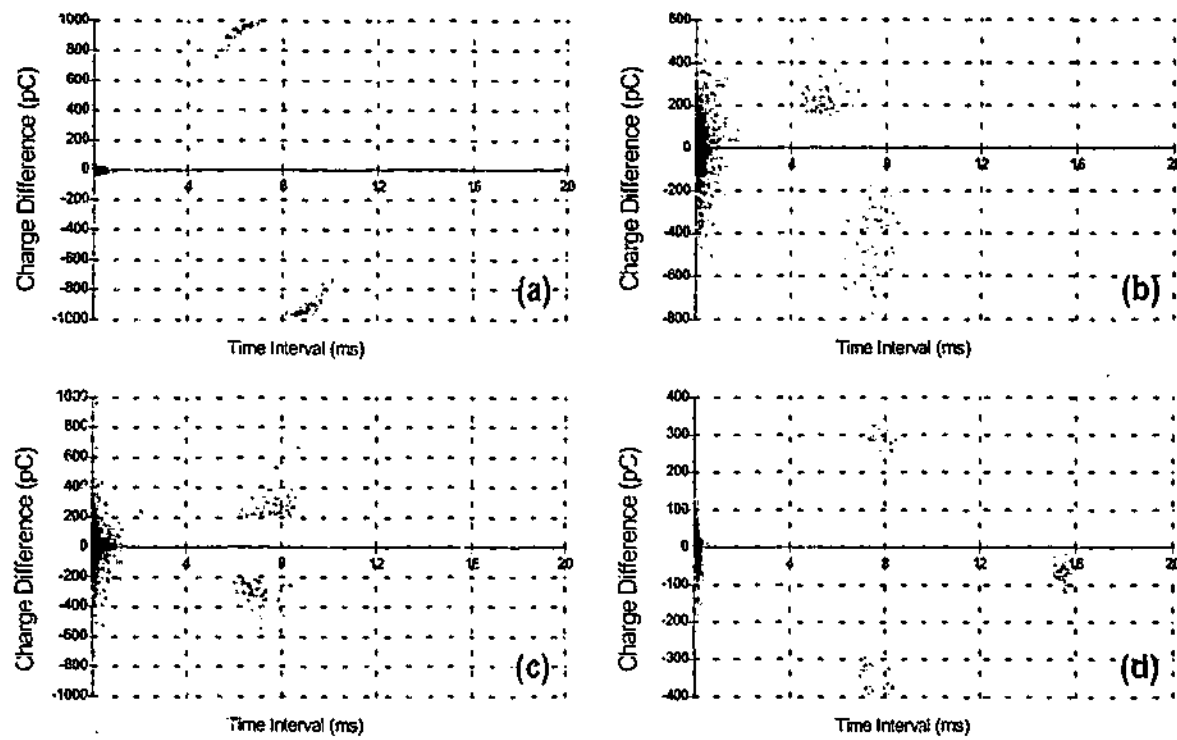
Fig. 6.4 Patterns of QD versus TD in a discharge sequence measured from
(a) a point -to-plane arrangement
(b) a point -to-dielectric arrangement
(c) an oil-impregnated pressboard sample
(d) an epoxy resin stator bar sample with an artificial defect inside
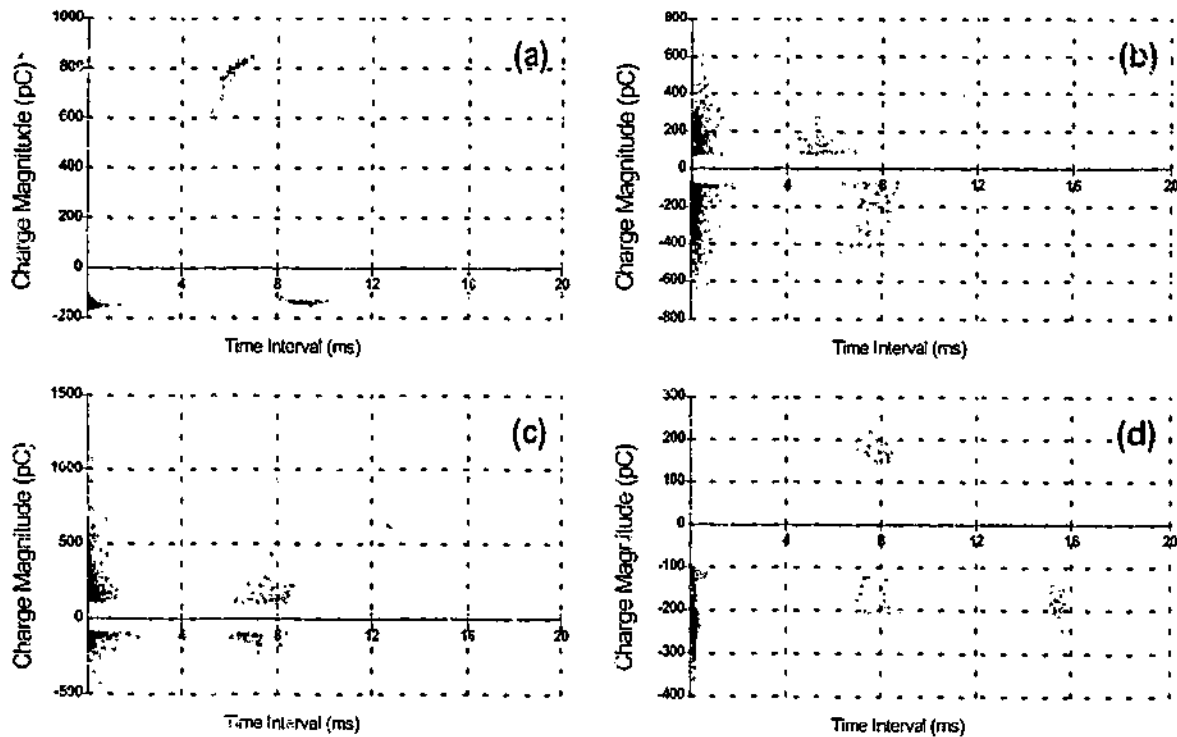
Fig. 6.5 Patterns of PD amplitude versus TD in a discharge sequence measured from
(a) a point -to-plane arrangement
(b) a point -to-dielectric arrangement
(c) an oil-impregnated pressboard sample
(d) an epoxy resin stator bar sample with an artificial defect inside

6.3   NEW VOLTAGE DIFFERENCE RESOLVED PATTERN

Under ac voltage, the local field strength is changed due to every PD event causing the redistribution of ions and electrons on the insulator surface. The changing local field will influence the external voltage trigging the next PD event. Thus, the voltage difference in a PD sequence is an indicator of discharge physical process. It is practically useful to examine some new distribution functions in relation to the voltage difference. Voltage difference (VD) resolved PD distribution patterns are established with newly defined distribution functions in this section. In VD resolved patterns, VD between consecutive PD pulses are normalized and equally divided.

6.3.1   Maximum and Minimum Discharge Magnitude

According to equation 6.1a and assuming q_λ is the PD amplitude of an arbitrary λ^{th} event in a sequence and it is neither the first nor the last event in a sequence. The maximum and minimum PD distribution functions can be defined as:

$$Q_{V.Max}(i) = \max(q_\lambda \mid q_\lambda > 0, \Delta V_{\lambda-1} \in VDW_i) \qquad (6.2a)$$

$$Q_{V.Min}(i) = \min(q_\lambda \mid q_\lambda < 0, \Delta V_{\lambda-1} \in VDW_i) \qquad (6.2b)$$

where i is the index of voltage difference window (VDW) that is the normalized voltage difference range equally divided by the number of partition windows. The maximum and minimum PD amplitude distribution functions are illustrated in figure 6.6 and 6.7 respectively. Apparently, the difference between patterns measured from different types of defect is obvious. Hence, the maximum and minimum distribution functions are useful in PD pattern recognition.
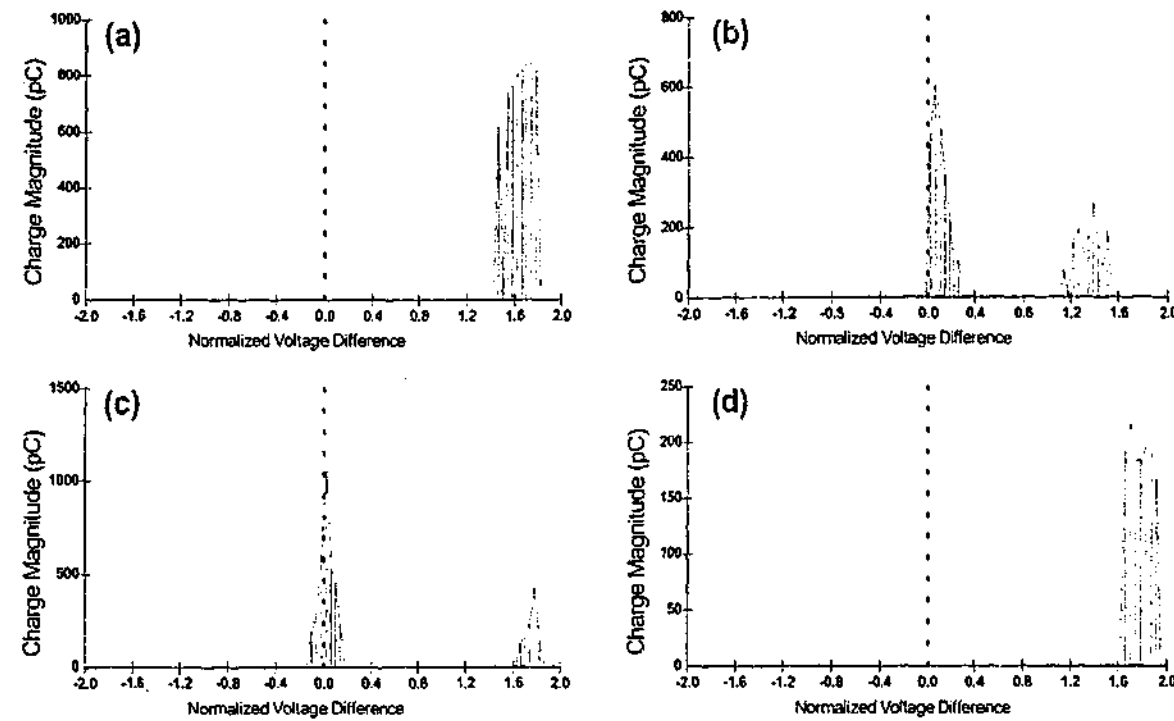
Fig. 6.6 Maximum PD amplitude distribution functions measured from
(a) a point-to-plane arrangement
(b) a point-to-dielectric arrangement
(c) an oil-impregnated pressboard sample
(d) an epoxy resin stator bar sample with an artificial defect inside
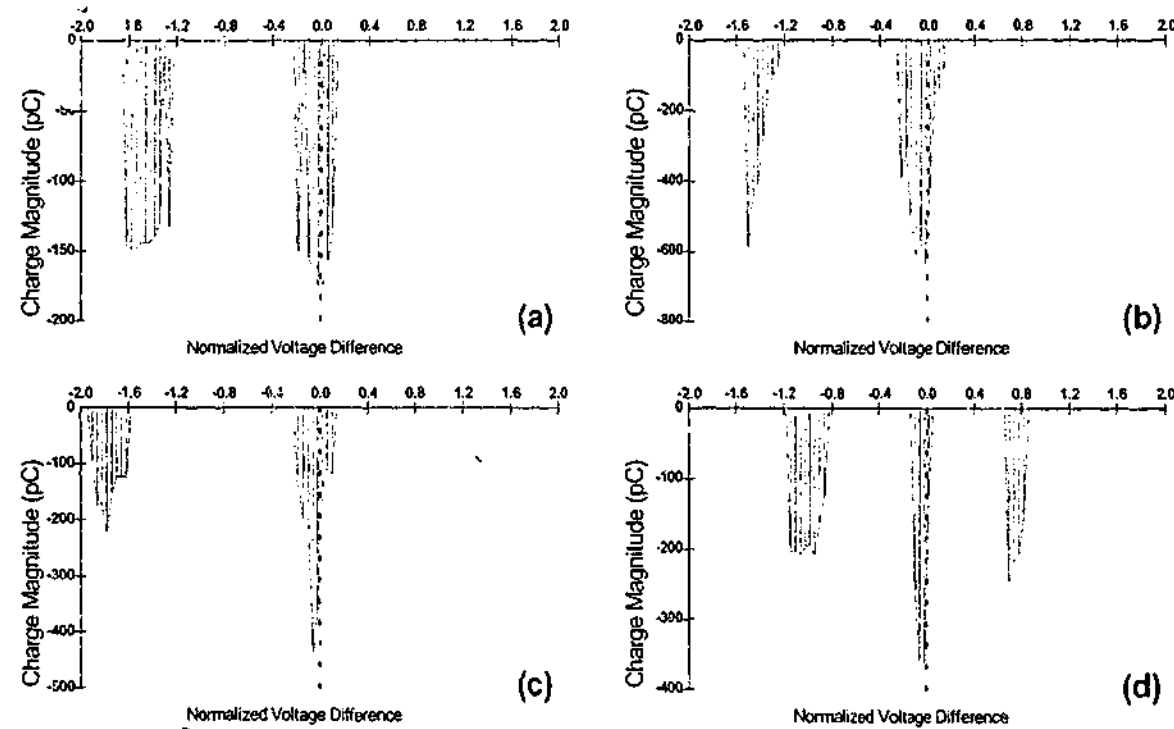
Fig. 6.7 Minimum PD amplitude distribution functions measured from
(a) a point-to-plane arrangement
(b) a point-to-dielectric arrangement
(c) an oil-impregnated pressboard sample
(d) an epoxy resin stator bar sample with an artificial defect inside

---

6.3.2 Maximum and Minimum Time Interval

The distribution functions of the maximum and minimum time interval between consecutive PD events charge can also be defined as:

$$TD_{V,Max}(i) = \max(\Delta T_{\lambda-1} \mid \Delta V_{\lambda-1} \in VDW_i) \tag{6.3}$$

$$TD_{V,Min}(i) = \min(\Delta T_{\lambda-1} \mid \Delta V_{\lambda-1} \in VDW_i) \tag{6.4}$$

where i is the index of VDW, T_i is the time interval between the $i\text{-}1^{th}$ and i^{th} events, and VDW_i is the voltage range in the ith VDW. The maximum and minimum time-interval distribution functions are illustrated in figure 6.8 and 6.9 respectively. Apparently, the difference between these functions is obvious for different types of defect.
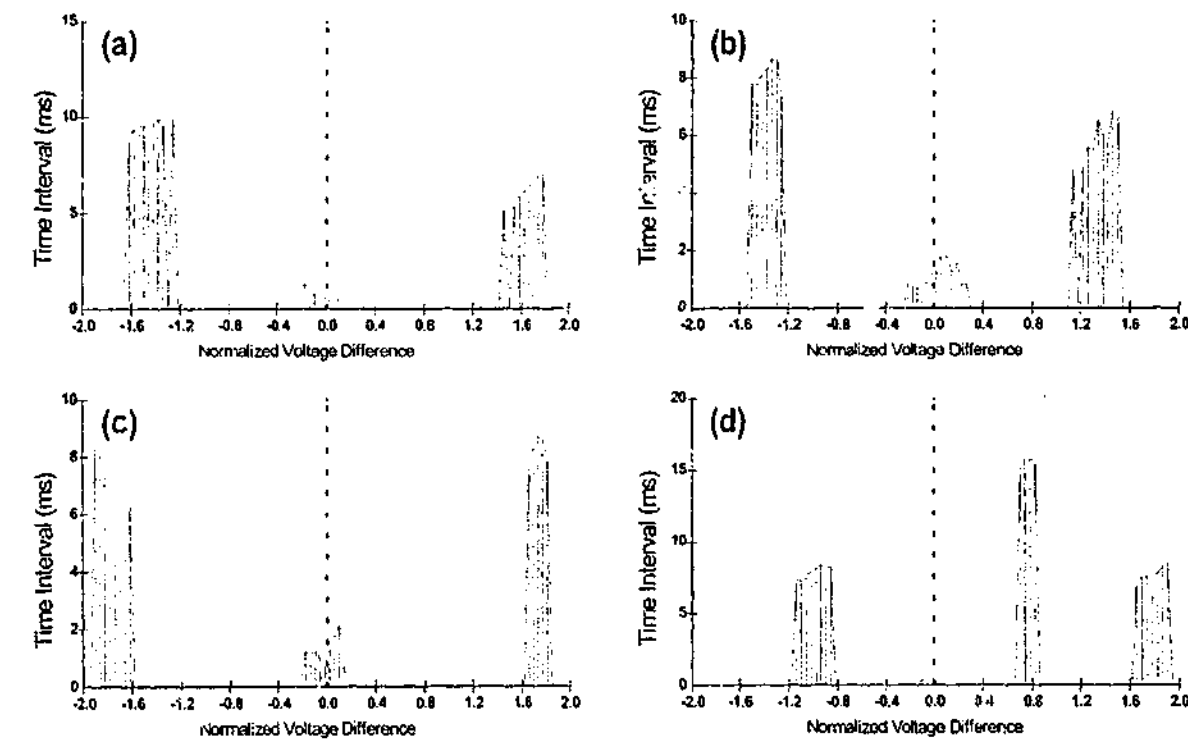

Fig. 6.8 Maximum time interval distribution functions measured from
(a) a point-to-plane arrangement
(b) a point-to-dielectric arrangement
(c) an oil-impregnated pressboard sample
(d) an epoxy resin stator bar sample with an artificial defect inside
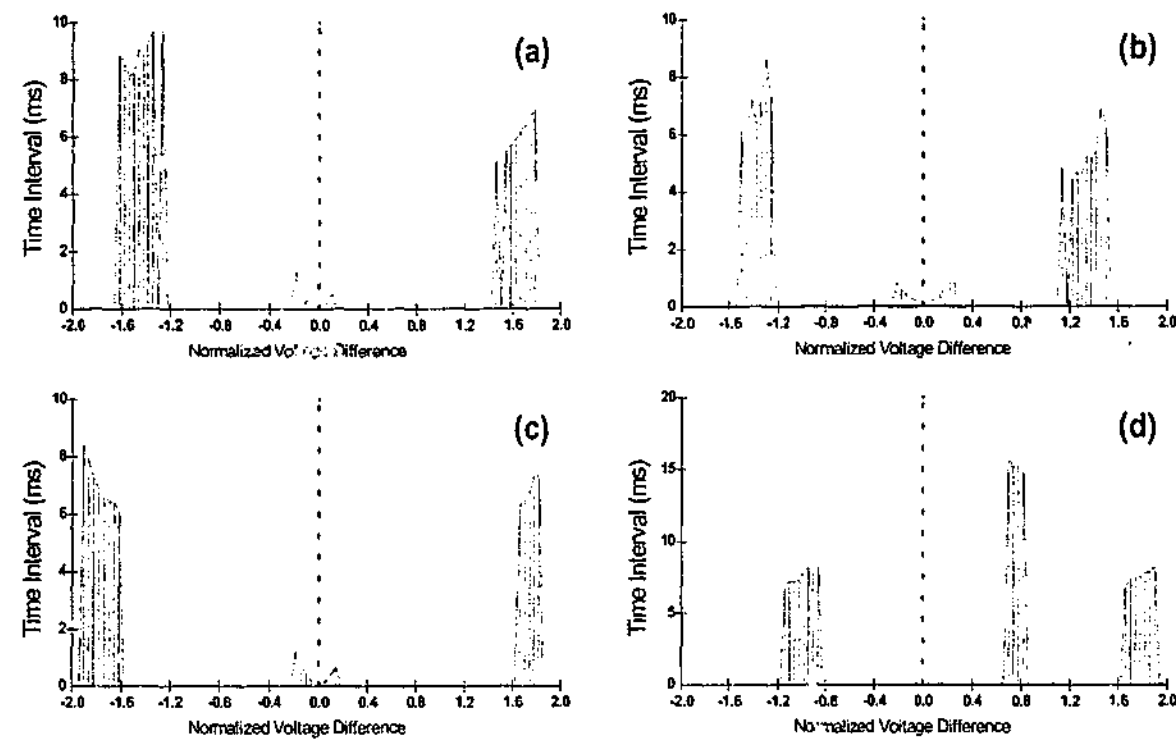
Fig. 6.9 Minimum time interval distribution functions measured from
(a) a point-to-plane arrangement
(b) a point-to-dielectric arrangement
(c) an oil-impregnated pressboard sample
(d) an epoxy resin stator bar sample with an artificial defect inside

6.4 NEW PD AMPLITUDE DIFFERENCE RESOLVED PATTERN

Reliable identification of a discharge source is likely to be efficient when physically related PD fingerprints can be extracted. To understand the physical basis of PD transients, Pedersen and his coworkers [102-109] studied the fundamental topic of induced charge in an ellipsoidal void. Having adopted a dipole representation, the influence of void parameters upon the induced charge has been studied. The induced charge is actually dependent on void location, geometry, physical dimensions, void gas and pressure as well as the permittivity of bulk dielectric. Meanwhile the induced charge can be separated into two components: (1) component q_μ directly related to the space charge in void and (2) component q_p represents the charge associated with the change in dielectric polarization. For a fixed void location, q_μ may be assumed as constant, therefore the variations in q_p reflect the characteristics of the PD in regard to geometry of the void, field orientation as well as permittivity of the bulk dielectric. With

this knowledge in mind, it is important to examine the charge magnitude difference (QD) between consecutive PD events.

6.4.1 Maximum Voltage Difference

QD resolved distribution functions are investigated with the different types of defect. The distribution function of the maximum VD can also be defined in equation 6.5.

$$TD_{q,Ext}(i) = \max(\Delta T_{\lambda-1} \mid \Delta Q_{\lambda-1} \in QDW_i, \Delta Q_{\lambda-1} > 0) \qquad (6.5a)$$

$$TD_{q,Ext}(i) = \min(\Delta T_{\lambda-1} \mid \Delta Q_{\lambda-1} \in QDW_i, \Delta Q_{\lambda-1} < 0) \qquad (6.5b)$$

where i is the index of charge difference window (QDW), $\Delta Q_{\lambda-1}$ is the time interval between the $\lambda\text{-}1^{th}$ and λ^{th} events, and QDW_i is the equally divided charge magnitude range in the ith QDW.
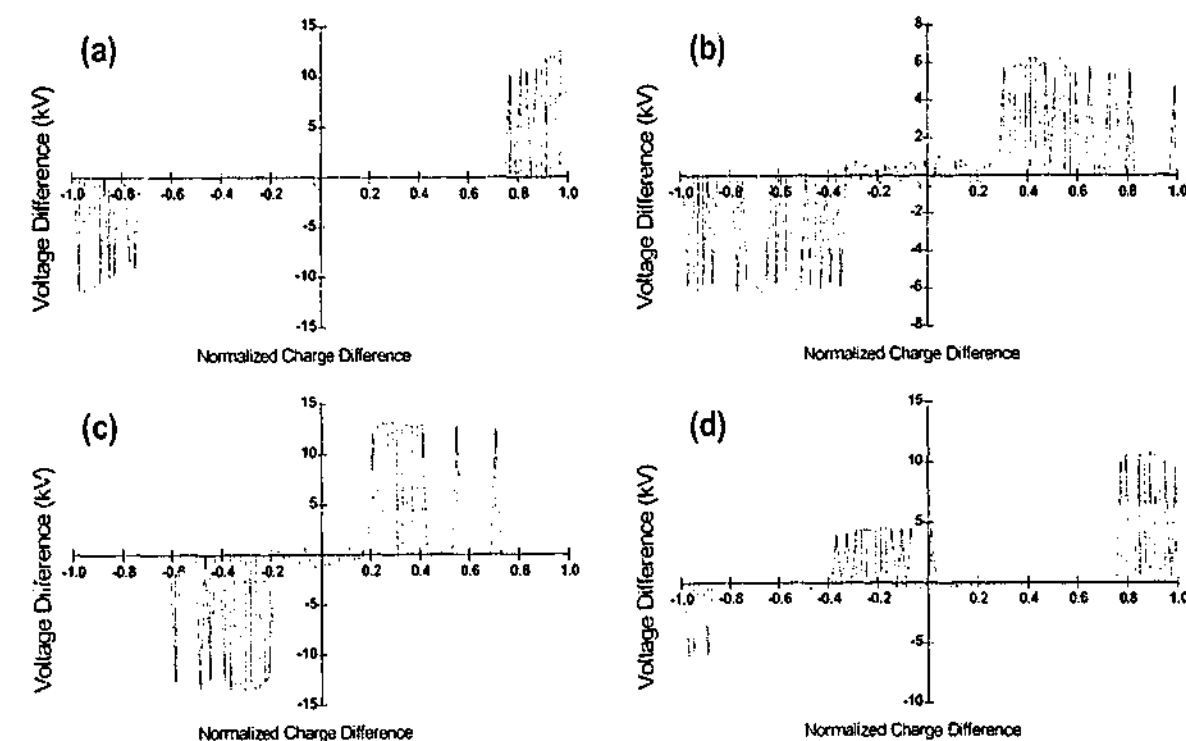

Fig. 6.10 Distribution functions of maximum voltage difference
(a) Pattern measured from a rod-to-plane arrangement
(b) Pattern measured from a rod-to-dielectric arrangement
(c) Pattern measured from a oil-impregnated pressboard sample
(d) Pattern measured from an epoxy resin stator bar sample with an artificial defect inside

6.4.2 Average and Maximum Time Difference

If $p_1(\lambda \mid \Delta Q_{\lambda-1} \in QDW_i)$ is the probability of a PD event λ having time separation $\Delta T_{\lambda-1}$ from its previous event falling into the ith QDW (QDW_i), the frequency distribution of the QDW_i can be defined as:

$$f_{\Delta Q}(i) = (N-1) \cdot p_1(\lambda \mid \Delta Q_{\lambda-1} \in QDW_i) \qquad (6.7)$$

where N is the total number of PD events in a sequence. Hence, the distribution function of average PD amplitude difference can also defined as follow:

$$TD_{Q,Ave}(i) = \frac{\sum (\Delta T_{\lambda-1} \mid \Delta Q_{\lambda-1} \in QDW_i)}{(N-1) \cdot p_1(\lambda \mid \Delta Q_{\lambda-1} \in QDW_i)} \qquad (6.8)$$

where $(N-1) \cdot p_1(\lambda \mid \Delta Q_{\lambda-1} \in QDW_i) > 0$, otherwise $TD_{Q,Ave}(i) = 0$, $\Delta Q_{\lambda-1}$ is the charge difference between the $\lambda-1^{th}$ and λ^{th} events, and QDW_i is the range of the ith charge difference window.

$$VD_{q,Ext}(i) = \max(\Delta V_{\lambda-1} \mid \Delta Q_{\lambda-1} \in QDW_i, \Delta V_{\lambda-1} > 0) \qquad (6.9a)$$

$$VD_{q,Ext}(i) = \min(\Delta V_{\lambda-1} \mid \Delta Q_{\lambda-1} \in QDW_i, \Delta V_{\lambda-1} < 0) \qquad (6.9b)$$

The average time difference distribution functions are plotted in figure 6.11, where the distribution features of different types of PD sources are unique and visually separable. The difference between these distribution functions may be quantified in order to enable a simple algorithm to separate them.
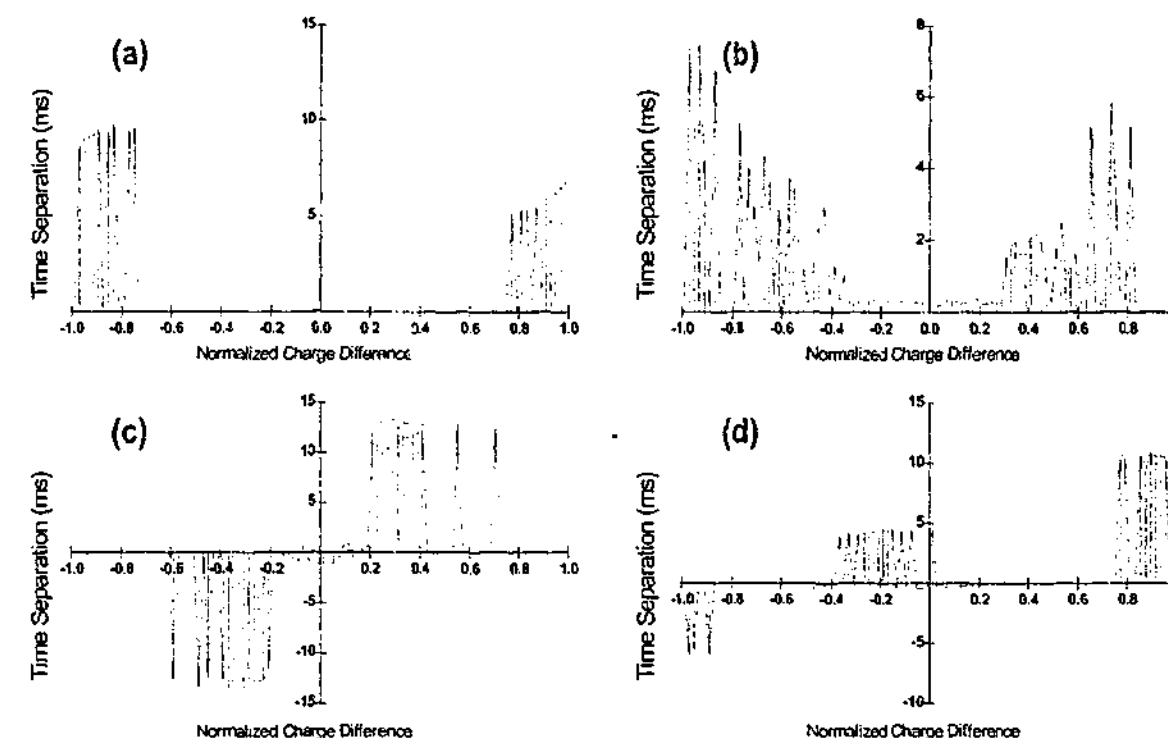
Fig. 6.11 Average time interval distribution functions measured from
(a) a point-to-plane arrangement
(b) a point-to-dielectric arrangement
(c) an oil-impregnated pressboard sample
(d) an epoxy resin stator bar sample with an artificial defect inside

6.5 NEW TIME INTERVAL RESOLVED PATTERN

As described in early sections, the PD amplitude of an event in a sequence is closely related to the time separation from its latest precedent event. Therefore, it is necessary to investigate discharge distribution properties associated with the distribution of time separation between consecutive PD events. Time interval (TD) resolved distribution is a useful tool to provide PD nature related information. In this approach, one cycle time is equally divided into a number of windows. Distribution functions are studied in relation to time difference window (TDW)

6.5.1 Average Discharge Amplitude

If $p_1(\lambda \mid \Delta T_{\lambda-1} \in TDW_i)$ is the probability of a PD event λ that having time separation $\Delta T_{\lambda-1}$ from its previous event falling into the ith TDW (TDW_i), the frequency distribution of the TDW_i can be defined as:

$$f_{\Delta T}(i) = (N-1) \bullet p_1(\lambda \mid \Delta T_{\lambda-1} \in TDW_i) \tag{6.10}$$

where N is the total number of PD events in a sequence. Hence, the distribution function of average PD amplitude difference can also defined as follow:

$$Q_{T.Ave}(i) = \frac{\sum (q_\lambda \mid \Delta T_{\lambda-1} \in TDW_i)}{(N-1) \bullet p_1(\lambda \mid \Delta T_{\lambda-1} \in TDW_i)} \tag{6.11}$$

where $(N-1) \bullet p_1(\lambda \mid \Delta T_{\lambda-1} \in TDW_i) > 0$ otherwise $Q_{T.Ave}(i) = 0$, $\Delta T_{\lambda-1}$ is the time interval between the $\lambda\text{-}1^{th}$ and λ^{th} events, and TDW_i is the range of the ith time difference window.

6.5.2 Average Discharge Amplitude Difference

Based on equation 6.7, the distribution function of average PD amplitude difference can be defined as:

$$QD_{T.Ave}(i) = \frac{\sum (\Delta q_{\lambda-1} \mid \Delta T_{\lambda-1} \in TDW_i)}{(N-1) \bullet p_1(\lambda \mid \Delta T_{\lambda-1} \in TDW_i)} \tag{6.12}$$

where $p_1(\lambda \mid \Delta T_{\lambda-1} \in TDW_i) > 0$, otherwise $QD_{T.Ave}(i) = 0$ and $\Delta q_{\lambda-1}$ is the charge difference between the $\lambda\text{-}1^{th}$ and λ^{th} discharge events.

6.5.3 Maximum Discharge Amplitude

The Distribution function of extreme charge amplitude in a consecutive PD sequence can be defined as:

$$Q_{T.Ext}(i) = \max(q_\lambda \mid \Delta T_{\lambda-1} \in TDW_i, q_\lambda > 0) \tag{6.13a}$$

$$Q_{T.Ext}(i) = \min(q_\lambda \mid \Delta T_{\lambda-1} \in TDW_i, q_\lambda < 0) \tag{6.14b}$$

where i is the index of TDW, $\Delta T_{\lambda-1}$ is the time interval between the $\lambda\text{-}1^{th}$ and λ^{th} events, and TDW_i is the range of the ith TDW.

6.6 ANALYSIS OF CORONA USING CONSECUTIVE PATTERN

With the advancement of electronics and computer systems, it is possible to interpret measurable PD distribution functions with discharge physical mechanisms. Earlier research work has found that the parameters of an arbitrary discharge event in a series are closely related to the time separation from the precedent events [1,2]. However, under ac criteria, parameters are difficult to calculate due to the add-on impact of periodical changing field. Obviously, the characteristics of pulse-to-pulse memory propagation of Trichel-pulse corona are influenced by the applied ac voltage. In order to evaluate the superimposed impact on discharge distributions, both PD amplitude and energy are employed to study the properties of negative Trichel-pulse corona. Relevant statistics of unconditional and conditional distributions are calculated for comparison and analysis. It is found in this study that there is a critical time interval t_c, which exists between consecutive PD pulses, under which ac voltage impact may be minimized. With the knowledge of t_c, it is possible to compute the discharge parameters relating to characteristics of discharge mechanism under ac voltage. The results obtained from a number of conditional distributions are discussed in order to interpret the behavior of negative Trichel-pulses in distribution profiles.

As many important discharge properties are embedded in patterns of various conditional distributions, it is important to study the observed features and their correlation with

discharge mechanism. Conditional distributions of consecutive negative Trichle-pulse events are investigated in this paper as an example using consecutive discharge variables.

6.6.1 Introduction

Experimental studies on the pulsating negative corona discharge have been carried out under various criteria. The quantitative model of corona discharge was proposed by Morrow within numerical solution of Poisson's equation [1]. The conditional and unconditional distributions of corona pulse-height and time separation from its precedent pulse as well as its repetition rates were measured. The results demonstrated that Trichel-pulse discharge phenomenon is a stochastic process in which memory effects play an important role [2-4]. The correlation between discharge amplitude and time separation from the precedent pulses has been extensively studied. However, most power apparatus is operated under ac voltage. It requires in-service condition monitoring of the insulation system to ensure the safe operation of power equipment. However, the recent progress in the development of PD pattern recognition could not interpret the physical mechanisms relating to PD phenomena. To characterize measurable discharge patterns with the physical mechanism under ac voltage, it is essential to extract physically related discharge parameters. For a point-to-plane arrangement, the ac field at the highly stressed needle electrode varies continuously, both in amplitude and polarity. Various corona modes could be observed during a single cycle if appropriate voltage applied. When the gap distance is greater than the critical distance, the observed pulses only appear on the negative half cycle of power frequency [5]. This is due to the ionic space charge created during one half-cycle. The created space charge and metastable species are not absorbed by the electrode but are drawn back to the field intensity region in the following half-cycle, which can influence discharge initiation and development. According to the Townsend corona current formula:

$$I_{av} \propto V_{gap} (V_{gap} - V_{onset})$$ (6.15)

Originally, the formula was developed for cylindrical coronas and later supported by the extensive investigation on point-to-plane Trichel-pulse corona in air. This study has found that the repetition rate of Trichel-pulse corona in air is dependent on voltage [6]. On the other hand, discharge amplitudes are strongly affected by the presence of ion space charge and metastable species from earlier discharge events. Hence, the physical mechanisms of pulse-to-pulse propagation under ac voltage are more complicated than those observed under dc voltage due to the add-on variability of external field. Discharge pulse energy is a parameter used to calculate discharge power in a given time interval and it is the product of discharge amplitude and the instantaneous voltage at the time discharge occurred. The energy of an individual discharge can be used to investigate the superimposed impact from the time separation of consecutive PD events as well as the changing external field. It is more appropriate to use discharge energy rather than amplitude since discharge energy contains the field information, which is critical for PD initiation and development. The discharge pulse propagation under ac voltage is illustrated in figure 6.12. Apparently, the memory propagation and the sinusoid voltage significantly affect the time separation resolved distributions. The energy of individual discharge can be expressed by

$$E_n = \sqrt{2} q_n V \sin(\varphi_n)$$ (6.16)

where V is the RMS value of applied voltage and φ_n and q_n are the instantaneous ac phase position and discharge amplitude of the nth discharge event respectively.
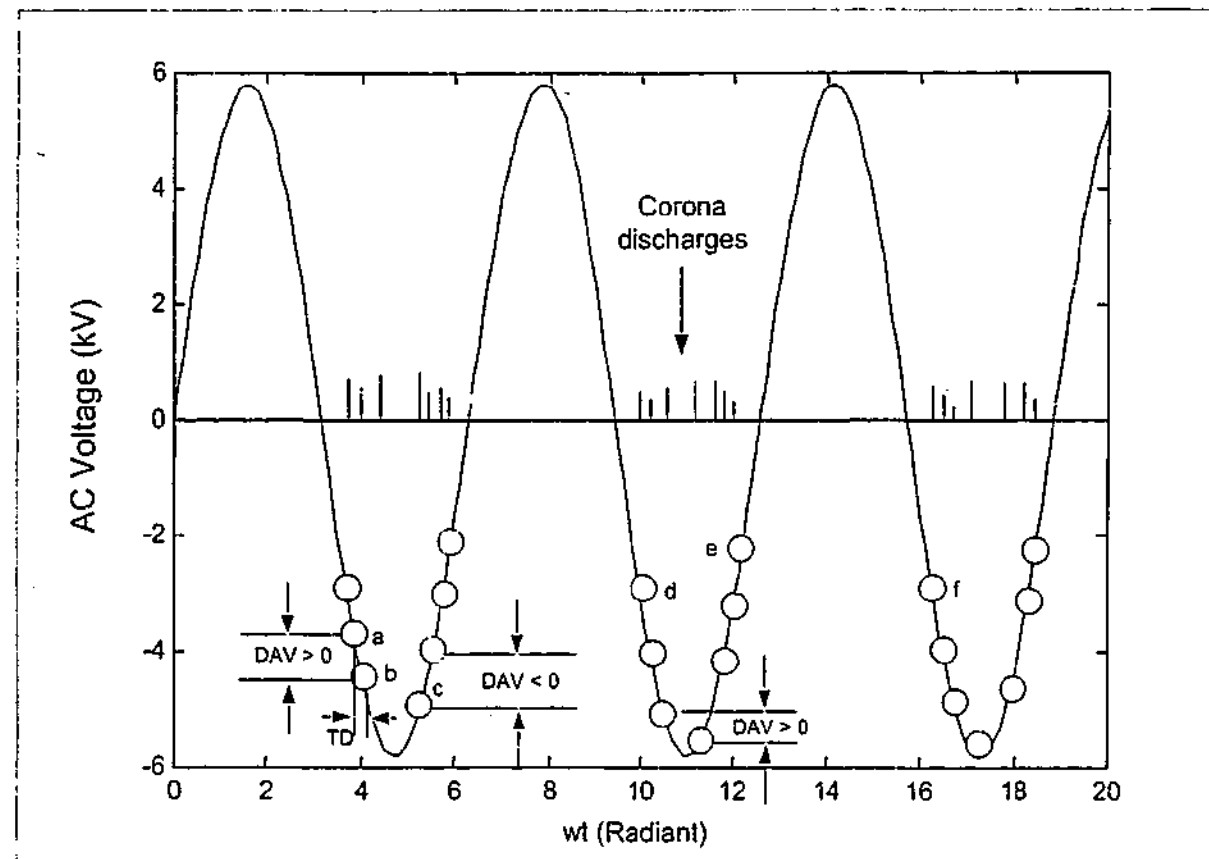
Fig. 6.12 Pictorial representation of Trichel-pulse phenomenon.
DAV: Difference of absolute voltage of consecutive discharges

It is proved in the earlier work that there is a strong correlation between PD pulse amplitude and the time separation due to the pulse-to-pulse memory effect. [3,4,5]. Consecutive PD pulse analysis under ac condition is based on the fact that the sinusoid voltage has a significant impact on the existing memory propagation, which determines the probability distributions of the corona discharge. As an arbitrary PD in a sequence, the pulse amplitude and energy are correlated with the previous event. Seen in figure 6.12, the sign of the difference of absolute voltage (DAV) between consecutive discharge pulses is a critical condition to evaluate the ac voltage impact on the pulse-to-pulse memory propagation. The difference of absolute voltage and the time separation can be defined as,

$$DAV_n = |V_n| - |V_{n-1}| \qquad (6.17)$$

$$\Delta t_{n-1} = t_n - t_{n-1} \qquad (6.18)$$

where DAV_n is the difference of absolute voltage between two consecutive PD events and Δt_{n-1} is the time separation between the n-1th and the nth discharge events. When $DAV_n > 0$, the nth PD event occurs on the down side slope of ac voltage. On the other hand, when $DAV_n < 0$, the nth PD event occurs upon the up side of ac voltage. The ac voltage impact on the pulse-to-pulse propagation may be evaluated by the comparison of the statistics calculated from PDs occurred on different side of ac voltage slope. The approach is implemented by analyzing various unconditional and conditional distributions of discharge amplitude and energy along with the statistics. The following unconditional and conditional distributions of discharge amplitude and energy are listed to investigate the impact of the memory effect under ac condition.

Unconditional distribution: $f_0(q_n)$, $f_0(E_n)$

Conditional distribution (1st order): $f_1(q_n \mid \Delta t_{n-1})$, $f_1(E_n \mid \Delta t_{n-1})$, $f_1(q_n \mid DAV_n)$, $f_1(E_n \mid DAV_n)$

Conditional distribution (2nd order): $f_2(q_n \mid \Delta t_{n-1}, DAV_n)$, $f_2(E_n \mid \Delta t_{n-1}, DAV_n)$

6.6.2 Time Separation Resolved Distribution Function

It is understood that discharge initiation and growth is affected by residuals produced from earlier pulses. This phenomenon is called the memory effects. Obviously, the impact of the memory effects is associated with the moving ion space charges produced from the most recent pulse. The presence of the space charge has a significant impact not only on the rate of electron release but on the initiation of subsequent pulses as well. It has shown that consecutive pulse time separations are strongly correlated with discharge physical phenomena under dc condition [4,5]. The scatter plot and the derived time-interval resolved distribution functions are shown in figure 6.13.
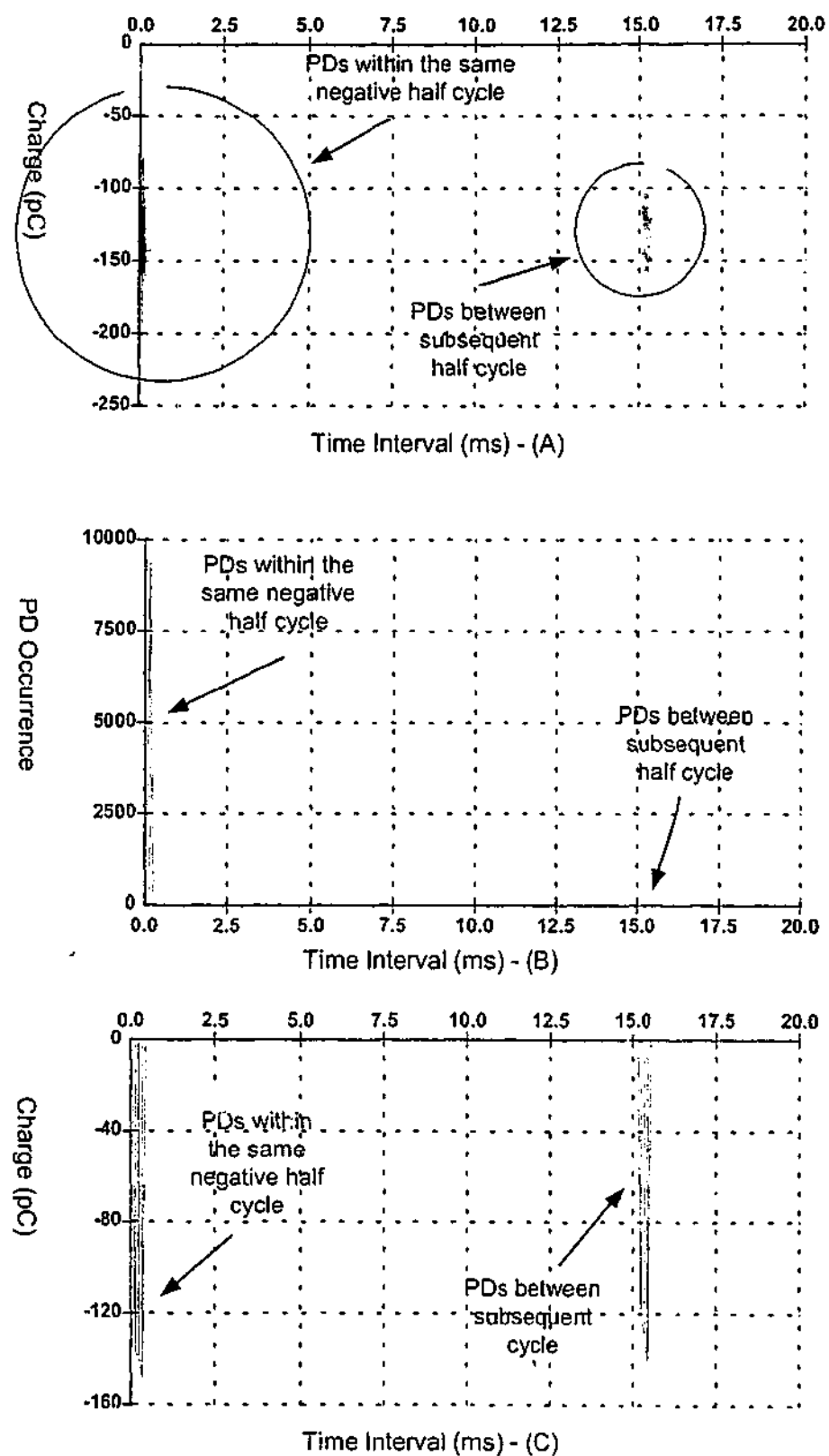
Fig. 6.13 Time interval restricted distribution of the negative discharge
A: Scatter plot of PD magnitude vs. time interval
B: PD occurrence vs. time interval
C: Average PD magnitude vs. time interval

As seen from figure 6.13, each distribution pattern has two regions separated by the time-interval of consecutive PD events. The region with shorter time interval represents the parameters of two consecutive PD events that appear in the same negative half cycle. On the other side, the region with longer time interval stands for the parameters of inception discharges. The memory propagation impact between subsequent pulses can be investigated in the first region. This is because (1) the time interval between the consecutive cross-cycle events are long and (2) the remaining ion space charges are cleaned away during the positive half cycles that affect the following discharge initiation and development.

Zooming into the region with shorter time interval of consecutive PD pulses illustrated in figure 3 (A), the detailed view of the discharge magnitude in relation to the time separation is shown in figure 4. It can be observed that the PD amplitude versus time interval is almost horizontally symmetric. The minimum time separation of consecutive discharge pulses is found about 14 microseconds, which dependents on the sample arrangement and the test criteria. It reflects the minimum time required to the initiation and development of the next discharge. The superimposed impact of pulse-to-pulse memory effect and the voltage on the Trichel-pulse corona can be analyzed by the comparison of various distributions with the restriction of time interval and the difference of absolute voltage of consecutive discharge events.
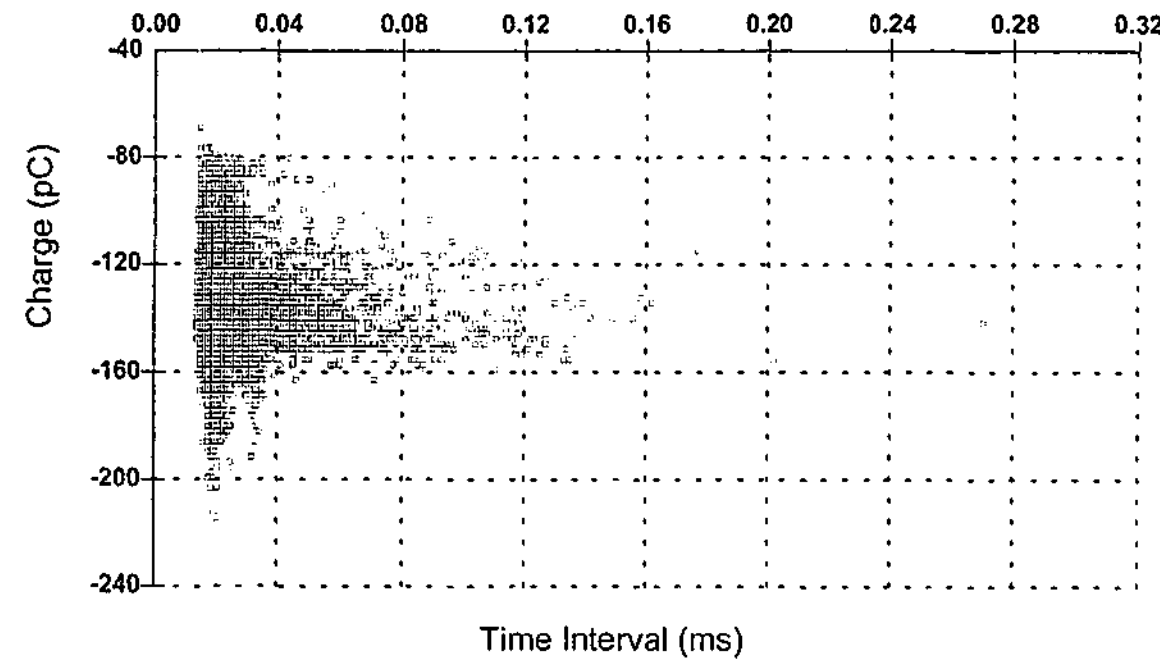
Fig. 6.14 Zoom-in picture of figure 6.13 (A)
Note the negative sign represents the polarity of PD amplitude

6.6.3 BEHAVIOR OF $f_1(q_n \mid DAV_n)$, $f_1(E_n \mid DAV_n)$, $f_1(q_n \mid \Delta t_{n-1})$, and $f_1(E_n \mid \Delta t_{n-1})$

As shown in Figure 6.15(A) and (B), the statistics of unconditional distribution of $f_0(q_n)$ and $f_0(E_n)$ are summarized at the indicated gap voltage and distance. The statistical results in figure 6.15 have shown the central tendency, the dispersion, and the distribution of PD amplitude as well as PD energy. Applying with 95% confidence level, the interval of both the arithmetical and the geometrical mean of PD amplitude are in the ranges of 0.761 and 0 respectively. The zero confidence interval of geometrical mean indicates the stability of PD amplitude as well as the symmetric of the distribution. Meanwhile the interval of the arithmetical and the geometrical mean of pulse energy are in the range of 0.00641 and 0.00702 µJ respectively. The detailed summary of the unconditional distribution statistics of discharge magnitude and energy are illustrated in figure 6.15(a) and (b) respectively. The individual pulse energy is accounted with micro-joule unit for convenience. Along with statistical results, the conditional distribution of discharge magnitude and energy are also shown together with the normal distribution curve for comparison. These statistical results provide useful information as to how the relevant discharge data spread over their ranges as shown in figure 6.16 and 6.17 respectively.
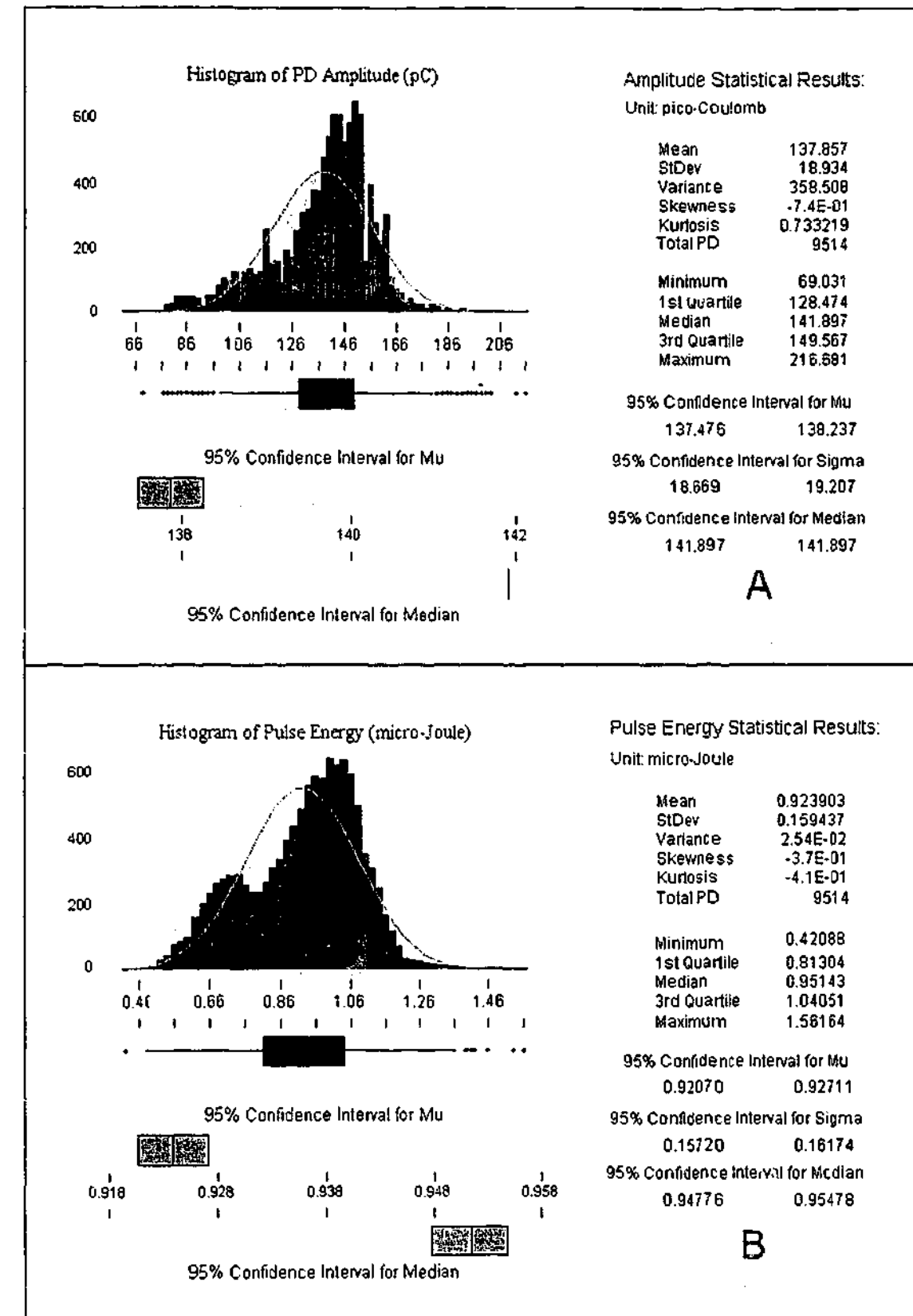

Fig. 6.15 Unconditional statistics of PD amplitude and energy.
Gap voltage: 5.1 kV   Gap distance: 12 mm
A: amplitude   B: energy
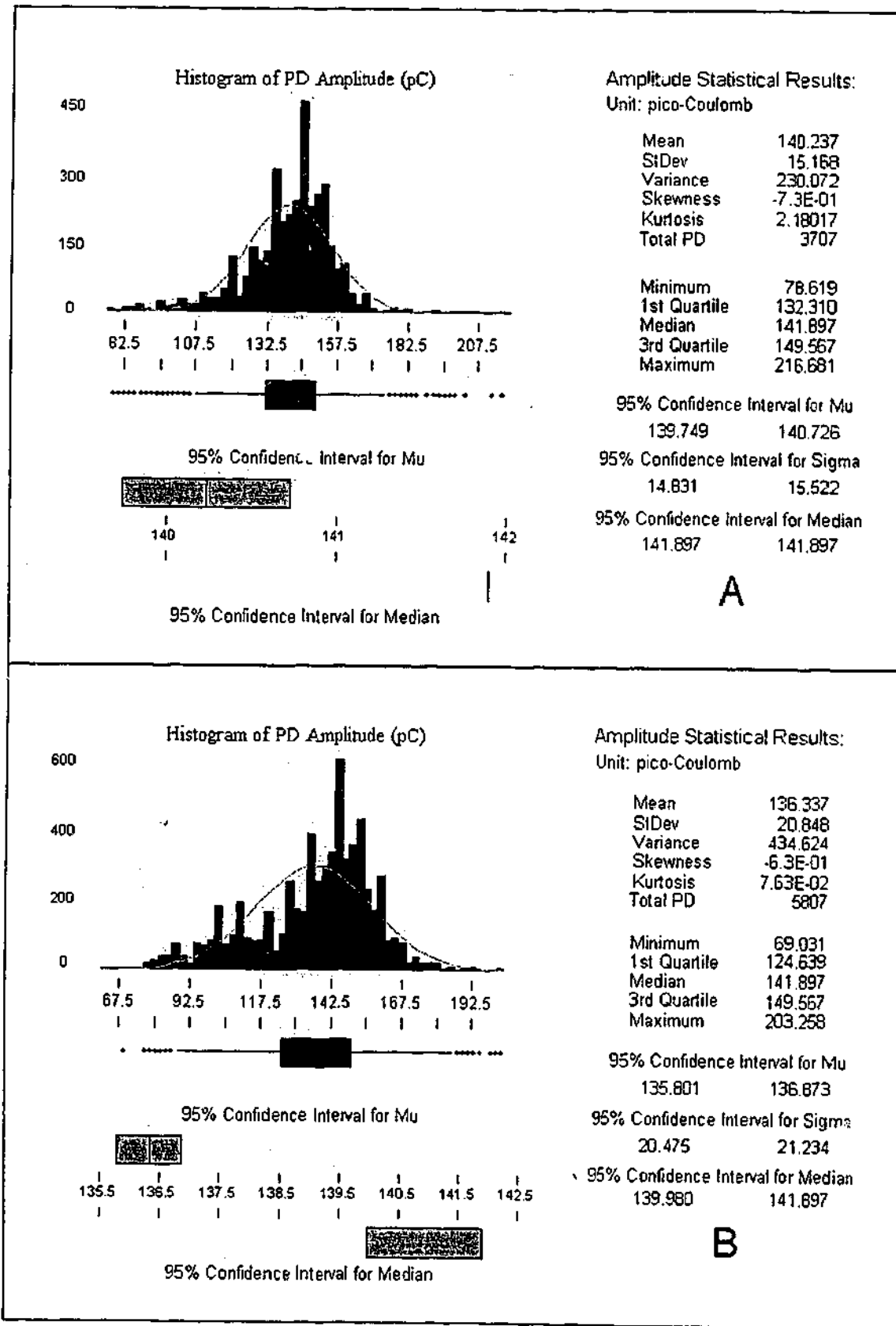
Fig. 6.16 Conditional statistics of PD magnitudes
A: DAV<0   B: DAV>0
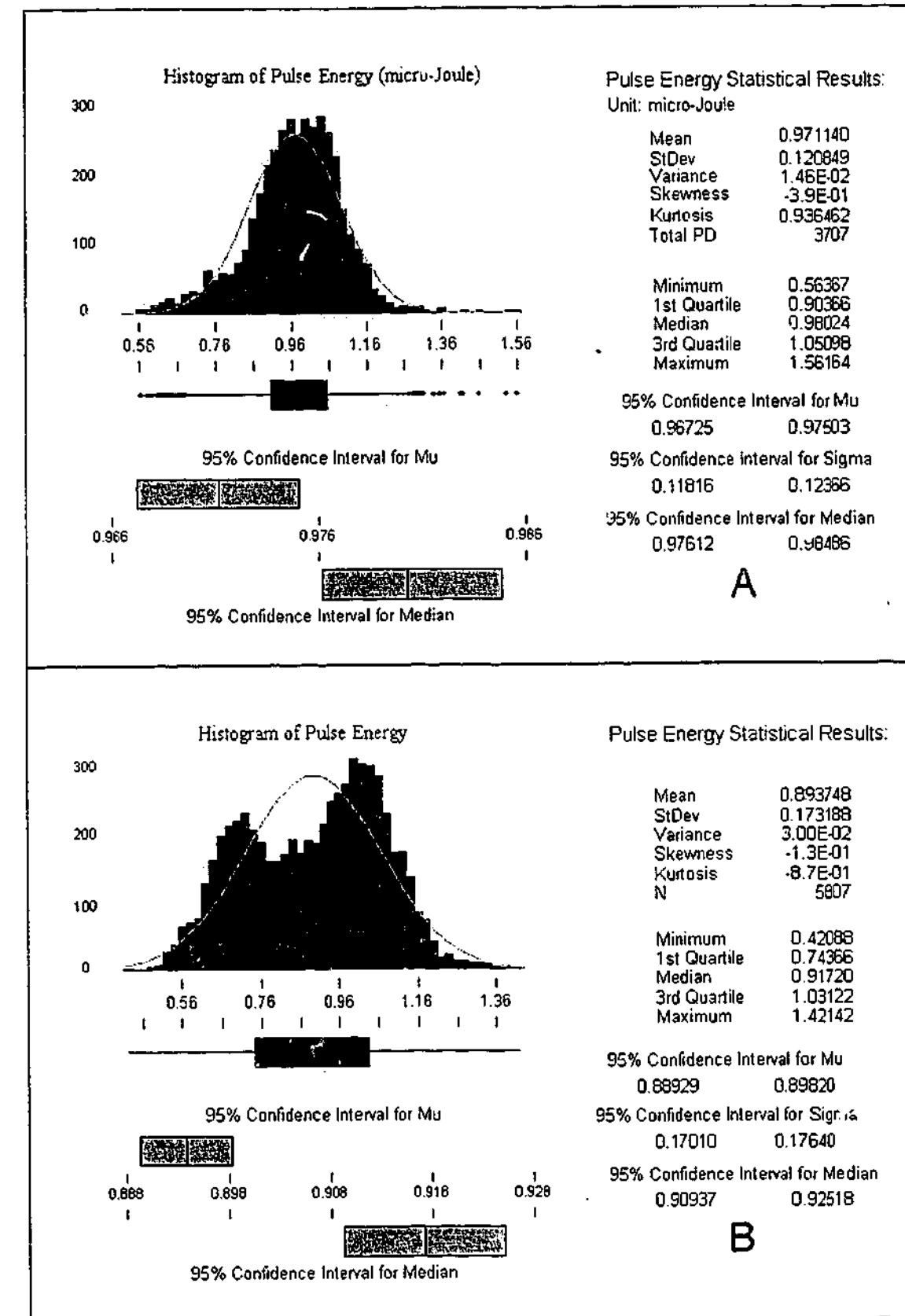
Fig. 6.17 Conditional statistics of PD energy
A: DAV<0   B: DAV>0

The conditional distributions of discharge magnitude and pulse energy are plotted with a number of different time separations as shown in figure 6.18 and 6.19 respectively. The impact of the pulse-to-pulse memory effect is obvious from the probability distributions especially when Δt_{n-1} is short. Meanwhile this impact becomes less significant at longer Δt_{n-1}, due to the influence of changing ac field.

Comparing to the conditional distribution of PD amplitude shown in figure 6.18, the dependency of PD energy distribution over the time interval is more distinguishable. This phenomenon is due to the influence of the changing ac field that is involved in the conditional distribution of PD energy.
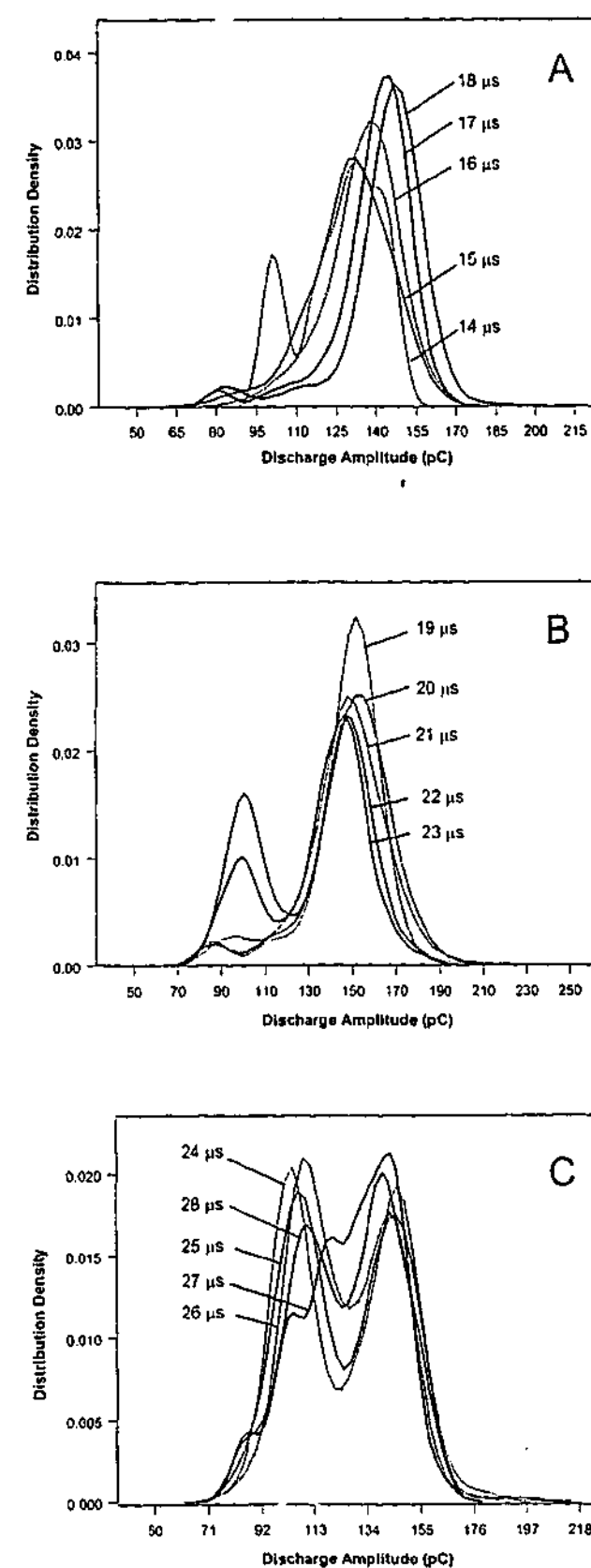
Fig. 6.18 Probability distribution of PD amplitude
A: pulse to pulse time separation range (14-18) μs
B: pulse to pulse time separation range (19-23) μs
C: pulse to pulse time separation range (24-28) μs
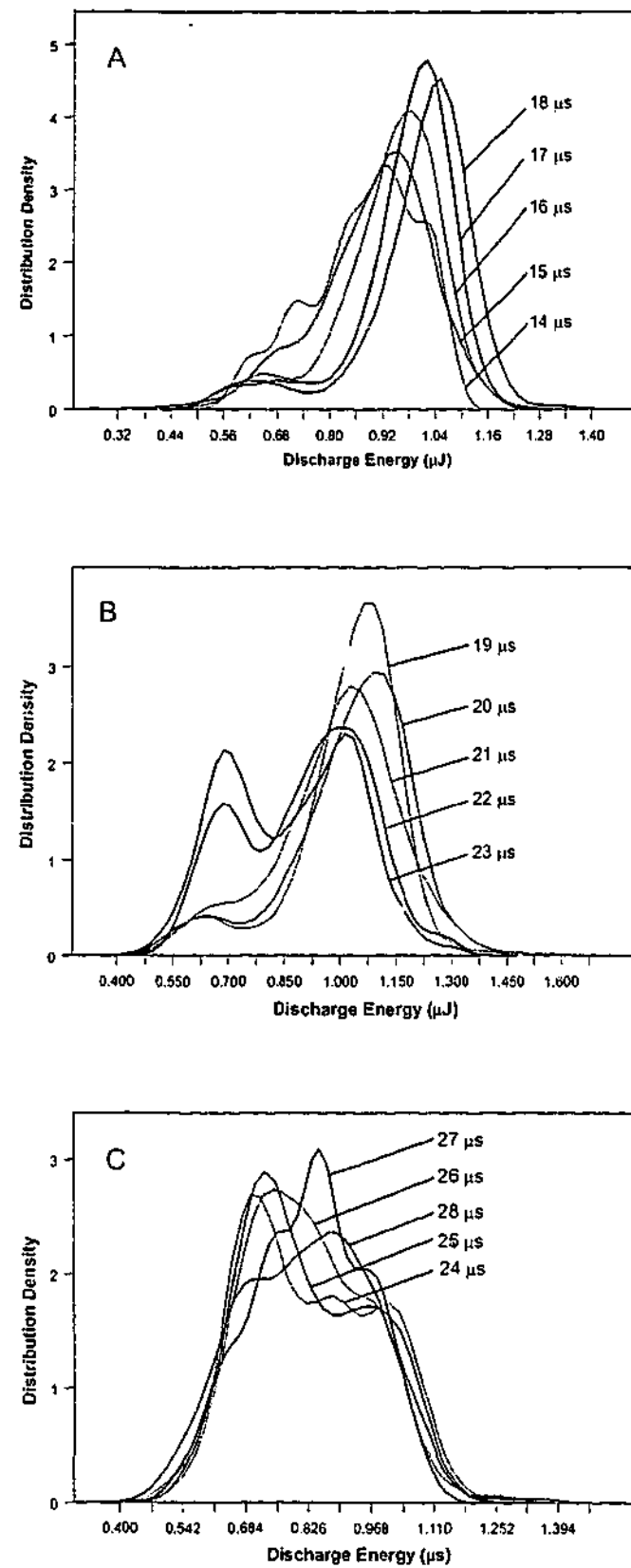
Fig. 6.19 Probability distribution of PD energy
A: pulse to pulse time separation range (14-18) µs
B: pulse to pulse time separation range (19-23) µs
C: pulse to pulse time separation range (24-28) µs

The selected descriptive statistics of PD amplitude and energy are illustrated in figure 6.20 where the arithmetical mean, standard deviation, and distribution range are plotted against the time separations from previous event. Apparently, there is a critical time interval t_c about 21 µs. When Δt_{n-1} is shorter than t_c, it is observed that both mean discharge amplitude and energy increase with Δt_{n-1} increases. The result is consistent with the earlier results suggested by van Brunt, that the longer the time interval separated from the previous PD event, the greater the probability of generating a PD of higher amplitude. In addition, the standard deviation of both PD amplitude and energy over the time interval range are quite stable. Meanwhile the amplitude and energy ranges increase with Δt_{n-1} when Δt_{n-1} is shorter than the critical time interval t_c.
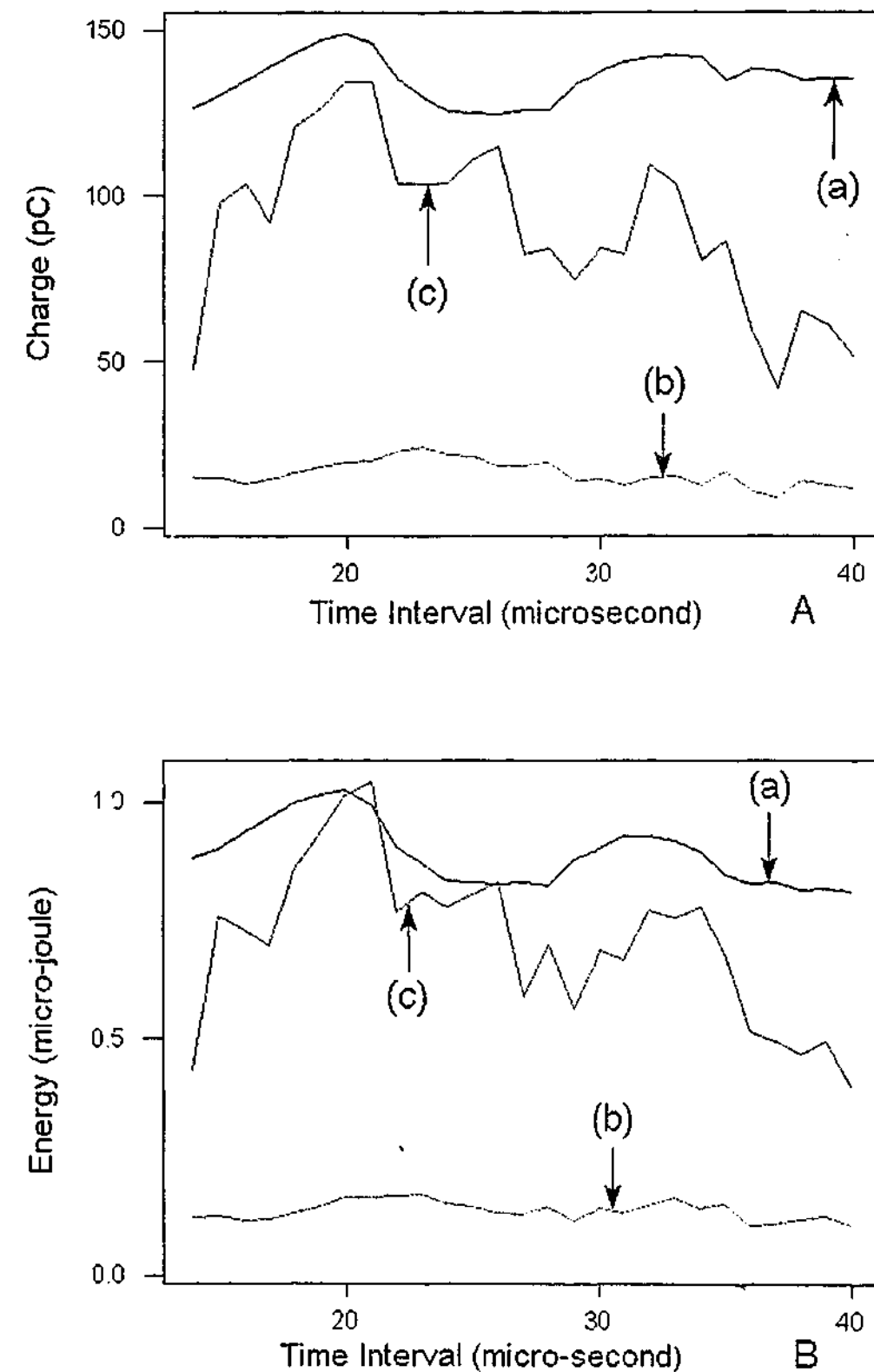
Fig. 6.20 Selected descriptive statistics of discharge amplitude and energy
A: Statistics of discharge amplitude   B: Statistics of discharge energy
(a): mean amplitude   (d) mean energy
(b): amplitude standard deviation   (e) energy standard deviation
(c): amplitude range   (f) energy range

6.6.4 BEHAVIOR OF $f_2(q_n \mid \Delta t_{n-1}, DAV_n)$ and $f_2(E_n \mid \Delta t_{n-1}, DAV_n)$

The second order conditional distributions have shown the dependency of q_n on Δt_{n-1} and DAV_n as well as the dependency of E_n on Δt_{n-1} and DAV_n. With the same time interval, the distribution of $f_2(X \mid DAV_n > 0)$ and $f_2(X \mid DAV_n < 0)$ are plotted together for comparison, where X represents either the PD amplitude or energy. The impact of the pulse-to-pulse memory effect as well as the influence of the ac periodical field can be revealed from the second order distributions as shown in figure 6.20 and 6.21 respectively. This phenomenon is observed by the comparison of $f_2(q_n \mid \Delta t_{n-1}, DAV_n > 0)$ and $f_2(q_n \mid \Delta t_{n-1}, DAV_n < 0)$ as well as by the comparison of $f_2(E_n \mid \Delta t_{n-1}, DAV_n > 0)$ and $f_2(E_n \mid \Delta t_{n-1}, DAV_n < 0)$. It is found in figure 6.20 that the similarity of conditional distribution shape at different side of ac voltage slope changes with time interval. The conditional distribution shapes are similar when time interval is short. It means that the ac voltage has less impact on memory effects. It may be summarized from the observation that the memory effect has a dominant impact on those consecutive discharges having short Δt_{n-1}. However, the impact of the ac field gradually becomes more significant for those consecutive discharges having longer Δt_{n-1}. The conditional distributions of $p_2(q_n \mid \Delta t_{n-1}, DAV_n)$ and $p_2(E_n \mid \Delta t_{n-1}, DAV_n)$ have been plotted in figure 6.21 and 6.22 for the investigation of PD distribution on different side of ac voltage slope. Experiment results of negative Trichel-pulse corona are analyzed using conditional distributions. Due to the complexity of discharge phenomena, especially under ac conditions, the impact of ac voltage can be investigated by comparing the Δt_{n-1} restricted distributions on different side of ac voltage slope. Referring to the earlier definition, the sign of DAV_n indicates which side of voltage slope q_n is allocated. As for negative Trichel-pulse, it is understood that q_n is found in the down side slope when DAV_n is greater then zero. Conversely, q_n is located in the up side slope when DAV_n is less than zero. With the same Δt_{n-1}, the PD amplitude and energy of different slope are plotted together for comparison. It is observable that q_n and E_n are dependent on Δt_{n-1} and DAV_n accordingly.
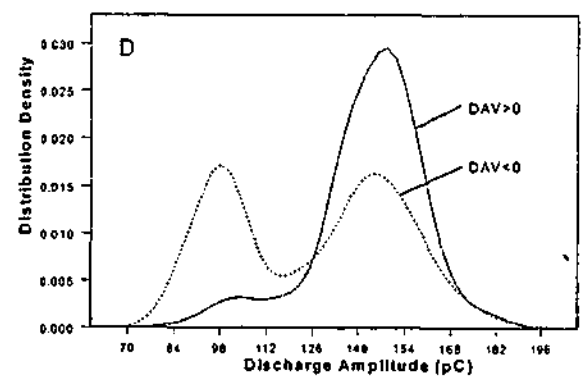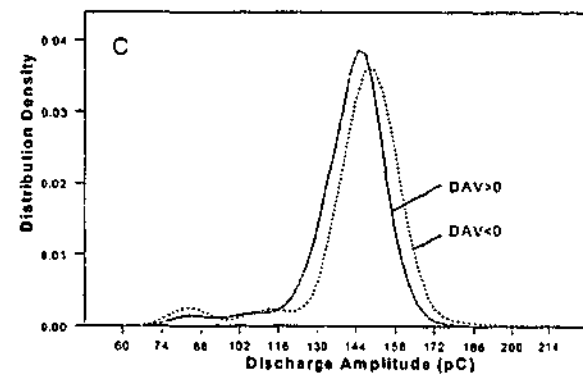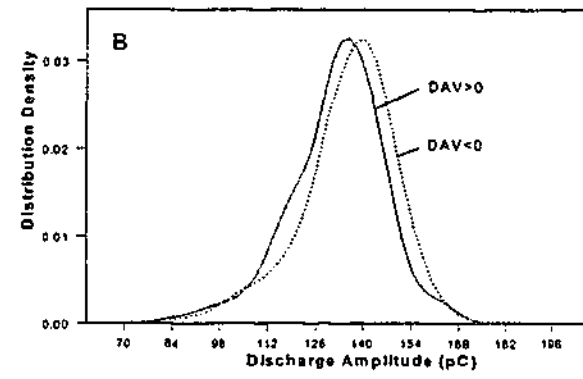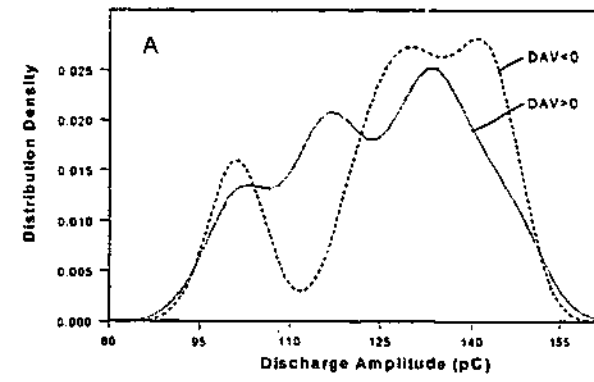
Fig. 6.21 Probability distribution of PD amplitude $p_2(q_n \mid \Delta t_{n-1}, DAV_n)$

A: time interval at 14 μs   B: time interval at 16 μs
C: time interval at 18 μs   D: time interval at 22 μs
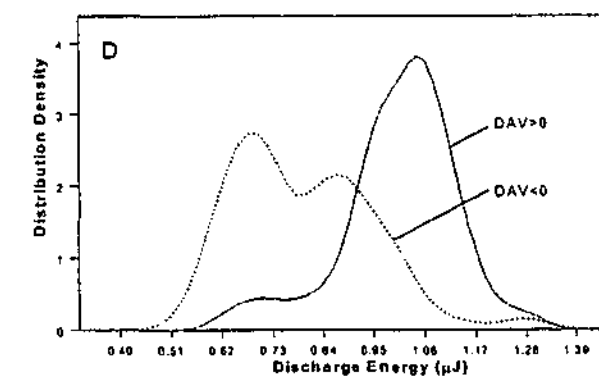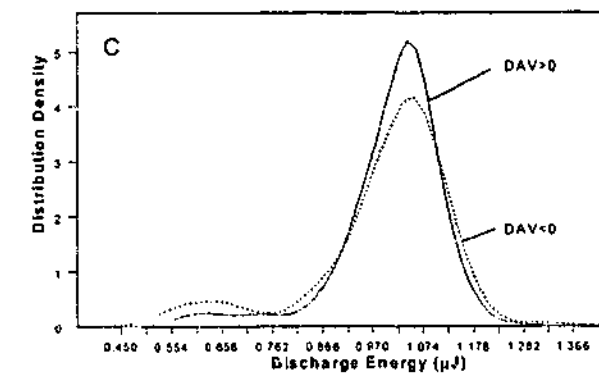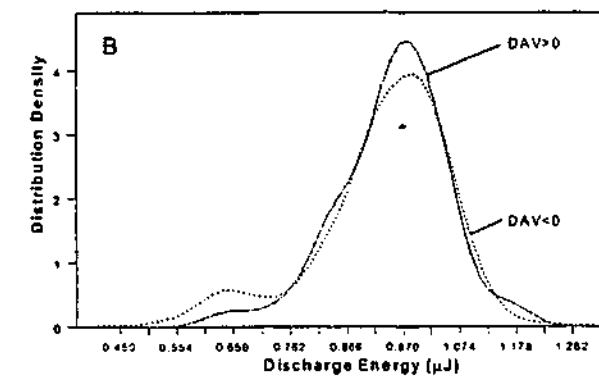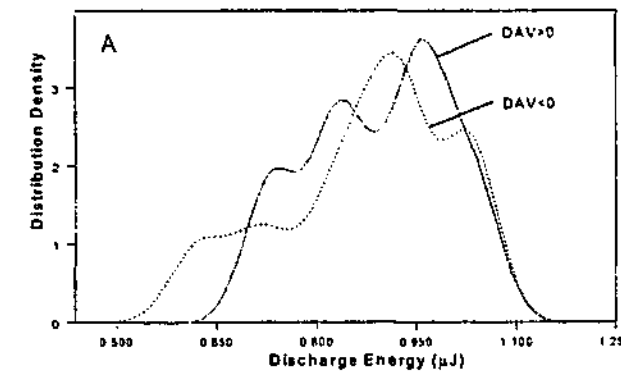
Fig. 22 Probability distribution of PD energy $p_2(E_n \mid \Delta t_{n-1}, DAV_n)$

A: time interval at 14 μs   B: time interval at 16 μs
C: time interval at 18 μs   D: time interval at 22 μs

The impact of ac voltage on pulse-to-pulse memory propagation can be further analyzed using the statistical results calculated from the first and second order of conditional distributions. The conditional distributions used for analysis are listed below:

$$p_1(q_n \mid \Delta t_{n-1}), \quad p_2(q_n \mid \Delta t_{n-1}, DAV_n > 0), \text{ and } p_2(q_n \mid \Delta t_{n-1}, DAV_n < 0)$$

$$p_1(E_n \mid \Delta t_{n-1}), \quad p_2(E_n \mid \Delta t_{n-1}, DAV_n > 0), \text{ and } p_2(E_n \mid \Delta t_{n-1}, DAV_n < 0)$$

The statistics of the first and the second order distributions such as occurrence, arithmetical mean of discharge amplitude and energy are shown in figure 6.23(A), (B), and (C) respectively. Within each plot, the Δt_{n-1} restricted discharge amplitude and energy occurred on different voltage slopes are drawn together to assess the ac voltage impact on the pulse-to-pulse memory propagation. It is found in figure 6.23(A) that more PD events are occurred on the up side of ac voltage slope. Restricted with the location of different side of ac voltage slope, the arithmetical mean of discharge amplitude and energy are very close when Δt_{n-1} is shorter than the critical time interval t_c. Meanwhile it is also observed that the consecutive discharges with longer Δt_{n-1} ($\Delta t_{n-1} > t_c$), the mean of PD amplitude and energy on different side of ac voltage slope are moving apart. In addition, the likeness of PD energy mean between the up and down side of ac voltage slope is more similar than that of PD amplitude as shown in figure 6.23(B) and (C). It indicates that using discharge energy to assess the ac voltage impact on pulse-to-pulse memory propagation is appropriate.
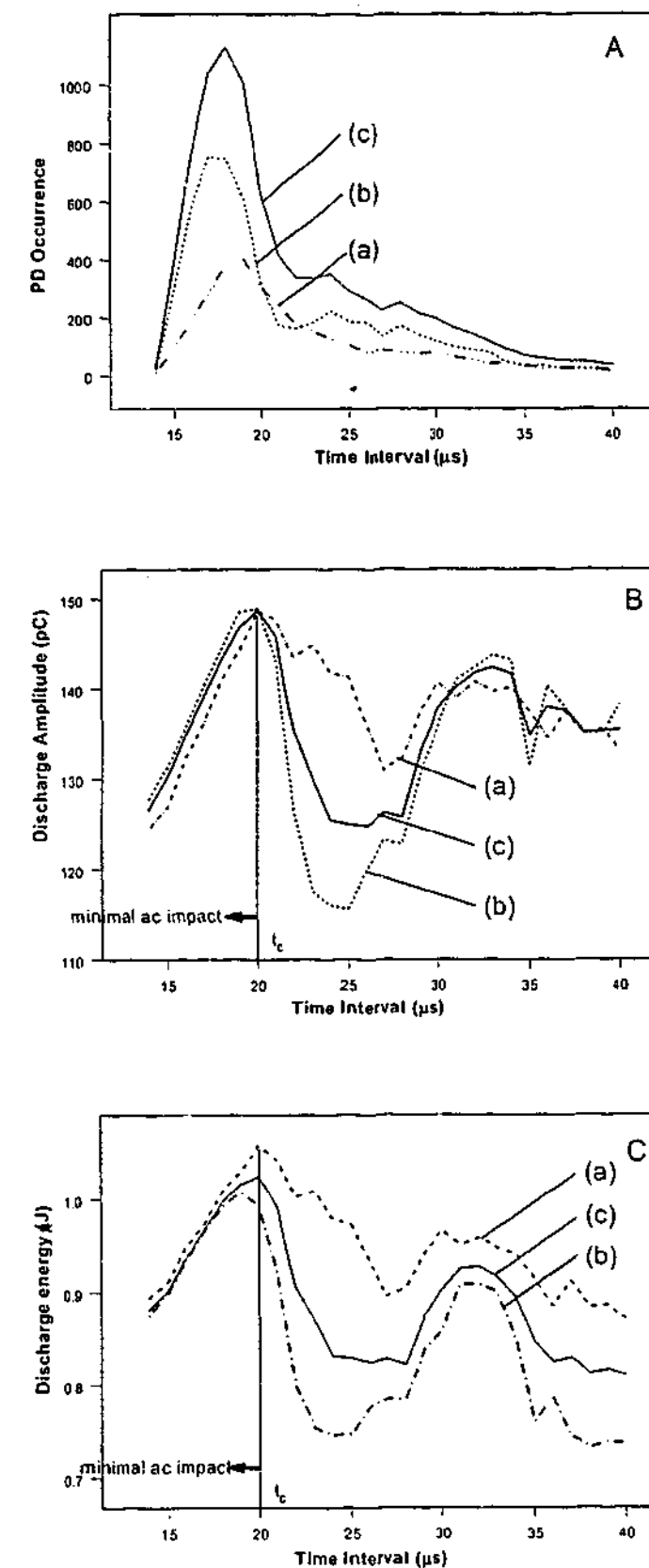
Fig. 6.23 Conditional distribution statistics of Trichel-pulse
A: PD occurrence   B: Amplitude mean   C: Energy mean
(a): up-trend slope;   (b): down-trend slope; and   (c): both up and down-slopes

Figure 6.24 has demonstrated the correlation between the minimum time separations Δt_{min} and ac RMS voltage under the test arrangement. It is shown that $f_1(\Delta t_{min} \mid DAV < 0) > f_2(\Delta t_{min} \mid DAV > 0)$ is in the indicated voltage range. It is understandable that the increase of voltage has the possibility to accelerate the initiation and development of the next discharge event. Hence, statistically, the minimum time separation tends to occur on the down side slope of ac voltage. It is also shown that the minimum time-separation reach a critical value Δt_{mc} that depends on the sample arrangement and test criteria.

In fact, each defect has its own particular degradation mechanism, which is significantly affected by the memory effects. Using pulse sequence analysis to investigate discharge physical process has become more and more important due to pulse sequence characteristics are mainly determined by the local inception field at the defect site. However, such an approach is quite limited under ac voltage. The critical time interval is a measure under which the impact from ac voltage can be minimized. It may be calculated from the distributions shown in figure 6.23. In practice, it can be calculated from the relationship between the arithmetical mean of corona amplitudes and Δt_{n-1}. When the mean of corona is increased in proportional to the increase of Δt_{n-1}, it means $\Delta t_{n-1} < t_c$, otherwise $\Delta t_{n-1} \geq t_c$.
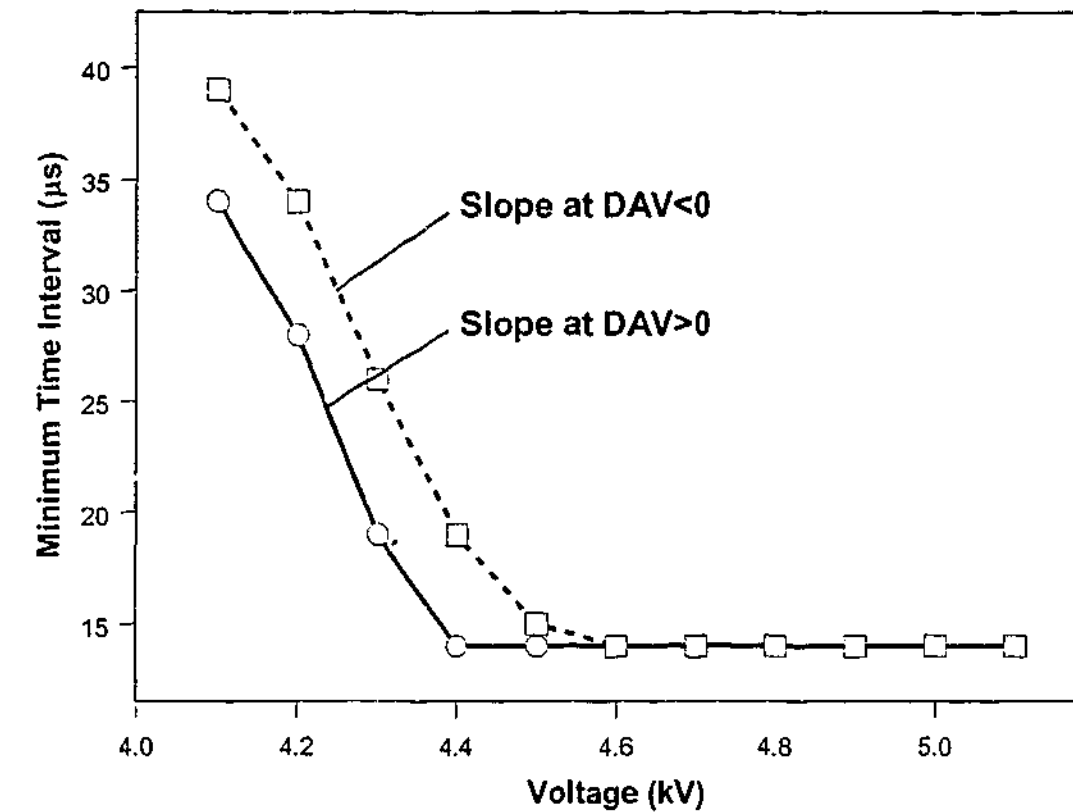
Fig. 6.24 The minimum time separation at different voltage slope vs. applied voltage

It has been observed that the impact of change of voltage is minimal when the pulse-to-pulse time separation is less than the critical time interval t_c. Before the minimum time separation Δt_{min} of both sides of ac voltage slope reaches the saturated value Δt_{mc}, the critical time interval t_c continues to decrease with the ac RMS voltage. Figure 6.25 demonstrates that the critical time interval t_c depends on the ac voltage. It is obvious that the higher is the applied ac voltage, the shorter the critical time interval t_c will be.
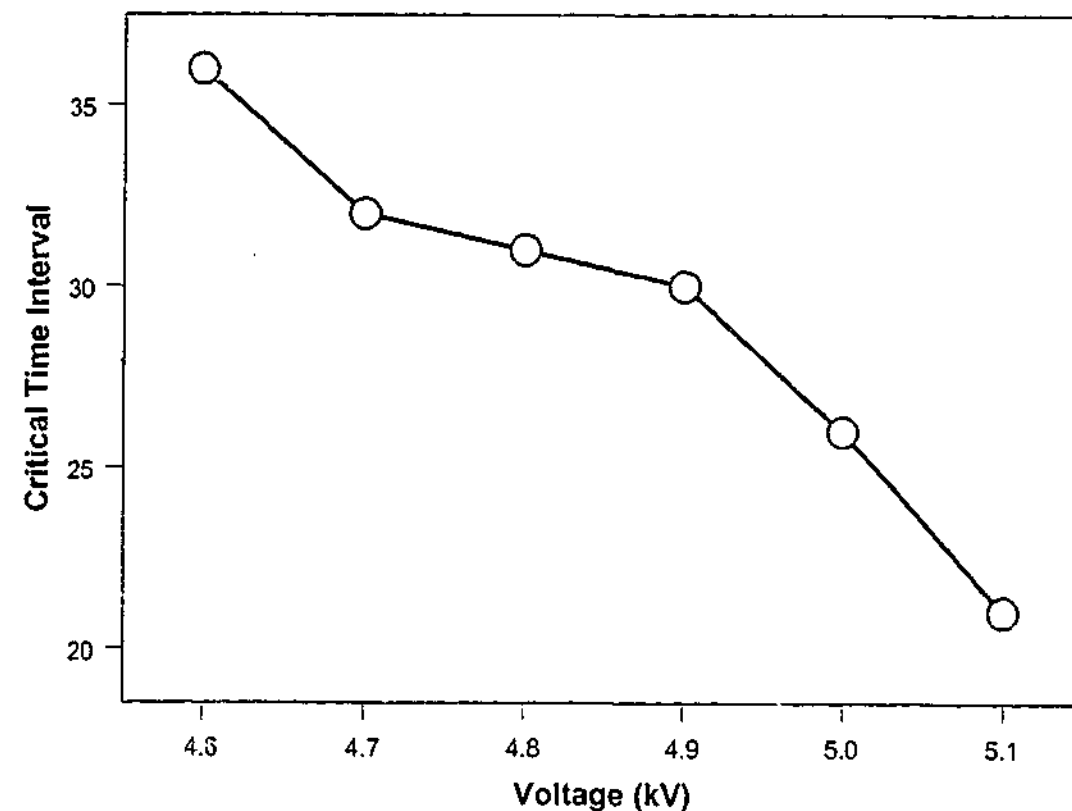
Fig. 6.25 Critical time interval versus applied voltage after reaching the minimum time separation

6.7 CONCLUDING REMARKS

Distribution functions derived from the differences of PD properties in a continuous sequence provide distinctive distribution information which is valuable for the study of discharge physical phenomena and for the classification of different types of defect. Distribution functions based on voltage, charge and time difference between consecutive PD events are new concepts that introduced in this research project. More importantly, the consecutive PD distribution functions are implemented in the PDD system for PD analysis and pattern recognition. With the help of this distribution category, PDD system can explore PD distribution information-base on the differences of consecutive PD properties. Using distribution functions based on the time interval between consecutive PD events, memory effects of negative air corona are investigated under ac circumstances as an example.

The pulse-to-pulse distribution behavior of negative, point-to-plane corona discharges in air has been investigated under ac voltage. The statistics of Trichel-pulse discharge properties were studied using the unconditional and conditional distributions of PD amplitude and energy. It has been shown that ac generated discharges within a point-to-plane gap have a complex stochastic behavior. Under the test criteria, both corona amplitude and energy are dependent on Δt_{n-1} and DAV_n. Apparently, the corona behavior is influenced or determined by its basic physical mechanisms. The statistical variation of discharge including the pulse-to-pulse memory propagation under dc voltage has been extensively studied because the memory effects are closely related to the probabilities of discharge initiation and growth [4]. However, the behavior of pulse-to-pulse memory propagation is more complicated under ac voltage than under dc, due to the change of external field. Therefore, the characteristic of memory effects can not be measured for the entire range of consecutive coronas, only for those with the time separation Δt_{n-1} shorter than the critical time interval t_c.

The experimental results presented in this paper have demonstrated explicitly that the Trichel-pulse discharge phenomenon is a stochastic process in which memory effects play an important role when q_{n-1} is shorter than the critical time interval. The time separation resolved distribution could be attributed to the superimposed influence of residual space charge from the previous pulse as well as from the change of applied ac voltage. It has been learned that the minimum time separation between consecutive pulses decreases with the increase of applied voltage. Statistically, the pulse-to-pulse memory effect has suffered a significant impact from the change of applied voltage. The minimum time separation becomes constant when the voltage is further increased. Before dropping to the constant value, the minimum time separation is always located in the voltage slope where $DAV_n > 0$.

In addition, the pulse-to-pulse memory effect has suffered a significant impact from the change of applied voltage, which has been demonstrated by the correlation between discharge properties and Δt_{n-1} when $\Delta t_{n-1} < t_c$. Apparently, the influence of the increase or decrease of the applied voltage is getting weaker when Δt_{n-1} is shorter. Conversely,

the influence would be stronger as Δt_{n-1} becomes longer. The conditional distribution patterns of consecutive discharge events may be used not only to explore discharge mechanisms but also to provide potential tools for interpreting insulation test results.

Finally, when extracting discharge parameters, cares must be taken. One must understand that the critical time interval t_c is not only dependent on the applied ac voltage and frequency, but also dependent on the sample arrangement and test environment such as the gap distance, temperature, gas type, density etc. Based on experimental results, The analysis may led to the conclusion that conditional distribution patterns of consecutive discharge events can be used, not only to explore discharge mechanisms, but also to provide potential tools for interpreting insulation test results.

Chapter 7

Partial Discharge Classification Using Neural Networks

In previous chapters, discharge distribution functions of four different categories have been established to analyze discharge phenomena and extract relevant parameters. Apparently, distribution functions contain details of discharge distributions that are associated with the nature of discharge mechanism. It is feasible to form discharge fingerprints using compressed information extracted from those distribution functions to discriminate different types of discharge source. In the past decades, a number of classification methods have been employed for the recognition of various discharge sources. These methods include conventional model, hidden Markov model, fuzzy logic, artificial neural networks, wavelet transforms, and fractal feature approaches etc. In this chapter, the PD pattern recognition techniques using neural networks are applied to the established discharge fingerprints. The usefulness and the effectiveness of the established PD fingerprints are proved by the results obtained from three different neural network topologies. Finally, sensitivity theory is employed in order to innovate a general method to find the most significant discharge parameters from the fingerprints. The sensitivity analysis is performed on the trained MLP network. The most significant parameters are found being associated with the nature of discharge mechanism.

7.1 OVERVIEW

As explained, PD measurement plays a vital role to monitor the quality and determine the reliability of insulation system of HV power equipment. The computer based PD monitoring and diagnosing system has opened a new era for insulation condition monitoring. It has been made possible the application of advanced technologies such as artificial neural networks and fuzzy logic to PD pattern recognition. Artificial neural networks have attracted the attention of scientists and technologists from a number of

disciplines. The discipline has attracted many scientists including computer scientists who are interested in opportunities that are opened by the massively parallel computational networks in artificial intelligence, modeling and simulation. A brief overview on the applications of PD pattern recognition using artificial neural network (ANN) is helpful in understanding what has been achieved and what is still required to be done. In spite of the growing number of applications in PD pattern recognition, only a limited number of distribution functions have been for the extraction of discharge distribution p ..... ‾ ‾ ‾‾lting in the possibility of missing significant PD parameters that have ... ‾‾ .. .. ‾ini:al‾‾g power for the classification of different types of PD source. I‾ ‾‾‾‾‾‾‾. ‾e ‾‾nber of statistics employed to represent a distribution function i‾ ‾ ‾ ‾‾‾‾‾‾‾‾ ‾‾‾ cover the detail of discharge distributions. There is a need to interpret the ‾‾‾ ‾‾‾‾‾.ship between the most significant parameters found from the sensitivity analysis and the types of PD sources used to train the network due to the imprecision and instability of the distribution functions themselves.

7.1.1 PD Recognition Using Distribution Function

Many types of distribution functions can be used for PD recognition. Most are derived directly or indirectly from the phase angle φ, discharge magnitude q, and PD repetition rate. In fact, the performance of the classifier engine is dependent on the quality of the training data as well as the type of neural network. Feature quantities are extracted to form an input vector to represent a defect under certain circumstances. In order to reliably and efficiently identify PD sources of different types, it is necessary to have fingerprints containing the significant feature quantities. To date, the distribution functions currently used to provide fingerprints for PD pattern recognition are summarized herewith.

(1) Distribution functions of the PRPD category

In PRPD distribution category, the following distribution functions have been utilized to provide distribution information.
- The phase of occurrence
- The average PD amplitude

182

- The maximum PD amplitude

(2) Distribution functions of the PHPD category

In PHPD distribution category, the pulse-height of occurrence distribution function is the only distribution function used to calculate feature quantities.

(3) Distribution functions of the inter-pulse distribution category

In this category, the following mapping patterns and distribution functions have been used to recognize PD patterns and to investigate PD physical characteristics such as memory effects as well.
- The mapping of $\Delta V_n \Delta V_{n-1}$ pattern
- The occurrence distribution function based on ΔV_{n-1}
- The occurrence distribution function based on ΔT_{n-1}

(4) Others

A few miscellaneous distribution patterns have been used
- The φ-q-n three-dimensional distributions
- The pulse energy of occurrence distribution function

The former pattern was used to calculate fractal dimensions that describe surface roughness, lacunary and denseness of the distribution. Discharge features can also be extracted from the latter distribution as part of the PD fingerprints.

7.1.2 ANN Architectures Used for PD Recognition

The development of artificial neural network was inspired by the studies of the brain and nervous system. Generally, artificial neural network consists of a network of processing nodes connected with uni-direction interconnection lines. The network takes a number of inputs and produces a number of outputs that are intended to describe the inputs. This kind of mapping process is utilized for a variety of purposes such as pattern recognition, filtering etc. It can be implemented using hardware and/or software methods.

183

Computer based PD detection offers an opportunity to scrutinize various derived distribution functions related to the nature of a defect. Unfortunately, even under laboratory conditions, no particular feature quantity has been regarded as the most appropriate or significant parameter that can separate different types of defect. Hence, the problem of finding a generalized approach to find out the most significant feature quantities has been raised for the application of PD pattern recognition.

Feature quantities extracted from distribution functions have been used to calculate boundaries of various different types of discharge source. Several network architectures have been adopted to classify PD sources of different types. Among those types of ANN used for PD pattern recognition, multilayer perceptron (MLP) topology with a back-propagation (BP) training algorithm is the most popular one used to classify various defects. In addition to MLP topology, there are a few applications successfully using Adaptive Neuro-Fuzzy Inference System to fulfill the task. Principal component transformation has also been adopted for a large-scaled approach.

In this chapter, the MLP neural network with BP training algorithm will be studied along with its extended models. The MLP neural network, a powerful classifier employed to classify defects, is trained with feature quantities extracted from PRPD, PHPD, CRPD and inter-pulse distribution functions. The performance of a special type of MLP, the modular neural network, trained with the same fingerprints, is compared with that of the MLP network. Finally, a hybrid topology constructed by an unsupervised and a supervised learning algorithm is trained with the same fingerprints for the classification purpose.

7.2 THE PD CLASSIFICATION SYSTEM AND FINGERPRINTS

Partial discharge involves complex physical and chemical processes. In an insulation system of HV equipment, different types of discharge produce different distribution patterns. Undoubtedly, an integrated PD measuring and evaluating system with pattern recognition technology can accomplish this task. With such an implementation, a

backend database is required to warehouse various types of known PD fingerprints that acquired and stored in the past so that PD pattern recognition can be performed on the unknown defect during the measuring phase. A general PD recognition procedure is illustrated in figure 7.1. It consists of a PD detector that yields PD distribution patterns. The classification process requires this reliable backend database support, which is followed by the calculation and extraction of feature quantities from distribution functions.
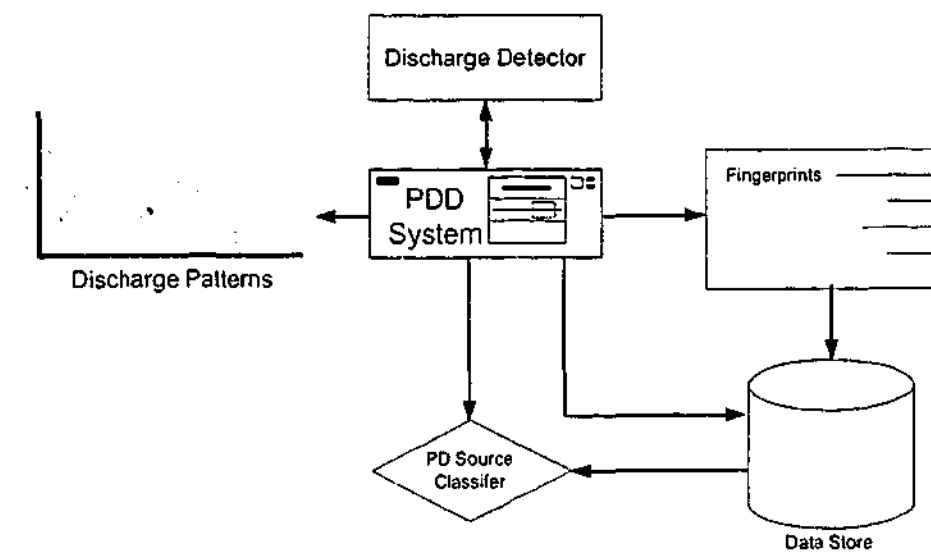
Fig.7.1 General procedure for PD source identification with PDD system

According to the measuring system shown in figure 2.1 of chapter 2, PD data are acquired and transferred to the PDD system in which many patterns of distribution functions can be displayed on a PC screen for visual comparison. Meanwhile feature quantities of distribution functions are calculated to form a fingerprint. The fingerprints of various defects are extracted from distribution functions of PRPD, PHPD, CRPD, and inter-pulse PD distribution categories. The calculated fingerprints can be compared with the existing fingerprints in the database to identify the type of defect. As an option, the recognition results can be chosen to add into the back-end database. The general PD fingerprints built in the PDD system consist of 360 feature quantities. The types of PD sources used in this project for training neural networks are listed in table 7.1.

Defect	Description
1	Corona discharge in air (a rod-to-plane arrangement)
2	A ball-type needle inside an epoxy resin stator bar at half distance between surface and conductor
3	A sharp needle inside a mica insulated stator bar at half distance between surface and conductor
4	A sharp needle inside an epoxy resin stator bar at half distance between surface and conductor
5	3 mm oil-impregnated pressboard under parallel electrodes (water contains: 20-25 ppm)
6	1 mm mylar film under parallel electrodes
7	Discharge from Point-to-dielectric arrangement
8	Corona discharge in Nynes oil (water contains: 10 ppm)
9	3 mm dry pressboard under parallel electrodes

Table 7.1 Discharge sources of different types for classification

7.3 CLASSIFICATION USING MLP NETWORKS

Multilayer perceptrons (MLPs) extend the perceptron with hidden layers. Hidden layers consist of processing elements that are not directly connected to the output. Conceptually, the multilayer perceptron constructs input-output mappings of any non-linearity. They are of the form

$$y = f(\sum f(\cdots f(\sum(\bullet))\cdots)) \qquad (7.1)$$

where the number of function compositions is given by the number of network layers. The resulting map is very flexible and powerful, but is hard to analyze.

7.3.1 MLP Theoretical Summary

Multilayer perceptrons are an extension of Rosenblatt's perceptron. The perceptron has only one input and one output layer. The perceptron can only solve pattern recognition problems where the classes are separated by hyperplanes, an extension of a plane for more than two dimensions. A large number of problems in practice such as PD pattern recognition do not fit into this description. MLPs extend the perceptron with hidden layers.

There are two important characteristics of the multilayer perceptron. First, processing elements are nonlinear and their transfer functions must be smooth. Second, they are fully interconnected so that any element of a given layer feeds all the elements of the next layer. The perception and the multilayer perceptron are trained with error correction learning, which means that the desired response for the system must be known. This is normally the case with pattern recognition. Error correction learning works as follows:

From the system response at the ith PE at iteration n, $y_i(n)$, and the desired response $d_i(n)$ for a given input pattern, an instantaneous error $e_i(n)$ is defined by:

$$e_i(n) = d_i(n) - y_i(n) \qquad (7.2)$$

Applying the theory of gradient descent learning, each weight in the network can be adapted by correcting the present value of the weight with a term that is proportional to the present input at the weight and the present error at the weight:

$$w_{ij}(n+1) = w_{ij}(n) + \eta \delta_i(n) x_j(n) \qquad (7.3)$$

The local error can be directly computed from $e_i(n)$ at the output PE or computed as the sum of errors at the internal PEs. The constant h is called the step size and the procedure is called the backpropagation algorithm. Backpropagation computes the error of the output with respect to each weight in the network and modifies each weight by a value that is proportional to the error. The beauty of the procedure is that it can be implemented with local information and is efficient because it requires just a few multiplications per weight. However, since it is a gradient descent procedure and only uses the local information, it can get caught in a local minimum. Moreover, the procedure is rather noisy since a poor estimate of the gradient is being used, resulting in possible slow convergence.

Momentum learning is an improvement to the straight gradient descent in the sense that

a memory term is utilized to speed up and stabilize the convergence. In momentum learning the equation to update the weights becomes:

$$w_{ij}(n+1) = w_{ij}(n) + \eta \delta_i(n) x_j(n) + \alpha(w_{ij}(n) - w_{ij}(n-1)) \qquad (7.4)$$

where α is the momentum which normally should be set between 0.1 and 0.9. The training can be implemented in two ways, either presenting one pattern and updating the weights one at a time or presenting all patterns and then updating the weights with the average weight update. To start backpropagation, an initial value for each weight is required and it proceeds until one of the stopping criteria is met. The stopping criteria are the number of iterations, the mean square error of the training set and the mean squared error of the cross validation set. Cross validation is the most powerful criterion of the three since it stops the training at the point of optimal generalization.

7.3.2 Topology and Configuration

MLP neural network with two-hidden-layer is chosen to train by the PD fingerprints as shown in figure 7.2. Like one-hidden-layer MLP, it is a universal classifier. It can realize any input-output map. However, existing theorems do not constrain the topology of MLP and can address any engineering problem such as how many PEs and layers does the MLP need to solve a particular problem. On the other hand, it is important to know that the MLP is a universal approximator. The number of PEs in the first hidden layer is associated with the number of linear discriminant functions required by size of the input vector. Generally, the number of PEs in the first hidden layer should cover the number of dimensions in the input space. The number of PEs in the second hidden layer creates the number of bumps in the input space that are needed for the approximation. A modified M-P PE in the second hidden layer forms a single bump. The beauty of backpropagation training algorithm is that it is a systematic, step-by-step procedure that can be applied independent of the topology of the network and the input dimensionality. Larger, more complex networks may require more training time, but backpropagation is still fully capable of training the network.
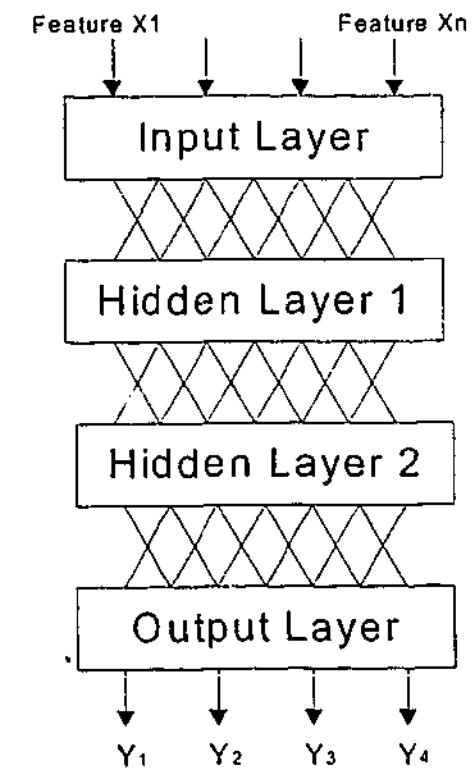
Fig. 7.2 The two-hidden-layer MLP system

The configuration of the MLP network was as follows:

Input Layer
- Number of PEs: 360

First Hidden Layer
- Number of PEs: 500
- Transfer function:hyperbolic tangent
- Step size: 1
- Momentum: 0.7
- Percentage to change the step size: 10

Second Hidden Layer
- Number of PEs: 100
- Transfer function:hyperbolic tangent
- Step size:0.1
- Momentum: 0.7
- Percentage to change the step size: 10

Output Layer

- Number of PEs: 4
- Step size: 0.01
- Momentum: 0.7
- Percentage to change the step size: 10

Training

- Batch training

Termination Criteria

- MSE threshold: 0.01
- Maximum epochs: 1000
- MSE of cross validation: 0.01

7.3.3 MLP Training Performance

After setting the MLP neural network, the training leads to the following results:

- The average number of epochs: 325
- The average elapsed time: 12:34 minutes

Training was conducted 5 times. The initial values of weights were randomly set. During training, one of the cost functions is shown in figure 7.3. It demonstrates the training process that takes 351 epochs to satisfy the stopping criteria.
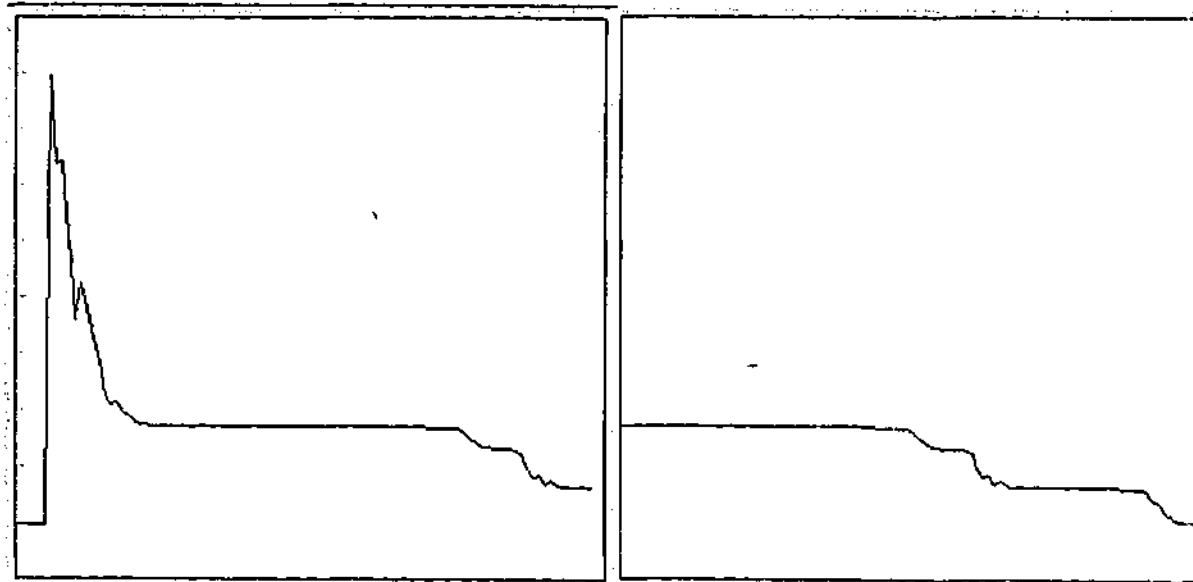
Fig 7.3 The cost function during the MLP network training

7.4 CLASSIFICATION USING MODULAR NETWORKS

The modular network is simply an extension to the multilayer perceptron networks. Therefore, the theory and learning rules are the same. The only aspect to note is that a modular network requires fewer weights versus a MLP with the same number of PEs. A modular network generally train faster than a MLP in speeding in the weight adaptation for the hidden and input layers due to PEs in hidden layers having partial connections to their previous and next layers as illustrated in figure 7.4.
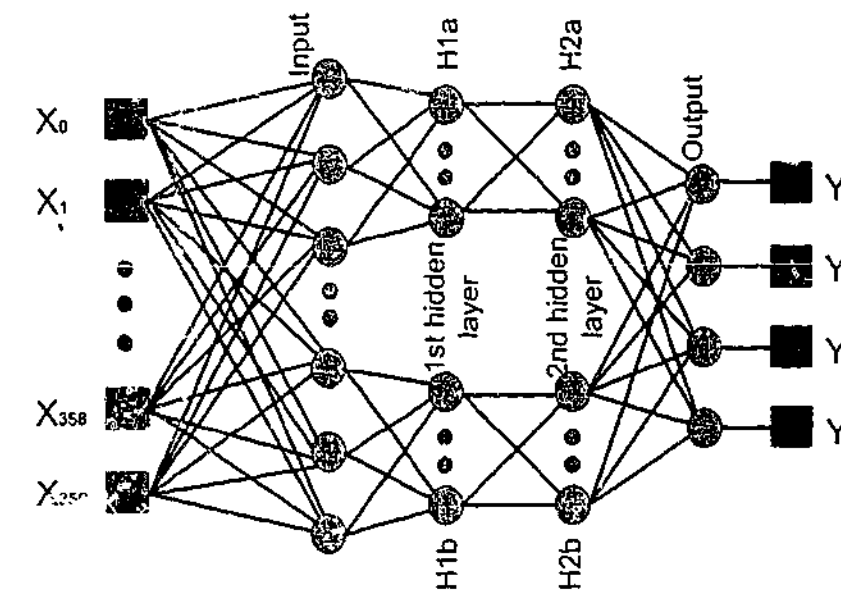
Fig. 7.4 The modular network topology

The modular network was configured as follows:

Input Layer

- Number of PEs: 360

First Hidden Layer (H1a)

- Number of PEs: 195
- Transfer function:hyperbolic tangent
- Step size: 1
- Momentum: 0.7
- Percentage to change the step size: 10

Second Hidden Layer (H2a)

- Number of PEs: 130

- Transfer function:hyperbolic tangent

- Step size: 0.11

- Momentum: 0.71

- Percentage to change the step size: 10

Output Layer

- Number of PEs: 4

- Step size: 0.01

- Momentum: 0.7

- Percentage to change the step size: 10

Training

- Batch training

Termination Criteria

- MSE threshold: 0.01

- Maximum epochs: 1000

- MSE of cross validation: 0.01

Note, settings of hidden layer H1b and H2b are same as H1a and H2a respectively. After setting the network, the backpropagation training was conducted 5 times. Before training the network, a set of small random initial value was assigned to each weight. One of the cost functions during training is shown in figure 7.5. The averaging number of epochs that the network required to satisfy the stopping criteria is 87 and the average lapsed time for training the network is 3:27 minutes.

Fig 7.5 The cost function during the modular network training

Comparing the required epochs for MLP and modular network, it is found that modular network has better performance in terms of training speed. This is because the modular network does not have full interconnectivity between the layers, which tends to speed up the training process.

7.5 CLASSIFICATION USING COMBINED PCA AND MLP

One of the fundamental concerns in pattern recognition is the technique of feature extraction that is important for the classification. The goal is to transform the input vectors into a new space so that the characteristics about the vectors are kept, but the dimensionality is significantly reduced. This transformation makes the classification process much easier.

7.5.1 Theoretical Briefing

Principal component analysis (PCA) is a useful technique. From the input space, it finds an orthogonal set of N directions where the input data has the largest energy and extracts M $(D \geq M)$ projections from D directions in an ordered fashion. The first principal component is the projection, which has the largest value, while the Mth principal component has the smallest value as in figure 7.6.
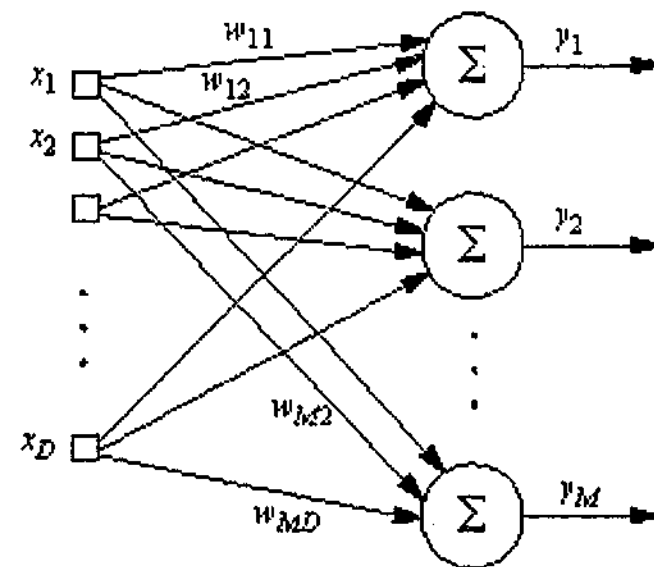
Fig 7.6 A PCA network to project data from D to M dimensions

If the largest projections are extracted, then the most significant information about the input data is kept. Principal component analysis is normally done by calculating eigenvalues from the input correlation matrix. Sanger's rule is applied in this application because it orders the projections. Principal component analysis can be used for data compression, producing M most significant linear features. When used in conjunction with a multilayer perceptron to perform classification, the separability of the classes is not always guaranteed. If the classes are not sufficiently separated, the PCA will extract the largest projections while the separability could be contained within some of the smaller projections. The importance of PCA used in conjunction with a MLP is that the number of inputs for the MLP classifier can be significantly reduced. Hence, it results in a reduction in the training times of the classifier. The topology of this hybrid network is illustrated in figure 7.7.
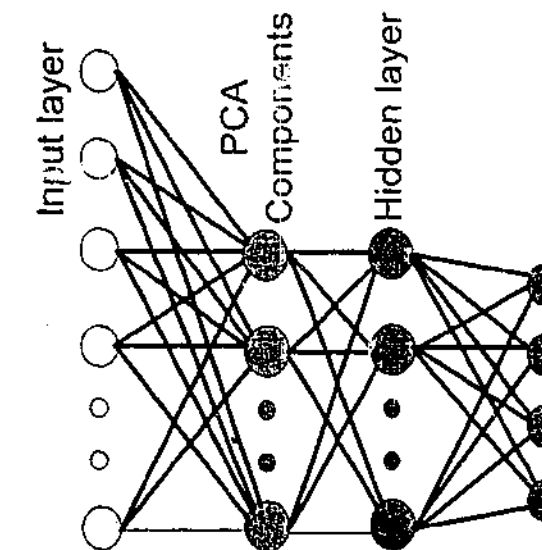
Fig 7.7 The topology of a PCA in connection with a MLP network

7.5.2 Configuration

The hybrid network was configured as follows:

Input Layer
- Number of PEs: 360

PCA Components (MLP Input)
- Number of PEs: 36
- Learning Rate: 0.01
- Learning Rate Decay: 0.0001

MLP Hidden Layer
- Number of PEs: 72
- Transfer function:hyperbolic tangent
- Step size:0.1
- Momentum: 0.7
- Percentage to change the step size: 10

Output Layer
- Number of PEs: 4
- Step size: 0.01
- Momentum: 0.7
- Percentage to change the step size: 10

Training

- Batch training

Termination Criteria

- MSE threshold: 0.01
- Unsupervised Maximum epochs: 200
- Supervised Maximum epochs: 800
- MSE of cross validation: 0.01

PCA is a linear procedure to find the direction in input space where most of the input energy lies. In other words, PCA performs feature extraction. The projections of these components correspond to the eigenvalues of the input covariance matrix. The MLP performs classification of these features. During the training phase, the principal component analysis is performed first, and then the MLP is trained. The value of this arrangement is (1) PCA network trains faster when it does not have to share computing resources with MLP and (2) there is no need to train the MLP until the eigenvalues become stable. After being extracted, principle components are fed to the MLP for training and the cost function is shown in figure 7.8.
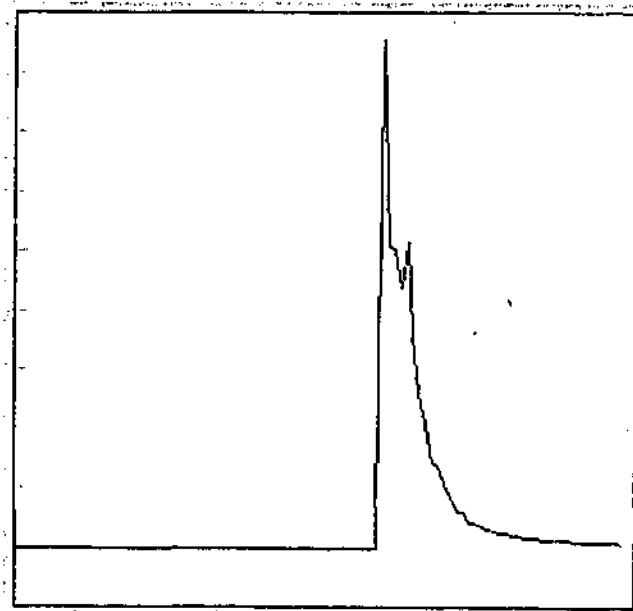
Fig 7.8 The cost function during MLP training for a combined PCA and MLP network

---

7.6   SENSITIVITY ANALYSIS

While training a network, it is important to know the effect that each of the network inputs is having on the network output. This provides feedback as to which input parameters are the most significant. In this project, sensitivity theory is adopted to conduct sensitivity analysis using the trained MLP network to find the most significant parameters that are associated with discharge distributions.

7.6.1   Introduction

Sensitivity may be defined as the partial derivative of a function with respect to one of its independent variables. It determines how small a change in one of the independent variables will affect the functional value. A sensitivity study may not only help to decide to prune the input space by removing the insignificant inputs but also help to find the most significant distribution functions. Thus, more feature quantities may be further explored from distribution functions having significant contributions on the classification. It is obvious that sensitivity analysis helps to build efficient PD fingerprints and reduce the size of the network, which in turn reduces the complexity and the training time.

Sensitivity analysis is a method for extracting the cause and effect relationship between the inputs and outputs of the network. The network learning is disabled during the operation of sensitivity analysis so that the network weights are not affected. The basic idea is that the inputs to the network are shifted slightly and the corresponding change in the output is reported as a percentage difference.

As defined, the nature of sensitivity analysis provides an efficient approach to catch the feature quantities that have significant contributions to establish the mapping between inputs and outputs. It provides an opportunity to trace back the feature quantities having significant discrimination power among defects for recognition. In addition, it is important to find the original distribution functions from which the significant feature quantities are extracted. It is worthwhile to further investigate the relationship between discharge physical processes and the distribution functions providing significant feature

quantities. This is one of the major contributions of this research project providing a general methodology to capture the most sensitive PD parameters.

7.6.2 Basic Definition

Sensitivity considerations have long been of concern in connection with dynamic systems. Sensitivity considerations have provided a fundamental motivation for the use of output error. Let the behavior of a dynamic system be characterized by $\vec{\alpha} = [\alpha_1 \alpha_2 \cdots \alpha_n]$ and quantity $\xi = \xi(\vec{\alpha})$. Here ξ is referred to a system function.

Let the nominal parameter vector be denoted by $\vec{\alpha_0} = [\alpha_{10} \alpha_{20} \cdots \alpha_{n0}]$ and the nominal system function by $\xi_0 = \xi(\vec{\alpha_0})$. Then, under certain continuity conditions, the following general definitions hold

$$\overline{S_j} = \frac{\partial \xi(\vec{\alpha})}{\partial \alpha_j} = \overline{S_j}(\vec{\alpha_0}) \text{ at } \vec{\alpha} = \vec{\alpha_0}, \qquad j=1, 2, ..., n \qquad (7.5)$$

System error caused by the jth parameter can be expressed

$$\Delta \xi_j = |\overline{S_j}| \bullet |\Delta \alpha_j| \qquad (7.6)$$

Hence, the overall system error caused by the variation of parameter vector

$$\Omega = \sum_{j=1}^{n} \Delta \xi_j = \sum_{j=1}^{n} |\overline{S_j}| \bullet |\Delta \alpha_j| \qquad (7.7)$$

The relative error of the system caused by the jth parameter

$$\varepsilon(j) = \frac{\Delta \xi_j}{\Omega} = \frac{|\overline{S_j}| \bullet |\Delta \alpha_j|}{\sum_{i=1}^{n} |\overline{S_i}| \bullet |\Delta \alpha_i|}, j=1, 2, ..., n \qquad (7.8)$$

7.6.3 Results

The sensitivity analysis has been conducted on the PD fingerprints that are large vectors consisting of 360 feature quantities. The feature quantities are statistics extracted from distribution functions discussed in chapter 3, 4, 5, and 6. Based on the trained MLP network presented early in this chapter, a small percentage of variation is applied to each feature quantity of the trained fingerprints on a one-to-to basis. The percentage effect of overall output performance is calculated using equation 7.8 and it is associated with the percentage variation of every input parameter. The output vector represents the total response to the variation of corresponding input. The variation of each input parameter is ranged from 1% to 5% at the step of 1%. The sensitivity output for each input parameter is shown in figure 7.9, where the output percentage effects are illustrated for 1%, 2%, 3% and 5% variation of input feature quantity.
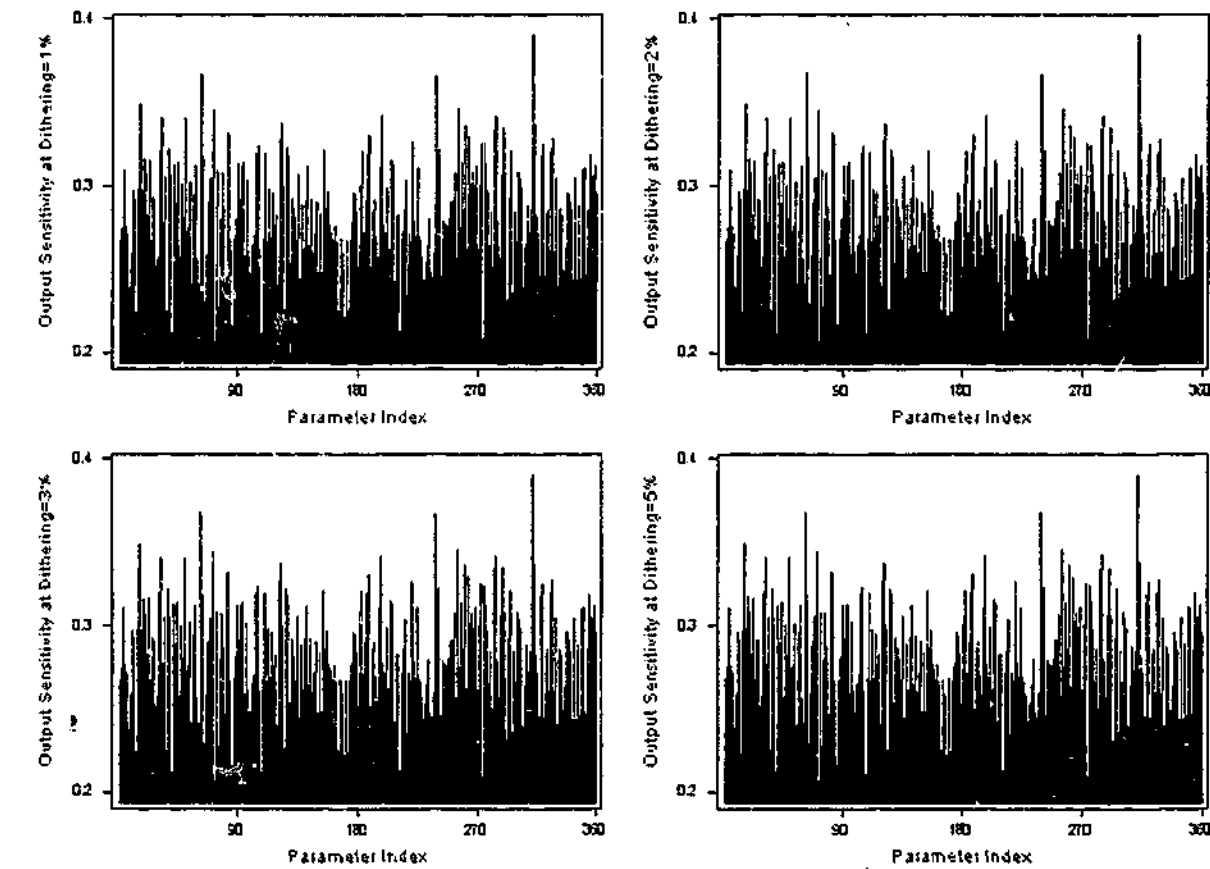
Fig 7.9 Results of sensitivity analysis after dithering the training data

After being sorted, the most sensitive parameters are listed in table 7.2, where the first parameter is the input parameter causing the most significant response of the overall output.

Parameter Index	Parameter Description
312	Range of positive Distribution of QD resolved pattern
61	Standard deviation of extreme parameter of PRPD pattern
239	Geometry mean of PD quadratic amplitude of PHPD pattern
16	Variance of negative PD events of PRPD pattern
255	Correlation between PHPD positive and negative maximum distribution functions
71	Accumulative positive PDs of PRPD pattern
285	Distribution range of positive side of consecutive VD pattern
197	Total number of negative PD events in PHPD pattern
49	Variance of positive maximum PD distribution function of PRPD pattern
32	Skewness of positive average PD distribution function of PRPD pattern

Table 7.2 Top 10 most sensitive discharge parameters

The top 10 most sensitive feature quantities are presented in order as listed in table 7.2. It is desirable to re-evaluate the distribution functions that provide the most significant feature quantities. Further research in this direction may determine the connection between the distribution functions and the discharge stochastic properties.

7.6.4 Discussions

Based on the results of the sensitivity analysis, it can be observed that the positive range of consecutive charge difference is the most significant feature quantity listed on top of table 7.2. The charge difference resolved distribution functions and the relevant analysis techniques are referred to in chapter 6. For a spherical void discharge model, the potential of the electrode and the associated charge are U and q respectively. Prior to a PD event in the void, the potential immediately after the discharge quenched has dropped to $U-\Delta U$ and the charge on the electrode has become $q+\Delta q$, where Δq is the charge transferred to the electrode. According to Green's theorem it yields

$$(U - \Delta U)q = U(q + \Delta q) + \int_S V\sigma dS \qquad (7.9)$$

where V is the scalar potential at the surface element dS, σ is the surface charge density, and $q = CU$, where C is the capacitance of the system. Equation 7.9 can be further

200

simplified as

$$q = C\Delta U + \Delta q \qquad (7.10)$$

If the impedance of the circuit is large, then Δq may be ignored. Hence, the induced charge is given approximately by

$$q \approx C\Delta U \qquad (7.11)$$

As illustrated in the above equation 7.10, the induced charge is directly related to the system capacitance and voltage difference between two consecutive PD events. Generally, the location and geometry and other properties of the defect are associated with the distribution of induced charge in or around the defect. Therefore, the charge difference between consecutive pulses may be treated as an important variable to model the PD process. It is understandable that the range of charge difference resolved distribution functions become the most significant feature quantity of the input parameters. The charge difference resolved voltage distribution functions of different types of PD sources are illustrated in figure 7.10.
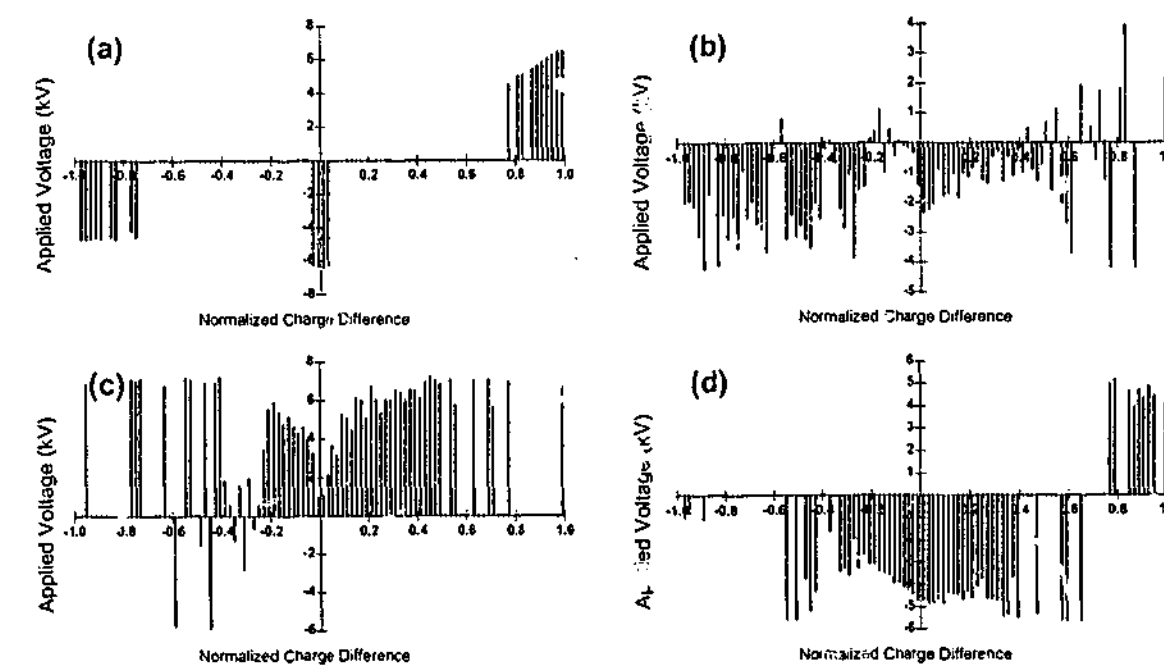
Fig. 7.10 Distribution functions of average applied voltage against QD measured from

201

(a) A rod-to-plane arrangement
(a) A rod-to-dielectric arrangement
(b) An oil-impregnated pressboard sample
(c) An epoxy resin stator bar sample with an artificial defect inside

As seen in table 7.2, the most of significant feature quantities are derived or calculated from PRPD, PHPD and consecutive inter-pulse VD, QD resolved distribution functions. The details of calculating feature quantities from these distribution functions have been discussed in the previous chapters. Referring to the second most significant feature quantity listed in table 7.2, the maximum distribution function of PRPD pattern category is illustrated in figure 7.11 and 7.12. In figure 7.11, PD data are measured from a point-to-dielectric after applying 3 kV voltage for 1, 3, 5, and 7 minutes while in figure 7.12 PD data are measured from point-to-plane arrangement under different applied voltages. According to the results of the sensitivity analysis, the dispersion of absolute PD magnitude from their central tendency is an important measure for classifying PD sources of different types.
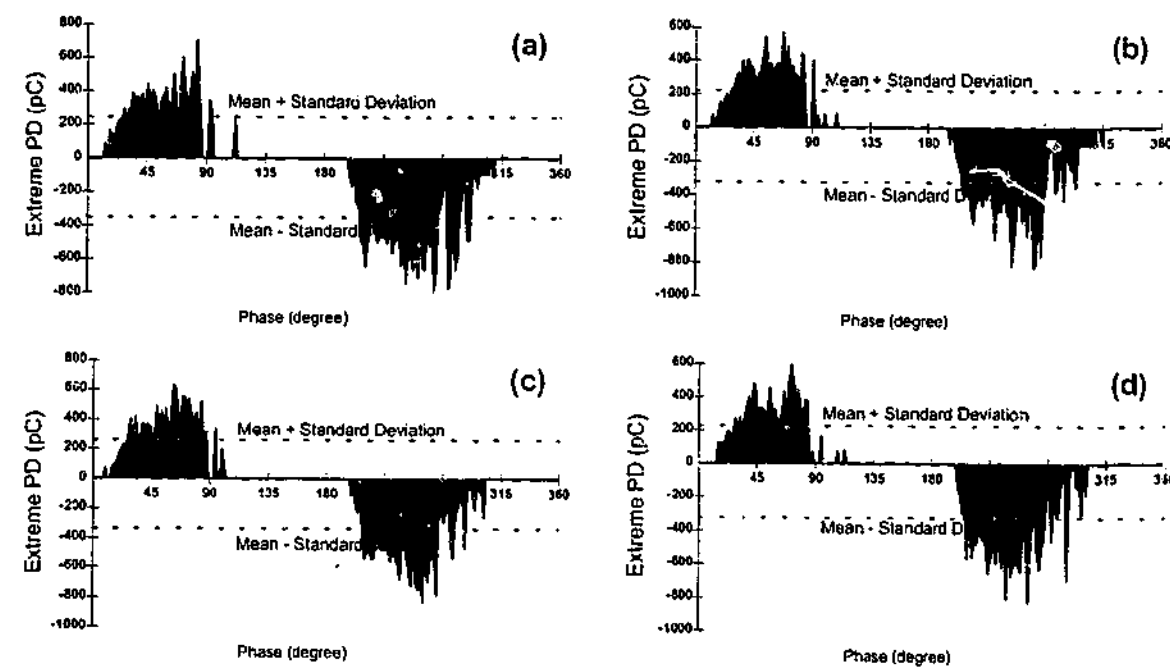
Fig. 7.11 Maximum distribution functions of PRPD category measured from a point-to-dielectric arrangement after applying 3 kV voltage
(a) for 1 minute   (b) for 3 minutes   (c) for 5 minutes   (d) for 7 minutes
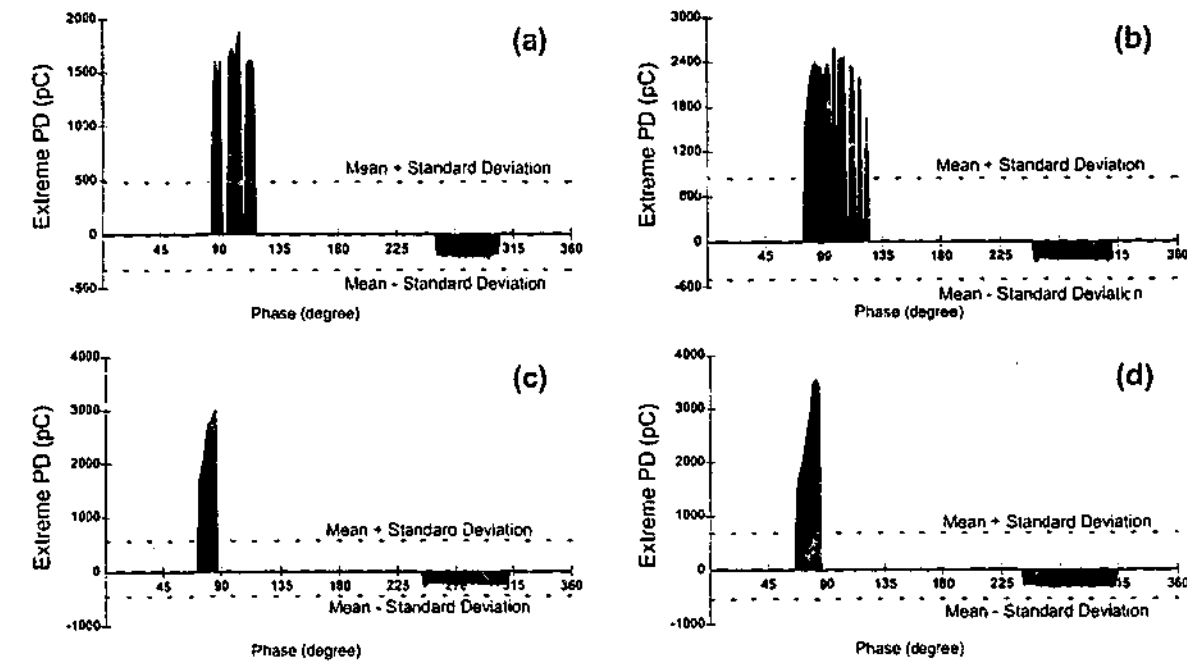
Fig. 7.12 Maximum distribution function of PRPD category measured from a point-to-plane arrangement
(a) at 4 kV   (b) at 4.2 kV   (c) at 4.4 kV   (d) at 4.6 kV

After sorting, feature quantities are re-organized in order from the most to the least significant. Prior to the sensitivity analysis, the parameter order of a fingerprint was organized in a standard list. The same topology of the MLP network was trained again using the found top 40 most significant feature quantities. The configuration of the network was scaled down according to the number of inputs. Fingerprints acquired from the types of defect used to train the network are the same, which is listed in table 7.2. The detail of the network configuration is illustrated as follows:

Input Layer

• Number of PEs: 40

First Hidden Layer

• Number of PEs: 60

• Transfer function:hyperbolic tangent

• Step size: 1

• Momentum: 0.7

• Percentage to change the step size: 10

Second Hidden Layer

- Number of PEs: 30
- Transfer function:hyperbolic tangent
- Step size: 0.1
- Momentum: 0.7
- Percentage to change the step size: 10

Output Layer

- Number of PEs: 4
- Step size: 0.01
- Momentum: 0.7
- Percentage to change the step size: 10

Training

- Batch training

Termination Criteria

- MSE threshold: 0.01
- Maximum epochs: 1000
- MSE of cross validation: 0.01

The cost function of the network is shown in figure 7.13. The average number of epochs required for the network to meet the stop criteria are 19 and the average lapsed time is 31seconds.
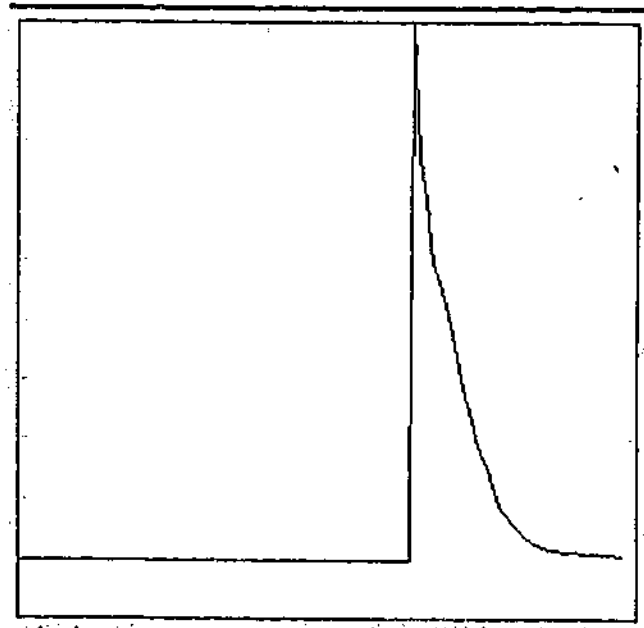
Fig 7.13 The cost function in the MLP training with top 40 most significant feature quantities

Further studies on sensitivity analysis were performed using different defects. The MLP network was trained again after removing those fingerprints that represent defect type 1 of table 7.1. After being trained, sensitivity analysis was performed again to find the most significant parameters. Then, in the similar fashion, the fingerprints representing defect type 1 and 2 were removed before training the same MLP network again. The results were obtained and compared with the significant parameters listed in table. It is clear that the found most significant parameters in the three cases are different. The top ten most significant parameters computed in each case are listed in table 7.3.

Case 1 Parameter Index	Case 2 Parameter Index	Case 3 Parameter Index
312	168	344
61	161	189
239	152	91
16	327	153
255	162	109
71	217	161
285	113	40
197	349	292
49	124	348
32	259	180

Table 7.3 Most significant parameters of 3 different cases listed in descending order
Case 1: With all the defects listed in table 7.1
Case 2: With all the defects listed in table 7.1 except defect type 1
Case 3: With all the defects listed in table 7.1 except defect type 1 and 2

Obviously, it may be concluded that most significant parameters are closely associated with the overall fingerprints stored in the database. It is dependent on the number of different types of discharge sources, the input space covered by fingerprint and the configuration of the classifier.

7.7 CONCLUDING REMARKS

One of the advantages of ANNs is that they are powerful enough to create arbitrary discriminant functions to achieve optimal classification. One of the central issues in neural network design is to utilize systematic procedures to modify the weights so that the effective classification is achieved. The accuracy is quantified by an error criterion.

The aim of PD pattern recognition or classification is to assign a label to a PD pattern of unknown origin based on known patterns. Generally, there are two major steps in PD pattern recognition (1) feature selection and (2) classification and identification. Obviously, the quality and the size of the training data have significant impacts on the selection of the network topology and the configuration of the neural network.

Apparently, a set of acquired PD data measured by PDD system generates many distribution functions classified into four distribution categories. Every distribution function provides unique distribution information associated with the nature of PD process. Distribution functions of the same or different categories are related. The quality of the training data is extremely important as PD patterns may vary significantly under different testing criteria. As a rule, one should make the training data cover as much input space as possible.

Many types of neural network can be used for PD pattern recognition. MLP is the most popular one due to its non-linear classification capability. With two hidden layers, they can approximate any input-output mappings. They can efficiently use the information contained in the input data. The disadvantage of using MLPs is that the input-output mapping depends only on the presented fingerprints. Therefore, it must be emphasized that PD fingerprints should cover as much input space as possible by acquiring PD data under a wide range of testing conditions. As a special case of MLPs, a modular network segments part of the input feature quantities into modules of different layer. This tends to create some structures that may be trained on a unique portion of the data within the topology. Obviously, it speeds up the training process and reduces the number of epochs needed to train the network to the same degree of accuracy. The main

disadvantage is that there are many ways to segment a MLP into modules. It demonstrates 4 possible different ways to construct a modular network in figure 7.14. It is unclear which one is the best design based on the given training data.
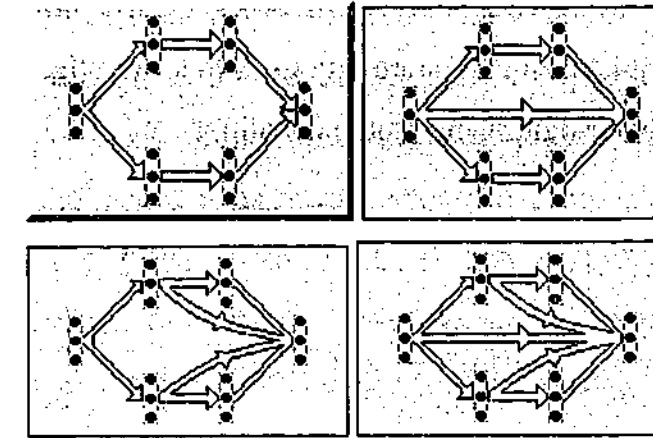
Fig. 7.14 Different ways to segment a MLP into modular networks

There is no guarantee that each module will be trained specially on a unique portion of the data. Principle component analysis is a well-known tool of orthogonalizing data. After PCA, the features are orthogonal and can easily train a MLP network. There are usually fewer features extracted than the number of inputs, so the PCA segment provides a means of data reduction. The disadvantage of using PCA is that the most discriminant features are not always the features having the largest eigenvalues. In addition, the choice of the number of features to extract is rather arbitrary.

In the application of PD pattern recognition, start by extracting as many feature quantities as possible from distribution functions of all categories. It is considered that the extracted features will be used to discriminate PD sources not only at present time but in the future as well. However, the larger the number of feature quantities, the longer the time required to calculate these feature quantities and train the network. After being trained, the weights of network are frozen to perform the sensitivity analysis in order to determine the most significant feature quantities. Feature quantities with significant discrimination power are found using the sensitivity analysis.

In summary, successful PD recognition requires PD patterns to have good discriminating power. To reduce the dimensions of PD fingerprints, feature quantities can be

compressed directly using a PCA network but there is no unique way to do this. The balance among the size of fingerprints, time for calculating fingerprints, discriminating power and the final speed of classification should be considered when designing the whole system. The most sensitive discharge parameters can be found using a trained MLP. As the discriminant power of the trained network is dependent on the quality of the training data, the results of sensitivity analysis open an opportunity to further investigate the relevant distribution functions that generate significant feature quantities.

Chapter 8

Conclusions and Future Work

Practically, it is impossible to achieve the reliable recognition of a PD source if the distribution patterns employed in the profile do not cover enough information regarding PD physical activities. However, it is possible to achieve this task or at least to improve the reliability of PD source recognition if enough PD feature quantities, derived from meaningful distribution functions, are extracted to form PD fingerprints.

Various distribution categories are systematically established and implemented in this research project. In order to clarify the way for PD pattern analysis, a few important concepts are defined such as the basic and integrated PD quantities, the partition window and its quantity and finally the distribution function and the feature quantity. In each distribution category, conventional and new developed distribution functions are combined together to provide a complete vision regarding the distributions of discharge activities against a specific independent variable.

This research project has achieved the characterization of discharge mechanisms using four categories of distribution functions. A distribution category is a group of distribution functions having the same independent variable such as ac phase angle, PD magnitude, ac cycle, and the difference between PD properties of consecutive pulses. With PRPD analysis, distribution functions are derived in relation to the phase of sinusoidal applied voltage and PRPD statistics are also presented over the phase partition window. For PHPD analysis, the six built-in distribution functions are made against discharge pulse-height partition window. PHPD distribution functions are not only interrelated but also correlated with the corresponding PRPD distribution functions. With CRPD analysis, the distribution functions are developed to analyze discharge stochastic properties under ac cycle voltage stress especially the inception and extinction properties. Pulse sequence analysis is another important approach to characterize PD phenomena since pulsating

PDs in a sequence are not independent but correlated. The voltage, charge and time differences between consecutive PD events are treated as independent variables that can be used to derive new distribution functions. It is proved that these distribution functions are indispensable to analyze PD phenomena. As an example, the memory effects of discharges measured from point-to-plane in air are investigated using pulse sequence distribution functions under ac voltage. However, it could be argued that the number of windows chosen to partition the phase and PD pulse-height may have some influence on the PRPD and PHPD distribution functions as well as on the feature quantities. In fact, the number of partition windows used to establish the distribution functions presented in this thesis is fixed at 200. Though the window number can be varied, it is restricted by the sampling rate, the number of resolution bits and the buffer size of the PDD system. In practice, the number of partition windows can be adjusted from a scroll bar which is located in the middle of the bottom of the main interface as shown in figure 2.4.

Successful PD source recognition is reported because feature quantities extracted for training the networks covers a wide range of PD distributions that represents the nature of discharge activities. They have stronger discriminating power than any other fingerprints used for this purpose. To reduce the dimension of PD fingerprints, feature quantities can be compressed directly using a PCA network. More importantly, the most significant feature quantities can be found using sensitivity analysis that is general method to find most sensitivity or significant discharge parameters. It is one of the major contributions made in this research project. Finally, it is important to note that the results of sensitivity analysis provide an opportunity to further investigate the relevant distribution functions and their correlation with the types of defect source under test.

An integrated PD measuring and evaluating system is necessary to effectively investigate discharge mechanisms using distribution patterns and to achieve the results claimed in each chapter. The PDD system is such a system that has been developed and implemented through out this project as a necessary tool. It is applicable to evaluate insulation conditions by assessing the various distribution functions acquired and calculated with PDD system in which more than 50 distribution functions are implemented not only for visual examination but also able to extract feature quantities

for PD pattern recognition. PDD system uses advanced digital signal processing techniques equipped with comprehensive database and analysis routines. Test results are saved together with the hardware settings under which PD data are acquired. In addition, the results can be analyzed and displayed instantly with the support of various distribution graphs and printable reports. The integrated quantities displayed are in compliance with the IEC Publication 270 standard. It is one of the significant contributions in this research project for discharge measuring and evaluating techniques. More over, PDD system carries out PD measurement and analysis with greater speed, flexibility and effortlessness. Visually impressive plots of two and three-dimensional diagrams depicting their evolvement with time are obtained with little effort. Feature quantities calculated from various distribution functions can be directly exported to become part of the PD fingerprints.

In all, evidence is provided in this thesis of significant progress that has been made in achieving a better understanding of PD phenomena through pattern analysis. As is often the case with basic research, the increase in knowledge about PD raises more questions and places greater demands on the quality of fundamental data needed to the next level of understanding. In pursuit of this next level, it is recommended that emphasis should be given to the following research fields:

(1) Study on basic PD phenomena and its distribution patterns

Further investigation and development works are suggested in PD theory, mathematical modeling, experimenting and analyzing PD distribution patterns. It is basic and important to develop better experimental and theoretical techniques to investigate PD behaviors. It is informative and useful to investigate the dynamics of dielectric surface discharge, to acquire more information about the changes in PD behavior during electrical tree formation in solids, to measure PD-induced decomposition of dielectric gases and to develop models that predict pulsating and glow discharges in highly non-uniform fields. Acquiring PD profiles against the change of testing environment for example, temperature, applied voltage and different background noise pattern is also crucial. It is practically useful to work on the establishment of close relationship between

PD distribution functions and PD physical phenomena.

(2) Improvement of PD measuring system

Future PD measuring system should be equipped with more reliable hardware and advanced techniques based on the existing PDD system. The improvement should be in the area such as increasing the speed as well as the resolution space for PD measurement, enhancing the real-time noise suppression technique, optimizing self-detected gain, filters and signal threshold settings, improving dynamic peak catching and reliable PD location techniques. The objects are achievable using multiple processor approach with which one enable high-speed execution algorithms to capture the first peak, one for noise reduction and real-time monitoring and one for handling the interrupts from host software.

(3) Improvement of host software and database

Component-based design strategy has been adopted in PDD system because it is the cornerstone of modern-day software development. With such a design, one software component controls the communication with the detection system, one handles the saving and retrieving data file as well as saving to and query from the backend database, one handles the graphics and one manages the pattern analysis. The performance can be improved in all the components mentioned, especially the communication and the database. In addition, the efficiency can be significantly improved by adding more stored procedures in the server side for data-manipulation, performance and security. This negates network latency in execution speed, because the processes that manipulate data reside in the same memory and processing space. In a networked environment, this can equate to large performance gains.

Finally, there is yet much more to be learned about PD. It is hoped to develop better diagnostic tools to evaluate insulation conditions as more details about PD are learned.

References

[1] Peek, F. Jr., "Dielectric Phenomena in HV Engineering", Mc Graw-Hill Book Company, Inc., 1915.

[2] Penning, F. M. "Electrical Discharges in Gases", The MacMillan Company, New York, 1957.

[3] Kuffel, K.; Zaengl, W. S. "HV Engineering Fundamentals", Pergamon Press, Oxford, England, 1984.

[4] Bartnikas, R. "Detection of Partial Discharges (Corona) in Electrical Apparatus", IEEE Trans. on Dielectrics and Electrical Insulation, Vol. 25, 1990. Page(s): 111-124.

[5] Danikas, M. G. "The Definitions Used for Partial Discharge Phenomena", IEEE Trans. on Dielectrics and Electrical Insulation, Vol. 28 No. 6, 1993. Page(s): 1075-1081.

[6] Bartnikas, R.; Novak, J. P. "On the Character of Different Forms of Partial Discharge and their Related Terminologies", IEEE Transaction on Dielectrics and Electrical Insulation, Vol. 28 No. 6, 1993. Page(s): 956-968.

[7] Sletbak, J. "The Influence of Cavity Shape and Sample Geometry on Partial Discharge Behavior", IEEE Trans. on Dielectrics and Electrical Insulation, Vol. 3 No. 1, 1996. Page(s): 126-130.

[8] Okamoto, T.; Hozumi, N.; Imajo, T. "Partial Discharge Pattern Recognition for Four Kinds of Electrode Systems", IEEE International Symposium on Electrical Insulation, Baltimore, MD USA June 7-10, 1992.

[9] Van Brunt, R. J. "Physics and Chemistry of Partial Discharge and Corona", IEEE Trans. on Dielectrics and Electrical Insulation, Vol. 1 No. 5, 1994. Page(s): 761-784.

[10] Pedersen, A.; Crichton, G. C.; McAllister, I. W. "The Theory and Measurement of Partial Discharge Transients", IEEE Trans. on Dielectrics and Electrical Insulation, Vol. 26 No. 3, 1991. Page(s): 487-497.

[11] McAllister, I. W. "Electric Field Theory and the Fallacy of Void Capacitance", IEEE Trans. on Dielectrics and Electrical Insulation, Vol. 26 No. 3, Page(s): 458-459, 1991.

[12] Kreuger, F. H. "Partial Discharge Detection in High Voltage Equipment", Temple Press, London, 1964, Butterworths & Co. 1989.

[13] Quinn, G. E. "Detection of the Ionization Point in Electrical Apparatus", AIEE Trans., Vol. 59, 1940. Page(s): 680-682.

[14] Starr, W. T. "Corona Measurement", in Engineering Dielectrics and Interpretation, Vol. I, R. Bartnikas and E. J. McMahon, Editors, STP 669, ASTM Press, Philadelphia, 1979.

[15] Bartnikas, R. "Effect of Pulse Rise Time on the Response of Corona Detectors", IEEE Trans. on Electrical Insulation, Vol. 7, 1972. Page(s): 3-8.

[16] Austin, J.; James, R. E. "On-line Digital Computer System for Measurement of Partial Discharges in Insulation Structures", IEEE Trans. on Electrical Insulation, Vol. EI-11, No. 4, December 1976.

[17] Tanaka, T.; Okamoto, T. "A Microcomputer Based Partial Discharge Measurement System", IEEE International Symposium on Electrical Insulation, Conference Record 78-CH1287-2-EI, June 1978. Page(s): 86-89.

[18] Muhr, M.; Scheucher, W. "Computer-Aided Measurement of Partial Discharges", 4th ISH Greece, Paper 63.12, September 1983.

[19] Matsuzaki, H.; Ehara, Y.; Sakai, T.; McKenny, P. A.; Hammen, M. S. A. A. "Internal Discharge Pulse Measurement Using a Microcomputer", IEEE Conference on Electrical Insulation and Dielectric Phenomena, 1986 Annual Report, November 1986. Page(s): 438-443.

[20] Rosch, P.; Boele, M. "A New Concept for Digital Partial Discharge Energy Measuring Device", 5th ISH Braunschewig, Paper 40.01, August 1987.

[21] Bartnikas, R. "Improved Pulsed Discharge Rate Measuring Apparatus for Ionization Discharge Rate Studies at Low Frequencies", Rev. Scientific Instruments, Vol. 37, 1966. Page(s): 1245-1251.

[22] Bartnikas, R.; Levi, J. H. E. "A Simple Pulse-height Analyzer for Partial Discharge Rate Measurements", IEEE Trans. on Instrumentation and Measurement, Vol. 18, 1969. Page(s): 341-345.

[23] Mazroua, A. A.; Bartnikas, R. "Neural Network System using the Multi-layer Perception Technique for the Recognition of PD Pulse Shapes due to Cavities and Electrical Trees", IEEE Trans. on Power Delivery, Vol. 10, 1995. Page(s): 92-96.

[24] International Standard IEC 60270, "Partial Discharge Measurements"

[25] Gulski, E. "Computer-Aided Measurement of Partial Discharge in HV Equipment", IEEE Trans. on Electrical Insulation, Vol. 28, No. 6, 1993. Page(s): 969-983.

[26] Kreuger, F. H.; Gulski, E.; Krivda, A. "Classification of Partial Discharge", IEEE Trans. on Electrical Insulation Vol.28, No. 6, Page(s): 917-931 December 1993.

[27] Gulski, E.; Kreuger, F. H. "Computer-aided Recognition of Discharge Sources", IEEE Trans. on Electrical Insulation Vol.27, No. 1, Page(s): 82-92 February 1992.

[28] Boggs, S. A. "Partial Discharge: Cavity-Induced PD in Solid Dielectric", IEEE Electrical Insulation Magazine, Vol. 6, N. 6, November/December 1990.

[29] Devins, J. C. "The Physics of Partial Discharge in Solid Dielectrics" 1984 Annual Report of the Conference on Electrical Insulation and Dielectric Phenomena (CEIDP), IEEE Publication 84CH1994-3, Page(s): 15-31.

[30] Gu, W.Y. Laurent, C.; Mayoux, C. "Characteristics of Discharges Inside Simulated Tree Channels Under Impulse Voltage" J. Phys. D. Appl. Phys. 19, 1986. Page(s): 2197-2207.

[31] Hantouche, C.; Fortune, D. "Digital Measurement of Partial Discharges in Full-sized Power Capacitors", IEEE Trans. on Dielectrics and Electrical Insulation, Vol. 28, No. 6, December 1993. Page(s): 1025-1032.

[32] Florkowska, B. "Partial Discharge Patterns in Polypropylene and Polyethyleneterephthalate Film", Proceedings of the 4th International Conference on Properties and Applications of Dielectric Materials, July 3-8 1994, Brisbane, Australia

[33] James, R. E.; Phung, B. T.; Su, Q.; Tychsen, R. C. "On-line Condition Monitoring by Partial Discharge Detection in Hydro-Generators", Electric Energy Conference, Canberra, Australia, October 1990. Page(s): 19-23.

[34] Su, Q.; Chang, C.; Tychsen, R. "Travelling Wave Propagation of Partial Discharges along Generator Stator Windings", International Conference on Properties and Application of Dielectric Materials, 25-30 May 1997, Seoul, Korea. Page(s): 1132-1135.

[35] Lloyd, B. A. Campbell, S. R.; Stone, G. S. "Continuous On-line Partial Discharge Monitoring of Generator Stator Windings" IEEE Transactions Energy Conversion Vol.14, No. 4, December 1999. Page(s): 1131-1138.

[36] James, R. E.; Phung, B. T.; Su, Q. "Application of a Computer-Based Measurement System for the Detection of PDs at Different Positions Within a Transformer Winding", Paper 43.06, 6th ISH, New Orleans, September 1989.

[37] Ahmed, N. H.; Srinives, N. N. "On-line Partial Discharge Detection in Transformer", IEEE International Symposium on Electrical Insulation, Virginia, USA, June 7-10, 1998.

[38] Sellars, A. G.; Farish, Q.; Hampton, B. F. "Characterizing the Discharge Development Due to Surface Contamination in GIS Using the UHF Technique", IEE Proceeding of Science, Measurement and Technology, Vol 141, No. 2, March 1994.

[39] Oki, I.; Haida, T.; Wakabayashi, S.; Tsuge, R.; Sakakibara, T. and Murase, H. "Development of Partial Discahrge Monitoring Technique Using a Neural Network in a Gas Insulated Substation", IEEE Transactions on Power system. Vol. 12, No. 2, May, 1997. Page(s): 1014-1021.

[40] Morin, R.; Gonzalez, A.; Poirier, B. "Partial-Discharge Detector for In-Service Cables and Joints Under Normal Network Operating Conditions", Proc. 1991 IEEE Power Engineering Society Transmission and Distribution Conference, 1991. Page(s): 23-28.

[41] Nakanishi, Y.; Suzuki, H.; Endoh, T. "Development of a Live-Line Partial Discharge Detection Method for XLPE-Insulated Copper Wire-Shielded Cable Using a Yoke Coil", Proceedings of 1991 IEEE Power Engineering Society Transmission and Distribution Conference. Published by IEE, IEE Service Center, Pitscataway NJ USA, 1992. Page(s): 17-22.

[42] Fukunaga, K.; Tan, M.; Takehana, H. "New Partial Discharge Detection Method for Live UHV/EHV Cable" IEEE Transactions on Electrical Insulation Vol.27, No. 3, June 1992. Page(s): 669-674.

[43] Ahmed, N. H.; Srinivas, N. N. "On-line Partial Discharge Detection in Cables", IEEE Annual Report – Conference on Electrical Insulation and Dielectric Phenomena, Minneapolis, October 19-22, 1997.

[44] Chang, C.; Su, Q. "Partial Discharge Measurement and Analysis Using an Integrated System", Australiasian University Power Engineering Conference, Perth, Australia, September 2001.

[45] Morrow, R. "Theory of Negative Corona in Oxygen", Physical Rev. A, Vol. 32, No. 3, September 1985. Page(s): 1799-1809.

[46] Van Brunt, R. J.; Kulkarni, S. V. "Stochastic Properties of Trichel-pulse Corona: A Non-Markovian Random Point Process", Physical Rev. A, Vol. 42, No. 8, , October 1990. Page(s): 4908-4932.

[47] Loeb, L. B. "Electrical Coronas", University of California Press, 1965.

[48] Fruth, B. and Niemeyer, L. "The Importance of Statistical Characteristics of Partial Discharge Data", IEEE Trans. on Electrical Insulation Vol.27, No. 1, February 1992. Page(s): 60-69.

[49] Trinh, N. G. "Partial Discharge XIX: Discharge in Air Part I: Physical Mechanisms", IEEE Electrical Insulation Magazine, Vol. 6, No. 2, March/April 1995.

[50] Krivda, A. "Automated Recognition of Partial Discharges", IEEE Trans. on Dielectrics and Electrical Insulation, Vol. 2, No. 5, October 1995. Page(s): 796 –821.

[51] Salama, M.M.A.; Bartnikas, R. "Fuzzy logic applied to PD pattern classification", Dielectrics and Electrical Insulation, IEEE Transactions on Volume: 7. Issue: 1, Feb. 2000. Page(s): 118 –123.

[52] Hoof, M.; Patsch, R. "A Physical Model, Describing the Nature of Partial Discharge Pulse Sequences", Properties and Applications of Dielectric Materials, 1997., Proceedings of the 5th International Conference on , Volume: 1 , 1997. Page(s): 283 - 286 vol.1.

[53] Hoof, M.; Freisleben, B.; Patsch, R. "PD source identification with novel discharge parameters using counterpropagation neural networks" Dielectrics and Electrical Insulation, IEEE Transactions on Volume: 4 Issue: 1, Feb. 1997. Page(s): 17 –32.

[54] Van Brunt, R. J.; Misakian, M. "Influence of Dielectric Barrier on the Stochastic Behavior of Trichel-pulse Corona", IEEE Trans. on Dielectrics and Electrical Insulation, Vol.26 No. 3, June 1991.

[55] Gulsik, E.; Kreuger, F. H. "Computger-aided Analysis of Discharge Patterns", J. Phys. D: Appl. Phys., Vol. 23, Page(s): 1569-1575, 1990.

[56] Gulsik, E.; Morshuis, P. H. F.; Kreuger, F. H. "Atomized Recognition of Partial Discharges in Cavities", Japanese Journal of Applied Physics, Vol. 29, Page(s): 1329-1335, 1990.

[57] Krivda, A. "Recognition of Discharges: Discrimination and Classification", Ph.D Thesis, Delft University Press, 1995.

[58] Krivda, A.; Gulski, E.; Satish, L.; Zaengl, W. S. "The Use of Fractal Features for Recognition of 3-D Discharge Patterns", IEEE Trans. on Dielectrics and Electrical Insulation, Vol.2 No. 5, October 1995.

[59] Van Brunt, R. J. "Stochastic Properties of Partial-Discharge Phenomena", IEEE Trans. on Dielectrics and Electrical Insulation, Vol. 26, No. 5, October 1991, Page(s): 902-948.

[60] Van Brunt, R. J.; Cernyar, E. W.; von Glahn, P. "Importance of Unraveling Memory Propagation Effects in Interpreting Data on Partial Discharge Statistics", IEEE Trans. on Electrical Insulation, Vol. 28, No. 6, Page(s): 905-916, December 1993.

[61] Bartnikas, R. "A Commentary on Partial Discharge Measurement and Detection", IEEE Trans. on Dielectrics and Electrical Insulation, Vol. 22, Page(s): 629-653, 1987.

[62] James, R.E.; Phung, B.T. "Development of Computer-based Measurement and their Application to PD Pattern Analysis", Dielectrics and Electrical Insulation, IEEE Transactions on Volume: 2 Issue: 5, Oct. 1995. Page(s): 838 –856.

[63] Kranz, H.-G. "Fundamentals in computer aided PD processing, PD pattern recognition and automated diagnosis in GIS", Dielectrics and Electrical Insulation, IEEE Transactions on Volume: 7 Issue: 1 , Feb. 2000. Page(s): 12 –20.

[64] Candela, R.; Mirelli, G.; Schifani, R. "PD recognition by means of statistical and fractal parameters and a neural network", Dielectrics and Electrical Insulation, IEEE Transactions on Volume: 7. Issue: 1, Feb. 2000. Page(s): 87 –94.

[65] Axelson, J. "Parallel Port Complete", Lakeview Research, 1997.

[66] Cacciari, M.; Contin, A.; Rabach, G.; Montanari, G. C. "An Approach to Partial-discharge Investigation by Height-distribution Analysis", IEE Proc. Science, Measurement and Technology Vol. 142, No. 1, January 1995.

[67] Van Brunt, R. J.; von Glahn, P.; Las, T. "Nonstationary Behaviour of Partial Discharge During Discharge Induced Aging of Dielectrics", IEE Proc. Science, Measurement and Technology Vol. 142, No. 1, January 1995.

[68] Malik, N. H.; Alrainy, A. A. "Statistical Variation of DC Corona Pulse Amplitudes in Point-to-Plane Air Gaps", IEEE Trans. on Electrical Insulation, Vol. 22, December 1987. Page(s): 825-829.

[69] Stricklett, K.L.; Von Glahn, P.; Van Brunt, R.J. " Phase behaviour in AC generated partial discharges: electro-convection and the moderation of discharges ", Electrical Insulation and Dielectric Phenomena, 1997. IEEE 1997 Annual Report, Conference on, Volume: 2, 1997. Page(s): 525 vol.2.

[70] Mole G.; Robinson, F. C. "A Versatile Corona Detector", 1962 Annual Report – Conference on Electrical Insulation, Nat. Acad. Sci., 1080, Page(s): 54-56, 1962.

[71] CIGRE Working Group 21.03 "Recognition of Discharges", Electra, Vol. 11, Page(s): 61-98, 1969.

[72] Braun, J. M.; Rizzetto, S.; Fujimoto, N.; Ford, G. L. "Modulation of Partial Discharge Activity in GIS Insulators by X-ray Irradiation", IEEE Trans. on Electrical Insulation. Vol 26, Page(s): 460-468, 1991.

[73] Fuhr, J.; Haessing, M.; Fruth, B.; Kaiser, T."PD Fingerprints of Some HV Apparatus", Conference Record – 1990 IEEE International Symposium on Electrical Insulation, IEEE Publication CH2727-6/90, Page(s): 129-132, 1990.

[74] Gulski, E.; Kreuger, F. H. "Computer-aided Analysis of Discharge Patterns", J. Phys. D: Appl. Phys., Vol. 23, Page(s): 1569-1575, 1990.

[75] Mirelli, G.; Schifani, R "A novel method for the recognition of PD patterns by neural network", Electrical Insulation and Dielectric Phenomena, 1999 Annual Report Conference on, 1999. Page(s): 206 -209 vol.1.

[76] Chang, C.; Su, Q. "Partial Discharge Distribution Patterns Analysis Using Combined Statistical Parameters", IEEE PES Winter Meeting 2000, Singapore, January 24-28, 2000.

[77] Chang, C.; Su, Q. "Partial Discharge Pattern Analysis with Correlation Coefficients", Australiasian Universities Power Engineering Conference, September 24-27, Brisbane, Australia. Page(s): 337-342,

[78] Mangiavacchi C.; Rabach, G. "The degradation processes in highly electrically stressed expoxy resins by the analysis of Partial Discharge Amplitude distribution". Proceedings of the 4th ISH, paper 22.08, Athens, Greece, September 1983.

[79] Boscolo, A.; Cimbrico, P. L.; Contin, A.; Rabach, G.; Tosato, F. "A Monitoring and Diagnostic Technology, Based on PDAD Detection and Analysis for HV Generator", Proceedings of the IEEE International Symposium on Electrical Insulation, Toronto, Canada, June 1990. Page(s): 137-140.

[80] Contin, A.; Rabach, G. "Partial Discharge Analysis of AC Rotating Machines", IEEE Trans. on Electrical Insulation, Vol. 28, No. 6, 1993. Page(s): 1033-1042.

[81] Krump, R.; Kranz, H. G. "Computer Aided Partial Discharge Evaluation about the Surface material of the PD-Source in GIS", Proceedings of IEEE IS EI, Boston, USA, Page(s): 246-249, 1988.

[82] Contin, A.; Cacciari. M. "A Calibration Procedure for Computer Controlled Multichannel Pulse-height Analyzer", Proceedings of IEE International Conference on Partial Discharge, Canterbury, UK, Page(s): 97-98, 1993.

[83] Contin, A.; Rabach, G. "Identification of Detection of Slot Discharges During Accelerated Aging Tests", Proceedings of IEE VRIFP' 92, Victoria, Canada, Page(s): 415-420, October 1992.

[84] Stone, G. C.; Goodeve, T. E."Unusual PD Pulse Phase Distributions in Operating Rotating Machines", IEEE Trans. on Electrical Insulation, Vol. 2, No. 4, Page(s): 567-577, August 1995.

[85] Montanari, G.C.; Contin, A.; Cavallini, A. "PD Source Recognition by Weibull Processing of Pulse Height Distributions", Dielectrics and Electrical Insulation, IEEE Transactions on, Volume: 7 Issue: 1 , Feb. 2000. Page(s): 30-39.

[86] Contin, A.; Montanari, G.C.; Ferraro, C. "PD Source Recognition by Weibull Processing of Pulse Height Distributions", Dielectrics and Electrical Insulation, IEEE Transactions on, Volume: 7 Issue: 1, Feb. 2000 Page(s): 48 –58.

[87] Contin, A.; Cavallini, A.; Montanari, G.C.; Pasini, G.; Puletti, F. "Artificial Intelligence Methodology for Separation and Classification of Partial Discharge Signals", Electrical Insulation and Dielectric Phenomena, 2000 Annual Report Conference on Volume: 2, 2000. Page(s): 522 -526.

[88] Di Lorenzo del Casale, M.; Schifani, R.; Holboll, J.T. "Partial Discharge Tests Using CIGRE Method II", Dielectrics and Electrical Insulation, IEEE Transactions on, Volume: 7 Issue: 1, Feb. 2000. Page(s): 133 –140.

[89] Contin, A.; Contessotto, G.; Montanari, G.C.; Cacciari, M. "Comparing Different Stochastic Models for the Identification and Separation of Concurrent Partial Discharge Phenomena", Dielectric Materials, Measurements and Applications, 2000. Eighth International Conference on, 2000. Page(s): 374 –379.

[90] Schifani, R.; Candela, R. "A New Algorithm for Mixed Weibull Analysis of Partial Discharge Amplitude Distributions", Dielectrics and Electrical Insulation, IEEE Transactions on Volume: 6 Issue: 2, April 1999. Page(s): 242 –249.

[91] Nerkar, Y.P.;Narayanachar, R.N.;Nema, R.S. "Characterisation of Partial Discharges in Oil Impregnated Pressboard Insulation Systems", High Voltage Engineering, 1999. Eleventh International Symposium on, Volume: 5, 1999. Page(s): 208 -211 vol.5.

[92] P. von Glahn and R. J. Van Brunt, "Continuous Recording and Stochastic Analysis of PD", IEEE Electrical Insulation, Vol. 2, No. 4, Page(s): 590-601, 1995.

[93] Imai, K.; Ito, K.; Shimizu, N.; Nawata, M. "Influence of Polymer Structure on Tree Growth from a Simulated Tree Channel", Electrical Insulation and Dielectric Phenomena, 2000 Annual Report Conference on, Volume: 1, 2000. Page(s): 337 -340 vol.1.

[94] Chia, P.Y.; Liew, A.C. "Defect Classification Based on Weibull Statistic of Partial Discharge Height Distribution with Wavelet Preprocessing", Power System Technology, 2000 Proceedings, PowerCon 2000. International Conference on, Volume: 2. Page(s): 1035 -1040 vol.2.

[95] Imai, K.; Suzuki, T.; Ito, K.; Shimizu, N.; Nawata, M. "Mechanism of Tree Propagation from a Simulated Tree Channel", Properties and Applications of Dielectric Materials, 2000. Proceedings of the 6th International Conference on, Volume: 1, 2000. Page(s): 239 -242 vol.1.

[96] Ryder, D.M.; Kouadria, D.; Howlett, R.J.; Bish, N. "The Use of Neural Network and Statistical Techniques for the Identification of Partial Electrical Discharges", Electrical Insulation and Dielectric Phenomena, 1998. Annual Report., Conference on, 1998. Page(s): 399 vol. 2.

[97] Patsch, R.; Berton, F.; Jung, J. "Space Charge, Local Electric Field and Partial Discharges", Dielectric Materials, Measurements and Applications, 2000., Eighth International Conference on, 2000. Page(s): 519 –522.

[98] Hoof, M.; Patsch, R. "Voltage-difference Analysis, a Tool for Partial Discharge Source Identification", Electrical Insulation, 1996. Conference Record of the 1996 IEEE International Symposium on, Volume: 1, 1996, Page(s): 401 -406 vol.1.

[99] Suwarno; Suzuoki, Y.; Mizutani, T. "Pulse-sequence Analysis of Partial Discharges in a Void and Electrical Treeing", Electrical Insulation, 1996., Conference Record of the 1996 IEEE International Symposium on , Volume: 1, 1996. Page(s): 130 -133 vol.1.

[100] Hoof, M.; Patsch, R. "Pulse-sequence analysis: A New Method for Investigating the Physics of PD-induced Aging", Science, Measurement and Technology, IEE Proceedings, Volume: 142 Issue: 1, Jan. 1995. Page(s): 95 –101.

[101] Hoof, M.; Patsch, R. "Pulse-sequence-analysis, A Way to Get a Better Insight into the Physics of discharges", Partial Discharge, 1993., International Conference on, 1993. Page(s): 49 –51.

[102] Trinh, N.G. "Partial Discharge XX. Partial Discharges in Air. II. Selection of Line Conductors", IEEE Electrical Insulation Magazine, Volume: 11 Issue: 3, May-June 1995. Page(s): 5 -11.

[103] Pedersen, A.; Crichton, G.C.; McAllister, I.W. "Partial Discharge Detection: Theoretical and Practical Aspects", Dielectrics and Electrical Insulation, IEEE Transactions on Volume: 2, Issue: 4, Aug. 1995. Page(s): 323 -326.

[104] Pedersen, A.; Crichton, G.C.; McAllister, I.W. "Influence of Bulk Dielectric Polarization Upon PD Transients", Electrical Insulation and Dielectric Phenomena, 1995. Annual Report., Conference on , 1995. Page(s): 323 -326.

[105] McAllister, I.W.; Crichton, G.C.; Pedersen, A. "PD-related Stresses in the Bulk Dielectric for Ellipsoidal Voids", Electrical Insulation and Dielectric Phenomena, 1994., IEEE 1994 Annual Report., Conference on, 1994. Page(s): 79 -84.

[106] Pedersen, A.; Crichton, G.C.; McAllister, I.W "PD-related Stresses in the Bulk Dielectric and Their Evaluation", Electrical Insulation and Dielectric Phenomena, 1993. Annual Report, Conference on, 1993. Page(s): 474 -480.

[107] McAllister, I.W.; Crichton, G.C. "Influence of Bulk Dielectric Polarization upon Partial Discharge Transients Effect of Heterogeneous Dielectric Geometry", Dielectrics and Electrical Insulation, IEEE Transactions on Volume: 7. Issue: 1, Feb. 2000. Page(s): 124 -132.

[108] Crichton, G.C.; Karlsson, P.W.; Pedersen, A. "Partial Discharges in Ellipsoidal and Spheroidal Voids", Electrical Insulation, IEEE Transactions on, Volume: 24 Issue: 2, April 1989. Page(s): 335 -342.

[109] Pedersen, A. "On the Electrical Breakdown of Gaseous Dielectrics - An Engineering Approach", Electrical Insulation and Dielectric Phenomena, 1989. Annual Report, Conference on, 1989. Page(s): 721 -739.

[110] Pedersen, A. "On the Electrodynamics of Partial Discharges in Voids in Solid Dielectrics", Conduction and Breakdown in Solid Dielectrics, 1989, Proceedings of the 3rd International Conference on, 1989. Page(s): 107 -116.

[111] G. E. Quinn, "Detection of the Ionization Point in Electrical Apparatus", AIEE Trans. 1940, Vol. 59, pp. 680-682.

[112] Y. Linde, A. Buzo and R. Gray, "An Algorithm for Vector Quantization Design", IEEE Trans. On Communications, COM-28 84-95, 1980.

[113] J. T. Tou and R. C. Gonzalez, "Pattern Recognition Principles", Addison-Wesley Publishing, 1974.

[114] Gallant and White, "On Learning Derivatives of an Unknown Function with MLPs", Neural Networks 5 (1), 129-138,1992.

Appendix A

Publications
(March 1998 – December 2001)

"Memory Propagation of Negative Point-to-Plane Corona under AC Voltage" -- IEE Science Measurement and Technology (Accepted).

"Partial Discharge Measurement and Analysis Using an Integrated System"-- Australiasian University Power Engineering Conference, Perth, Australia September, 2001. (Published)

"PD Classification with Novel Parameters Using Combined Topology of PCA and MLP"-- Australiasian University Power Engineering Conference, Perth, Australia, September, 2001. (Published)

"Neural Network Based PD Source Classification Using a Combined Topology of Unsupervised and Supervised Learning Algorithm"-- IEEE PES Summer Meeting, Vancouver, BC. Canada, July, 2001. (Published)

"Analysis of PD Patterns with Integrated Distribution Parameters Using Modular Neural Networks"-- IEEE Proceedings on PowerCon, Perth, Western Australia, Australia, December, 2000. (Published)

"Extraction of PD Fingerprints Using Correlation Learning"—Proceedings of the 5th International Conference on APSCOM 2000, Hong Kong, October, 2000. (Published)

"Partial Discharge Source Identification Using SOFM and MLP Neural Networks" -- the first international conference on Insulation Condition Monitoring of Electrical Plant (ICMEP'2000), Wuhan, China, July, 2000. (Published)

"Partial Discharge Pattern Analysis Using Correlation Coefficients"-- Australiasian University Power Engineering Conference, Brisbane, Australia, September, 2000. (Published)

"Partial Discharge Distribution Pattern Analysis Using Combined Statistical Parameters", IEEE PES Winter Meeting 2000, Singapore, January, 2000. (Published)

"Statistical Characteristics of Partial Discharges from a Rod to Plane Arrangement"-- Australasian Universities Power Engineering Conference, Darwin, Australia, September, 1999. (Published)

"Comparison Between Pattern Recognition Techniques For Partial Discharge Identification", Proceedings of Australasian University Power Engineering Conference, Hobart, Australia, Sep. 1998. (Published)

"Analysis of Partial Discharge Patterns from a Rod to Plane Arrangement"-- IEEE Symposium on Electrical Insulation, Anaheim, CA., April, 2000. (Published)

Appendix B

Partial Discharge Energy Resolved Distribution Function

Great effort has been directed towards the development of PD distribution functions of various categories. In addition to PRPD, PHPD, CPRD and inter-pulse distribution categories, PD pulse energy resolved distribution function (ERPD) is a new distribution category which consists of a recently developed group of distribution functions based on discharge pulse energy partition window.

Unfortunately, the ERPD distribution category has been only partly implemented in the PDD system. Feature quantities of ERPD distribution functions have not been calculated and transformed into PD fingerprints used to classify different PD sources and analyze discharge stochastic properties. Along with the enhancement of the PDD system, ERPD distribution categories will be fully implemented in the system in the near future. ERPD distribution functions are briefly introduced and discussed in this section as complementary distribution information to measure discharge activities. The analytical diagram of ERPD distribution is illustrated in figure B.1, where the discharge distributions in the i-1th and ith partition windows are demonstrated.

Similar to PRPD, PHPD and CRPD distribution category, there has been considerable interest in using occurrence distribution function to assess the quality of electrical insulation system under ac electrical stress. In fact, the occurrence distribution function has been used to provide feature quantities for PD pattern recognition [25, 55]. However, it is the only distribution function of this category has been used to extract identification parameters.
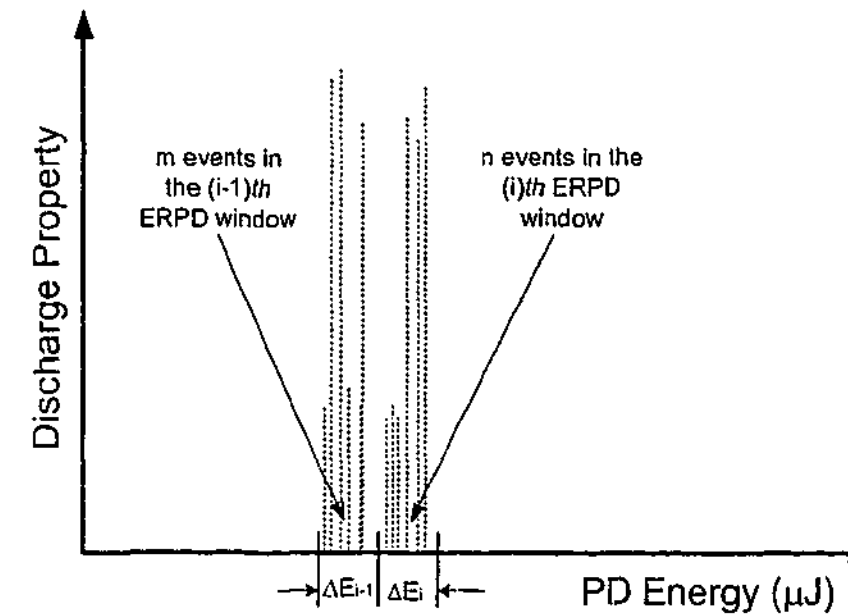
Fig. B.1 Discharge distribution in the i-1th and ith ERPD windows

B.1   OCCURRENCE DISTRIBUTION FUNCTION

For ERPD pattern analysis, many feature quantities can be calculated from occurrence distribution functions as identification parameters of PD fingerprints. Discharge energy of occurrence is an important distribution function describing the probability of PD events along ERPD partition window. If $p_1(\lambda \mid E_\lambda \in \Delta E_i)$ is the probability that a PD event λ occurred with pulse energy E_λ and $E_\lambda = \Delta E_i = E_{i+1} - E_i$, the occurrence distribution function in the ith partition window may be defined as:

$$f_E(i) = N \bullet p_1(\lambda \mid E_\lambda \in \Delta E_i) \qquad (B.1)$$

where N is the total number of PD events acquired in a measurement and i is the equally divided ERPD partition window index. The occurrence distribution functions measured from different types of defects are shown in figure B.2.
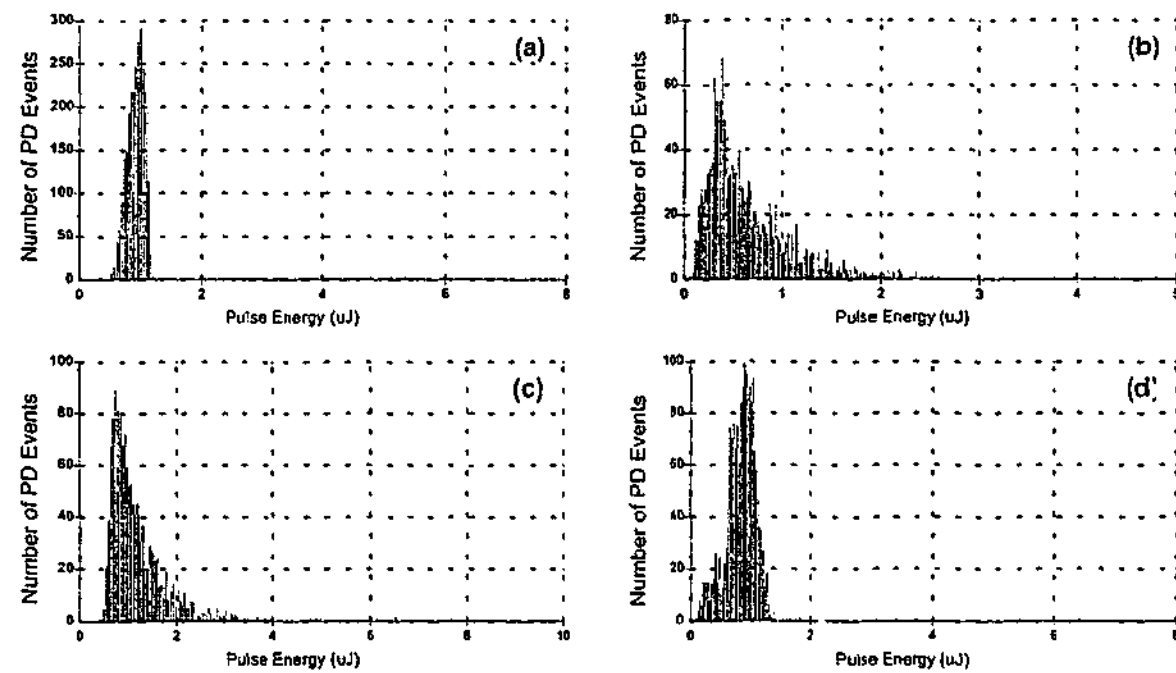
Fig. B.2 PD energy of occurrence distribution functions measured from
(a) a point-to-plane corona
(b) a point-to-dielectric discharge
(c) an oil-impregnated pressboard discharge
(d) an epoxy resin stator bar with an artificial defect inside

B.2 AVERAGE VOLTAGE DISTRIBUTION FUNCTION

The distribution function of average voltage along ERPD partition window is an interesting distribution property that has not been used in any applications either to classify discharge sources of different types or to analyze discharge stochastic properties. It is the relationship between the average external stress required for triggering discharges and the energy released when the discharges happen. Average distribution function is defined as:

$$V_{A,E}(i) = \frac{\sum (V_\lambda \mid E_\lambda \in \Delta E_i)}{N \bullet p_1(\lambda \mid E_\lambda \in \Delta E_i)} \tag{3.2}$$

where $p_1(\lambda \mid E_\lambda \in \Delta E_i) > 0$ otherwise $V_{A,E}(i) = 0$, and $V_\lambda \mid E_\lambda \in \Delta E_i$ is the voltage when the λ PD event occurs under the given condition that PD energy is in the *i/h* ERPD partition window $\Delta E_i = E_{i+1} - E_i$.

The distribution functions of average voltage of different types of discharge source are shown in the figure B.3. Obviously, the difference can be easily found between the patterns.
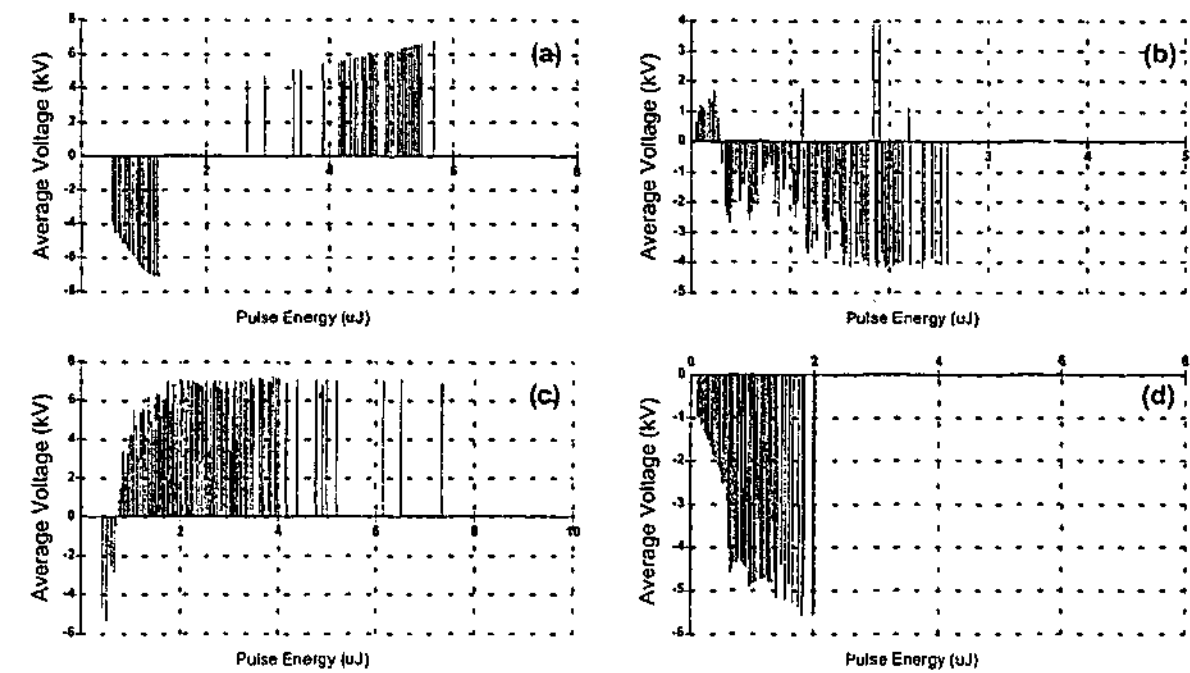
Fig. B.3 Distribution functions of average voltage measured from
(a) a point-to-plane corona
(b) a point-to-dielectric discharge
(c) an oil-impregnated pressboard discharge
(d) an epoxy resin stator bar with an artificial defect inside

B.3 MAXIMUM VOLTAGE DISTRIBUTION FUNCTION

After examining the average voltage distribution, it is important to know the maximum voltage distribution over the ERPD partition windows. With the help of the maximum distribution function, it is convenient to observe the maximum voltage required to trigger a discharge event at every ERPD partition window. It is defined as:

$$V_{M,E}(i) = \max(V_\lambda \mid E_\lambda \in \Delta E_i), \text{ when } q_\lambda > 0 \qquad (B.3a)$$

$$\text{or } V_{M,E}(i) = \min(V_\lambda \mid E_\lambda \in \Delta E_i), \text{ when } q_\lambda < 0 \qquad (B.3b)$$

The maximum distribution functions measured from different types of defect are shown in the following figure B.4 in which a visual comparison among the four different types of discharge can be easily conducted.
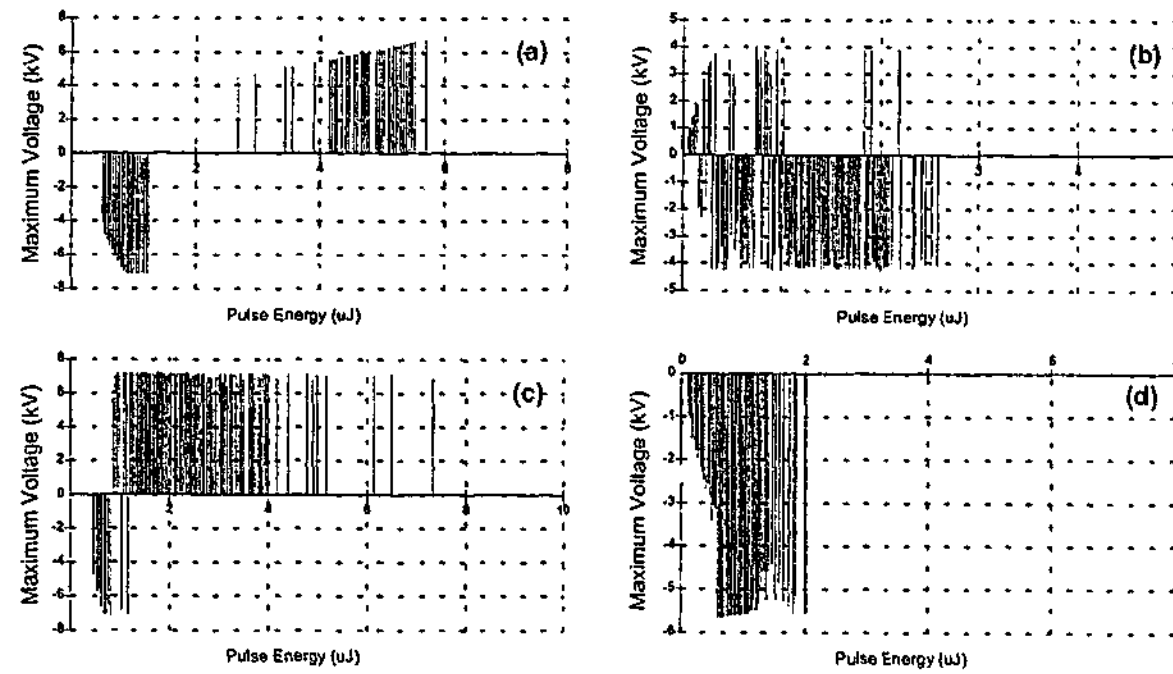
Fig. B.4 Distribution functions of maximum voltage measured from
(a) a point-to-plane corona
(b) a point-to-dielectric discharge
(c) an oil-impregnated pressboard discharge
(d) an epoxy resin stator bar with an artificial defect inside

B.4   AVERAGE PD AMPLITUDE DISTRIBUTION FUNCTION

The distribution function of average PD amplitude along ERPD partition window is an important distribution property which is a new distribution function. It describes the relationship between the average amplitude of discharges and the energy released when the discharges happen. Average PD amplitude distribution function is defined as:

$$q_{A,E}(i) = \frac{\sum(q_\lambda \mid E_\lambda \in \Delta E_i)}{N \bullet p_1(q \mid E_\lambda \in \Delta E_i)} \qquad (B.4)$$

where $p_1(\lambda \mid E_\lambda \in \Delta E_i) > 0$ otherwise $q_{A,E}(i) = 0$, and $q_\lambda \mid E_\lambda \in \Delta E_i$ is the voltage when the λ PD event occurs under the given condition that PD energy is in the ith ERPD partition window $\Delta E_i = E_{i+1} - E_i$.

The average PD distribution functions of different types of discharge source are illustrated in the figure B.5.
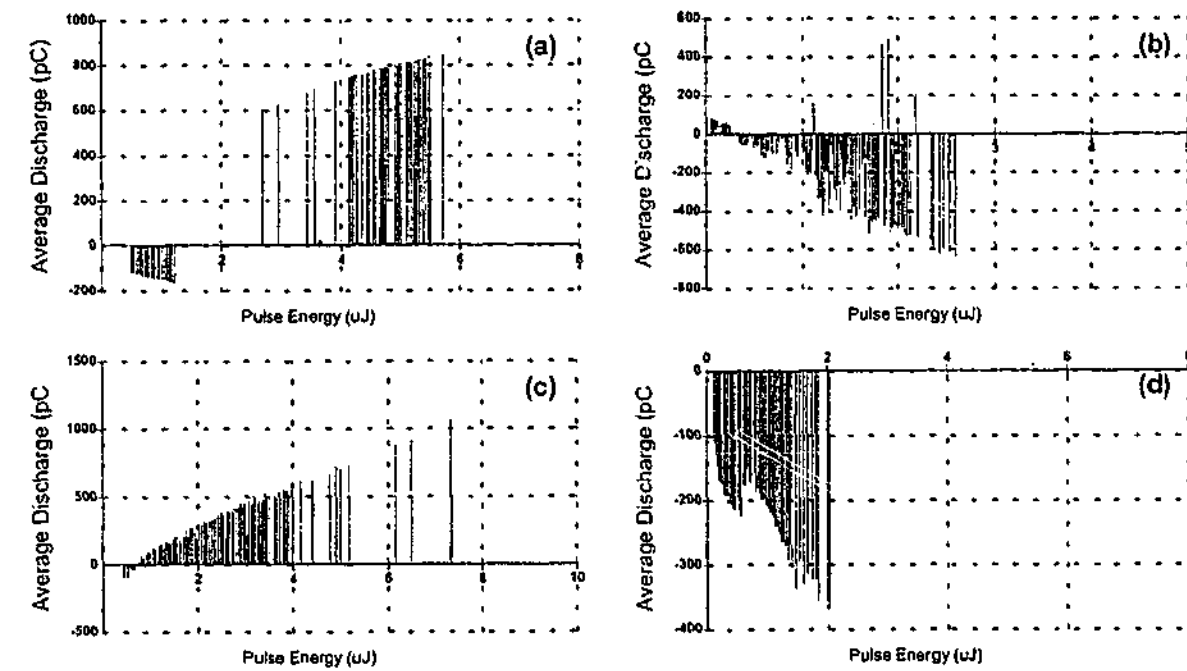
Fig. B.5 Distribution functions of average PD amplitude measured from
(a) a point-to-plane corona
(b) a point-to-dielectric discharge
(c) an oil-impregnated pressboard discharge
(d) an epoxy resin stator bar with an artificial defect inside

B.5 MAXIMUM PD AMPLITUDE DISTRIBUTION FUNCTION

It is essential to know the maximum PD amplitude distribution over the ERPD partition windows since maximum discharge is sometimes regarded as an important property for the interpretation of measurement results. With the help of the maximum PD distribution function, it is helpful to observe the maximum PD occurred at every ERPD partition window. It is defined as:

$$q_{M,E}(i) = \max(q_\lambda \mid E_\lambda \in \Delta E_i), \text{ when } q_\lambda > 0 \qquad \text{(B.5a)}$$

$$\text{or } q_{M,E}(i) = \min(q_\lambda \mid E_\lambda \in \Delta E_i), \text{ when } q_\lambda < 0 \qquad \text{(B.5b)}$$

The maximum distribution functions measured from different types of defect are shown in the following figure B.6 in which a visual comparison among the four different types of discharge can be easily performed.
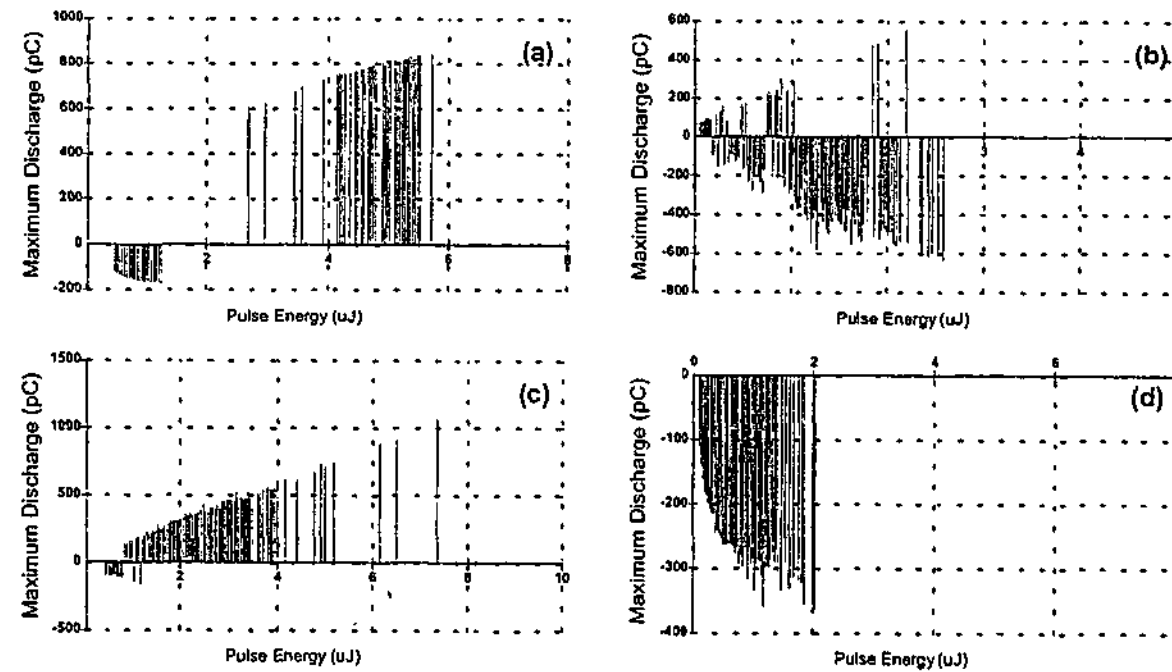
Fig. B.6 Distribution functions of maximum PD amplitude measured from
(a) a point-to-plane corona
(b) a point-to-dielectric discharge
(c) an oil-impregnated pressboard discharge
(d) an epoxy resin stator bar with an artificial defect inside

Appendix C

List of Symbol, Figure and Table

C.1 Symbol Table

Symbol	Physical Meaning	Unit
τ	The period of the power cycle	Second
ξ	Cycle index number	N/A
λ	An arbitrary discharge event neither the first nor the last	N/A
q_λ	Discharge amplitude of the λ PD event	PC
φ_λ	Phase angle of the λ PD event	Degree
E_λ	Discharge Energy of the λ PD event	μJ
P	Discharge power	W
D	Discharge quadratic rate	pC*pC/S
Q_S^-	The sum of PD amplitudes in negative half cycle	PC
Q_S^+	The sum of PD amplitudes in positive half cycle	PC
N^-	The number of PD events in the negative half cycle	N/A
N^+	The number of PD events in the positive half cycle	N/A
φ_{inc}^-	The mean inception phase angle in the negative half cycle	Degree
φ_{inc}^+	The mean inception phase angle in the positive half cycle	Degree
$H_{qn}(\varphi)$	The parameter measures the asymmetry of a distribution	N/A
CC	The cross correlation between two distributions	N/A
μ, Mu	Arithmetical mean of a distribution	N/A
S_K	The skewness of a distribution	N/A

K_U	The kurtosis of a distribution	N/A
σ	The standard deviation of a distribution	N/A
N	Total discharge events acquired a measurement	N/A
i	Partition window index	N/A
$f_\varphi(i)$	Phase of occurrence distribution function	N/A
$A_\varphi(i)$	Phase resolved average PD distribution function	pC
$M_\varphi(i)$	Phase resolved maximum PD distribution function	pC
$I_\varphi(i)$	Phase resolved PD current distribution function	μA
$P_\varphi(i)$	Phase resolved PD power distribution function	μW
$Q_\varphi(i)$	Phase resolved PD quadratic rate distribution function	nC^2/S
$f_q(i)$	Pulse-height of occurrence distribution function	N/A
$A_q(i)$	Pulse-height resolved average distribution function	N/A
$M_q(i)$	Pulse-height resolved maximum distribution function	N/A
$I_q(i)$	Pulse-height resolved PD current distribution function	μA
$P_q(i)$	Pulse-height resolved PD power distribution function	μW
$Q_q(i)$	Pulse-height PD quadratic rate distribution function	nC^2/S
$f_T(i)$	Cycle of occurrence distribution function	N/A
$A_T(i)$	Cycle resolved average PD distribution function	pC
$M_T(i)$	Cycle resolved maximum PD distribution function	PC
$I_T(i)$	Cycle resolved PD current distribution function	μA
$P_T(i)$	Cycle resolved PD power distribution function	μW
$Q_T(i)$	Cycle resolved PD quadratic rate distribution function	nC^2/S
I_{av}	Average PD current in a given time interval	S
V_{gap}	Rod-to-plane gap voltage	V
V_{onset}	Discharge onset voltage	V

E_n	n-th discharge pulse energy	J
t_c	The critical time interval – the maximum time separation between consecutive discharges that minimizing the influence of ac voltage.	μs
Δt_{min}	The minimum time separation between consecutive PDs	μs
Δt_{mc}	The saturated value of Δt_{min}	μs

C.2 Acronyms Table

A/D	Analog to digital
CRPD	Cycle resolved partial discharge
DAV	Difference of absolute voltage
EPC	Extended capability port
ERPD	Energy resolved partial discharge
ISA	Industrial Standard Architecture
MSSD	The half mean of successive squared differences
PD	partial discharge
PDD	Partial discharge detector
PHPD	Pulse height resolved partial discharge
PRPD	Phase resolved partial discharge
QD	Successive charge difference in a discharge series
QDPD	Charge difference resolved partial discharge
TD	Successive time difference in a discharge series
TDPD	Time difference resolved partial discharge
VD	Successive voltage difference in a discharge series
VDPD	Voltage difference resolved partial discharge

C.3 List of Figures

C.4 List of Tables

Appendix D

Other Partial Discharge Quantity

With digital processing technology, the results of a PD measurement can be displayed as a φ-q-n three-dimensional graph as shown in figure D1. In such a graph, the number of PD events is shown as a function of the magnitude and phase information of PD events. To analyze the measurement results with a computer-based system, fractal features can be calculated directly from this three-dimensional graph to describe naturally occurring complex shapes such as mountain, range, and cloud etc. However, the algorithms used with such an approach is more complicated than those applied to two-dimensional distributions. In addition, the fractal features calculated from the φ-q-n distribution are not directly associated with PD physical mechanism [58].
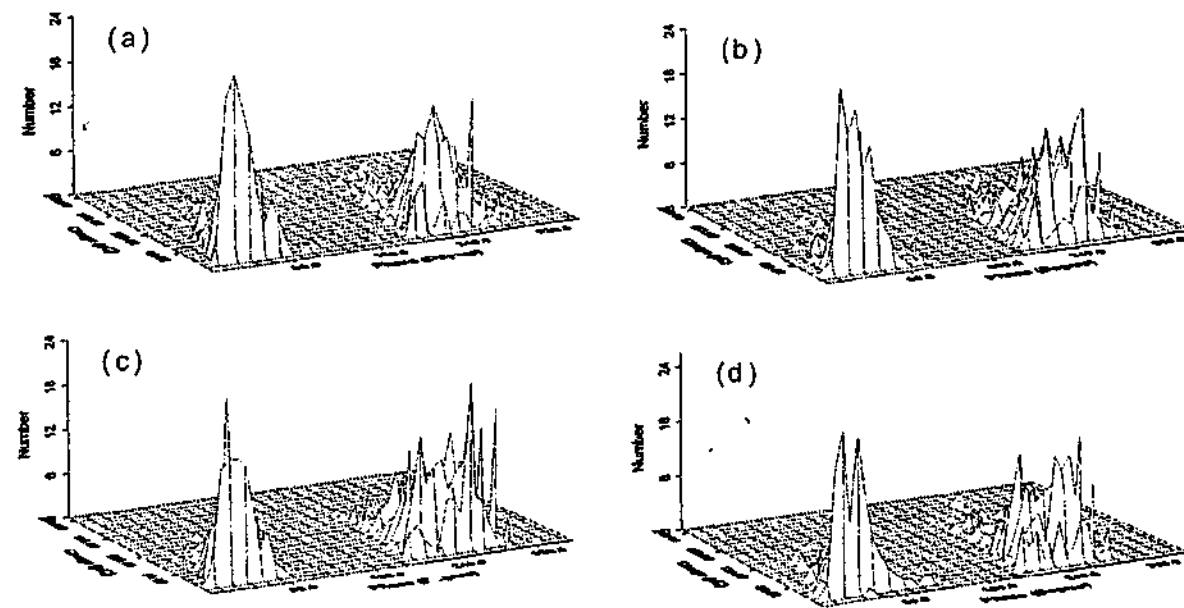
Figure D1 Patterns of φ-q-n measured at 8mm gap of a point-to-dielectric arrangement after applying 3 kV voltage for (a) 16 minutes; (b) 18 minutes; (c) 20 minutes; and (d) 25 minutes

Appendix E

Exportable Parameters for PRPD, PHPD and CRPD Distributions

Table E.1 illustrates the available statistics calculated based on PHPD window for exportation. Similar to statistics calculated based on PRPD window, the statistics listed in table E1 provide detailed information about the nature of discharge characteristics in terms of PHPD based statistical variations against discharge magnitude. In the same manner, table E.2 has shown statistics for CRPD window. Like listed statistics calculated from PRPD and PHPD based window, the distribution of these statistics provides indispensable information regarding the nature of PD phenomena.

Parameter Name	Interpretation
Count	Total observable number of PD events
Vave	Average value of applied voltage (kV)
Vmax	Maximum absolute value of applied voltage (with polarity)
Vmin	Minimum absolute value of applied voltage (with polarity)
Vmean	Mean value of applied voltage (kV)
Vrange	Range of applied voltage (kV)
Vvar	Variance of applied voltage
Vstdev	Standard deviation of applied voltage (kV)
Vmssd	Half mean of squared difference in applied voltage
Vsk	Skewness of applied voltage
Vku	Kurtosis of applied voltage
Current	Integrated PD current (uA)
Power	Integrated PD power (mW)
Quadratic	Quadratic rate of PD amplitude (nC*nC/s)
PhaseMax	Maximum ac voltage phase position in degree
PhaseMin	Minimum ac voltage phase position in degree
PhaseRange	Range of ac voltage phase in degree
PhaseMean	Mean value of ac voltage phase position in degree
PhaseVar	Variance of ac voltage phase
PhaseStdev	Standard deviation of ac voltage phase
Qrange	Range of PD amplitude (pC)
Qvar	Variance of PD amplitude
Qstdev	Standard deviation of PD amplitude
Qmssd	Half the mean of successive squared difference of PD amplitude

Table E.1 Exportable statistical parameters based on pulse-height partition window

Parameter Name	Interpretation
NumPos	Total number of PD events occurred in ac positive half cycle
QmaxPos	Maximum PD amplitude in ac positive half cycle (pC)
QintgPos	The sum of PD amplitude in ac positive half cycle (pC)
IavePos	PD current in ac positive half cycle (uA)
PowerPos	PD Power in ac positive half cycle (mW)
QuadPos	Quadratic rate of PD amplitude occurred in ac positive half cycle (nC*nC/s)
SkPos	Skewness in ac positive half cycle
KuPos	Kurtosis in ac positive half cycle
MeanPos	Mean value of PD amplitude in ac positive half cycle (pC)
VarPos	Variance of PD amplitude in ac positive half cycle
StdDevPos	Standard deviation of PD amplitude in ac positive half cycle
NumNeg	Total number of PD events occurred in ac negative half cycle
QmaxNeg	Maximum PD amplitude in ac negative half cycle (pC)
QintgNeg	The sum of PD amplitude in ac negative half cycle (pC)
IaveNeg	PD current in ac negative half cycle (uA)
PowerNeg	PD Power in ac negative half cycle (mW)
QuadNeg	Quadratic rate of PD amplitude occurred in ac negative half cycle (nC*nC/s)
SkNeg	Skewness in ac negative half cycle
KuNeg	Kurtosis in ac negative half cycle
MeanNeg	Mean value of PD amplitude in ac negative half cycle (pC)
VarNeg	Variance of PD amplitude in ac negative half cycle
StdDevNeg	Standard deviation of PD amplitude in ac negative half cycle
Count	Total number of PD events in a whole cycle
Qmean	Mean value of PD amplitude in a whole cycle (considering polarity) (pC)
Qmax	Maximum PD amplitude in a whole cycle (considering polarity) (pC)
Qmin	Minimum PD amplitude in a whole cycle (considering polarity) (pC)
Qrange	Range of PD amplitude in a whole cycle (considering polarity) (pC)
QstdDev	Standard deviation of PD amplitude in a whole cycle (considering polarity) (pC)
Qsum	Total sum of PD amplitude in a whole cycle (considering polarity) (pC)
Qinception	PD amplitude of first event in a cycle (pC)
Qextinction	PD amplitude of last event in a cycle (pC)
Vmean	Mean value of applied voltage (considering polarity) (kV)
Vmax	Maximum applied voltage (considering polarity) (kV)
Vmin	Minimum applied voltage (considering polarity) (kV)

Vrange	Range of applied voltage (considering polarity) (kV)
VstdDev	Standard deviation of applied voltage (considering polarity) (kV)
Vsum	Total sum of applied voltage (considering polarity) (kV)
Vinception	Instantaneous value of ac voltage when first PD event occurs in a cycle (kV)
Vextinction	Instantaneous value of ac voltage when last PD event occurs in a cycle (kV)

Table E.2 Exportable statistical parameters based on ac cycle

The following figure E.1 has shown part of the PRPD distribution results in a text delimited file that can be imported by other commercial packages for further analysis of PD distribution patterns.

WinNum	LFCount	LFAvePD	LFMaxPD	LFIa
23	3	32.2740	33.86773	0.00005
24	6	40.7460	50.83159	0.00012
25	9	44.9147	58.09325	0.00020
26	5	60.029.	87.13987	0.00015
27	1	79.8782	79.87822	0.00004
29	5	40.6653	60.51380	0.00010
30	1	38.7288	38.72883	0.00002
31	2	30.2569	31.46718	0.00003
32	3	83.1056	154.91533	0.00012
35	1	33.8877	33.88773	0.00002
36	9	232.9103	394.54999	0.00105
37	29	329.5289	469.58710	0.00478
38	52	344.3235	534.94202	0.00695
39	12	387.8934	539.78308	0.00233
40	1	534.9420	534.94202	0.00027
43	2	36.3083	36.30828	0.00004
44	4	47.8059	55.67270	0.00010
45	10	56.8830	96.82208	0.00028
46	14	39.2475	91.98098	0.00027
47	16	44.3264	106.50429	0.00035
48	17	49.2654	188.80305	0.00042
49	18	45.8560	77.45766	0.00041
50	17	80.0206	244.47575	0.00068
51	24	62.4301	213.00858	0.00075
52	19	64.4631	137.97147	0.00061
53	21	76.8814	171.85919	0.00081
54	15	62.9343	196.06471	0.00047
55	14	55.3269	96.82208	0.00039
56	7	92.6726	382.44720	0.00032
57	18	69.9271	210.58803	0.00063

Figure E.1 Part of the exported PRPD feature quantities in a text editor
WinNum: PRPD window index number (missing number means no PD events recorded)
LFCount: Discharge occurrence
LFAvePD: Average PD amplitude
LFMaxPD: Maximum PD amplitude
LFIa: Discharge current

Appendix F

PD Quadratic Rate of Various Distribution Categories

Quadratic rate of PD amplitude is an important measure to PRPD distribution functions. Figure F.1 has demonstrated the patterns of this important distribution function measured from various PD sources.
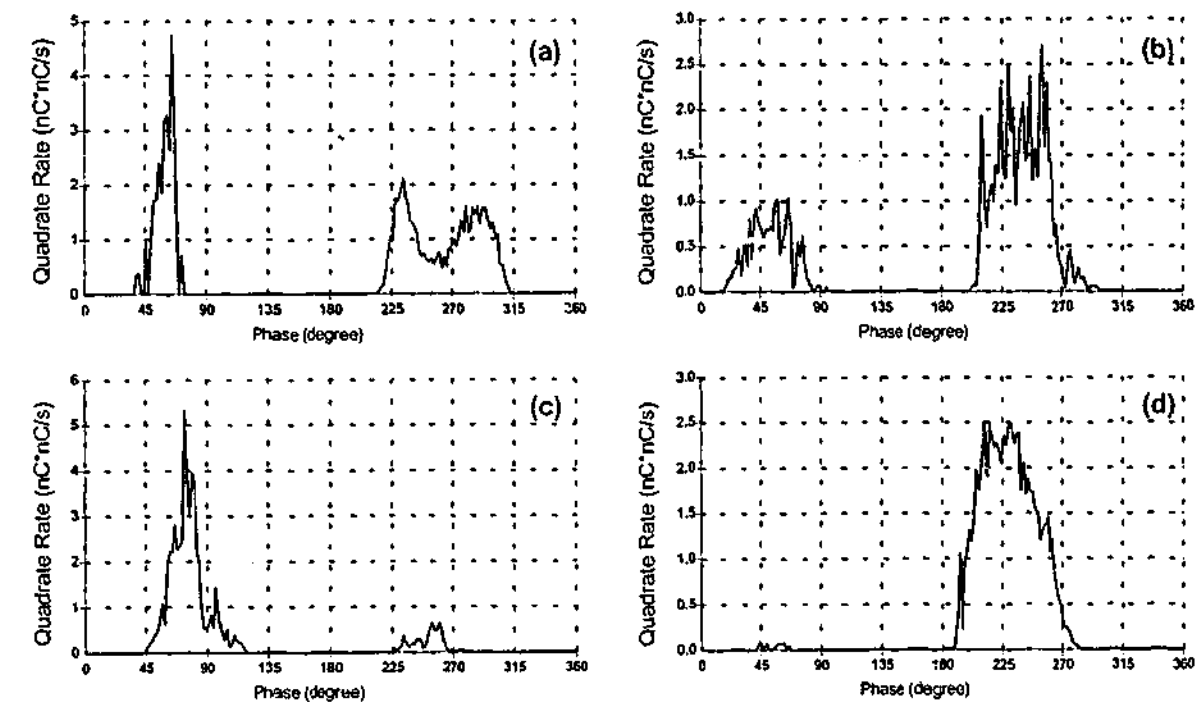

Figure F.1 Distribution functions of quadratic rate of discharge amplitude measured from
(a) a point-to-plane corona
(b) a point-to-dielectric discharge
(c) an oil-impregnated pressboard discharge
(d) an epoxy resin stator bar with an artificial defect inside

Quadratic rate of PD amplitude is also an important distribution parameter to quantify PHPD distribution functions. Figure F.2 has demonstrated the patterns of this important distribution function measured from various PD sources.
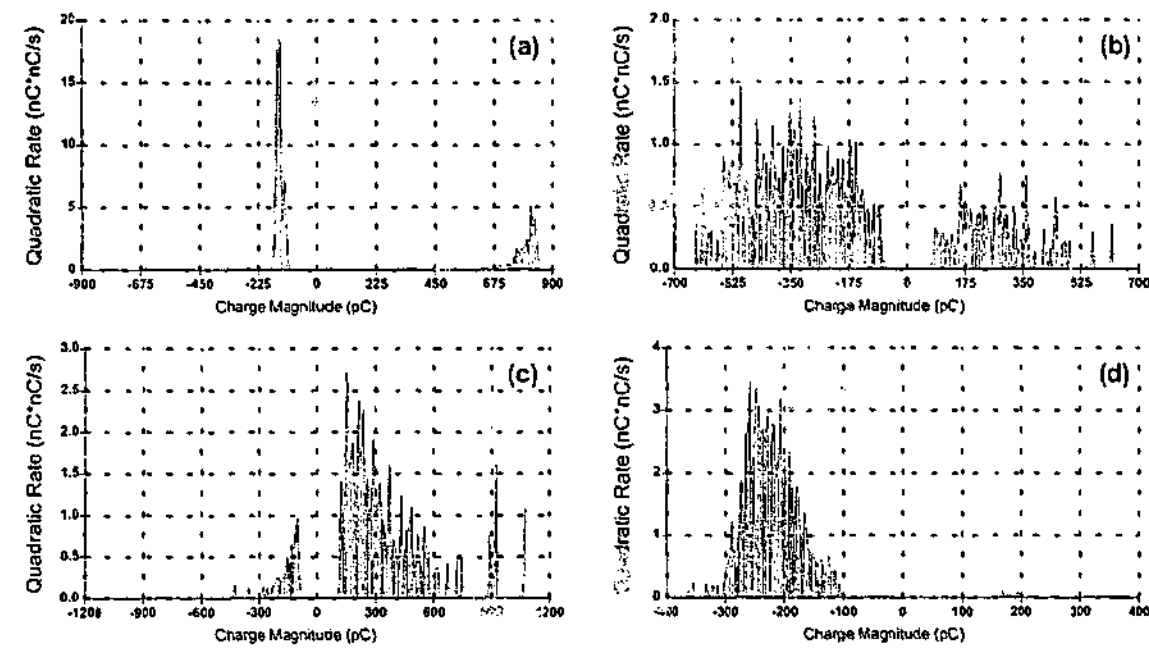

Figure F.2 Distribution functions of discharge amplitude quadratic rate measured from
(a) a point-to-plane corona
(b) a point-to-dielectric discharge
(c) an oil-impregnated pressboard discharge
(d) an epoxy resin stator bar with an artificial defect inside

Beside the PRPD and PHPD distribution, Quadratic rate of PD amplitude can also be used to observe the distribution function with CRPD pattern. Figure F.3 has demonstrated such distribution patterns obtained from experiments on various PD sources.
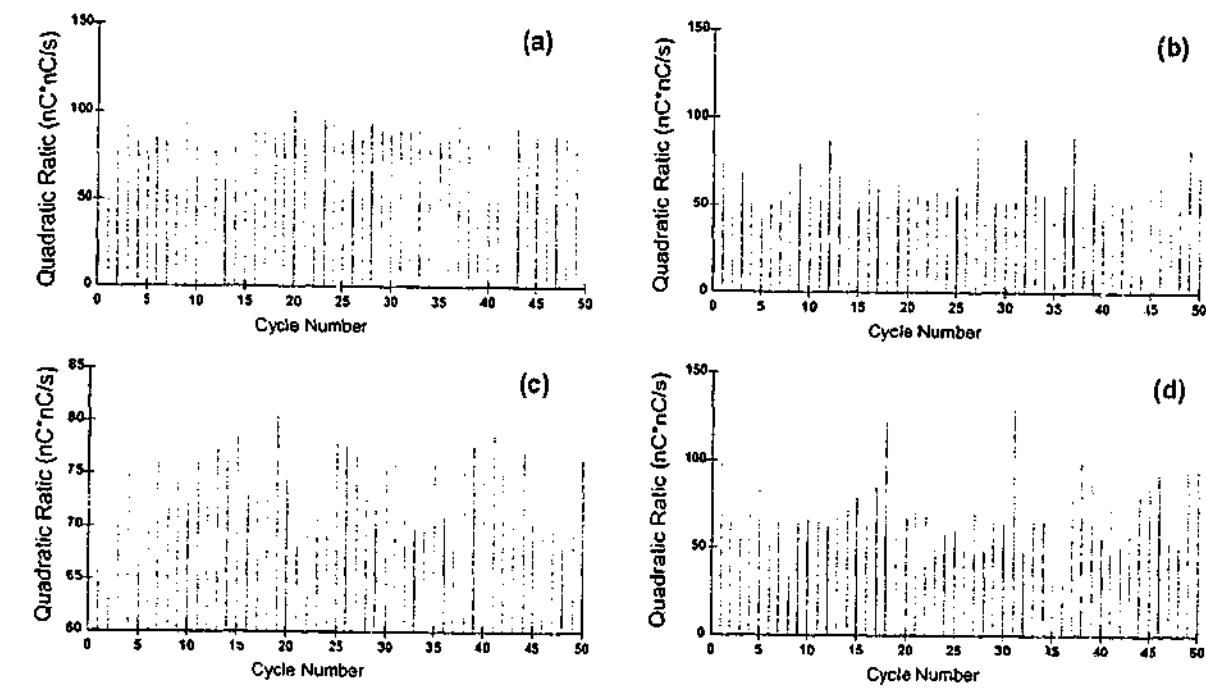

Figure F.3 CRPD quadratic rate distribution functions measured from
(a) a point-to-plane arrangement
(b) an oil-impregnated pressboard sample
(c) an epoxy resin stator bar
(d) a point-to-dielectric arrangement

Appendix G

Basic Concepts of Artificial Neural Networks

G.1 Background

In the first part of this chapter, the work has been focused on using neural networks for the classification with input PD fingerprints. The most important attribute of a multilayer network is that it can learn a mapping of any complexity. The network learning is based on repeated presentations of the training samples. To understand the nature of mapping performed by multilayer networks and the training of such networks, it is necessary to brief some basic fundamentals. It should be understood that detailed discussion of ANNs and their complicated algorithms are beyond the scope of this thesis. However, the following introduction and discussion may help readers to understand the applications.

G.2 Artificial Neural Networks

There are actually many definitions of ANNs. Generally ANNs are distributed, adaptive and nonlinear learning machines built from many different processing elements (PEs). Each PE receives connections from other PEs and/or itself. The interconnectivity defines the topology. The signals flowing on the connections are scaled by adjustable parameters called weights, W_{ij} and it is associated with every connection as seen in figure G.1. As illustrated in the figure, a PE sums all contributions and produces an output that is a nonlinear function of the sum. The output of the PE becomes either system output or is conveyed to the same or other PEs.
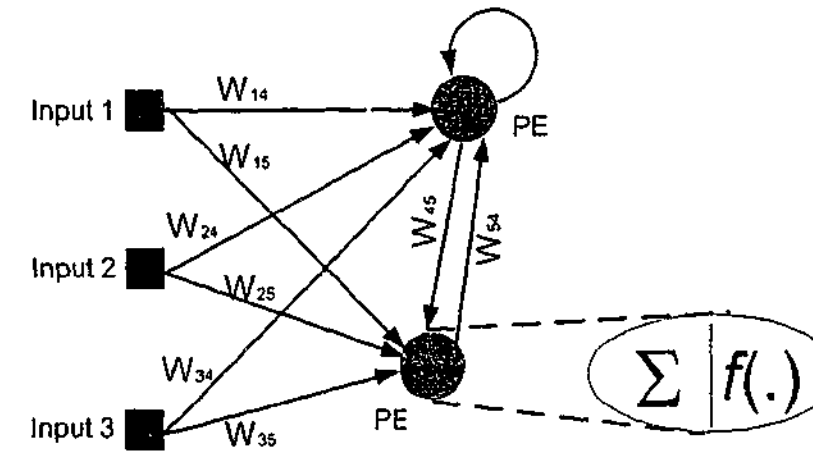
Figure G.1 An artificial neural network

The ANN builds discriminant functions from its PEs. The ANN topology determines the number and shape of the discriminant functions. In other words, the discriminant functions change with the topology [113]. The placement of the discriminant functions is controlled by the network weights. Following the ideas of non-parametric training, the weights are adjusted directly from the input vector by training without any assumptions about their statistical distribution.

G.3 Pattern Recognition Ability of the McCulloch-Pitts PE

The McCulloch-Pitts (M-P) processing element is simply a sum of products followed by a threshold non-linearity. Its input-output equation is as follows:

$$y = f(net) = f(\sum_{i=1}^{N} w_i x_i + b) \qquad (G.1)$$

where N is the number of inputs, x_i are the inputs to the PE, w_i are the weights and b is a bias term. The activation function f is a threshold function defined by equation G.2.

$$f(net) = 1, \qquad net \geq 0 \qquad (G.2a)$$
$$f(net) = -1, \qquad net < 0 \qquad (G.2b)$$

Such a system is able to separate two classes (one class associated with 1 and the other with the –1 response). In general, the output of the network y is dependent on $\sum_{i=1}^{n} w_i x_i + b$, where n is the number of connections of the PE. Apparently, the boundary $\sum_{i=1}^{n} w_i x_i + b = 0$ is a multidimensional space and the output of the network is difficult to obtain analytically. In practice, the computation of the corresponding output is conducted by injecting every input vector into the network. It is understood that M-P PE is restricted to classifying only two classes. To classify the input as one of M classes, the topology has to be modified to include a layer of M M-P PEs so that each one is able to create its own linear discriminant function in a N-dimensional space. The advantage of having multiple PEs versus single M-P PE is the ability to tune each PE to respond to an input space region. Each PE is essentially deciding if the input is in a particular class or not. Figure G.2 represents a two inputs, one output M-P PE network.
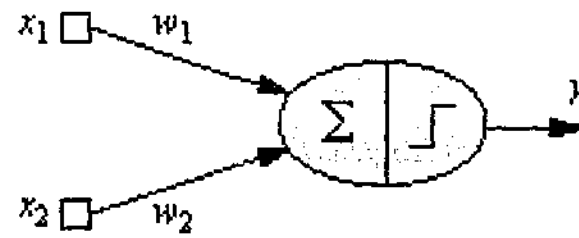

Figure G.2 Two inputs, one output (2-1) McCulloch-Pitts PE

G.4 The Perceptron

Rosenblatt's perceptron is a pattern recognition machine that was invented in the early 50s. The perceptron has multiple inputs fully connected to an output layer with multiple M-P PEs. According to figure G.3, each input value is multiplied by an adjustable weight before being fed to a processing element in the output layer, thus yielding

$$y_i = f(net) = f(\sum w_{ij} x_j + b_i) \qquad (G.3)$$

where b_i is the bias for each PE and the number of outputs is usually determined by the number of classes to be separated. These PEs add the individual scaled contributions and respond to the entire input space.
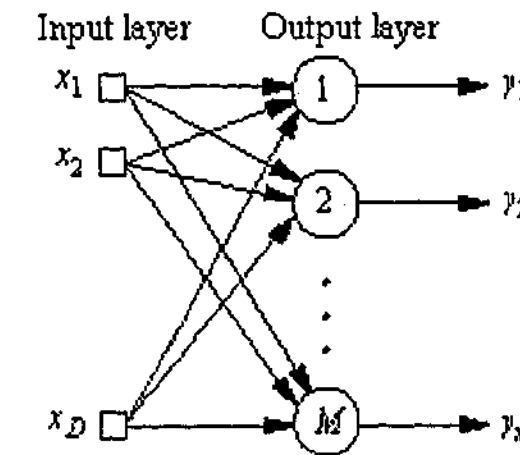
Figure G.3 The perceptron with D inputs and M outputs

An N-output perceptron can divide the pattern space into N distinct regions. The decision regions of the perceptron are always convex regions, because only one of the outputs is required to be positive during training. When a PE responds maximally to an input pattern, it means that the input is inside the region represented by the PE. Hence, each PE identifies patterns that belong to a class.

When there are M outputs of a network, the cost function can be computed as a sum over the training set as well as a summation of each output PE. If J is denoted as the cost function, it becomes

$$J = \frac{1}{2N} \sum_{p=1}^{N} \sum_{i=1}^{M} \varepsilon_{pi}^2 \qquad (G.4)$$

where p is the index over the patterns and i over the output PEs.